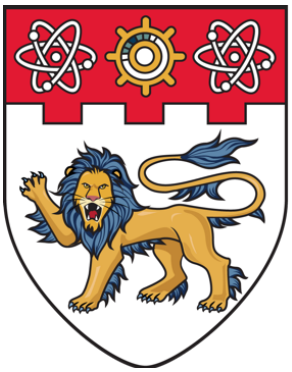

NANYANG TECHNOLOGICAL UNIVERSITY
SINGAPORE

CHEMISTRY OF OPEN-SHELL π-EXTENDED AZACORANNULENES

HAMAMOTO YOSUKE

SCHOOL OF CHEMISTRY, CHEMICAL ENGINEERING AND BIOTECHNOLOGY

2024

CHEMISTRY OF OPEN-SHELL π-EXTENDED AZACORANNULENES

HAMAMOTO YOSUKE

SCHOOL OF CHEMISTRY, CHEMICAL ENGINEERING AND BIOTECHNOLOGY

A thesis submitted to the Nanyang Technological University in partial fulfilment of the requirement for the degree of Doctor of Philosophy

2024

Statement of Originality

I hereby certify that the work embodied in this thesis is the result of original research done by me except where otherwise stated in this thesis. The thesis work has not been submitted for a degree or professional qualification to any other university or institution. I declare that this thesis is written by myself and is free of plagiarism and of sufficient grammatical clarity to be examined. I confirm that the investigations were conducted in accord with the ethics policies and integrity standards of Nanyang Technological University and that the research data are presented honestly and without prejudice.

2 Aug 2024

. . . . . .

Date

. . . . . .

[HAMAMOTO YOSUKE]

Supervisor Declaration Statement

I have reviewed the content and presentation style of this thesis and declare it of sufficient grammatical clarity to be examined. To the best of my knowledge, the thesis is free of plagiarism and the research and writing are those of the candidate's except as acknowledged in the Author Attribution Statement. I confirm that the investigations were conducted in accord with the ethics policies and integrity standards of Nanyang Technological University and that the research data are presented honestly and without prejudice.

2 Aug 2024

. . . . . .

Date

. . . . . .

[ITO SHINGO]

Authorship Attribution Statement

This thesis contains material from 2 papers published in the following peer-reviewed journal in which I am listed as an author.

Chapter 2 is published as Hamamoto, Y., Ochiai, K., Li, Y., Tapavicza, E., Ito, S. Synthesis and Properties of Azahomocorannulenyl Cations and Radicals. *Angew. Chem. Int. Ed*. **2024**, *63*, e202319022. DOI: 10.1002/anie.202319022.

The contributions of the co-authors are as follows:

- Prof. S. Ito provided the initial project direction and edited the manuscript drafts.
- I prepared the manuscript drafts.
- I co-designed the study with Prof S. Ito and Mr. K. Ochiai and performed all the laboratory work at the School of Chemistry, Chemical Engineering and Biotechnology.
- Dr. Y. Li assisted in collecting and interpreting the X-ray Crystal analysis.
- DFT calculations were performed and written by Prof S. Ito, Prof. E. Tapavicza and the author.

Chapter 4 is published as Li, Q.-Q., Hamamoto, Y. Kwek, G., Xing, B., Li, Y., Ito, S. Diazapentabenzocorannulenium: A Hydrophilic/Biophilic Cationic Buckybowl. *Angew. Chem. Int. Ed*. **2022**, *61*, e202112638. DOI: 10.1002/anie.202112638.

The contributions of the co-authors are as follows:

- Prof. B. Xing and Prof. S. Ito directed and conceived the project.
- Dr. Q.-Q. Li performed most of the synthetic work.
- The author performed the theoretical studies with DFT calculation.
- Dr. Q.-Q. Li and the author performed most of measurements for analysis.
- Dr. G. Kwek performed the biological experiments.
- Dr. Y. Li assisted in collecting and interpreting the X-ray Crystal analysis.
- Dr. Q.-Q. Li and the author contributed equally as the first authors of this work. All the authors discussed the results and contributed to the manuscript.

2 Aug 2024

. . . . . .

Date

. . . . . .

[HAMAMOTO YOSUKE]

Abstract

Open-shell aromatic molecules have garnered attention due to their applications in various fields. Designing such molecules by incorporating non-hexagonal structures or hetero atoms into the π-surface of aromatic molecules is an effective approach. This thesis investigates multiple analogs of open-shell aromatic molecules based on the azacorannulene skeleton. Chapter 1 provides a general introduction to the development of carbon-centered radical chemistry from the perspective of fragment molecules of carbon-defective graphene, highlighting the significance of organic open-shell molecules. Chapter 2 discusses the synthesis and properties of monoradical molecules, modified by incorporating one carbon into azapentabenzocorannulene, and the isolation of a single crystal of the rare tropyl radical form. Chapter 3 presents open-shell molecules with two sp^2 carbons added to azacorannulene, featuring a small singlet-triplet gap and a singlet ground state. Chapter 4 details the synthesis of diazapentabenzocorannulenium cation, which incorporates another nitrogen atom in the central pyrrole ring of the corannulene structure and serves as a potential precursor to diazapentabenzocorannulene radical. This cation molecule itself exhibits high affinity for water despite its large π-surface. These carbon-defective modifications enable the design of functional open-shell molecules. Chapter 5 describes the conclusion and perspective of this research.

Acknowledgements

First and foremost, I wish to express my deepest gratitude to my supervisor, Professor Shingo Ito. His extensive knowledge and insightful discussions have been invaluable throughout this PhD journey.

I am deeply thankful to my lab mates, Dr. Qiang-Qiang Li, Dr. Weifan Wang, Dr. Hui Han, Dr. Xinjiang Zhang, Dr. Hanindita Fiona, and Mr. Glen Goh Wee Zhuan. Their expertise, valuable contributions, and stimulating discussions have greatly enriched my research experience. Their camaraderie has also made the demanding work environment much more manageable.

My heartfelt appreciation extends to all my co-authors, Professor Enrico Tapavicza, Professor Bengang Xing, Mr. Kotaro Ochiai, and Dr. Germain Kwek. Their collaborative efforts, guidance, and support have been instrumental in advancing the experimental work for our publications. I am grateful to the CBC technical and administrative staff, particularly Dr. Yongxin Li, Ms. Goh Ee Ling, and Ms. Zhu Wenwei, for their invaluable assistance with experimental analyses. I would also like to express my appreciation to Nanyang Technological University for providing me with a research scholarship, which supported me throughout my pursuit of this degree.

I would also like to acknowledge all the individuals who have supported and influenced my PhD journey, especially Dr. Kei Ota, Dr. Yoshiya Sekiguchi, Dr. Kota Koshino, and my roommate Mr Tomoki Furuhashi. The connections and interactions with them have helped me navigate through the tough times.

Lastly, I express my deepest appreciation to my parents, sisters. Their encouragement and understanding during my prolonged absence while pursuing my PhD in Singapore, especially amid the challenging societal circumstances, have been a constant source of strength and motivation.

Table of Contents

Chapter 1. General Introduction

1.1. Polycyclic Aromatic Hydrocarbons (PAHs) based radicals

1.1.1. PAHs

Polycyclic aromatic hydrocarbons (PAHs) are a class of organic molecules composed of multiple aromatic rings. Representative structures include naphthalene, which has two adjacent benzene rings, and anthracene, which features three benzene rings attached continuously(**Figure 1.1a**). Due to their intrinsic properties, PAHs have been studied extensively in diverse research fields for over centuries[1,2]. The origin of this chemistry began with Faraday's discovery of benzene in 1825[3a]. Subsequently, Kekulé proposed the structural formula of benzene, which was a milestone in modern organic chemistry[3b]. In the realm of quantum chemistry, Hückel's theory of 4n+2π aromaticity demonstrated the prediction for planar cyclic hydrocarbons of the aromaticity in 1931[3c]. Clar further extended this idea with the π-sextet rule in 1972[4], accelerating research by enabling predictions of the stability and geometry of these intriguing molecules. The development of organic chemistry has enabled the synthesis of a vast array of PAHs[5], while advancements in physical chemistry have facilitated the creation of functional PAHs for applications[6].

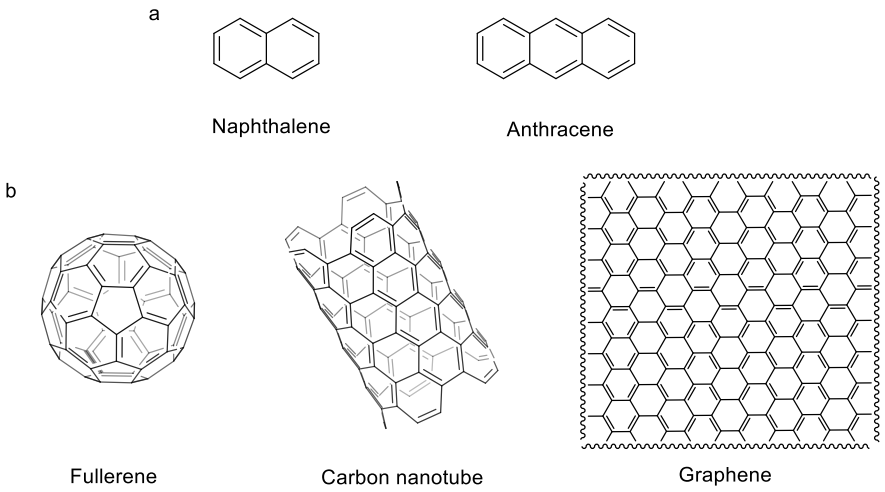

Figure 1.1. Chemical structures of PAHs (a) Naphthalene and Anthracene. (b) Carbon materials.

Additionally, three groundbreaking PAHs were reported. In 1985, fullerenes were reported as their unique closed-cage structure[7], marked a breakthrough in carbon chemistry and later won the Nobel Prize in 1996. Carbon nanotubes (CNTs), reported in 1991[8], introduced a new dimension to carbon materials with their mechanical and electrical properties. The isolation of graphene in 2004[9], a single layer of carbon atoms arranged in a honeycomb lattice, won the Nobel Prize in 2010 (**Figure 1.1b**). Furthermore, molecules that incorporate partial structures of fullerenes, CNTs, and graphene provide deeper insights into the properties of these carbon materials and can serve as precursors for synthesizing carbon materials[5,6].

Corannulene (**Figure 1.2**)[10,11], a bowl-shaped polycyclic aromatic hydrocarbon also called buckybowl which means the fragment of fullerenes, was first synthesized in 1966. Scalable synthesis methods were established by Scott and Siegel in separate groups[12], contributing to its widespread applications today[13]. Additionally, Sakurai and Hirao achieved the synthesis of sumanene (**Figure 1.2**) in 2003[14], which is another representative buckybowl molecule. (The author discusses buckybowls in more detail in **Chapter 1.2**.) In 2001, Scott *et al*. achieved the total synthesis of fullerenes C_{60} by laser irradiation at 337 nm to the precursor molecule $C_{60}H_{30}$[15a]. The next year, they successfully synthesized it by flash vacuum pyrolysis as well[15b] (**Figure 1.2**).

Significant progress has also been made recently in the synthesis of substructures of CNTs[16]. Cycloparaphenylene (CPP) (**Figure 1.2**)[17], representing the smallest unit of the armchair type of CNTs, was successfully synthesized in 2008[18]. This development has paved the way for synthesizing topologically complex molecules based on CPP[19]. Moreover, Segawa and Itami achieved a breakthrough in 2017 by synthesizing carbon nanobelts (**Figure 1.2**)[20], which are fully conjugated by continuous benzene rings to form a circle. Numerous synthetic studies have been reported regarding the partial structures of graphene as well[5,6].

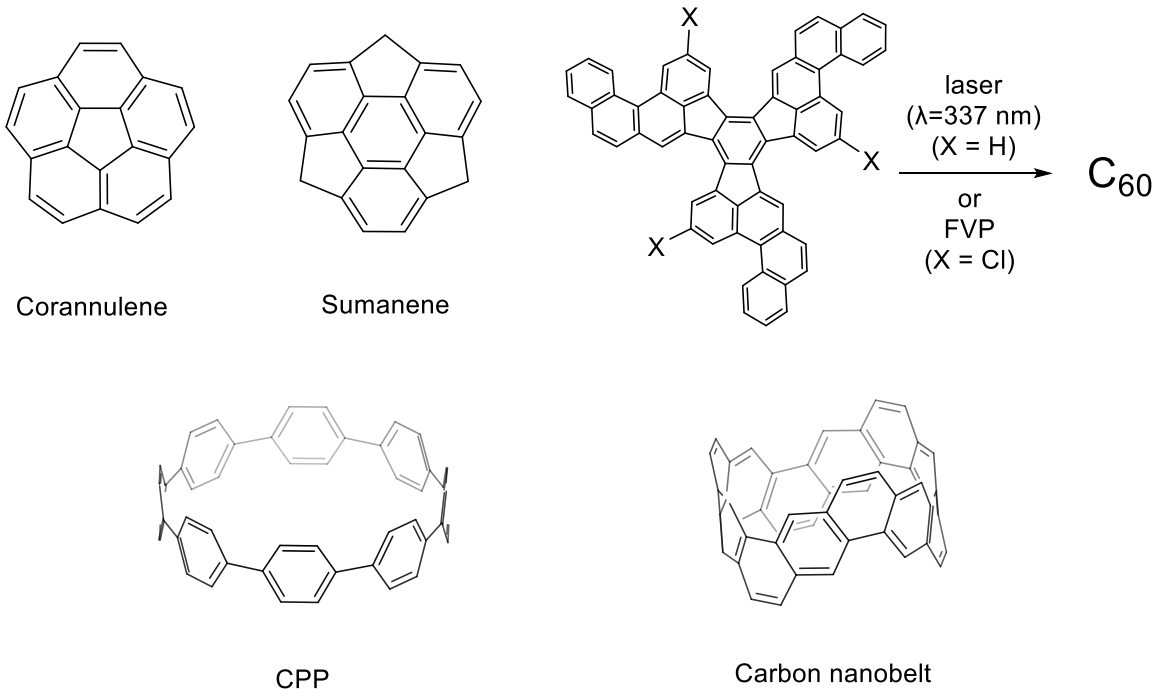

Figure 1.2. Fragments of Carbon materials.

1.1.2. Defective carbon-based PAHs

Graphene stands out as one of the most promising materials in science[21]. It typically exhibits exceptional electron [22] and mechanical [23] properties; however, during synthesis, structural defects can inadvertently contaminate its "pristine" structure due to the second law of thermodynamics [24] . These defects sometimes compromise graphene's properties. Paradoxically, the defects can also impart graphene with unique properties distinct from "pristine" graphene, influencing electron behavior and topological factors. These properties hold significant implications for nanomaterials[24].

There are typical types of defects in graphene structures. The graphene lattice can incorporate non-hexagonal rings, such as five- and seven-membered rings, where dislocation-like defects occur as alternating pentagon-heptagon pairs from the original hexagon-hexagon pairs (**Figure 1.3a**). The Stone-Wales defect is a straightforward example, as it involves bond rearrangement without atom removal (**Figure 1.3b**). Additionally, vacancies of single or

multiple atoms, as well as the inclusion of additive atoms—including heteroatoms—have been predicted and experimentally investigated. Reports of experimental investigations for carbon defects are increasing year by year. Meanwhile, many phenomena caused by these defects, such as optical, electronic, and magnetic properties, still require further exploration[24]. Additionally, controlling these defects remains a challenging issue. To understand the defined structure and properties of carbon defects, it is crucial to develop partial fragments of these defects and explore synthetic routes for them using bottom-up synthesis[25].

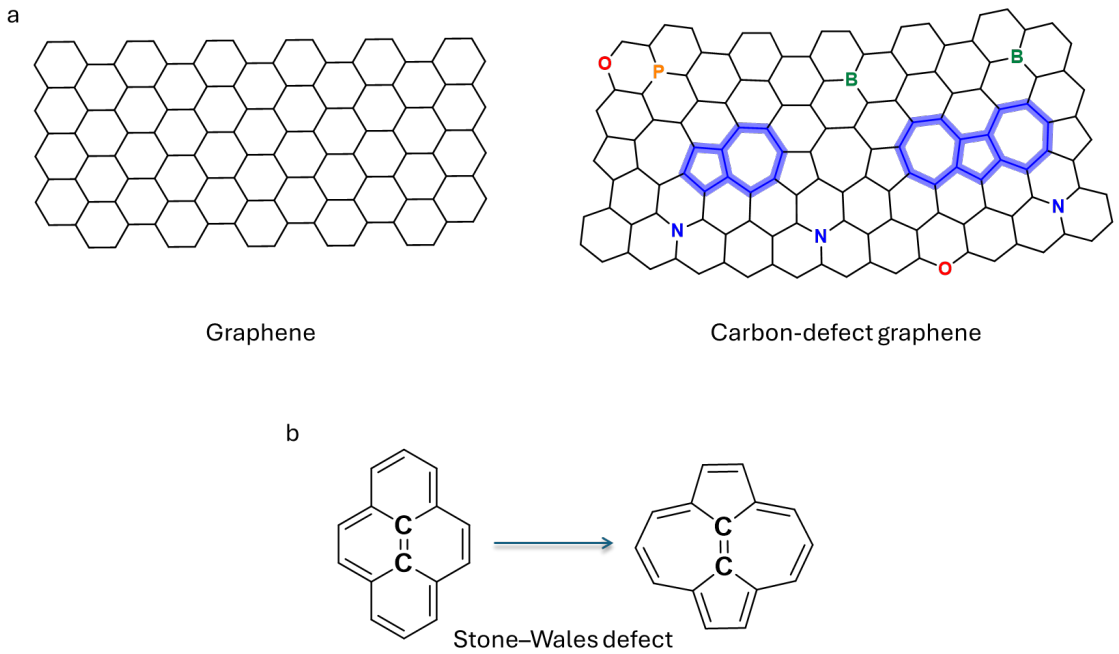

Figure 1.3. (a) Example structure of Carbon-defect graphene. (b) Stone-Wales defect.

Buckybowl molecules, mentioned above, are also classified as fragments with defective carbon structures. These are characterized by their Gaussian curvature typically caused by including five-membered rings. PAHs containing non-hexagonal rings, especially odd-membered rings, are classified as nonalternant hydrocarbon molecules[25].

Azulene, the most representative molecule of nonalternant hydrocarbons, consists of one five-membered ring and one seven-membered ring, making it a structural isomer of naphthalene[26]. This structure is commonly observed in carbon defects as well. Azulene exhibits

different properties from naphthalene. Comparing the frontier orbitals, the HOMO and LUMO orbital coefficients in naphthalene are of equal magnitude and symmetrically distributed on the same carbon atoms (**Figure 1.4**). In contrast, in azulene, the HOMO and LUMO orbital coefficients differ in both magnitude and distribution. The HOMO orbital coefficients are biased toward the five-membered ring, while the LUMO orbital coefficients are biased toward the seven-membered ring. This asymmetry in nonalternant hydrocarbons leads to unique properties not found in alternant hydrocarbons, such as dipole moments and low excitation energies.

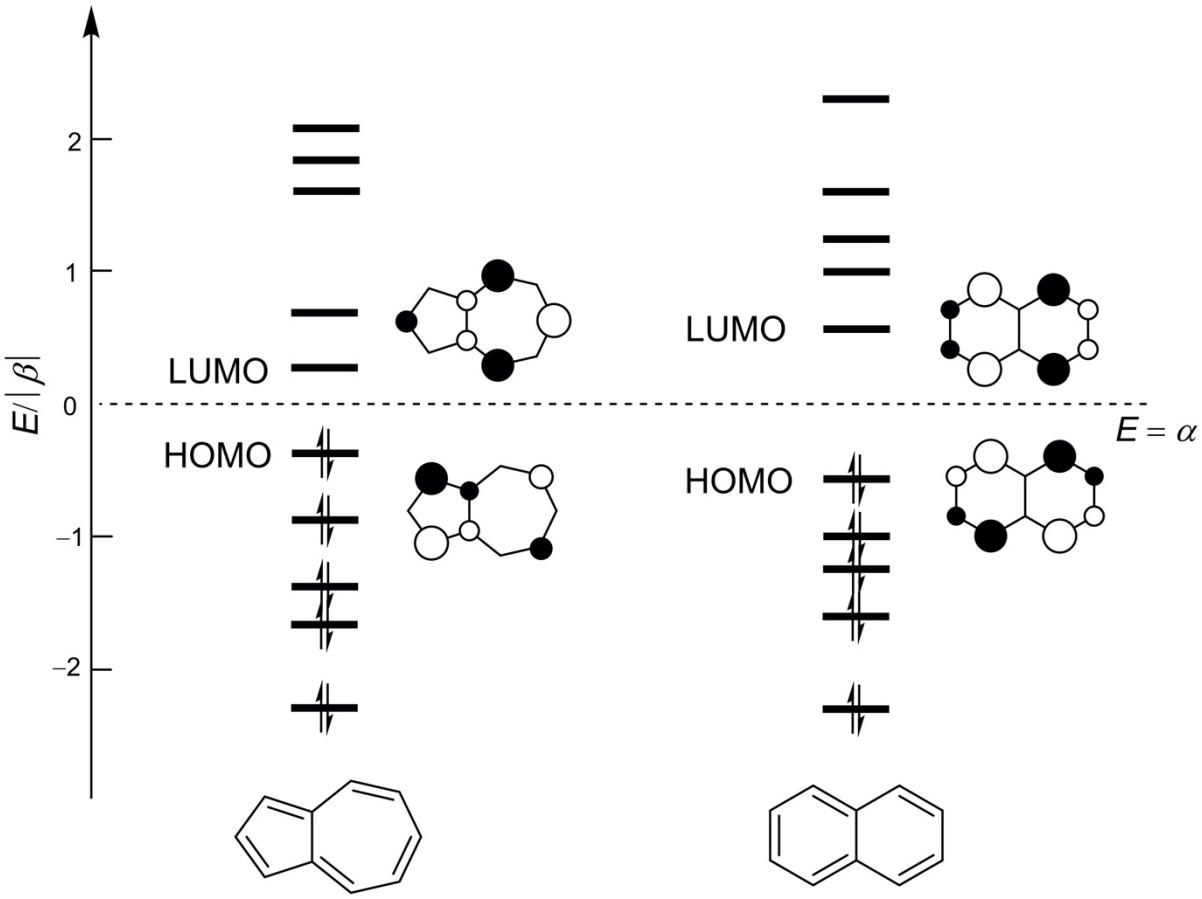

Figure 1.4. Frontier orbitals of azulene and naphthalene.

In recent years, there has been considerable progress in synthesizing PAHs containing odd-membered rings, and their physical properties have been extensively studied[25]. Research has also been conducted on molecules where two odd-membered rings are connected or

enclosed by benzene rings. Some of them have not been successfully synthesized due to their high reactivity caused by antiaromaticity or open-shell character. PAHs containing more than two odd-membered rings have also been attempted actively, with attention given to their (anti)aromaticity and topological properties[25].

1.1.3. Defective carbon-based open-shell PAHs

Open-shell molecules have unpaired electrons in one or more orbitals, making them highly reactive and often unstable. On the other hand, some stable radicals have been utilized for their unique unpaired electron characteristics in applications such as magnetic materials, secondary batteries, and specialized optical materials[27]. A representative example of open-shell organic species is the carbon-centered radical. Triphenylmethyl radical was discovered by M. Gomberg in 1900, marking the first recognition of a neutral chemical species with a trivalent carbon (**Figure 1.5a**)[28]. Gomberg reported that the dimer of the triphenylmethane was formed via radical species by the reduction of bromotriphenylmethane and exists in equilibrium between the radicals and dimer.

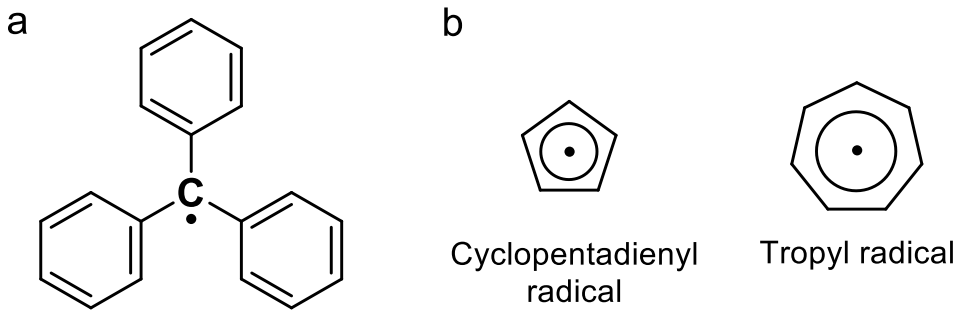

Figure 1.5. (a) Triphenylmethyl radical. (b) Odd-membered ring radicals.

Carbon-centered radical molecules often incorporate nonalternant hydrocarbon structures. One reason is that it is simple to design molecules with an odd number of π-electrons in odd-membered rings. Particularly common in molecular design are cyclopentadienyl

radicals with a five-membered ring structure and tropyl radicals with a seven-membered ring structure (**Figure 1.5b**). These structures are known to be highly unstable on their own. However, cyclopentadienyl radicals **1**[29] and **2**[30] can be isolated as crystals by introducing bulky substituents (**Figure 1.6a**). On the other hand, highly delocalizing the unpaired electrons on the π-surface, as seen in compound **3**[31], eliminates bulky substituents. The Koelsch radical **4**[32], stabilized by both delocalization of unpaired electrons and steric protection by fluorene skeletons, earns high stability even under air. Although examples of tropyl radicals are fewer and less stable compared to cyclopentadienyl radicals, some have been successfully isolated (**Figure 1.6b**). For instance, compound **5**[33] has been crystallized by Fukazawa and Yamaguchi. Additionally, the anthracen-9-yl-ligated dibenzotropyl radical **6** [34] and the hexapyrrohexaazahomocoronenyl radical **7**[35] have also been reported to be isolated in solution.

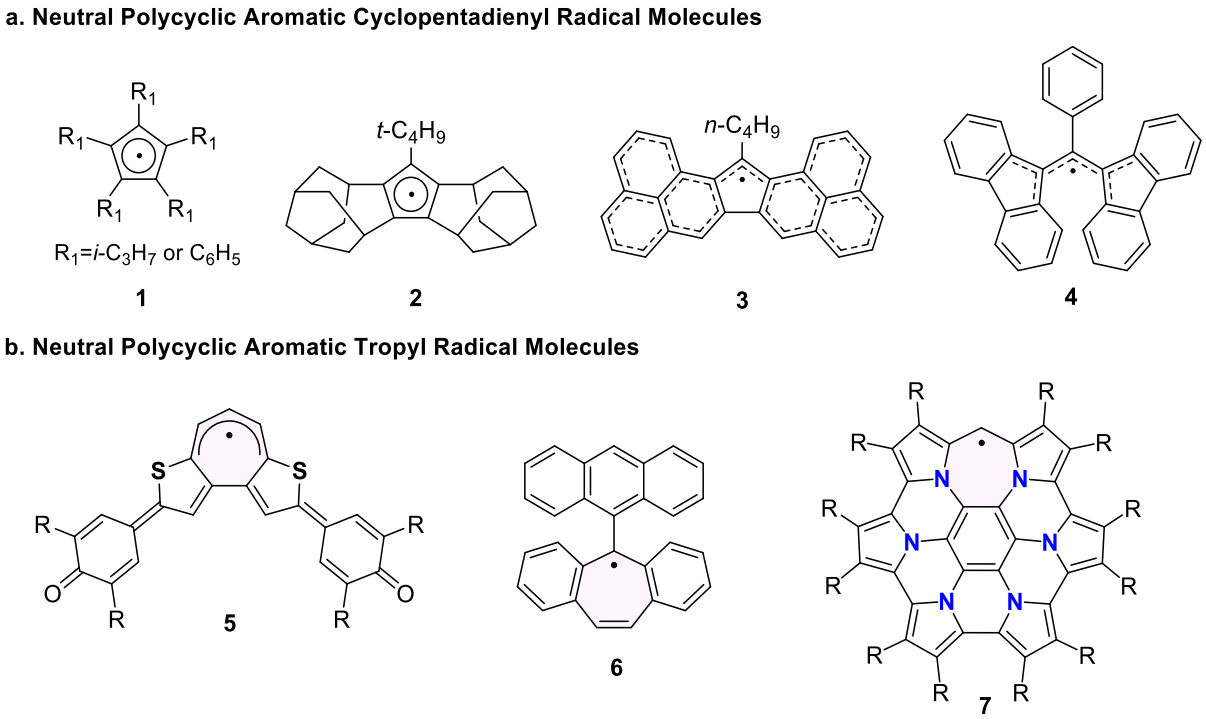

Figure 1.6. (a) Cyclopentadienyl radical based molecules. (b) Tropyl radical based molecules.

There are also many reports of incorporating two or more odd-membered rings into PAHs to induce an open-shell character. Particularly, diradicals, which have two electrons in

degenerate molecular orbitals, are of interest due to their unique physical properties[36]. The diradical properties vary depending on whether their ground state is a singlet or a triplet. The multiplicity of the ground state is an important topic. These were affected by factors such as the distance between the two spins, drawing attention to how these interactions work in the molecules.

Since odd-membered rings tend to localize spin density more than hexagonal rings, they are often used as spin centers in diradicals, as well as linkers for radical units. Specifically, odd-membered rings are frequently utilized in Kekulé, twisted ethylene, and antiaromatic diradical molecules (**Figure 1.7**).

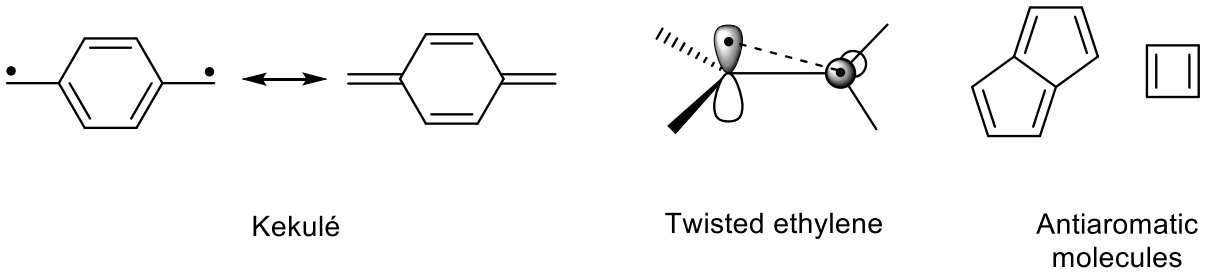

Figure 1.7. Representative types of diradical molecules.

Quinodimethane structure is one of the typical (non)Kekulé type structures to induce diradical characters.

o-Quinodimethane structure is one of the promising structures for inducing diradical character. In the trial of stabilizing the *o*-quinodimethane diradical, a naphthyl ring was introduced to incorporate a 7-membered ring. However, this was not isolated (**Scheme 1.1**)[37].

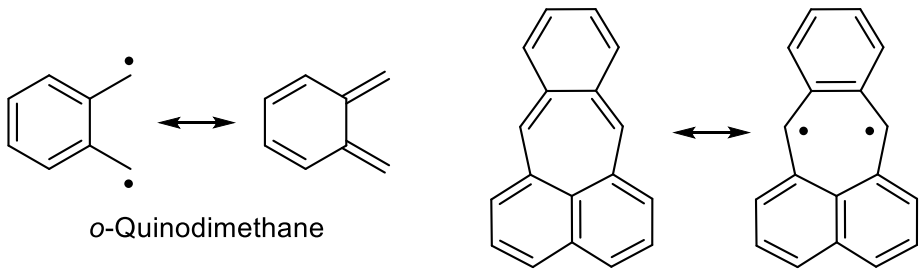

Scheme 1.1. *o*-Quinodimethane and *o*-quinodimethane based 7-membered diradical which has not been isolated.

s-Indacene/*as*-indacene, which partially features quinodimethane structure, is versatile and widely used for diradicals(**Figure 1.8**)[25]. Although parent *s*-indacene/*as*-indacene have never been isolated, tetra-*t*-butyl *s*-indacene derivative **8** was isolated by X-ray single crystal analysis[38]. The X-ray structure of derivative **8** revealed the D_{2h} form, while the ground state of derivative **8** is considered to have C_{2h} symmetry.

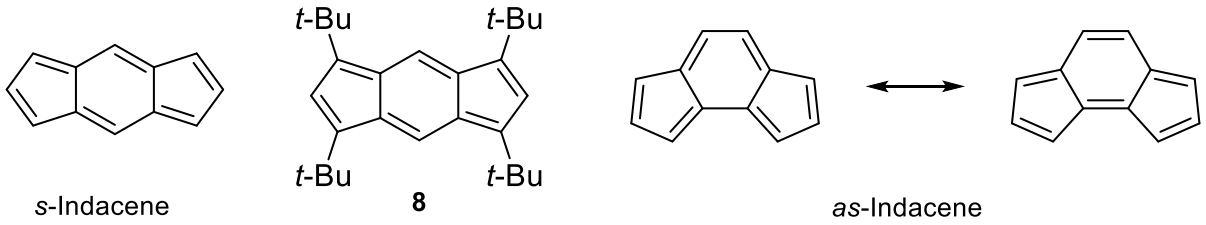

Figure 1.8. The structures of *s*-indacene and *as*-indacene.

Kubo and co-workers synthesized a series of biphenalenoindacene **9**, which feature two phenalenyl structures attached to *s*-indacene structure (**Figure 1.9a**)[39]. They reported that the diradical character increases with the number of benzene rings incorporated into the indacene structure.

The series of indenofluorene isomers **10-14**, which incorporate benzene rings at both ends of the indacene structure, are important for understanding electron behaviors based on s-indacene/as-indacene structures (**Figure 1.9a**)[40]. Derivatives **10** and **11** have demonstrated open-shell character, while **12-14** have experimentally shown a closed-shell ground state nature. The parent indenofluorene structure of **10** is unstable due to its open-shell character. However, introducing bulky mesityl (2,4,6-trimethylphenyl) groups to the five-membered rings, which serve as formal spin centers, sterically protects the reactive sites of the radicals, enabling their isolation. The molecule **11** has been synthesized in solution but has not yet been isolated as a single crystal. Electron behaviors of all isomers were investigated using scanning tunneling microscopy (STM) and atomic force microscopy (AFM) as well.

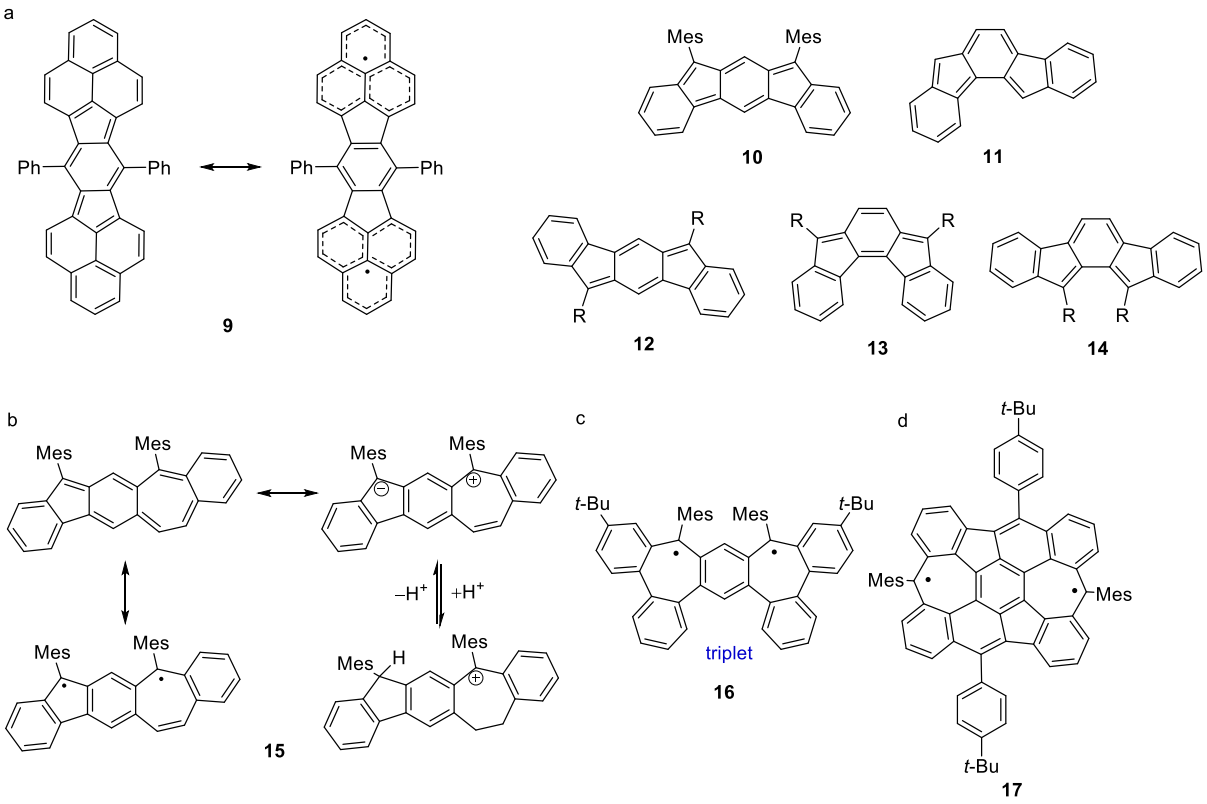

Figure 1.9. (a) Chemical structure of biphenalenoindacene and representative derivatives of indenofluorene isomers. (b) Resonance structures of cyclohepta[*f*]indene dervatives and its protonated form. (c) Chemical structure of triplet ground state dicyclohepta[*a,d*]benzene derivatives. (d) π-Extended dicyclohepta[*cd,ij*]-*s*-indacene.

Additionally, the molecule **15** of quinodimethane with one five-membered ring and one seven-membered ring added to both sides of a benzene ring has been reported (**Figure 1.9b**)[41]. Due to the aromatic nature of the odd-membered rings, resonance structures can be drawn with the five-membered ring as an anion and the seven-membered ring as a cation. This molecule exhibits the characteristics of a singlet ground state diradical and shows pH responsiveness by adding a proton to the seven-membered ring.

Derivatives **16** of dicyclohepta[*a,d*]benzene, which has two seven-membered rings added, have also been synthesized recently. This molecule has a triplet ground state. The structure is distorted due to the influence of the two seven-membered rings (**Figure 1.9c**)[42].

Additionally, π-extended molecules **17** combining the structures of s-indacene and dicyclohepta[a,d]benzene have been reported by Müllen and Feng group. These molecules exhibited a singlet ground state (**Figure 1.9d**)[43]. They achieved synthesis in solution and on metal surfaces, observing properties.

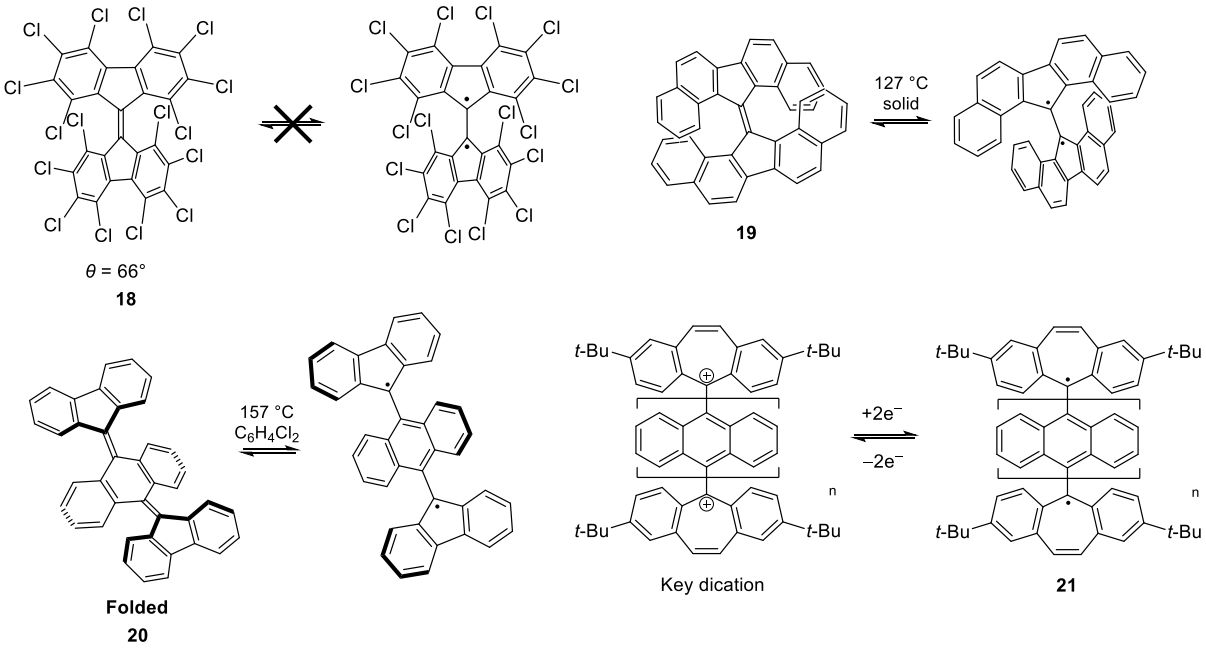

Scheme 1.2. Twisted ethylene types of diradicals based on odd-membered rings as radical center.

Twisted ethylene-type diradicals have also been a hot topic recently[36c]. This type of diradical arises when parallel p-orbitals of carbon-carbon double bond twist, weaking the double bond character and resulting in two radicals (**Figure 1.7**). As the twist angle of the double bond increases from 0° to vertical, the singlet and triplet states begin to degenerate. Then, the molecule starts to be observed as a singlet diradical[36c,44,45]. 9,9'-Bifluorenylidene structures have been extensively studied as a framework that generates diradicals through such twisted ethylene (**Scheme 1.2**)[46]. Molecule **18**, in which all the hydrogens of 9,9'-bifluorenylidene are substituted with chlorine, achieves a twist angle of 66°. However, no ESR

signal was observed. Twisted bifluorenylidene derivative **19**, with benzene rings added to both ends of the fluorene units, shows a triplet state signal in ESR spectra with a twist angle of approximately 90° upon heating[47]. Additionally, diradicals using bulky 9,9'-bifluorenylidene have been reported recently[48]. Diradicals **20** of the type where multiple anthracene units are inserted between the two fluorene units of 9,9'-bifluorenylidene have also been reported as metastable[49]. This molecule has a ground state as closed-shell which C-C double bonds are not twisted. Upon heating in dichlorobenzene solution, the form of twisted diradical is mixed. Likewise, twisted diradicals using seven-membered rings instead of five-membered rings have been studied[50]. These molecules adopt a folded structure in their closed-shell state due to the flexibility of seven-membered rings and C-C double bonds. However, upon oxidation, the rings become planar and each aromatic cores cross perpendicularly. When two-electron reduction is performed from the dication state, a diradical form **21** is generated. If there are three or more anthracene units incorporated inside, the molecules do not form the folded structures. A similar mechanism has been reported for diradicals with both five-membered and seven-membered rings at each end recently[51].

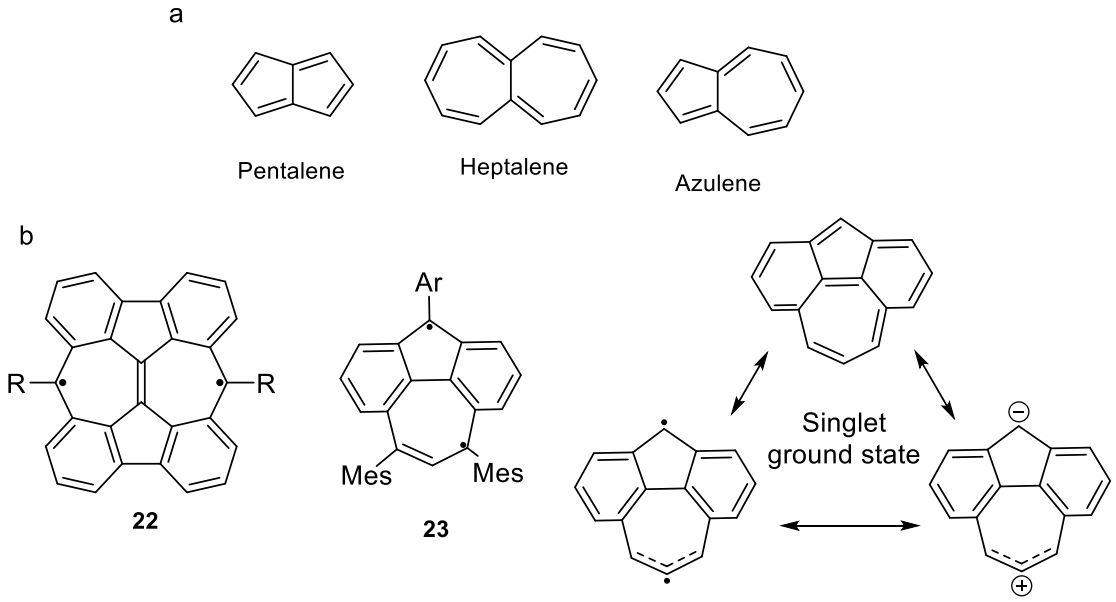

Figure 1.10. (a) Structure of pentalene, heptalene, and azulene. (b) structures of diradicals based on heptalene or azulene.

Some antiaromatic molecules incorporating two connected odd-membered rings have also been reported as having diradical character. Notably, multiple reports exist for pentalene, which features two adjacent five-membered rings[25]. In contrast, in 2019, Yasuda and Konishi reported molecule **22**, a diradical incorporating two adjacent seven-membered rings (heptalene subunit) (**Figure1.10b**)[52]. This planar molecule is a nonalternant isomer of bisanthene. The molecule **22** has 12π electron of antiaromaticity and shows an open-shell character with a singlet ground state.

Diradicals incorporating one azulene subunit have been reported by the groups of Yasuda and Konishi, as well as Liu group (**Figure1.10b**)[53]. Notably, molecule **23** can adopt a resonance structure displaying intramolecular dipolarity.

1.2. Corannulene Based Aromatic Molecules

1.2.1. Corannulene

As mentioned earlier in **Chapter 1.1.1**, buckybowls are bowl-shaped PAHs that represent partial structures of fullerenes. The most representative examples are corannulene and sumanene. These molecules and their derivatives are technically classified as nonalternant molecules and exhibit various physical properties due to their curved structures.

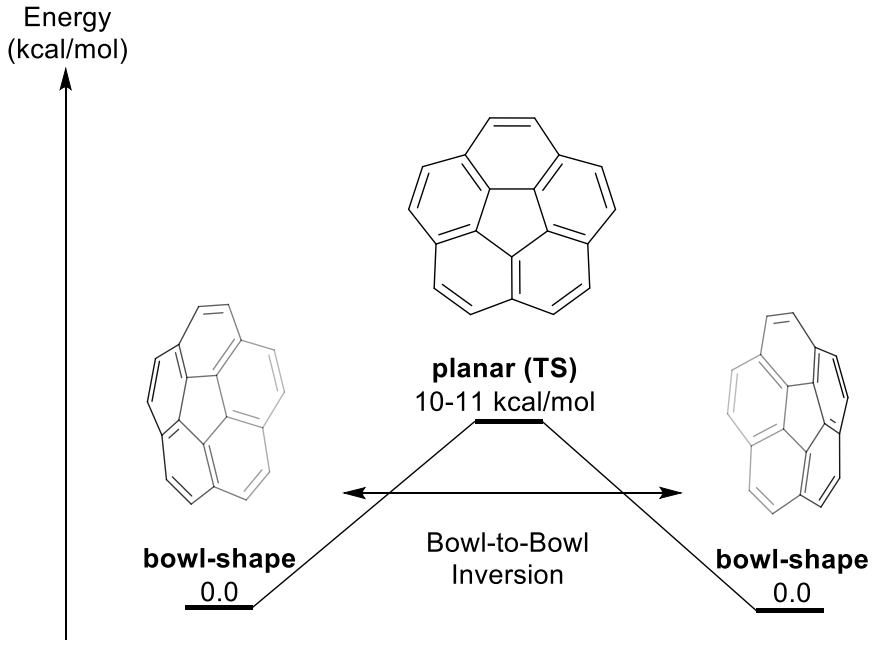

Figure 1.11. Bowl-to-bowl inversion of corannulene

The bowl-inversion capability of corannulene is one of their well-known properties. This inversion barrier is experimentally determined at 10-11 kcal/mol (**Figure 1.11**)[54]. The rapid inversion occurs in room-temperature solutions. Recent research has extended its π-electron system to synthesize larger, curved PAHs. Besides, corannulene can form inclusion complexes with fullerenes leveraging this curved shape. Other studies have explored supramolecular interactions where corannulene molecules interact with each other due to the bowl shape[12,13].

1.2.2 Heteroatom-doped Corannulene derivatives

Recent advancements have seen the synthesis of corannulene derivatives, where heteroatoms are inserted into the framework. These modified corannulenes are anticipated to serve as model compounds for studying heterofullerenes, heteroatom-doped carbon nanotubes, and carbon defect structures. Although examples of heteroatom-doped corannulene is still limited, these hold great potential for a wide range of applications, promising further exploration and innovation in the field.

In 2015, two research groups, Nozaki and Ito (our group)[55], and Shinokubo and Hiroto[56], respectively synthesized the first heteroatom-doped corannulene derivative **26** through different synthetic routes (**Scheme 1.3a**).

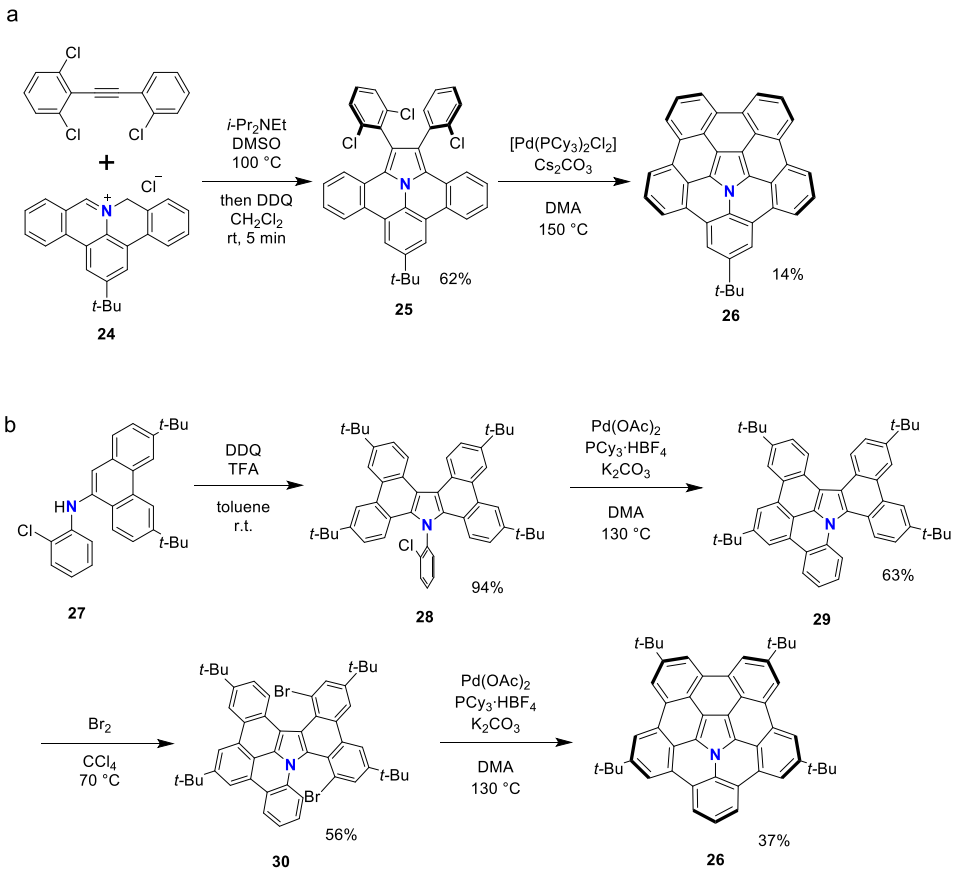

Scheme 1.3. Synthetic scheme of azapentabenzocorannulene (a) by Nozaki and Ito group, (b) by Shinokubo and Hiroto group.

In our group's route (**Scheme 1.3a**), a reactive azomethine ylide is generated from the iminium salt, which undergoes a 1,3-dipolar cycloaddition with halogenated diphenylacetylene. Subsequent dehydrogenation with DDQ yields the pyrrole-containing PAHs. This intermediate is subjected to an intramolecular Heck-type Pd-catalyzed cyclization to afford the target azacorannulene.

In the alternative route by the group of Shinokubo and Hiroto (**Scheme 1.3b**), the oxidative dimerization of 9-aminophenanthrene is performed to synthesize the pyrrole-containing PAHs. Repeated Heck-type Pd-catalyzed cyclization reactions then led to the formation of the azacorannulene.

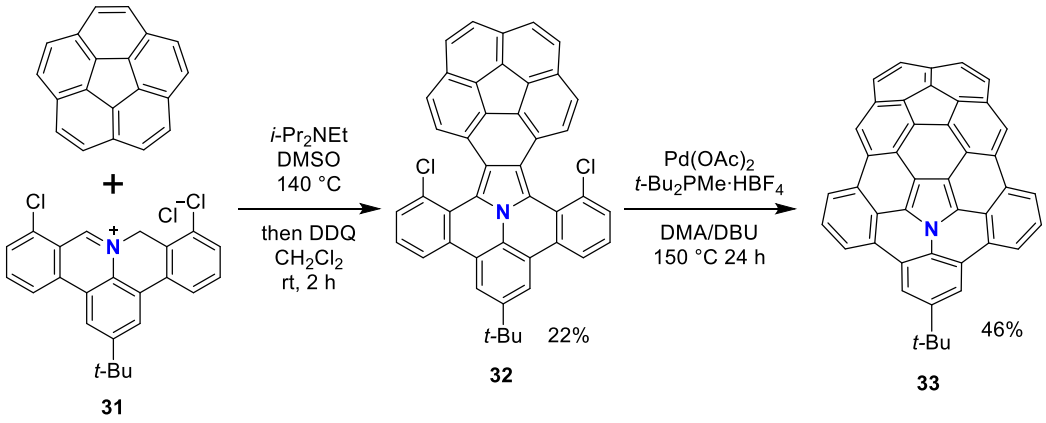

Scheme 1.4. Synthetic scheme of azabuckybowl **33**

In 2018, our group reacted corannulene with an azomethine ylide, followed by a similar Pd-catalyzed intramolecular cyclization to synthesize an azacorannulene derivative with a larger π-surface than molecule **33**[57]. This molecule is an azabuckybowl, a fragment of the $C_{79}N$ azafullerene. Compared to molecule **33**, it possesses a deeper bowl depth and a narrower HOMO-LUMO gap.

In 2017, Scott *et al.* reported the synthesis of the π-extended azacorannulene, 5-azadibenzo[*a,g*]corannulene **35**, using the FVP method with a yield of 26%[58]. This molecule

features a nitrogen atom at the rim position, which imparts basicity and results in instability due to hydrolysis on silica gel.

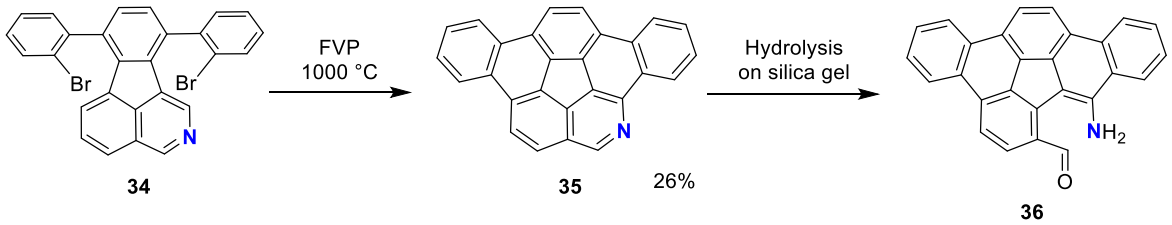

Scheme 1.5. Synthetic scheme of 5-azadibenzo[*a,g*]corannulene **35**.

In 2017, Hatakeyama *et al*. reported the multi-gram scale synthesis of BN-embedded dibenzocorannulene **37**. They incorporated two B-N units into the corannulene framework, achieving this through a four-step synthesis starting from commercially available compounds[59]. This molecule **37** exhibited strong blue fluorescence, indicating potential as a highly efficient blue light-emitting diode. Furthermore, in 2022, they developed a method for synthesizing BN-embedded dibenzocorannulenes using alkynes (**Figure 1.12** right)[60]. The method facilitated the introduction of substituents via cross-coupling reactions, demonstrating potential for efficient OLED materials.

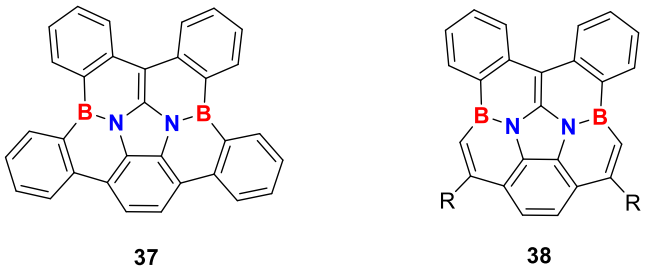

Figure 1.12. BN embedded dibenzocorannulenes.

In 2021, the author of this thesis and our group reported the synthesis of π-extended diazapentabenzocorannulenium cation. We incorporated two nitrogen atoms into the central

five-membered ring of the corannulene framework, resulting in an imidazolium cation core[61]. The detailed chemistry of this compound will be discussed in **Chapter 4**.

While there are not many examples of heteroatom-doped corannulene derivatives, those that have been successfully stabilized exhibit unique properties, such as fluorescence, and hold significant potential for various applications. π-extended aza-corannulene **26**, in particular, has been reported in multiple studies due to its straightforward synthesis and high scalability[62].

1.3. Objectives and Outlines

As discussed in the previous sections, fragmental structures of carbon-defective graphene exhibit various intrinsic properties and potential applications. These structures are also crucial for understanding and precisely synthesizing carbon-defective graphene. Therefore, the synthesis and characterization of new carbon-defective graphene substructures are significant tasks for organic chemists and physical organic chemists. In particular, some nonalternant hydrocarbons display unique properties such as asymmetrical molecular orbitals, topology, antiaromaticity, and open-shell character. The open-shell character of PAHs can be designed by the position and numbers of odd-membered rings, leading to one radical, diradicals, and multiradicals.

Meanwhile, corannulene, with its non-alternant hydrocarbon structure featuring a 5-membered ring, is not only a carbon-defective structure but also a buckybowl substructure of fullerenes. Heteroatom-doped corannulene derivatives have been reported to exhibit properties distinct from corannulene derivatives. However, the difficulty of synthesizing those derivatives is still an issue.

Given this context, introducing further carbon-defect-like chemical modifications to heteroatom-doped corannulenes is crucial. This approach not only enhances the understanding of carbon-defect structures but also expands potential applications for these molecules. Therefore, it is essential to develop organic synthesis methods for these and investigate their properties comprehensively. In this thesis, we focus on azacorannulene derivatives **26**, the first reported heteroatom-doped corannulene. We synthesize its derivatives incorporating additional carbon-defect structures to investigate their properties. The design of the molecules is based on two main ideas for incorporation of carbon-defect: "homo-" modification or the imidazolium skeleton.

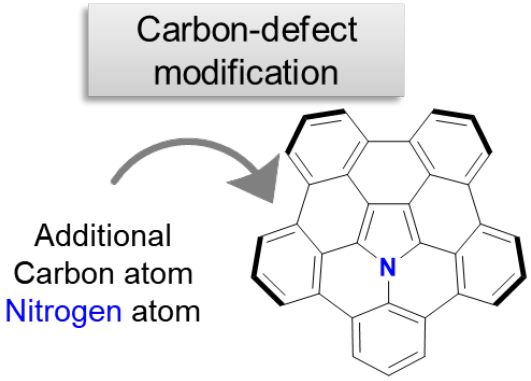

26

Figure 1.13. Concept of carbon-modification for azacorannulene **26**

1.3.1 Inspiration from "homo-" for insertion of sp^2 carbon

According to the IUPAC Compendium of Chemical Terminology[63], "homo-" is an affix used to denote a ring that expands by a methylene group. This "homo-"modification is one of the effective methods for expanding variety of PAHs. Several examples of homo-analogs of PAHs include homo-perylene **39**[64], homo-sumanene **40**[65] (technically resulting in sp^2 carbon) and homo-coronene **41**[66]. The homo-modification changes their properties significantly, not only in topological aspects such as structural flexibility and solubility but also in electronic aspects such as antiaromatic properties and two-photon absorption[66]. Inspired by the concept of homo-modification, this study involves incorporating carbon atoms into the azacorannulene framework to form seven-membered rings. Instead of inserting methylene groups, we applied sp^2 carbon atoms to investigate the impact of extra π-electrons by modification on the π-conjugation system of azacorannulene.

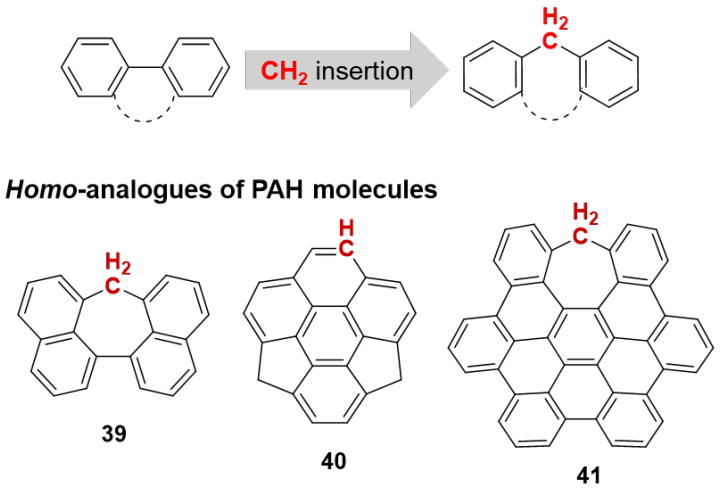

Figure 1.14. Homo insertion and precedented examples of homo-analogues of PAHs.

Chapter 2 discusses the synthesis and properties of molecule **42**, which incorporates one sp^2 carbon into the azacorannulene framework. The introduction of the seven-membered ring results in odd number of π-electrons within the molecule, imparting an open-shell character. Isolation of molecules containing a tropyl radical is rare due to their instability, and even rarer as single crystals. However, **42** was successfully isolated in single-crystal form. Its structure reveals that incorporating the azaazulene structure into corannulene results in a planar configuration. The optical properties and aromatic characteristics of molecule **42** are also discussed in this chapter.

Chapter 3 discusses the synthesis and properties of molecule **43**, which incorporates two sp^2 carbons into the azacorannulene framework. The addition of two seven-membered rings to the azacorannulene structure allows for the formation of diradical resonance structures. This molecule was isolated as single crystals. Its open-shell characteristics and aromaticity were evaluated as well. Based on computational and experimental results, it was revealed that the molecule is a singlet ground state diradical.

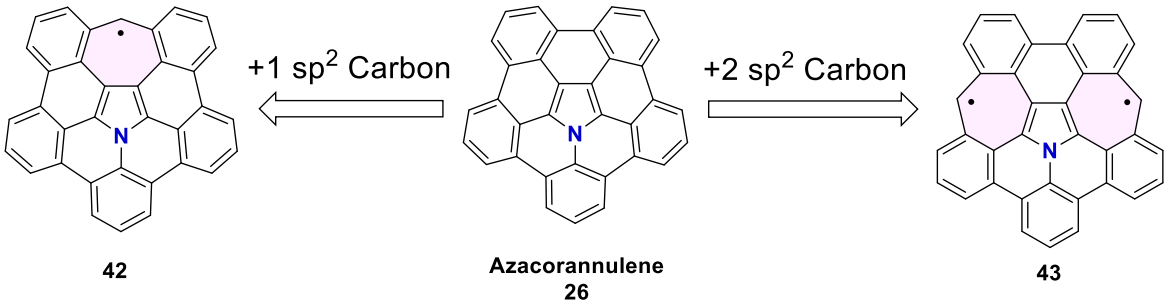

Figure 1.15. Azacorannulene derivatives which are inserted sp^2 carbons.

1.3.2 Incorporation of imidazolium skeleton

Imidazolium cations have long been used in chemistry and materials science, notably as precursors to N-heterocyclic carbenes (NHCs)[67] and in ionic liquids[68]. This five-membered ring structure is thermally and chemically stable in its cationic state due to its aromaticity. We designed molecule **45** by adding a nitrogen atom to the pyrrole ring at the center of the azacorannulene framework. Upon one-electron reduction, this molecule has the potential to become the first corannulene-centered doublet species **46**. **Chapter 4** discusses the synthesis and properties of this cationic molecule **45**. In previous research, we investigated a synthetic method for polycyclic aromatic molecules with imidazolium cations using azomethine ylide **44**[69]. By applying this reaction, we successfully synthesized molecule **45**. Despite its larger π-conjugated system compared to corannulene, this cationic molecule exhibited high hydrophilicity, dispersing well in water and showing fluorescence.

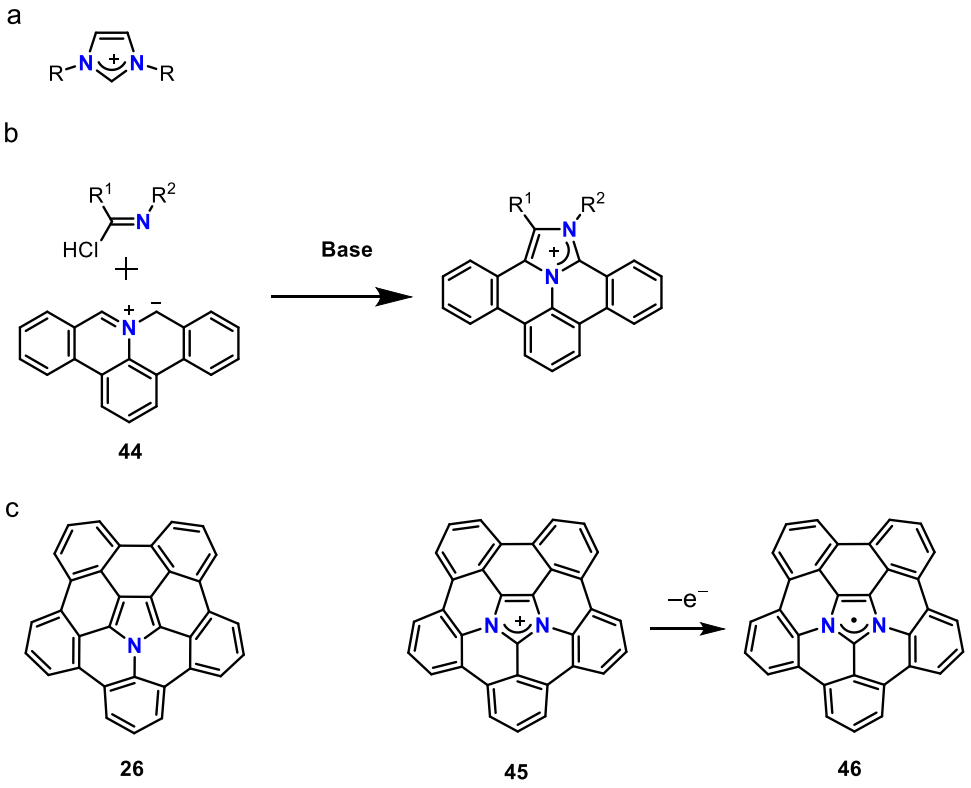

Scheme 1.6. (a) Imidazolium cation. (b) Synthetic method for polycyclic aromatic molecules with imidazolium cations (c) Target molecules **45** and target molecules **46**

References

1. Clar, E. *Polycyclic Hydrocarbons*. **1964**, Springer Berlin, Heidelberg.

2. Harvey, R, G. *Polycyclic Aromatic Hydrocarbons*. **1997**, Wiley-VCH, Weinheim.

3. (a) Faraday, M. *Phil. Trans. R. Soc. Lond.* **1825**, *115*, 440. (b) Kekulé, A. *Ann. Chem*. **1872**, *162*, 77. (c) Hückel, E. *Z. Phys*. **1931**, *70*, 204.

4. Clar, E. *The Aromatic Sextet.* **1972**, Wiley-VCH, London.

5. (a) Randić, M. *Chem. Rev*. **2003**, *103*, 3449–3605. (b) Narita, A., Wang, X. Y., Feng, X., Müllen, K. *Chem. Soc. Rev*. **2015**, *44*, 6616–6643. (c) Stępień, M., Gońka, E., Żyła, M.,

Sprutta, N. *Chem. Rev.* **2017**, *117*, 3479–3716. (d) Borissov, A. *et al*. *Chem. Rev.* **2022**, *122*, 565–788.

6. (a) Wu, J., Pisula, W., Müllen, K. *Chem. Rev.* **2007**, *107*, 718–747. (b) Ye, Q., Chi, C. *Chem. Mater.* **2014**, *26*, 4046–4056. (c) Lee, E. K. *et al*. *Adv. Mater.* **2017**, *29*, 1703638. (d) Aumaitre, C., Morin, J-C. *Chem. Rec.* **2019**, *19*, 1142–1154.

7. Kroto, H. W. *et al*. *Nature* **1985**, *318*, 162–163.

8. Iijima, S. *Nature* **1991**, *354*, 56–58.

9. Novoselov, K. S. *et al*. *Science* **2004**, *306*, 666–669.

10. Barth, W. E., Lawton, R. G. *J. Am. Chem. Soc*. **1966**, *88*, 380–381.

11. Hanson, J. C., Nordman, C. E. *Acta Cryst*. **1976**, *B32*, 1147–1153.

12. (a) Scott, L. T., Hashemi, M. M., Meyer, D. T., Warren, H. B. *J. Am. Chem. Soc*. **1991**, *113*, 7082–7084. (b) Scott, L. T. *et al*. *J. Am. Chem. Soc*. **1997**, *119*, 10963–10968. (c) Butterfield, A. M., Gilomen, B., Siegel, J.S. *Org. Process Res. Dev*. **2012**, *16*, 664–676.

13. (a) Saito, M., Shinokubo, H., Sakurai, H. *Mater. Chem. Front.* **2017**, *2*, 635–661. (b) Rice, A. M., Dolgopolova, E. A., Shustova, N. B. *Chem. Mater*. **2017**, *29*, 7054–7061. (c) Nestoros, E., Stuparu, M. C. *Chem. Commun.,* **2018**, *54*, 6503–6519.

14. Sakurai, H., Daiko, T., Hirao, T. *Science* **2003**, *301*, 1878.

15. (a) Boorum, M. M., Vasil'ev, Y. V., Drewello, T., Scott, L. T. *Science* **2001**, *294*, 828−831. (b) Scott, L. T. *et al*. *Science* **2002**, *295*, 1500−1502.

16. (a) Petrukhina, M. A., Scott, L. T. *Fragments of Fullerenes and Carbon Nanotubes* **2012**, Wiley-VCH: New York.

17. (a) Darzi, E. R., Jasti, R. *Chem. Soc. Rev*., **2015**,*44*, 6401-6410. (b) Wu, D., Cheng, W., Ban, X., Xia, J. *Asian J. Org. Chem.* **2018***, 7,* 2161–2181.

18. Jasti, R., Bhattacharjee, J., Neaton, J. B., Bertozzi, C. R. *J. Am. Chem. Soc*. **2008**, *130*, 17646–17647.

19. Segawa, Y., Levine, D. R., Itami, K. *Acc. Chem. Res.* **2019**, *52*, 2760–2767.

20. Povie, G. *et al*. *Science*. **2017**, *356*, 172–175.

21. (a) Geim, A. K., Novoselov, K. S. *Nat. Mater*. **2007**, *6*, 183–191. (b) Zhu, Y. *et al*. *Adv. Mater*. **2010**, *22*, 3906–3924. (c) Inagaki, M., Kim, Y. A., Endo, M. *J. Mater. Chem*. **2011**, *21*, 3280–3294.

22. Castro Neto, A. H. *et al*. *Rev. Mod. Phys*. **2009**, *81*, 109–162.

23. Lee, C., Wei, X., Kysar, J. W., Hone, J. *Science* **2008**, *321*, 385–388.

24. (a) Coraux, J., N'Diaye, A. T., Busse, C., Michely, T. *Nano Lett*. **2008**, *8*, 565–570. (b) Loginova, E. *et al*. *Phys. Rev. B* **2009**, *80*, 085430. (c) Banhart, F., Kotakoski, J., Krasheninnikov, A. V. *ACS Nano* **2011**, *5*, 26−41. (d) Zhao, Z. *et al*. *Mater. Adv*., **2023**, *4*, 835−867. (e) Jia, Y., Yao, X. *Acc. Chem. Res*. **2023**, *56*, 8, 948–958.

25. (a) Tobe, Y. *Chem. Rec*. **2015**, *15*, 86–96. (b) Tobe, Y. *Top. Curr. Chem*. **2018**, *376*, 12. (c) Konishi, A., Yasuda, M. *Chem. Lett*. **2021**, *50*, 195–212. (d) Konishi, A., Yasuda, M. *Adv. Phys. Org. Chem*. **2021**, 55, 17–40. (e) Fei, Y., Liu, J. *Adv. Sci.* **2022**, *9*, 2201000.

26. Xin, H., Hou, B., Gao, X. *Acc. Chem. Res*. **2021**, *54*, 7, 1737–1753.

27. (a) Hicks, R. G. *Stable Radicals*; Hicks, R. G., Ed.; Wiley, **2010**. (a) Chen, Z. X., Li, Y., Huang, F. *Chem*. **2021**, *7*, 288–322. (b) Mizuno, A., Matsuoka, R., Mibu,T., Kusamoto, T. *Chem. Rev*. **2024**, *124*, 1034–1121.

28. Gomberg, M. *J. Am. Chem. Soc*. **1900**, *22*, 757–771.

29. (a) Sitzmann, H., Boese, R. *Angew. Chem. Int. Ed*. **1991**, *30*, 971– 973. (b) Janiak, C., Weimann, R., Görlitz, F. *Organometallics* **1997**, *16*, 4933–4936.

30. Kitagawa, T., Ogawa, K., Komatsu, K. *J. Am. Chem. Soc*. **2004**, *126*, 9930– 9931.

31. Kubo, T. *et al*. *J. Am. Chem. Soc*. **2011**, *133*, 14240–14243.

32. Koelsch, C. F. *J. Am. Chem. Soc*. **1957**, *79*, 4439–4441.

33. Asai, K., Fukazawa, A., Yamaguchi, S. *Angew. Chem. Int. Ed*. **2017**, *56*, 6848–6852.

34. Nishiuchi, T. *et al*. *Chem. Asian J.* **2019**, *14*, 1830–1836.

35. Moshniaha, L. *et al*. *J. Am. Chem. Soc.* **2020**, *142*, 3626–3635.

36. (a) Borden, W. T., *Diradicals*; Borden, W. T., Ed.; **1982** Wiley-Interscience: New York. (b) Abe, M. *Chem. Rev*. **2013**, *113*, 7011–7088. (c) Ishigaki, Y., Harimoto, T., Shimajiri, T., Suzuki, T. *Chem. Rev*. **2023**, *123*, 13952–13965.

37. (a) Kolc, J., Michl, J. *J. Am. Chem. Soc*. **1970**, *92*, 4147–4148. (b) Kolc, J., Michl, J. *J. Am. Chem. Soc*. **1973**, *95*, 7391–7401.

38. Hafner, K. *et al*. *Angew. Chem. Int. Ed*. **1986**, *25*, 630–632.

39. Kubo, T. *et al*. *Angew. Chem. Int. Ed.* **2005**, *44*, 6564–6568.

40. (a) Shimizu, A. *et al*. *Angew. Chem. Int. Ed*. **2013**, *52*, 6076–6079. (b) Chase, D. T. *et al*. *Angew. Chem. Int. Ed*. **2011**, *50*, 1127–1130. (c) Chase, D. T. *et al*. *Angew. Chem. Int. Ed*. **2011**, *50*, 11103–11106. (d) Nishida, J., Tsukaguchi, S. Yamashita, Y. *Chem. Eur. J*. **2012**, *18*, 8964–8970. (e) Chase, D. T. *et al*. *J. Am. Chem. Soc*. **2012**, *134*, 10349–10352. (f) Shimizu, A., Tobe, Y. *Angew. Chem. Int. Ed.* **2011**, *50*, 6906–6910. (g) Fix, A. G. *et al*. *Org. Lett*. **2013**, *15*, 1362–1365. (h) Dressler, J. J. *et al*. *Angew. Chem., Int. Ed*. **2017**, *56*, 15363–15367. (i) Di Giovannantonio, M. *et al*. *J. Am. Chem. Soc*. **2019**, *141*, 12346–12354. (j) Majzik, Z. *et al*. *Nat. Commun*. **2018**, *9*, 1198. (k) Di Giovannantonio, M. *et al*. *J. Am. Chem. Soc*. **2018**, *140*, 3532–3536. (l) Di Giovannantonio, M. *et al*. *J. Am. Chem. Soc*. **2020**, *142*, 12925–12929. (m) Mishra, S. *et al*. *Nat. Chem*. **2024**, *16*, 755–761.

41. Fu, X. *et al*. *Chem. Sci.*, **2020**, *11*, 5565–5571.

42. Shimizu, A. *et al*. *Angew. Chem. Int. Ed*. **2022**, *61*, e202205729.

43. Liu, J. *et al*. *J. Am. Chem. Soc*. **2019**, *141*, 12011−12021.

44. Nakano, M. *et al*. *J. Chem. Phys*. **2010**, 133, 154302.

45. (a) Hirao, Y., Hamamoto, Y., Nagamachi, N., Kubo. *Phys. Chem. Chem. Phys.*, **2019**, *21*, 12209−12216. (b) Hamamoto, Y., Hirao, Y., Kubo, T. *J. Phys. Chem. Lett*. **2021**, *12*, 4729–4734.

46. (a) Ballester, M. *et al*. *J. Org. Chem*. **1985**, *50*, 2287–2292. (b) Molins, E., Miravitlles, C.; Espinosa, E., Ballester, M. *J. Org. Chem*. **2002**, *67*, 7175−7178. (c) Herbstein, F. H. *Acta Crystallogr*. **1991**, *47*, 288–298.

47. Wentrup, C., Regimbald-Krnel, M. J., Müller, D., Comba, P. *Angew. Chem., Int. Ed*. **2016**, *55*, 14600–14605.

48. (a) Prajapati, B. *et al*. *Nat. Chem*. **2023**, *15*, 1541–1548 (b) Kang, H. W. *et al*. *Nat. Commun*. **2023**, *14*, 5248.

49. (a) Zeng, Z. *et al*. *J. Am. Chem. Soc*. **2012**, *134*, 14513– 14525. (b) Yin, X. *et al*. *Chem. Sci.* **2019**, *10*, 10733–10739.

50. (a) Ishigaki, Y., Hayashi, Y., Suzuki, T. *J. Am. Chem. Soc*. **2019**, *141*, 18293–18300 (b) Jiménez, V. G. *et al*. *Chem. Commun*. **2020**, *56*, 12813–12816. (c) Hayashi, Y., Suzuki, S., Suzuki, T., Ishigaki, Y. *J. Am. Chem. Soc*. **2023**, *145*, 2596–2608.

51. Nishiuchi, T., Uchida, K., Kubo, T. *Chem. Commun*. **2023**, *59*, 7379–7382.

52. Konishi, A. *et al*. *J. Am. Chem. Soc*. **2019**, *141*, 10165–10170.

53. (a) Horii, K. *et al*. *J. Am. Chem. Soc*. **2022**, *144*, 3370–3375. (b) Wu, F. *et al*. *Angew. Chem., Int. Ed*. **2022**, *134*, e202202170.

54. L. T. Scott, L. T., Hashemi, M. M., Bratcher, M. S. *J. Am. Chem. Soc*. **1992**, *114*, 1920–1921.

55. Ito, S., Tokimaru, Y., Nozaki, K. *Angew. Chem. Int. Ed*. **2015**, *54*, 7256–7260.

56. Yokoi, H. *et al*. *Nat. Commun*. **2015**, *6*, 8215.

57. Tokimaru, Y., Ito, S., Nozaki, K. *Angew. Chem. Int. Ed*. **2018**, 57, 9818–9822.

58. Tsefrikas, V. M., Greene, A. K., Scott, L. T. *Org. Chem. Front*. **2017**, *4*, 688–698.

59. Nakatsuka, S., Yasuda, N., Hatakeyama, T. *J. Am. Chem. Soc*. **2018**, *140*, 13562–13565.

60. Okada, N. *et al*. *Chem. Eur. J*. **2023**, *29*, e202202627.

61. Li, Q., Hamamoto, Y., Kwek, G., Xing, B., Li, Y., Ito, S. *Angew. Chem. Int. Ed*. **2022**, *61*, e202112638.

62. (a) Nagano, T. *et al*. *Chem.–Eur. J*. **2018**, *24*, 14075–14078. (b) Zhou, Z. *et al*. *Angew. Chem., Int. Ed*. **2019**, *58*, 12107–12111. (c) W. Wang, F. Hanindita, Y. Hamamoto, Y. Li, S. Ito, *Nat. Comm*. **2022**, *13*, 1–7. (d) Zhang, X., Mackinnon, M. C., Bodwell, G. J., Ito, S. *Angew. Chem., Int. Ed*. **2022**, *61*, e202116585. (e) Yokoi, H., Hiroto, S., Sakamaki, D., Seki, S., Shinokubo, H. *Chem. Sci*. **2018**, *9*, 819–824. (f) Takeda, M. *et al*. *J. Am. Chem. Soc*. **2018**, *140*, 6336–6342. (g) Yokoi, H., Hiroto, S., Shinokubo, H. *J. Am. Chem. Soc*. **2018**, *140*, 4649–4655.

63. *IUPAC Compendium of Chemical Terminology*, 3rd ed. International Union of Pure and Applied Chemistry; **2006**, Blue Book, p. 500.

64. (a) Ohishi, T., Kojima, T., Matsuoka, T., Shiro, M., Kotsuki, H. *Tetrahedron Lett*. **2001**, *42*, 2493–2496. (b) Odajima, M., Tajima, K., Fukui, N., Shinokubo, H. *Angew. Chem., Int. Ed*. **2021**, *60*, 15838–15843.

65. (a) Hishikawa, S. *et al*. *Chem. Lett*. **2017**, *46*, 1556–1559. (b) Yakiyama, Y., Hishikawa, S., Sakurai, H. *Beilstein J. Org. Chem*. **2020**, *16*, 681–690. (c) Nishimoto, M. *et al*. *J. Org. Chem*. **2022**, *87*, 2508–2519.

66. (a) Luo, J., Xu, X., Mao, R., Miao, Q. *J. Am. Chem. Soc*. **2012**, *134*, 13796–13803. (b) Márquez, I. R. *et al*. *Chem. Sci*. **2017**, *8*, 1068–1074. (c) Castro-Fernández, S. *et al*. *Angew. Chem., Int. Ed.* **2020**, *59*, 7139–7145. (d) Gońka, E., Chmielewski, P. J., Lis, T., Stępień, M. *J. Am. Chem. Soc*. **2014**, *136*, 16399–16410. (e) Oki, K., Takase, M., Mori, S., Uno, H. *J. Am. Chem. Soc*. **2019**, *141*, 16255–16259. (f) Moshniaha, L. *et al*. *J. Am. Chem. Soc*. **2020**, *142*, 3626–3635.

67. Herrmann, W. A., Köcher, C. *Angew. Chem. Int. Ed. Engl*. **1997**, *36*, 2162–2187. (b) de Frémont, P., Marion, N., S. Nolan, S. P. *Coord. Chem. Rev*. **2009**, *253*, 862–892. (c) Hopkinson, M. N., Richter, C., Schedler, M., Glorius, F. *Nature* **2014**, *510*, 485–496.

68. (a) Lei, Z., Chen, B., Koo, Y.-M., MacFarlane, D. R. *Chem. Rev*. **2017**, *117*, 6633–6635. (b) Vekariya, R. L. *J. Mol. Liq*. **2017**, *227*, 44–60. (c) Singh, S. K., Savoy, A. W. *J. Mol. Liq*. **2020**, *297*, 112038.

69. Li, Q.-Q., Hamamoto, Y., Tan, C. C. H., Sato, H., Ito, S. *Org. Chem. Front.* **2022**, *9*, 4128–4134.

Chapter 2. Synthesis and Properties of Azahomocorannulenyl Cations and Radicals

Abstract

Cycloheptatrienyl (tropyl) molecules are representative non-alternant hydrocarbons that offer interesting chemistry because of their unique structures and properties. However, there have been a limited number of polycyclic aromatic tropyl cations and radicals reported in the literature. Herein, we report the synthesis of a series of azahomocorannulene derivatives, where the key reactions are a 1,3-dipolar cycloaddition of polycyclic aromatic azomethine ylides with dibenzotropone and a subsequent palladium-catalyzed cyclization. X-ray diffraction analysis revealed that the obtained azahomocorannulenyl cation and radical adopt planar structures and exhibit unique packing structures. Their electronic and optical properties were investigated experimentally and theoretically to reveal their aromatic character.

2.1. Introduction

Cycloheptatrienyl, also known as tropyl, ions and radicals are one of the simplest non-alternant hydrocarbon molecules, which contain odd-membered rings. These molecules have attracted the attention of researchers over the span of a century due to their intriguing structure and properties. The tropylium cation ($C_7H_7^+$; **A**; **Figure 2.1A**), first discovered in 1891[1,2], stands as a cyclic, planar molecule endowed with 6π electrons and a positive charge delocalized over the entire 7-membered ring. According to the Hückel rule, this species is classified as aromatic and displays notable stability, as demonstrated by the isolation of stable tropylium compounds[3,4,5,6,7]. Despite their aromaticity, tropylium cations exhibit electrophilic reactivity as Lewis acids and oxidants, which has led to their utilization as catalysts and stoichiometric

reagents in a diverse array of organic transformations [8,9], and as functional organic dyes/chromophores in material sciences[10,11,12,13,14,15,16,17].

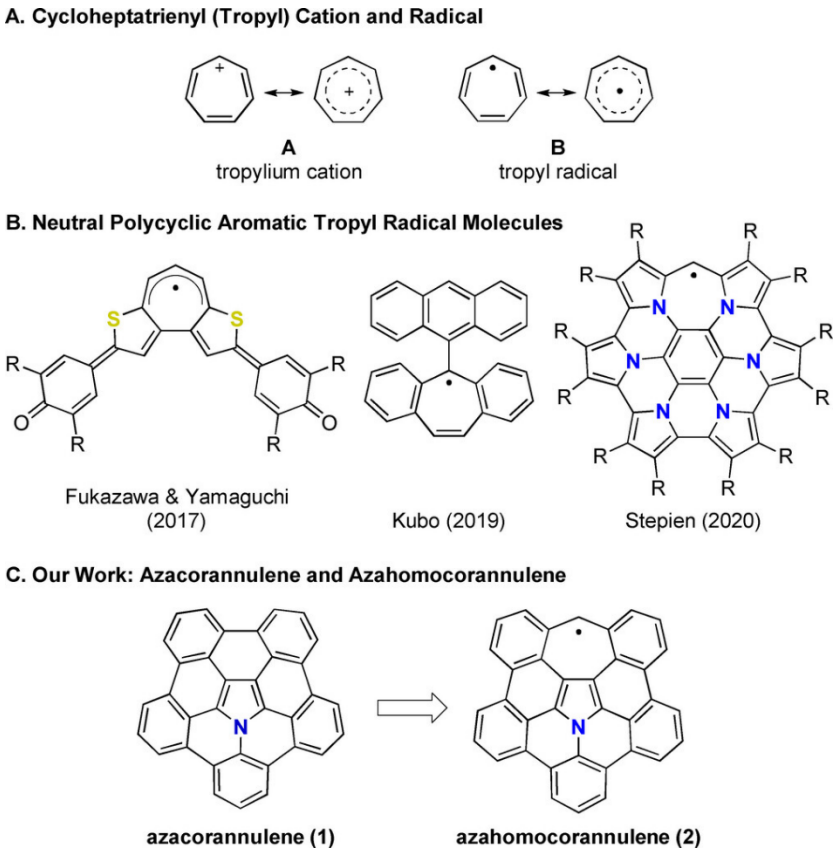

Figure 2.1. (A) Cycloheptatrienyl (tropyl) cation and radical. (B) Stable tropyl radical molecules reported in the literature. (C) Our work on azacorannulene and azahomocorannulene (this work).

In contrast, the neutral tropyl radical ($C_7H_7\cdot$;**B**), first experimentally observed in 1960[18], represents a more elusive species due to its structural and electronic complexity primarily attributed to the presence of 7π electrons.[19,20] Notably, the aromaticity of the tropyl radical is of particular interest because the Hückel 4n and 4n+2 rule cannot be applied to molecules possessing an odd number of electrons.[21,22,23] Theoretical calculations have indicated that this radical exhibits antiaromatic character[24], and thus it is known to be highly reactive and generally difficult to isolate and characterize. Indeed, reports on the isolation and

characterization of neutral tropyl radicals are scarce, with notable examples such as a thiophene-fused tropyl radical[16], an anthracen-9-yl-ligated dibenzotropyl radical[25], and a hexapyrrolohexaazahomocoronenyl radical (**Figure 2.1B**)[26]. Given its elusive nature and potential significance in structural organic chemistry, there is a pressing need to synthesize and investigate novel tropyl radical molecules.

Previously we reported azapentabenzocorannulene **1**[27,28] and diazapentabenzocorannulenium[29] as nitrogen-embedded corannulene molecules (**Figure 2.1C**).[30,31] In our continuous research, we decided to design and synthesize a ring-expanded analog of molecule **1**. Herein, we report on the synthesis and properties of azahomocorannulene derivatives **2**,[32,33,34] in which one of the hexagons in the corannulene core of **1** is substituted by a heptagon ring. With the introduction of the heptagon ring, it acquires a 2-azaazulene structure[35,36,37] in its center, which is a non-alternant structure of 2-azanaphthalene. This study presents rare examples of a polycyclic aromatic tropylium cation and tropyl radical.

2.2. Results and discussion

As shown in **Scheme 2.1**, the synthesis of azahomocorannulenes **2** started with a 1,3-cycloaddition reaction of dibenzotropone **4** and a polycyclic azomethine ylide formed from iminium salt **3**, which proceeded at 120 °C. Subsequently the oxidative dehydrogenation by 2,3-dichloro-5,6-dicyano-*p*-benzoquinone (DDQ) afforded the corresponding π-extended pyrrole **5** in 29 % yield within 2 steps. Next, a palladium-catalyzed intramolecular cyclization reaction of **5** was performed to yield π-extended azahomocorannulene ketone **6**. While **6** could not be fully identified by NMR analysis due to its poor solubility, its formation was indicated by clear signals of m/z=521.1773 (M^+) observed in mass spectrometric analysis. Then, ketone **6** was treated with an excess amount of mesitylmagnesium bromide in the presence of cerium(III) chloride to generate azahomocorannulenyl alcohol **7** in 40 % yield. The subsequent

dehydroxylation with tin(II) chloride afforded azahomocorannulenium cation **2 a**$^{+}\cdot$**SnCl$_3$**$^{-}$ in quantitative yield. Finally, single-electron reduction of **2 a**$^{+}\cdot$**SnCl$_3$**$^{-}$ with cobaltocene in acetonitrile effectively produced azahomocorannulenyl radical **2 a** as a black solid in 91 % yield.

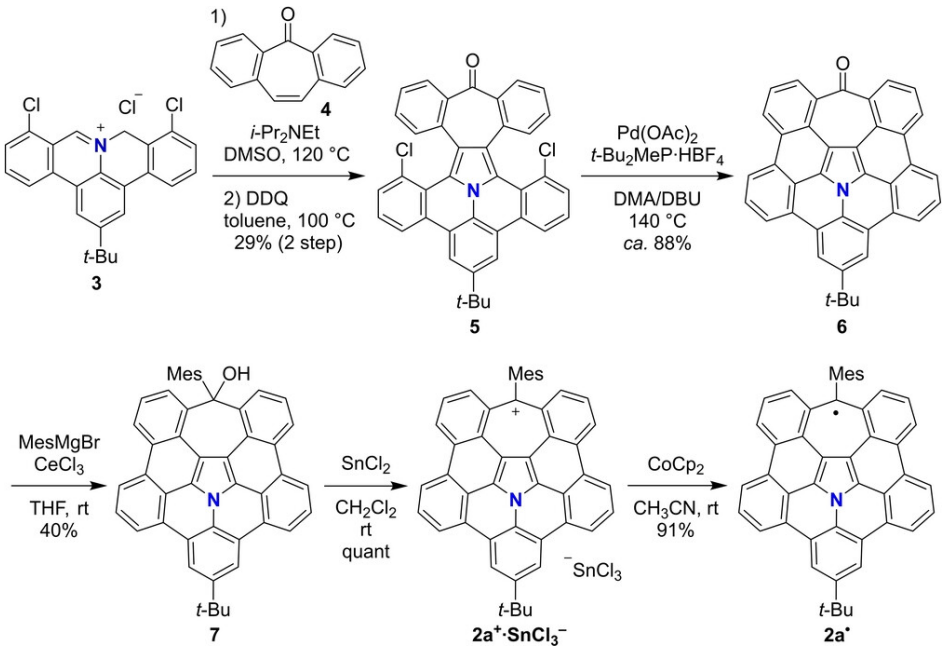

Scheme 2.1. Synthesis of azahomocorannulenes **2 a**.

Single crystals of cation **2 a**$^{+}\cdot$**SnCl$_3$**$^{-}$ suitable for X-ray diffraction analysis were obtained by slow evaporation of its solution in dichloromethane and toluene at −10 °C (**Figure 2.2A**)[38]. The cation **2 a**$^{+}\cdot$**SnCl$_3$**$^{-}$ crystallized in the triclinic space group *P*-1 and consisted of four ionic pairs including solvent molecules in a single unit cell. On the other hand, the crystals of radical **2 a·** were obtained by slow evaporation of its solution in benzene and carbon disulfide (**Figure 2.2B**). A unit cell of radical **2 a·** consisted of four molecules without any solvent molecules in the monoclinic space group $P2_1/c$. The dihedral angles between the mesityl group and the main π skeleton (i.e., seven-membered ring) are 83.1° (mean) for **2 a**$^{+}$ and 89.9° for **2 a·**, indicating that the mesityl group has a minimal electronic perturbation to the π-cores.

In both crystal structures, the main π-cores of azahomocorannulene adopt an almost planar structure, with average deviations of each atom from the mean plane of the main π-core of 0.058 Å for cation **2 a**$^+$ and 0.041 Å for radical **2 a**·. This is in a sharp contrast to the bowl shape of azacorannulene **1**[27], indicating that the positive curvature of the bowl shape of **1** caused by the central pyrrole ring is structurally relieved by the incorporation of the fused 7-membered ring.

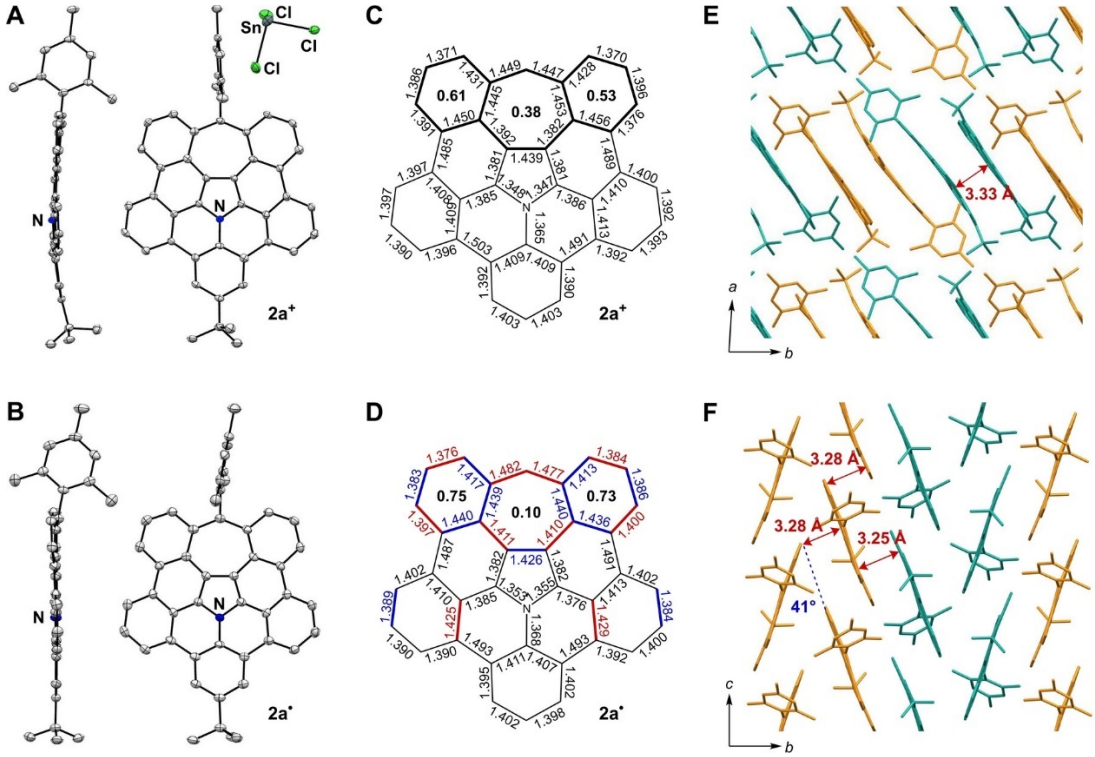

Figure 2.2. ORTEP structures of (A) **2 a**$^+ \cdot$ **SnCl**$_3^-$ and (B) **2 a**·. Bond lengths (Å) and some HOMA values (shown bold) in (C) **2 a**$^+ \cdot$ **SnCl**$_3^-$ and (D) **2 a**· (red: elongated, blue: shortened upon conversion of **2 a**$^+ \cdot$ **SnCl**$_3^-$ into **2 a**·). Crystal packing structures of (E) **2 a**$^+ \cdot$ **SnCl**$_3^-$ and (F) **2 a**·.

The bond lengths of **2 a**$^+$ and **2 a**· are shown in **Figure 2.2C** and **Figure 2.2D**, respectively. Upon reduction from **2 a**$^+$ to **2 a**·, significant changes in bond lengths were observed in the fused 6–7–6 membered ring unit (shown in bold in **Figure 2.2C**). The harmonic

oscillator model of aromaticity (HOMA) analysis[39] as one of the aromaticity indices (**Figures 2.2C, D** and **Figure 2.3**) revealed the HOMA values of the 6- and 7-membered rings are 0.61 (0.53) and 0.38, respectively, which are in good agreement with those of a polycyclic aromatic tropylium cation (0.63 and 0.36)[7]. Upon conversion from cation to radical, the value in the 7-membered ring decreased to 0.10, indicating less efficient delocalization, while the aromaticity of its adjacent benzene rings was slightly enhanced.

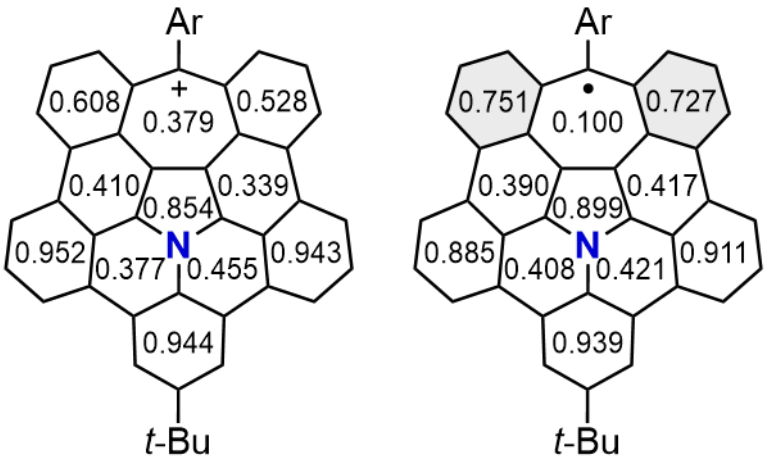

Figure 2.3. Harmonic oscillator model of aromaticity (HOMA) of $\mathbf{2a^{+}{\cdot}SnCl_3^{-}}$ and $\mathbf{2a^{\bullet}}$.

Note) With the conversion from cation to radical, the benzene rings adjacent to the 7-membered ring (shown in gray) undergo more efficient delocalization in terms of bond lengths alternation, while the 7-membered ring shows the opposite trend.

In the packing structure of $\mathbf{2\,a^{+}\cdot SnCl_3^{-}}$ (**Figure 2.2E**), four molecules of cation $\mathbf{2\,a^{+}}$ are packed in one unit cell, complementarily filling the empty space vacated by the counterions and solvent molecules. Two of the four $\mathbf{2\,a^{+}}$ molecules overlap face-to-face in an antiparallel manner, with the shortest intermolecular distance being 3.33 Å. These results suggest that the two molecules form a pair with π–π interactions, considering that the sum of the van der Waals radii of two carbon atoms is 3.4 Å. In contrast, radical $\mathbf{2\,a^{\cdot}}$ exhibits an interesting packing structure, as shown in **Figure 2.2F**: The molecules are slip-stacked parallel

to the π-surface. There are two types of interactions between the π-stacked molecules: one is between orange and orange at a distance of 3.28 Å, while the other is between orange and green at a distance of 3.25 Å. Given that the molecular orbitals bearing the π-spin density (see **Figure 2.5B**) do not overlap with each other, it was concluded that this π-stacking structure is formed by conventional intermolecular dispersion forces and that no σ-dimer is formed. Furthermore, each pair of adjacent layers in the brick stack arrangement adopts a herringbone structure with an angle of 41°, where CH-π interactions with a distance of 2.75–2.92 Å are observed (**Figure 2.4**). To the best of our knowledge, this "brick block-herringbone" structure was observed for the first time in the crystal packing of PAH molecules. It is also worth noting that radical **2 a**· offers a remarkably rare example of polycyclic aromatic heptagonal carbon-centered neutral radicals that are characterized by X-ray diffraction analysis[16]. Notably, there are a few examples of polycyclic aromatic heptagonal radical cations[40,41,42] and radical anions[43] that were characterized by X-ray diffraction analysis.

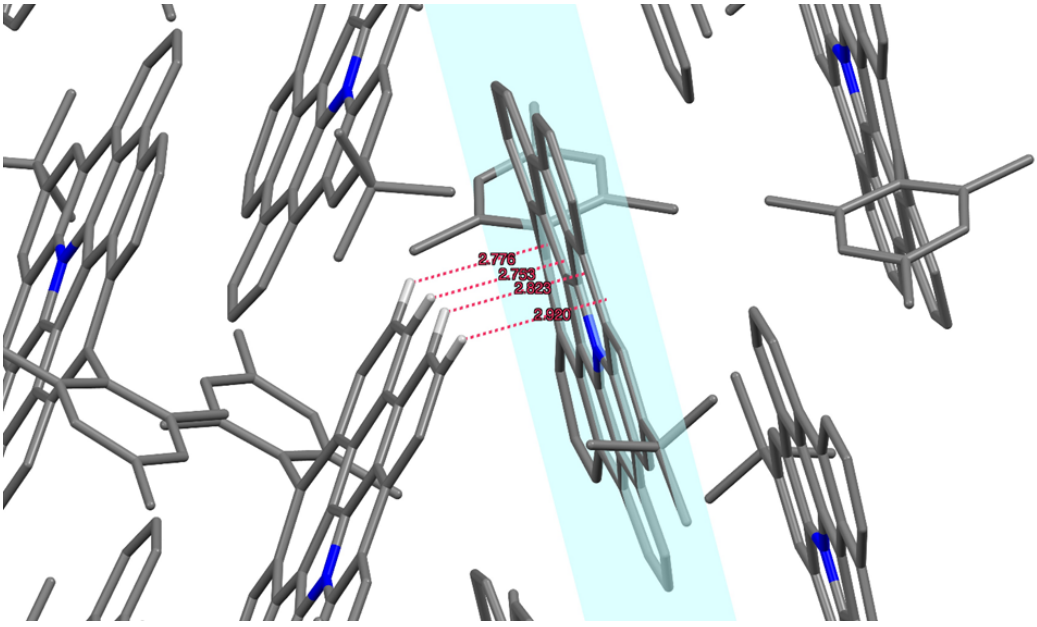

Figure 2.4. Distances (Å) between the π-plane of **2a**• to each hydrogen atom in the crystal packing structure.

To investigate the spin distribution on the π-surface of radical **2 a·**, electron spin resonance (ESR) analysis was conducted in its dilute toluene solution at room temperature (**Figure 2.5A**). The ESR spectrum shows several broad signals with a *g*-tensor of 2.0027, which is commonly observed with carbon centered radicals. The spectral simulation analysis afforded two sets for proton hyperfine coupling constants (α_H^1, α_H^2) of 0.348 and 0.442 mT, respectively, as well as a nitrogen hyperfine coupling constant of 0.176 mT. The density functional theory (DFT) calculation in **Figure 2.5B** indicated that the spin density is predominantly distributed mainly over the diphenylmethyl unit and extends to the nitrogen atom in the central pyrrole ring.

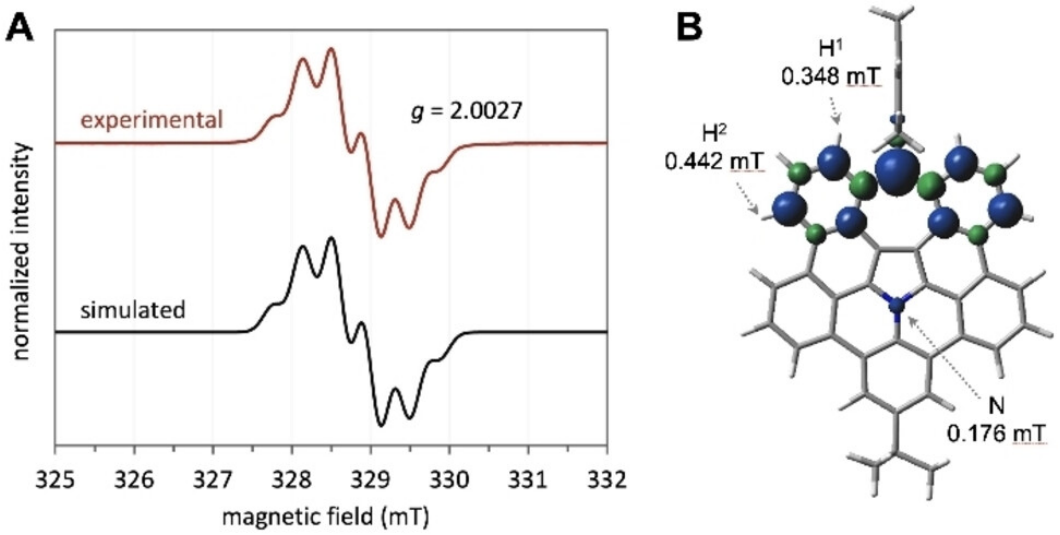

Figure 2.5. (A) ESR spectra (experimental in red; simulation in black) of radical **2 a·** (4.6×10^{-5} M in toluene at 298 K). (B) Spin density map of radical **2 a·** calculated at the UB3LYP/6–31G(d,p) level.

The photophysical properties of cation **2 a**$^+$ and radical **2 a·** were investigated (**Figure 2.6**). A solution of cation **2 a**$^+$ in dichloromethane exhibits a dark blue color and shows a broad absorbance signal ranging from 300 nm to 1400 nm with relatively sharp peaks observed at 803 nm and 734 nm. To elucidate the origin of the absorptions, we performed time-

dependent(TD)-DFT calculations of **2 b**$^{+}$ (which refer to compounds in which the *t*-butyl group of **2 a**$^{+}$ is replaced by a hydro group; see **Figure S2.23** for the details; **Figure S2.32** and **Table S2.2**) and vibronic spectra simulation of **2 d**$^{+}$ by using the RADLESS module of TURBOMOLE software (**Figures S2.35** and **S2.36**). [44,45] These calculations revealed that the peaks experimentally observed at 1210/1051 nm are attributed to the S_0–S_1 transition with vibrational bands, while the peaks at 803/734 nm are attributed to the S_0–S_2 transition with vibrational bands (see Section 5-7 in the **2.4. Experimental Section**)[46]. In contrast, a solution of radical **2 a·** in dichloromethane exhibits dark green color and has broad absorbance signals between 300 nm and 700 nm with a sharp signal at 575 nm. This experimental result is well consistent with the simulated result by unrestricted TD-DFT calculations (**Figure S2.34** and **Table S2.4**). The calculated transition band at 634 nm was assigned to the transitions from SOMO(α) (−4.19 eV) to LUMO(α) (−1.59 eV) and from HOMO(β) (−5.01 eV) to SOMO(β) (−2.31 eV). On the other hand, the experimental sharp band at 575 nm could be attributed to the transition from HOMO-1(β) (−5.24 eV) to SOMO(β) (−2.31 eV).

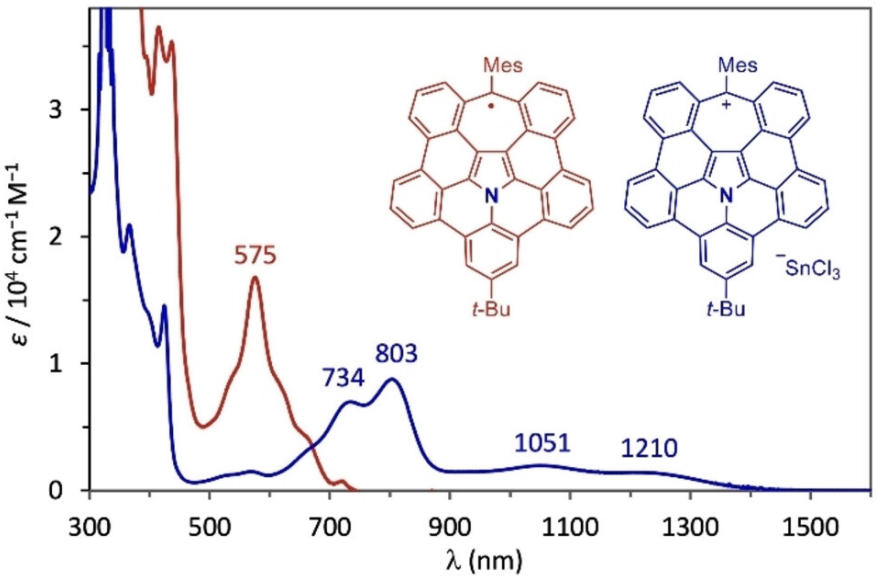

Figure 2.6. UV/Visible absorption spectra of cation **2 a**$^{+}$ · **SnCl**$_3^{-}$ (blue; 1.3×10^{-4} M) and radical **2 a·** (red; 1.0×10^{-5} M) in dichloromethane.

The cyclic voltammogram (CV) of radical **2 a·** in dichloromethane exhibited a reversible oxidation wave at $E_{ox1/2}$=−0.36 V and an irreversible reduction wave at E_{red}=−1.59 V, indicating an estimated SOMO-LUMO gap of 1.20 V (**Figure 2.7A**). The irreversible reduction wave suggests that the formed anionic species is not stable and decomposes even within the CV timescale. This could be attributed to the 8π anti-aromatic character of the 7-membered ring, as evident from its nucleus independent chemical shift ($NICS(1)_{zz}$) value of +47.7 ppm (**Figure 2.7B**).

For further investigation of aromaticity, isotropic chemical shielding surface at 1 Å of *Z* axis ($ICSS(1)_{zz}$)[47,48,49] (**Figure 2.7B**) were calculated for **2 b**$^+$, **2 b·**, and **2 b**$^-$ and the anisotropy of the current induced density (ACID)[50] (**Figure 2.7C**) calculations were performed for **2 c**$^+$, **2 c·**, and **2 c**$^-$ (which refer to compounds in which the *t*-butyl and mesityl groups of **2 a**$^+$, **2 a·**, and **2 a**$^-$, respectively, are replaced by hydro groups). For cation **2 b**$^+$, the $NICS(1)_{zz}$ value of −50.7 ppm at the central pyrrole ring and the values of −26.5 to −29.7 ppm at the peripheral benzene rings indicate their aromatic character. These results indicate that **2 a**$^+$ can be considered to have six fused 6π rings (1 pyrrole and 5 benzenes; **Figure 2.7D**), which is similar to the azacorannulene **1**[27]. The 7-membered ring shows a value of +1.9 ppm, which corresponds to non-aromatic character, although it formally has a cyclic 6π-electron conjugation[25]. This is also supported by the ACID plot of **2 c**$^+$, which does not show a clear clockwise diatropic ring currents around the 7-membered ring. Instead, it shows global diatropic ring currents along the outside peripheral rings with 26π aromaticity. The positive charge is mainly delocalized in the central azaazulene structure, as shown in its electrostatic potential map (**Figure S2.26**).

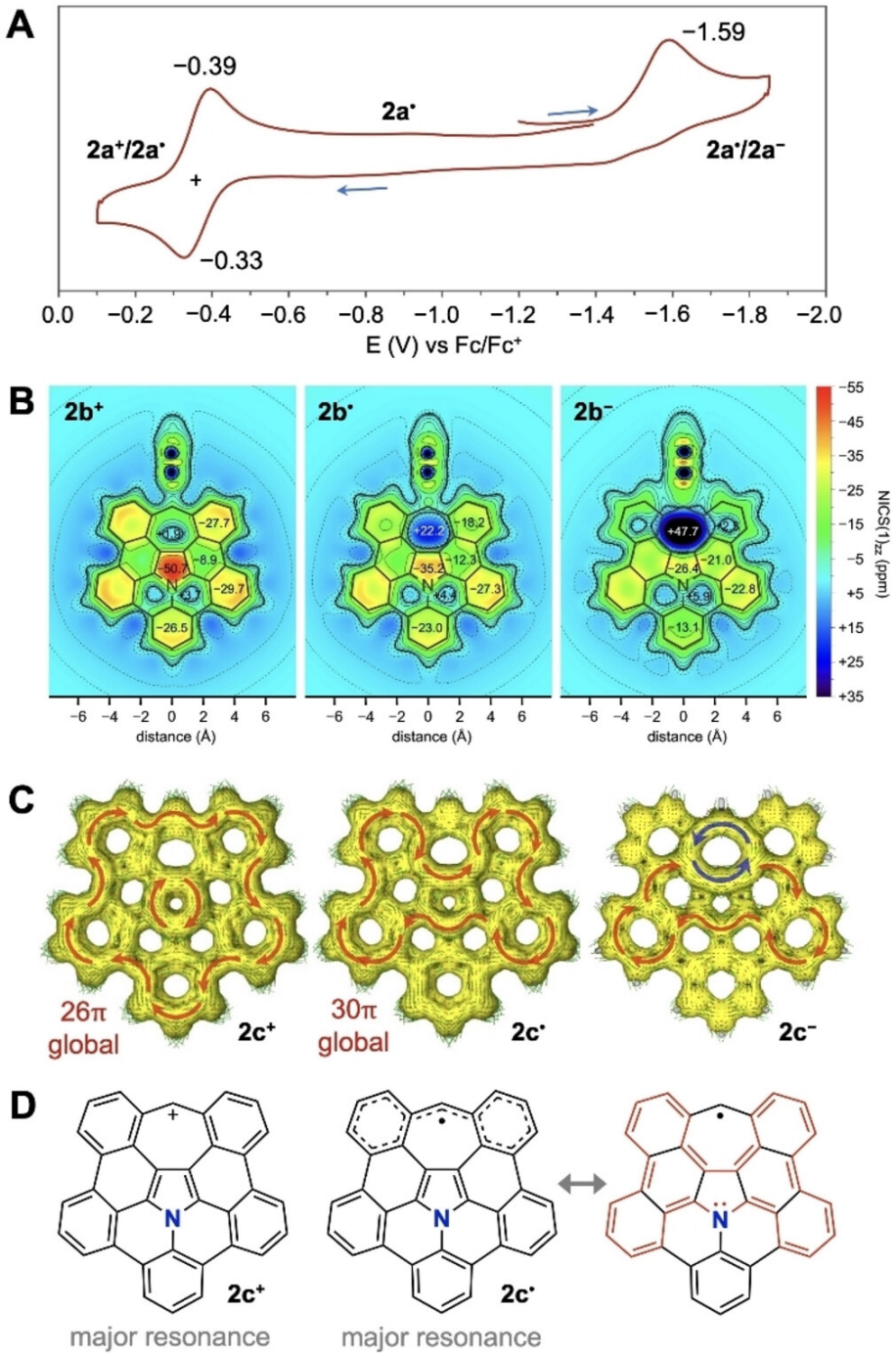

Figure 2.7. (A) Cyclic voltammogram of **2 a·** measured in dichloromethane with 0.10 M Bu_4NPF_6 at a scan rate of 100 mV/s. (B) $ICSS(1)_{zz}$ and $NICS(1)_{zz}$ values of **2 b**$^+$, **2 b·**, and **2 b**$^-$ calculated at the (U)B3LYP/6–31G(d,p) level. (C) ACID plots of **2 c**$^+$, **2 c·**, and **2 c**$^-$ calculated at the (U)B3LYP/6–31G(d,p) level (isovalue=0.03). The direction of the external magnetic field is from the back of the paper to the front. (D) Resonance structures of **2 c**$^+$ and **2 c·**.

Next, we scrutinized the aromaticity of radical **2·**, since the aromaticity of open-shell molecules is of great interest.[21-24] The tropyl radical is known to exhibit antiaromatic character albeit with 7π electrons[24]. When cation $\mathbf{2}^+$ is converted into radical **2·**, the $NICS(1)_{zz}$ values are decreased to −35.2 ppm for the pyrrole ring and −18.2 to −23.0 ppm for the benzene rings, suggesting a weakened overall aromatic character. The value at the 7-membered ring increases from +1.9 ppm (for $\mathbf{2\ b}^+$) to +22.2 ppm (for **2 b·**), suggesting a significant deshielding effect at its center. To elucidate the origin of the deshielding effect, the NICS(0) values of azacorannulene **1** and various fragmental molecules of radical **2·** were calculated (Figure S36). The comparison of NICS(0) values in the 7-membered ring between **2 c·** (+9.3 ppm) and the non-bridged compound (**I**; +5.6 ppm) indicates that the bridging CH group in **2 c·** contributes to enhancing the deshielding effect inside the 7-membered ring. However, the positive values of the 7-membered ring in compounds **I** (+5.6 ppm), **II** (+3.2 ppm), and **IV** (+4.2 ppm) indicate that there is a deshielding effect by the adjacent aromatic rings even without the bridging CH group. Indeed, the ACID plot of **2 c·** exhibits global diatropic ring currents with 30π global aromaticity, which go through the fjord-region around the 7-membered ring and contribute to the deshielding effect. Upon conversion of radical **2·** to anion $\mathbf{2}^-$, clear counterclockwise paratropic ring currents around the 7-membered ring in the ACID plot and an $NICS(1)_{zz}$ value of +47.7 ppm were observed, indicating the strong anti-aromatic character of the heptagon moiety in $\mathbf{2}^-$. This is a reasonable consequence because the 7-membered ring has 8π electrons, which satisfies the Hückel's 4nπ rule.

2.3. Conclusion

In conclusion, we have successfully synthesized azahomocorannulenyl cation $\mathbf{2\ a}^+$ and radical **2 a·**. The key to this achievement lies in the 1,3-dipolar cycloaddition of polycyclic aromatic azomethine ylides with dibenzotropone followed by palladium-catalyzed

intramolecular cyclization. The resulting azahomocorannulene molecules adopt planar structures that were unambiguously revealed by single crystal X-ray diffraction analysis. In the crystal packing, radical **2 a·** crystalizes to form a unique brick block-herringbone structure as a result of π–π and CH–π interactions. ESR analysis elucidated that the spin density is predominantly localized around the fused diphenylmethyl moiety. Their electronic and optical properties were thoroughly investigated experimentally and theoretically to reveal their aromatic character.

2.4. Experimental section

1. Experimental section

General: Reactions were carried out under argon atmosphere using standard Schlenk techniques. Thin-layer chromatography (TLC) was performed using glass plates pre-coated with silica gel impregnated with a fluorescent indicator (Merck, #1.15685.0001). Silica gel column chromatography was performed with silica gel (Davisil, 60 Å, 40–63 micron) purchased from Sigma-Aldrich.

Instrumentation: NMR spectra were recorded on JEOL JNM-ECZL-500 (^{1}H: 500 MHz), Bruker Avance 400 (^{1}H: 400 MHz and ^{13}C: 101 MHz) NMR spectrometers. Chemical shift values for protons are referenced to the signal of tetramethylsilane (δ 0.00) or the residual signals of chloroform-*d* (δ 7.26) and methylene chloride-d_2 (δ 5.32). Chemical shift values for carbons are referenced to the signal of tetramethylsilane (δ 0.00) or the carbon resonance of chloroform-*d* (δ 77.2) and dichloromethane-d_2 (δ 53.8). Preparative high-pressure liquid chromatography (HPLC) separation was carried out with a LaboACE (Japan Analytical Industry Co. Ltd.) equipped with a Buckyprep column (Nacalai, Co. Ltd.; 20 mm i.d. × 250 mm) by eluting with toluene (8.0 mL/min) at room temperature. High-resolution mass (HRMS) spectra were taken on a Waters Q-Tof Premier mass spectrometer with the electron spray

ionization time-of-flight (ESI-TOF) method and JEOL JMS-S3000 SpiralTOF with matrix-assisted laser desorption/ionization time-of-flight (MALDI-TOF) method. Melting temperatures and decomposition temperatures were recorded on an OptiMelt MPA-100 apparatus. Infrared (IR) spectra were recorded on a Shimadzu FTIR-8400 spectrometer with an attenuated total reflection (ATR) system. ESR spectrum was measured using a JEOL FA200 X-band spectrometer and g-value was determined by the Mn^{2+}/MgO solid as a standard. Ultraviolet–visible (UV–vis) absorption spectra were recorded on a Shimadzu UV-3600 spectrometer. Cyclic voltammograms were recorded on a Biologic SP-50 electrochemical analyzer. Cyclic voltammogram was recorded with a glassy carbon working electrode, a Pt counter electrode, and a $Ag/AgNO_3$ reference electrode in dichloromethane containing 0.1 M Bu_4NPF_6 as a supporting electrolyte. Electrochemical experiments were done under argon atmosphere at room temperature.

Materials: The following reagents were purchased from the indicated suppliers and used as received: dibenzo[*b*,*f*]tropone (5*H*-dibenzo[*a*,*d*][7]annulen-5-one; **4**; Sigma), cesium(I) fluoride (CsF; Sigma), *N,N*-diisopropylethylamine (*i*-Pr_2NEt; TCI), 2,3-dichloro-5,6-dicyano-*p*-benzoquinone (DDQ; Fluorochem), palladium(II) diacetate ($Pd(OAc)_2$; Sigma), di-*t*-butyl(methyl)phosphonium tetrafluoroborate (*t*-$Bu_2PMe{\cdot}HBF_4$; Sigma), 1,8-diazabicyclo[5.4.0]undec-7-ene (DBU, Sigma), tin(II) chloride ($SnCl_2$; Sigma), cobaltocene ($CoCp_2$; Sigma), and tetrafluoroboric acid diethyl ether complex ($HBF_4{\cdot}Et_2O$; 51–57 wt% solution in diethyl ether; Sigma). Cerium(III) trichloride ($CeCl_3$) was prepared by heating cerium(III) trichloride heptahydrate ($CeCl_3{\cdot}7H_2O$; Sigma) for 24 h at 200 °C under vacuum. Mesitylmagnesium bromide (MesMgBr) was prepared from bromomesitylene and magnesium using a standard method and titrated before use. Dimethylacetamide (DMA; Sigma) was pre-dried over activated 4 Å molecular sieves and distilled over calcium hydride under nitrogen atmosphere. Anhydrous toluene, tetrahydrofuran (THF), dichloromethane (CH_2Cl_2), and

acetonitrile (CH_3CN) were purchased from Sigma. Anhydrous dimethyl sulfoxide (DMSO) was purchased from Alfa Aesar. 2-*t*-Butyl-7,11-dichloro-8*H*-isoquinolino[4,3,2-*de*]phenanthridin-9-ium chloride (**3**) was prepared according to the literature procedure[51].

A Procedure for 1,3-Dipolar Cycloaddition of Azomethine Ylide Prepared from Iminium Salt 3 with Dibenzotropone 4:

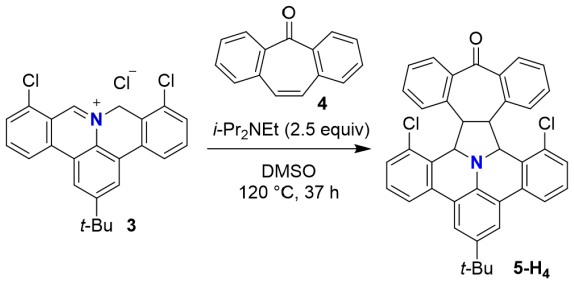

To a solution of iminium salt **3** (0.25 g, 0.58 mmol) and dibenzotropone **4** (0.12 g, 0.58 mmol) in DMSO (12 mL) was added *N*,*N*-diisopropylethylamine (0.25 mL, 1.45 mmol), and the mixture was stirred for 37 h at 120 °C. The black-green solution was cooled to room temperature and poured into a mixed solution of toluene and ethyl acetate (50/25 mL). The organic phase was washed with water three times and dried over sodium sulfate. After filtration, the filtrate was concentrated under reduced pressure to leave black solids. The solids were purified by silica gel column chromatography using a mixed solvent of dichloromethane and hexane (1/3, v/v) as eluent to yield *exo*-pyrrolidene **5-H$_4$** as a colorless solid (0.22 g, 0.37 mmol, 63%); R_f: 0.19 (dichloromethane:hexane = 1:1); mp 221–224 °C (decomp); IR (neat); cm^{-1} 2957, 1664, 1598, 1572, 1475, 1445, 1415, 1292, 1248, 1056, 937, 870, 793, 725, 670; ^1H NMR (400 MHz, $CDCl_3$, 300 K) δ 7.86 (s, 2H), 7.78 (d, J = 7.7 Hz, 2H), 7.67 (dd, J = 7.6 Hz, 1.2 Hz, 2H), 7.33 (t, J = 7.6 Hz, 2H), 7.31 (t, J = 7.9 Hz, 2H), 7.23 (dt, J = 7.4 Hz, 1.3 Hz, 2H), 7.13 (dd, J = 7.4 Hz, 0.8 Hz 2H), 6.64 (d, J = 7.1 Hz, 2H), 4.82–4.73 (m, 2H), 3.66–4.56 (m, 2H), 1.48 (s, 9H). ^{13}C NMR (101 MHz, CD_2Cl_2, 300 K) δ 200.8, 144.5, 143.1 (2C), 137.7, 136.7 (2C), 134.3 (2C), 133.5 (2C), 131.8 (2C), 131.6 (2C), 130.0 (2C), 129.6 (2C), 129.0 (2C),

128.4 (2C), 127.7 (2C), 122.2 (2C), 122.0 (2C), 121.8 (2C), 70.2 (2C), 54.9 (2C), 35.0, 31.7 (3C); HRMS (ESI) *m*/*z* calcd for $C_{39}H_{29}Cl_2NO$ $[M+H]^+$ 598.1704, found 598.1718.

A Procedure for Oxidation of π-Extended Pyrrolidine 5-H$_4$:

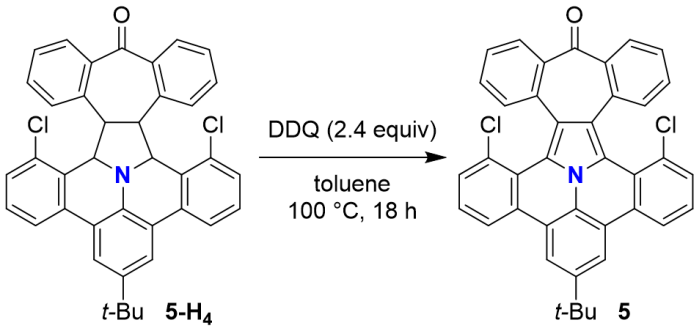

A solution of DDQ (0.20 g, 0.89 mmol) and **5-H$_4$** (0.22 g, 0.37 mmol) in toluene (15 mL) was stirred for 18 h at 100 °C. After the reaction was quenched with a saturated aqueous solution of sodium bicarbonate, the mixture was extracted with dichloromethane three times and washed with brine. The organic phase was dried over sodium sulfate. After filtration, the filtrate was concentrated under reduced pressure to obtain brown solids. The crude mixture was suspended in ethyl acetate. The precipitation was collected by filtration and washed with ethyl acetate and hexane to yield **5** as a yellow solid (0.10 g, 0.17 mmol, 46%); R_f: 0.25 (dichloromethane:hexane = 1:1); mp 331–336 °C (decomp); IR (neat); cm^{-1} 2959, 1665, 1596, 1556, 1442, 1397, 1300, 1058, 929, 796, 745, 683; ^{1}H NMR (400 MHz, $CDCl_3$, 300 K) δ 8.34 (s, 2H), 8.24 (dd, *J* = 7.8 Hz, 1.2 Hz, 2H), 7.74 (dd, *J* = 7.6 Hz, 1.1 Hz, 2H), 7.50–7.37 (m, 8H), 7.33 (dt, *J* = 7.5 Hz, 1.4 Hz, 2H), 1.57 (s, 9H); ^{13}C NMR (101 MHz, $CDCl_3$, 300 K) δ 200.3, 147.1, 141.9 (2C), 133.1 (2C), 131.3 (2C), 130.9 (2C), 130.7 (2C), 130.5 (2C), 128.7, 128.6 (2C), 127.7 (2C), 127.6 (2C), 127.2 (2C), 125.4 (2C), 123.2 (2C), 121.5 (2C), 121.5 (2C), 119.9 (2C), 119.6 (2C), 35.3, 31.8 (3C); HRMS (MALDI) *m*/*z* calcd for $C_{39}H_{25}Cl_2NO$ $[M]^+$ 593.1308, found 593.1289.

A Procedure for Palladium-Catalyzed Cyclization of 5:

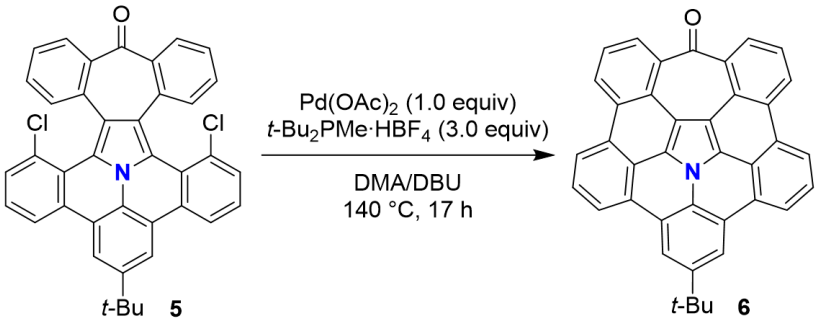

To a mixture of **5** (0.10 g, 0.17 mmol), palladium(II) diacetate (38 mg, 0.17 mmol), and *t*-$Bu_2PMe{\cdot}HBF_4$ (0.15 g, 0.51 mmol) in a Schlenk tube were added DBU (2.0 mL) and DMA (10 mL) via a syringe. The solution was degassed by a repeated freeze-pump-thaw method three times. The solution was stirred for 17 h at 140 °C to gradually afford orange precipitate of ketone **6**. The solution was cooled to rt and poured into methanol. The precipitate was collected by filtration and washed with methanol and hexane to obtain orange solid **6** (78 mg, 0.15 mmol, *ca.* 88%) (Note: Compound **6** has extremely low solubility in organic solvents and would be contaminated with a small amount of palladium black as a byproduct formed during the cyclization reaction, but it can be used for the next reaction); mp 359–363 °C (decomp); IR (neat); cm^{-1} 2945, 1664, 1612, 1582, 1538, 1482,1451, 1375, 1343, 1292, 1236, 1024, 953, 866, 803, 739; ^1H NMR (500 MHz, CD_2Cl_2/CS_2, 300 K) δ 8.99 (d, J = 7.0 Hz, 2H), 8.89 (d, J = 8.0 Hz, 2H), 8.73 (d, J = 8.5 Hz, 2H), 8.54 (s, 2H) 8.49 (d, J = 6.5 Hz, 2H), 8.00–7.90 (m, 2H), 7.87–7.78 (m, 2H), 1.69 (s, 9H). (Note: Clear signals could not be obtained in ^{13}C NMR analysis due to the low solubility of **6**); HRMS (MALDI) *m*/*z* calcd for $C_{39}H_{23}NO$ $[M]^+$ 521.1774, found 521.1773.

A Procedure for Addition of Grignard Reagent to Ketone 6:

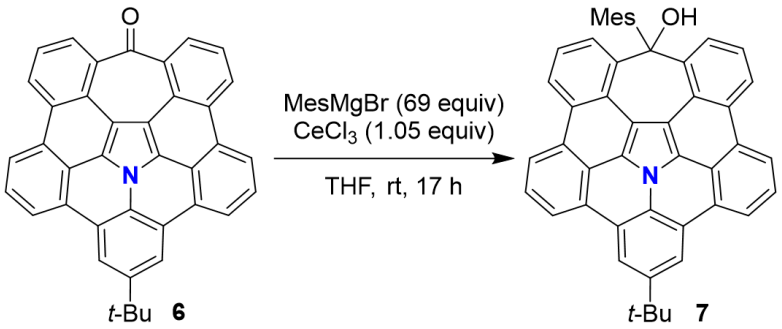

To a mixture of **6** (30 mg, 0.058 mmol) and cerium trichloride (15 mg, 0.061 mmol) in a 25-mL Schlenk tube was added mesitylmagnesium bromide (2.0 M solution in THF, 2.0 mL, 4.0 mmol) at 0 °C. The reaction mixture was stirred for 17 h at room temperature. The reaction mixture was quenched with an aqueous solution of ammonium chloride and extracted with dichloromethane three times. The combined organic phase was washed with water and brine. The organic layer was dried over sodium sulfate. After filtration, the solvent removed under reduced pressure to leave orange solids and oil. The crude mixture was purified by preparative HPLC using Buckyprep columns eluted with toluene (fraction: 11.2 min). The collected fraction was evaporated to yield **7** as a yellow solid (15 mg, 0.023 mmol, 40%); R_f: 0.27 (dichloromethane:hexane = 1:2); mp 246–249 °C (decomp); IR (neat); cm^{-1} 3553, 2953, 1659, 1614, 1573, 1540, 1455, 1404, 1376, 1341, 1297, 1234, 1027, 986, 870, 797, 748, 697; ^1H NMR (400 MHz, $CDCl_3$, 300 K) δ 8.76 (d, J = 7.9 Hz, 2H), 8.76 (d, J = 8.1 Hz, 2H), 8.56 (s, 2H), 8.52 (d, J = 7.6 Hz, 2H), 7.95 (t, J = 7.9 Hz, 2H), 7.61 (d, J = 7.7 Hz, 2H), 7.50 (t, J = 8.0 Hz, 2H), 7.11 (s, 1H), 6.74 (s, 1H), 2.99 (s, 3H), 2.74 (s, 1H), 2.38 (s, 3H), 1.66 (s, 12H); ^{13}C NMR (101 MHz, $CDCl_3$, 300 K) δ 147.3, 146.1 (2C), 143.7, 136.6, 136.0, 131.8, 131.1, 130.1 (2C), 129.7 (2C), 128.4 (2C), 128.0 (2C), 127.1 (2C), 126.1 (4C), 124.6 (2C), 124.2 (C), 123.3 (2C), 123.1, 122.7 (2C), 120.4 (2C), 120.2 (2C), 120.0 (2C), 109.9 (2C), 92.2 (2C), 35.8, 32.1 (3C), 22.7, 20.7(2C); HRMS (MALDI) m/z calcd for $C_{48}H_{35}NO$ $[M]^+$ 641.2713, found 641.2728.

A Procedure for Dehydroxylation of Alcohol 7 with Tin(II) Chloride:

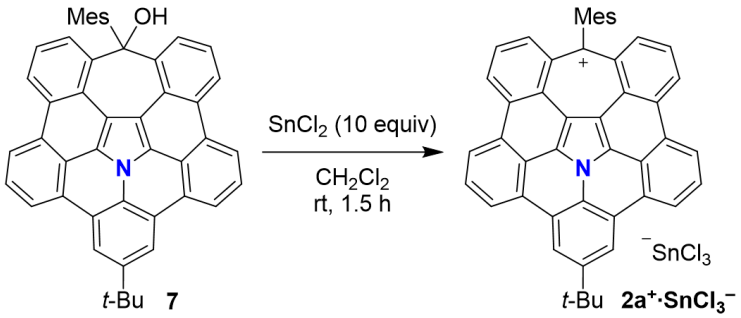

To a mixture of **7** (7.0 mg, 0.011 mmol) and tin(II) chloride (21 mg, 0.11 mmol) in a 10 mL Schlenk tube were added dichloromethane (3.0 mL). After stirring for 1.5 h at room temperature, the reaction mixture was filtered, and the filtrate was concentrated under reduced pressure to leave black solids. The residue was recrystallized from dichloromethane/hexane to afford **2a**$^{+}$**·SnCl**$_3^{-}$ as a dark blue solid (9.8 mg, 0.011 mmol, quant.); mp 291–296 °C (decomp); IR (neat); cm^{-1} 2920, 1674, 1618, 1589, 1571, 1542, 1506, 1477, 1452, 1413, 1391, 1347, 1327, 1295, 1243, 1221, 1174, 1132, 1089, 1035, 970, 916, 857, 826, 806, 769, 745, 691; ^{1}H NMR (400 MHz, CD_2Cl_2 with CF_3SO_3H (0.06%), 300 K) δ 9.86 (d, J = 7.6 Hz, 2H), 9.23 (d, J = 8.2 Hz, 2H), 9.00 (d, J = 7.8 Hz, 2H), 8.98 (s, 2H), 8.52 (d, J = 8.8 Hz, 2H), 8.41 (t, J = 8.0 Hz, 2H), 8.27 (t, J = 8.3 Hz, 2H), 7.33 (s, 2H), 2.61 (s, 3H), 1.93 (s, 6H), 1.74 (s, 9H); ^{13}C NMR (101 MHz, CD_2Cl_2 with CF_3SO_3H (0.06%), 300 K) δ 183.8, 153.7, 140.6, 139.5 (2C), 139.0 (2C), 138.3 (2C), 137.4 (2C), 135.8 (2C), 135.6 (2C), 131.8 (2C), 130.1 (2C), 129.8 (2C), 129.7 (2C), 127.9 (2C), 126.4, 125.9, 124.9 (2C), 123.9 (2C), 123.1, 122.3 (2C), 120.7 (2C), 119.9, 117.6 (2C), 115.9 (2C), 36.9, 32.1 (3C), 21.5, 20.0 (2C); HRMS (MALDI) *m*/*z* calcd for $C_{48}H_{34}N$ $[M-SnCl_3]^{+}$ 624.2686, found 624.2665.

A Procedure for Dehydroxylation of Alcohol 7 with Tetrafluoroboric Acid:

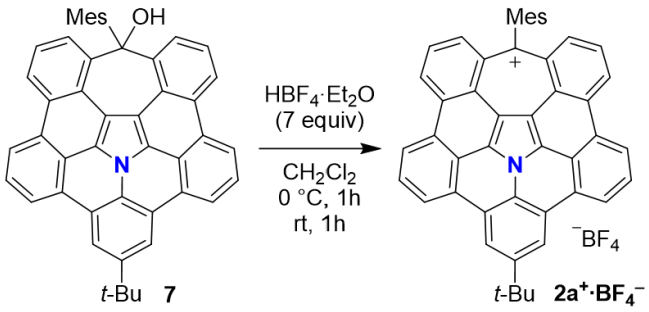

To a solution of **7** (7.0 mg, 0.011 mmol) in dichloromethane (1.5 mL) in a 10 mL Schlenk tube was added tetrafluoroboric acid diethyl ether complex (51–57 wt% solution in diethyl ether, 11 μL, 0.078 mmol) at 0 °C. The reaction mixture was stirred for 1 h at 0 °C and made it warm to room temperature gradually. After additional strring for 1 h, diethyl ether (8 mL) was added to the solution to give black precipitation. The black precipitates were collected by filtration and washed with diethyl ether and hexane to afford $\mathbf{2a^{+}\cdot BF_4^{-}}$ as a dark blue solid (7.6 mg, 0.011 mmol, quant.); mp 282–286 °C (decomp); IR (neat); cm^{-1} 2921, 1674, 1617, 1589, 1569, 1542, 1524, 1506, 1479, 1453, 1439, 1393, 1349, 1327, 1295, 1266, 1244, 1220, 1174, 1134, 1088, 1032, 970, 916, 858, 825, 809, 772, 745, 727, 700; ^{1}H NMR (400 MHz, $CDCl_3$, 300 K) δ 9.94 (d, J = 7.4 Hz, 2H), 9.18 (d, J = 8.2 Hz, 2H), 8.63 (d, J = 7.8 Hz, 2H), 8.53 (s, 2H), 8.45 (d, J = 8.8 Hz, 2H), 8.35 (t, J = 8.2 Hz, 2H), 8.22 (t, J = 7.9 Hz, 2H), 7.32 (s, 2H), 2.62 (s, 3H), 1.98 (s, 6H), 1.55 (s, 9H); ^{13}C NMR (101 MHz, $CDCl_3$, 300 K) δ 182.9, 152.9, 140.1, 139.0, 138.2 (2C), 138.2 (2C), 137.5 (2C), 135.2 (3C), 134.9 (2C), 131.2 (2C), 129.5 (4C), 128.1 (2C), 126.6 (2C), 125.2, 125.1 (3C), 125.0 (2C), 123.0 (2C), 122.2 (2C), 121.2 (2C), 118.9 (2C), 115.1 (2C), 36.6, 31.9 (3C), 21.4, 20.0 (2C); HRMS (MALDI) m/z calcd for $C_{48}H_{34}N$ $[M-BF_4]^{+}$ 624.2686, found 624.2676.

A Procedure for Reduction of Cation $2a^{+}\cdot SnCl_3^{-}$:

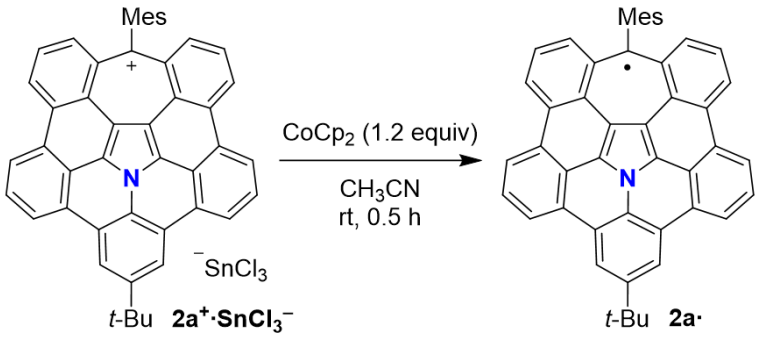

To a solution of $2a^{+}\cdot SnCl_3^{-}$ (9.3 mg, 0.011 mmol) in acetonitrile (1.5 mL) in a vial was added a solution of cobaltocene (2.5 mg, 0.013 mmol) in acetonitrile (1.5 mL). The mixture was stirred in the glove box for 0.5 h at room temperature to afford dark green precipitates. The precipitates were collected by filtration and washed with acetonitrile and hexane to obtain **2a**$^{\bullet}$ (6.2 mg, 0.010 mmol, 91%). Recrystallization from benzene/carbon disulfide in the glove box afforded black plate single crystals with X-ray quality; mp: 330–333 °C (decomp); IR (neat); cm^{-1} 2921, 2853, 1661, 1618, 1552, 1532, 1477, 1450, 1419, 1394, 1375, 1361, 1341, 1332, 1311, 1296, 1259, 1249, 1228, 1202, 1160, 1094, 1013, 949, 870, 848, 802, 788, 755, 732, 703, 693; HRMS (MALDI) *m*/*z* calcd for $C_{48}H_{34}N$ $[M]^{+}$ 624.2686, found 624.2710.

2. NMR Spectra

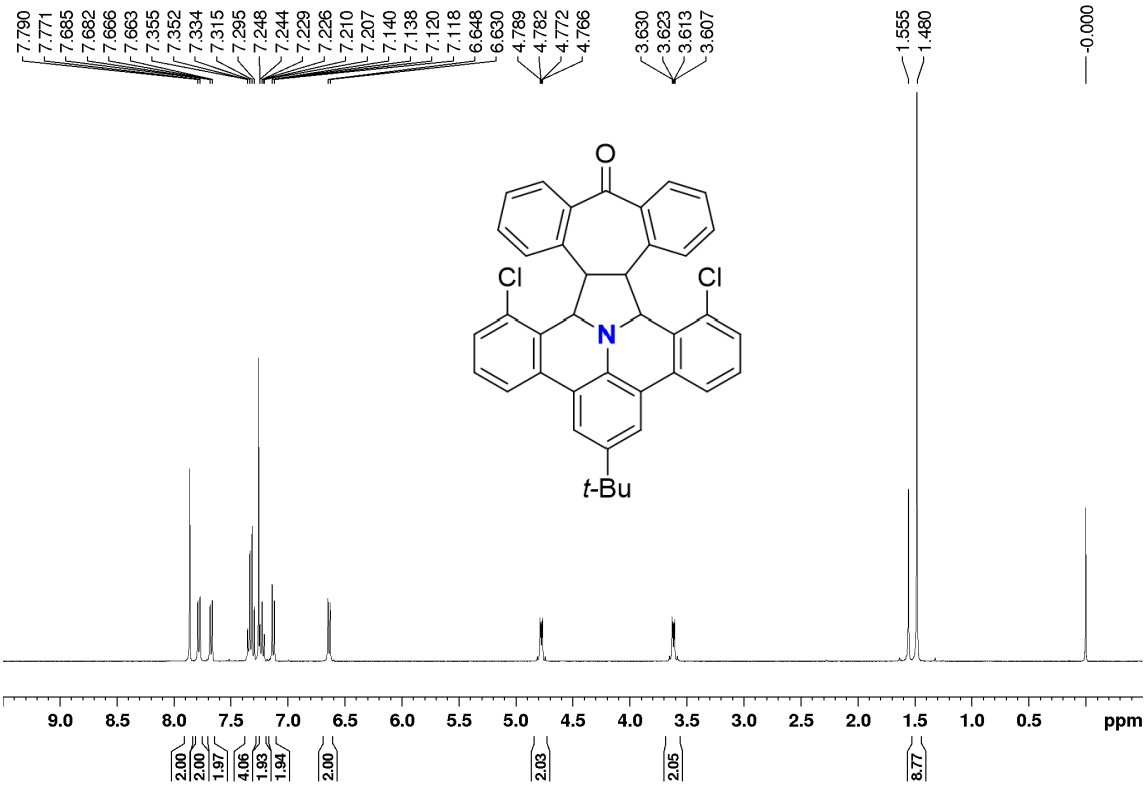

Figure S2.1. ^{1}H NMR spectrum of **5-H$_4$** (400 MHz, $CDCl_3$, 300 K).

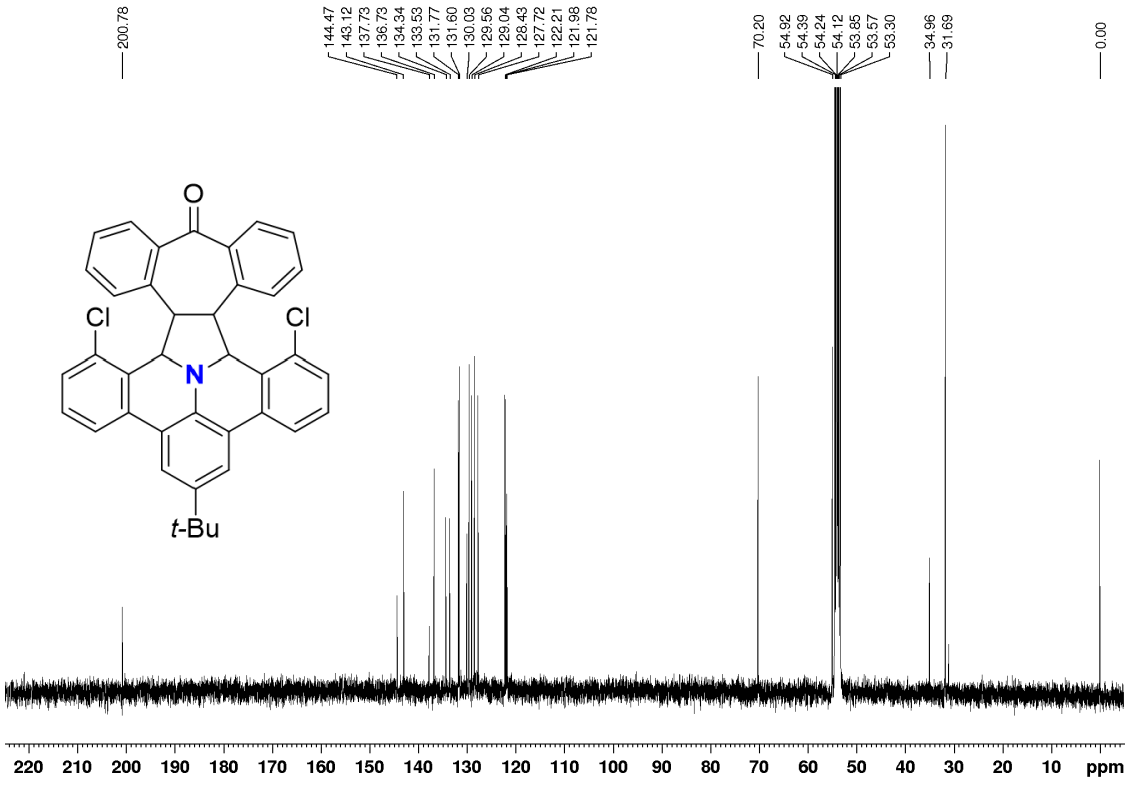

Figure S2.2. ^{13}C NMR spectrum of **5-H$_4$** (101 MHz, CD_2Cl_2, 300 K).

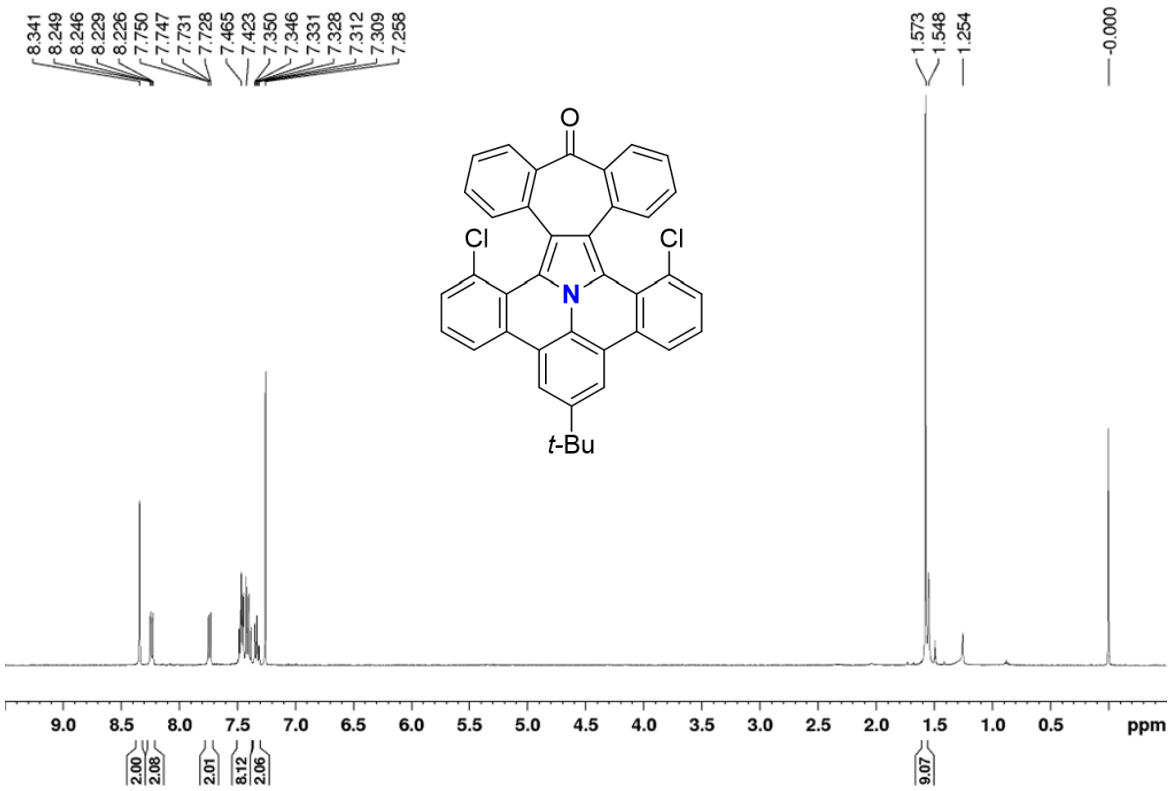

Figure S2.3. ^{1}H NMR spectrum of **5** (400 MHz, $CDCl_3$, 300 K).

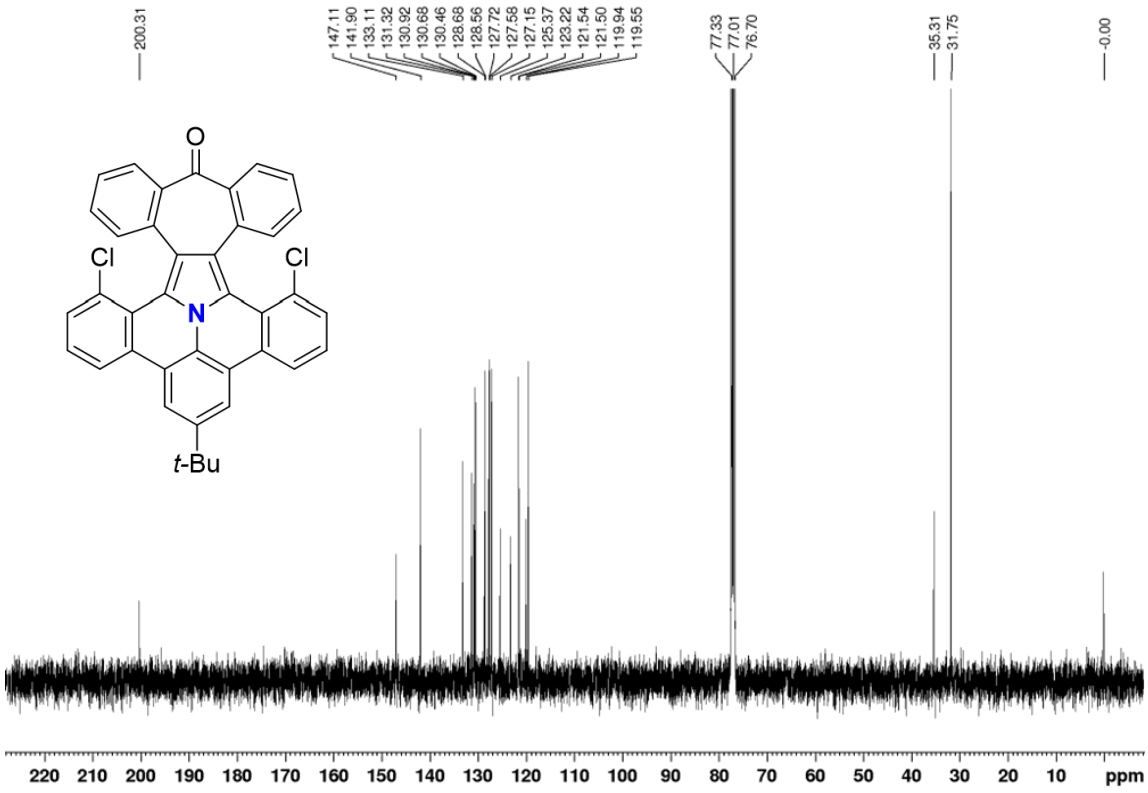

Figure S2.4. ^{13}C NMR spectrum of **5** (101 MHz, $CDCl_3$, 300 K).

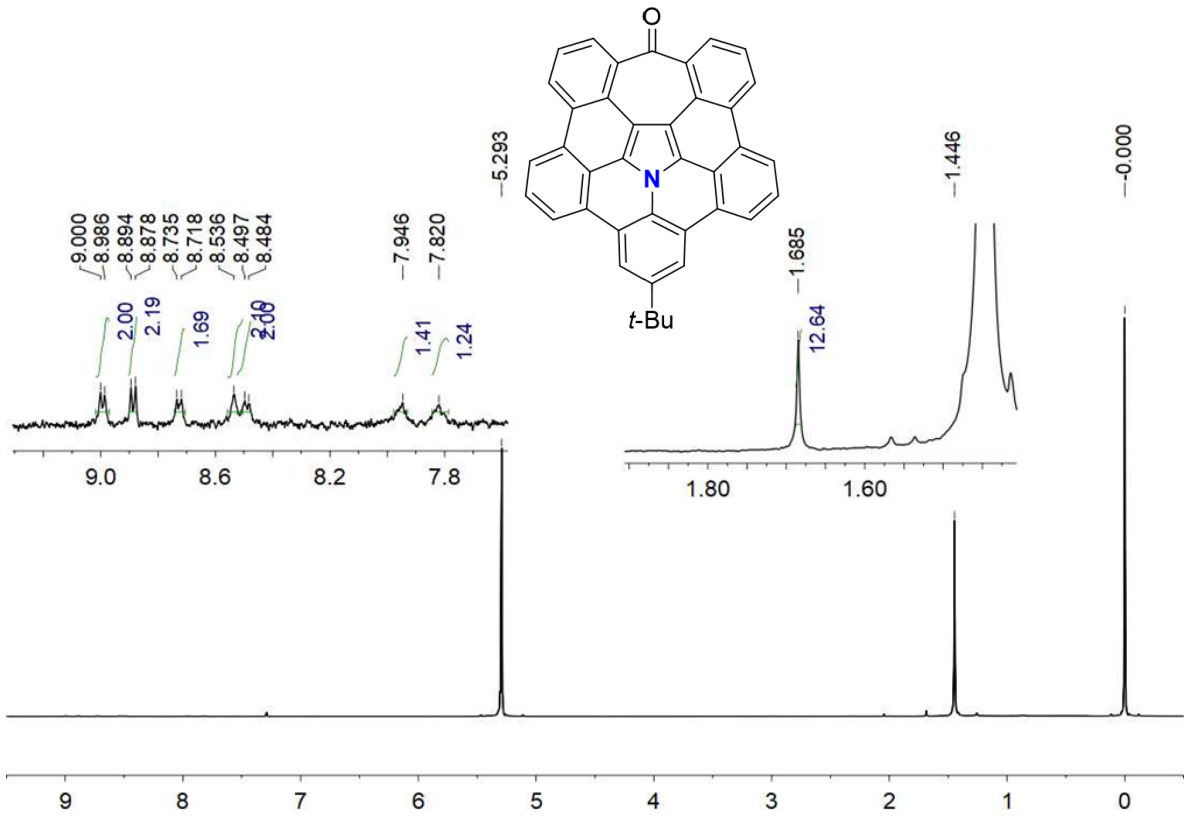

Figure S2.5. ^{1}H NMR spectrum of **6** (500 MHz, CD_2Cl_2/CS_2, 300 K).

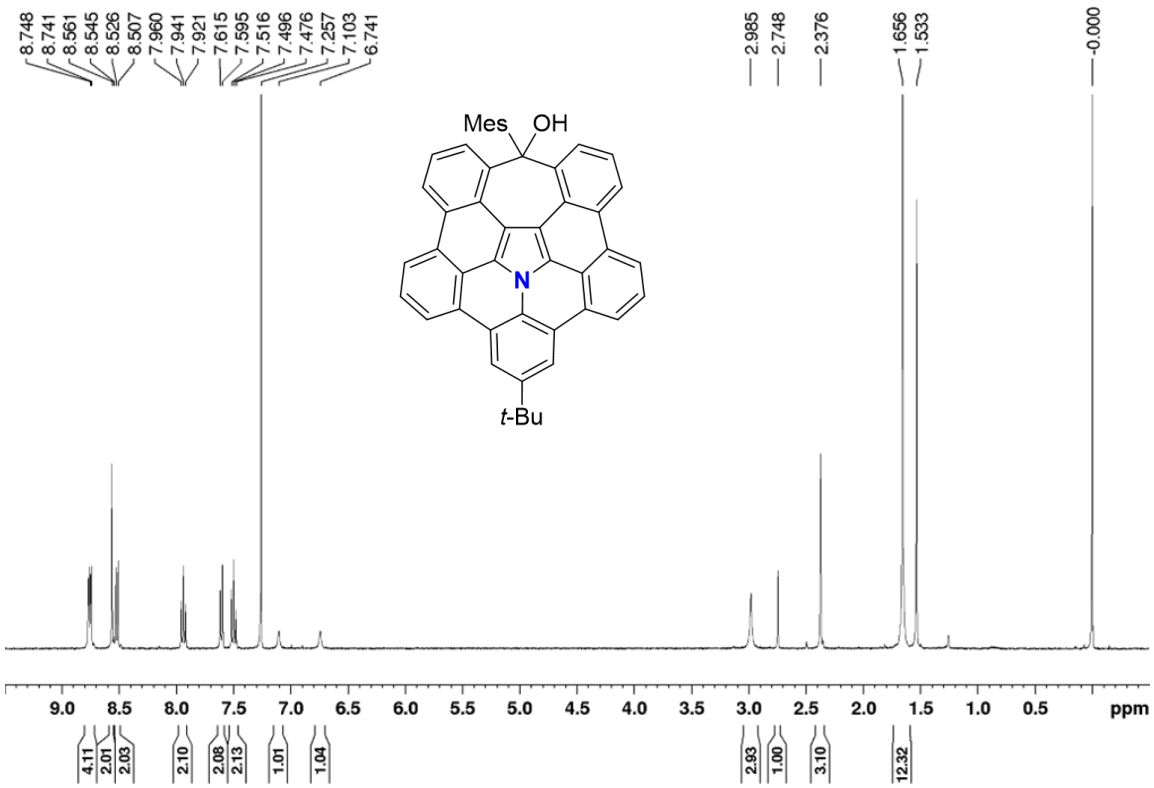

Figure S2.6. ^{1}H NMR spectrum of **7** (400 MHz, $CDCl_3$, 300 K).

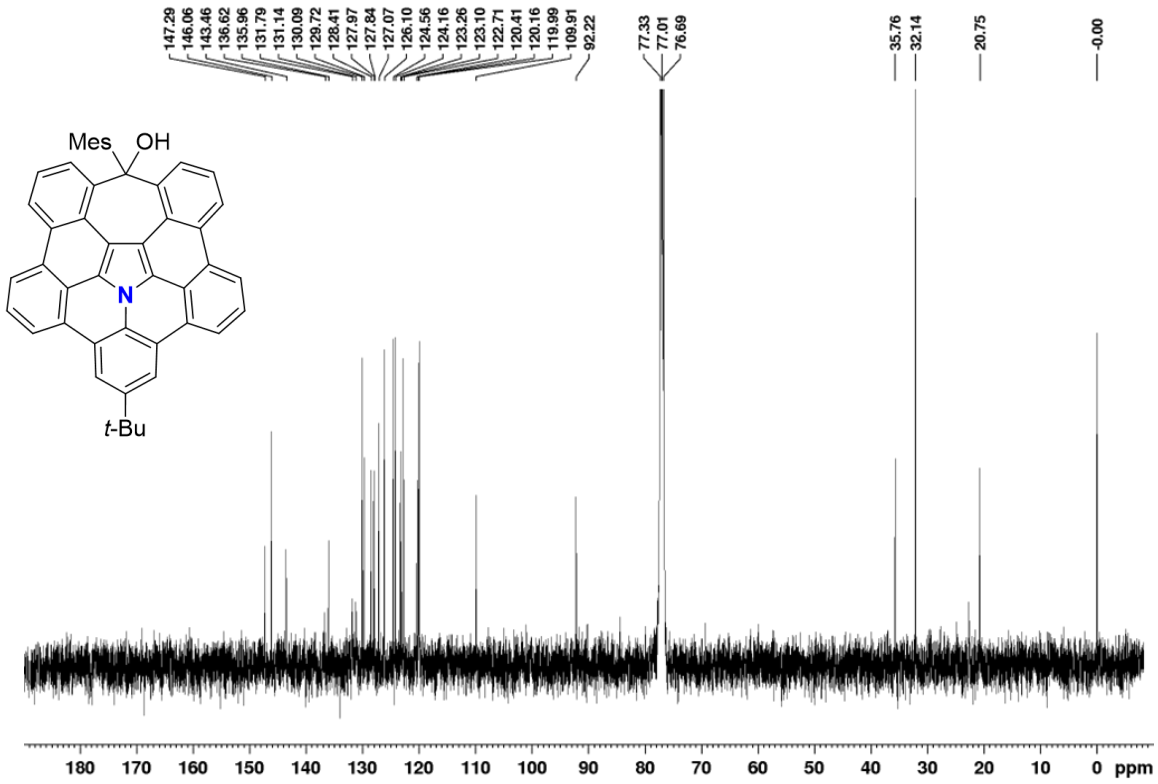

Figure S2.7. ^{13}C NMR spectrum of **7** (101 MHz, $CDCl_3$, 300 K).

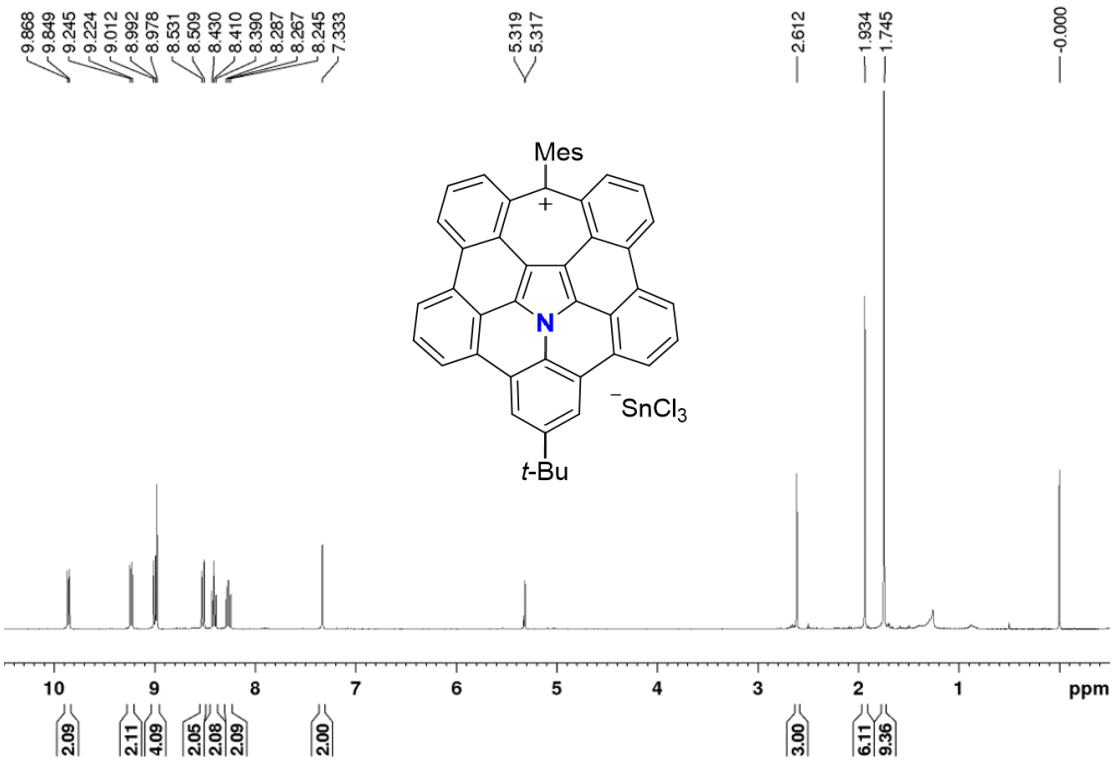

Figure S2.8. ^{1}H NMR spectrum of **2a**$^{+}$**·SnCl**$_3^{-}$ (400 MHz, CD_2Cl_2 with CF_3SO_3H (0.06%), 300 K).

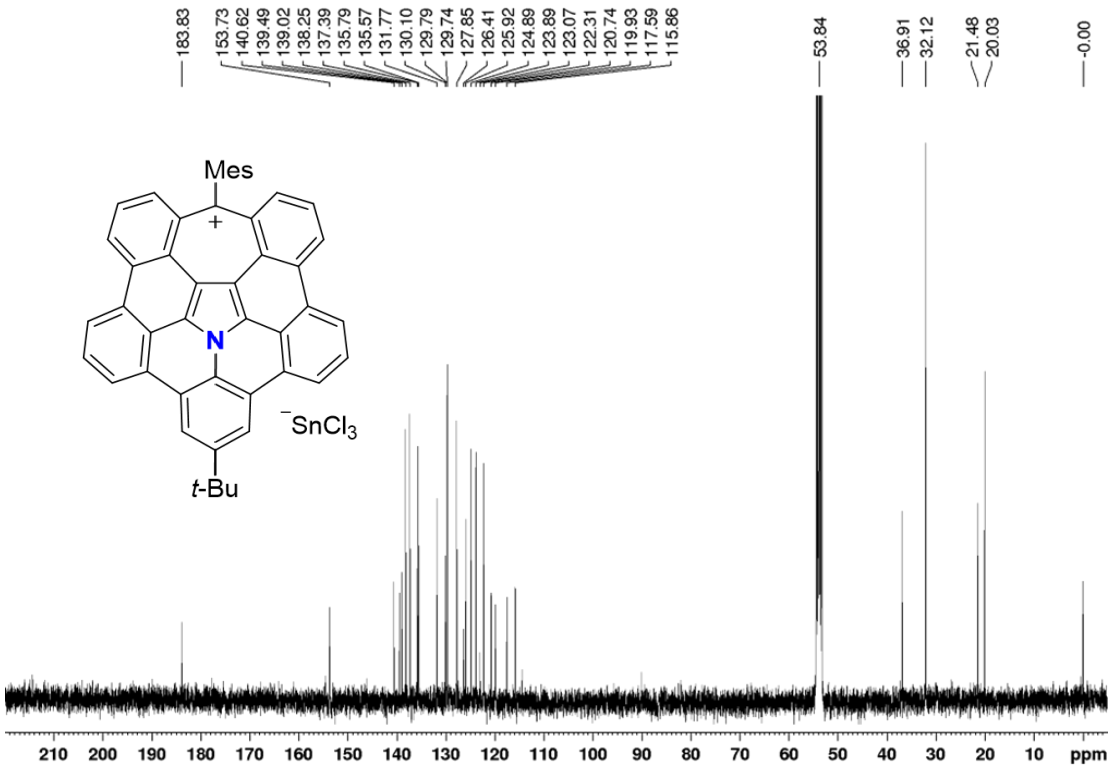

Figure S2.9. ^{13}C NMR spectrum of **2a**$^{+}$ **SnCl**$_3^{-}$ (101 MHz, CD_2Cl_2 with CF_3SO_3H (0.06%), 300 K).

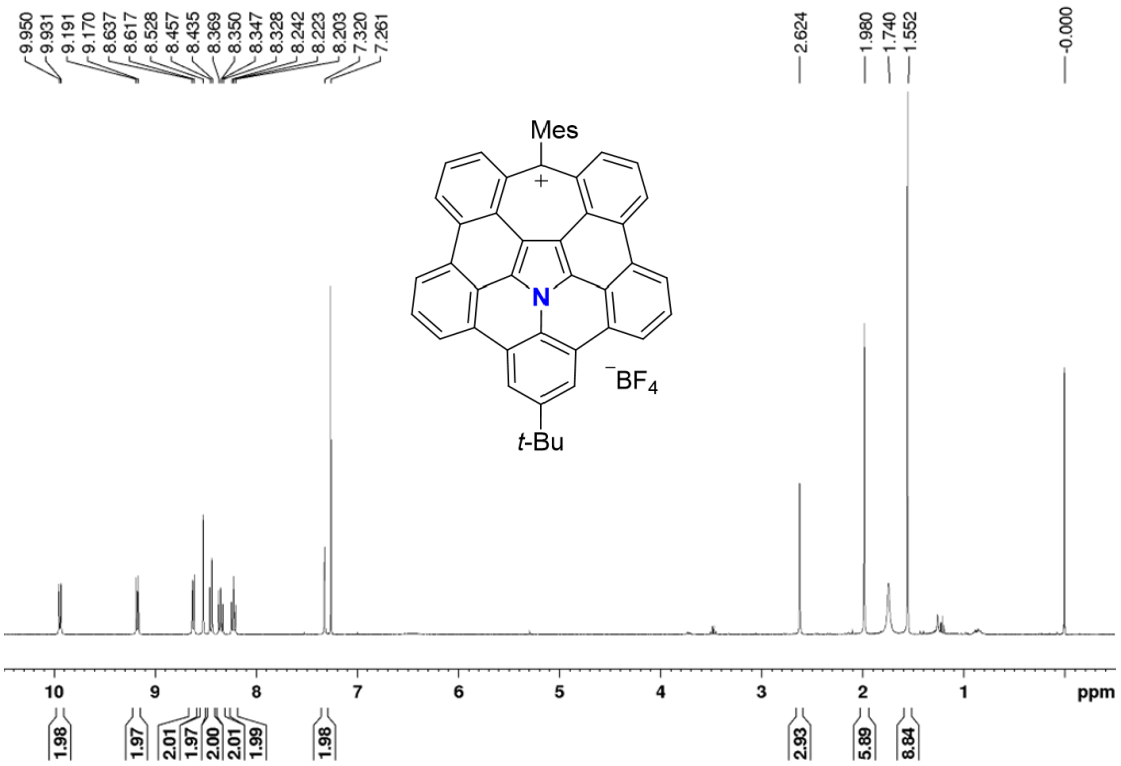

Figure S2.10. ^{1}H NMR spectrum of **2a**$^{+}$**·BF**$_4^-$ (400 MHz, $CDCl_3$, 300 K).

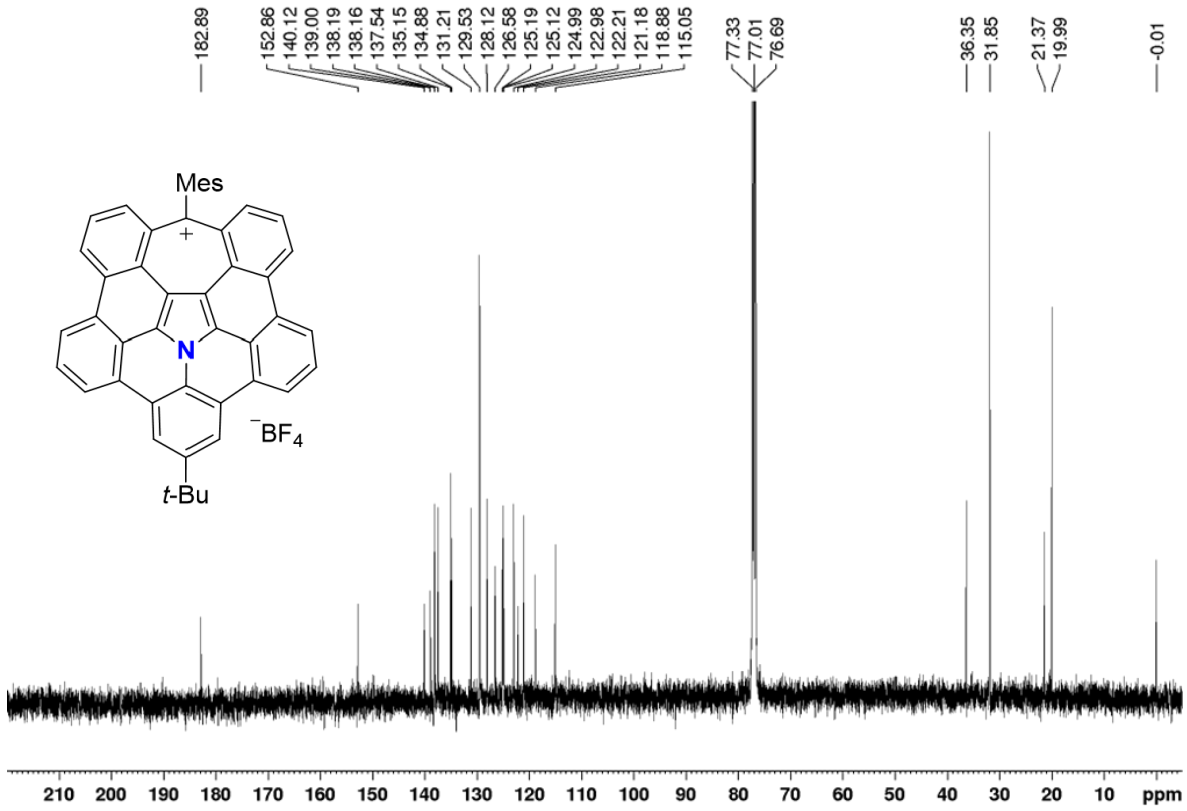

Figure S2.11. ^{13}C NMR spectrum of **2a**$^{+}$**·BF**$_4^-$ (101 MHz, $CDCl_3$, 300 K).

3. Optical Properties

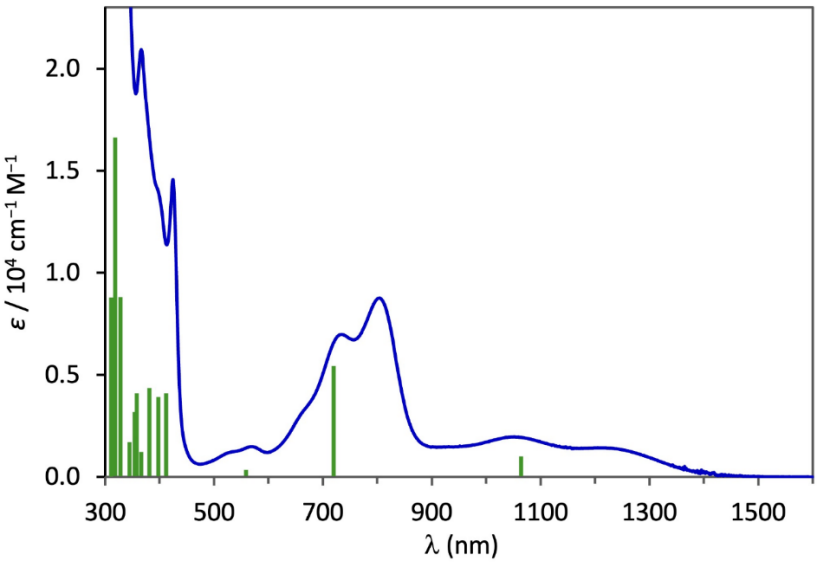

Figure S2.12. UV–vis absorption spectrum of $\mathbf{2a^{+}{\cdot}SnCl_3^{-}}$ (1.3×10^{-4} M) in dichloromethane. Green bars indicate simulated excitations by TD-DFT calculation with B3LYP/6-311+G(2d,p) (See Section 5-7).

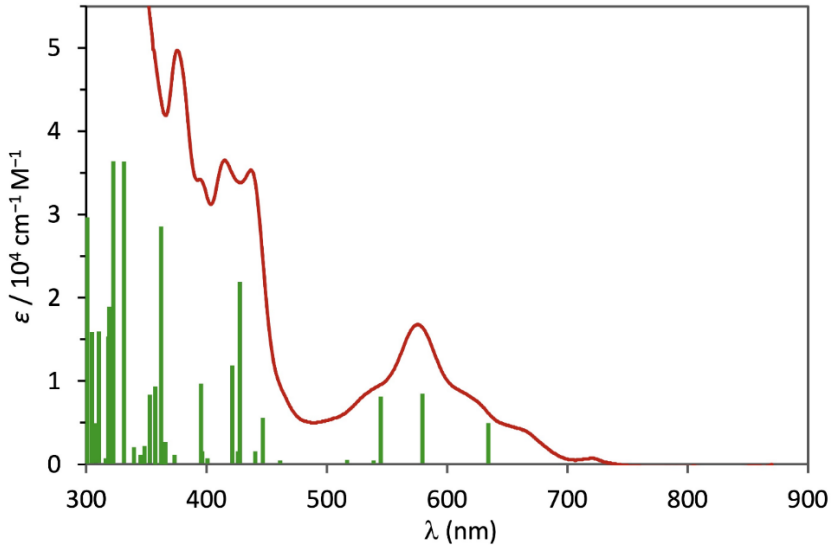

Figure S2.13. UV–vis absorption spectrum of $\mathbf{2a^{\bullet}}$ (1.0×10^{-5} M) in dichloromethane. Green bars indicate simulated excitations by TD-DFT calculation with UB3LYP/6-311+G(2d,p) (See Section 5-5).

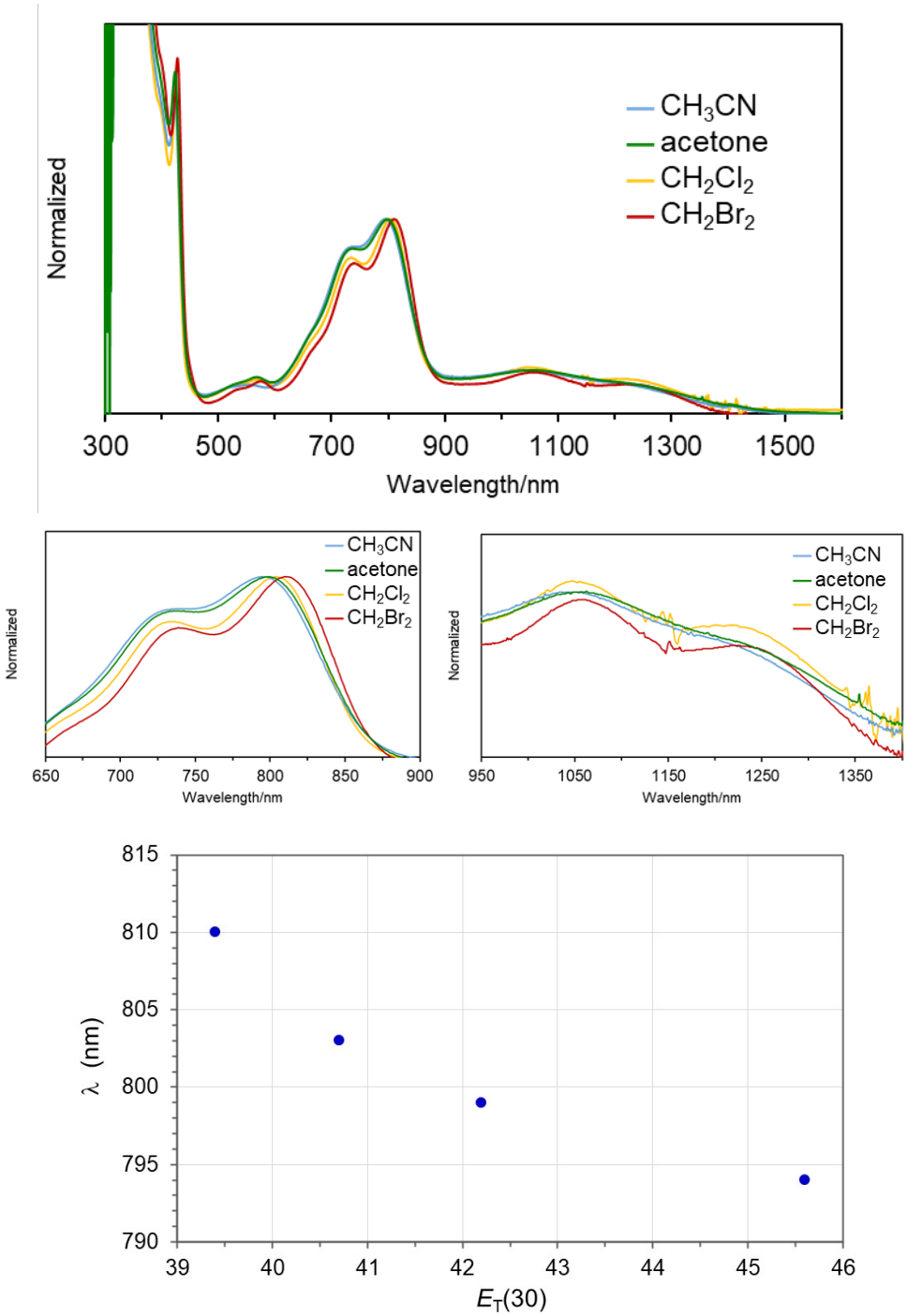

Figure S2.14. UV–vis absorption spectra of **2a**$^{+}$**·SnCl**$_3^{-}$ in acetonitrile (blue; 1.3×10^{-4} M), acetone (green; 8.8×10^{-5} M), dichloromethane (yellow; 1.3×10^{-4} M), and dibromomethane (red; 8.8×10^{-5} M). Correlation diagram of peak-top wavelengths (nm) and the solvent parameters of *E*t(30)[*].

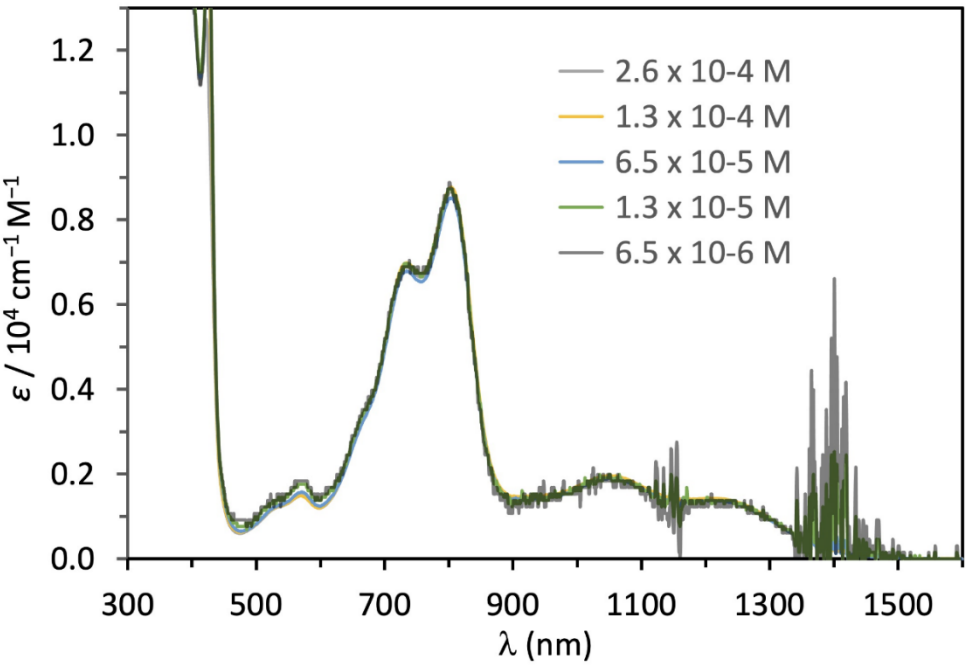

Figure S2.15. Concentration-dependent UV–vis absorption spectra of **2a**$^{+}$**·SnCl**$_3^-$ in dichloromethane (2.6×10^{-4} M to 6.5×10^{-6} M).

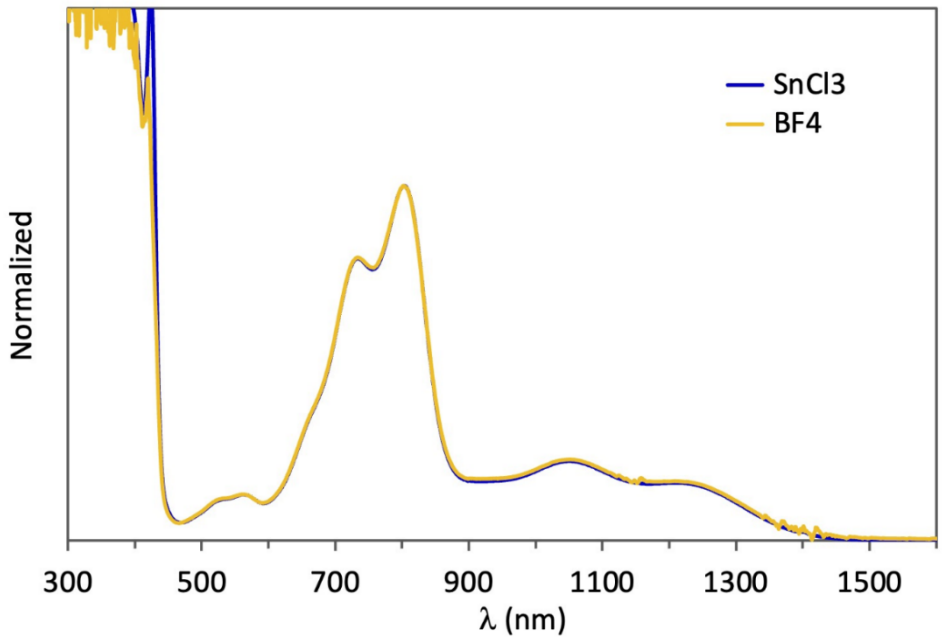

Figure S2.16. Normalized UV–vis absorption spectra of **2a**$^{+}$**·SnCl**$_3^-$ (1.0×10^{-4} M) and **2a**$^{+}$**·BF**$_4^-$ (1.8×10^{-4} M) in dichloromethane.

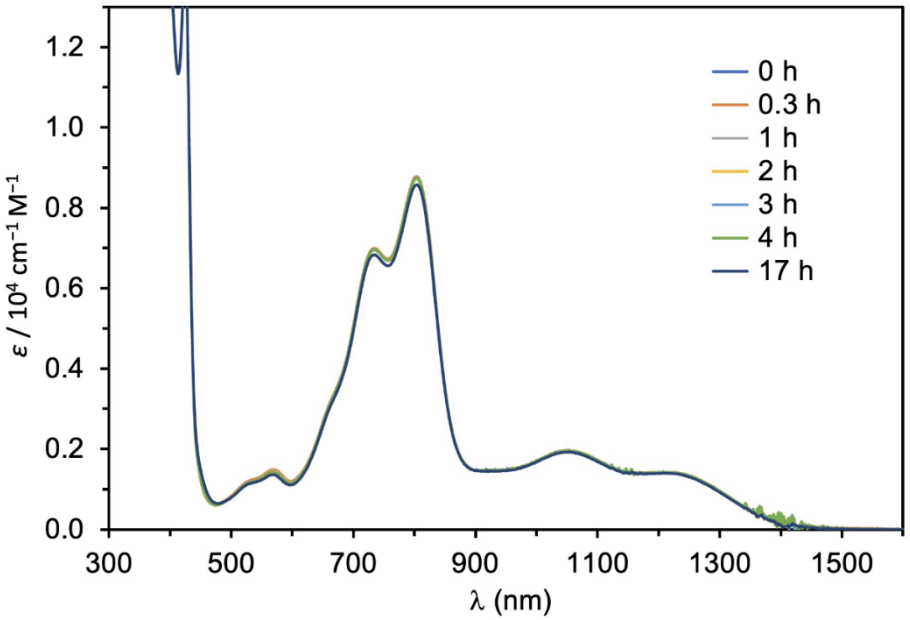

Figure S2.17. Time-dependent UV–vis absorption spectra of **2a**$^{+}$·**SnCl**$_3^-$ (1.3×10^{-4} M) in air in dichloromethane.

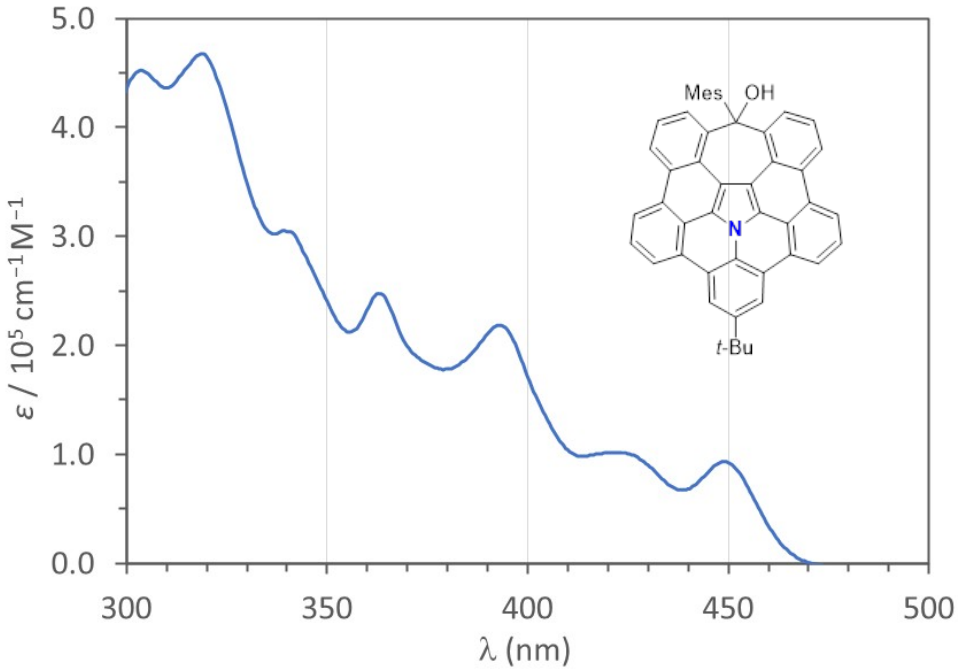

Figure S2.18. UV–vis absorption spectrum of **7** (1.0×10^{-6} M) in dichloromethane.

4. X-Ray Crystallographic Data

Single crystals suitable for X-ray analysis of **5-H$_4$** and **5** were obtained by slow evaporation of solvent from their solution in dichloromethane at room temperature, those of **2a**$^+$**·SnCl$_3$**$^-$ were obtained by slow evaporation of its solution in dichloromethane and toluene at −10 °C, and those of **2a**$^\bullet$ were obtained by slow evaporation of its solution in benzene and carbon disulfide under argon atmosphere at room temperature. A single crystal was mounted with mineral oil on a loop-type mount and transferred to the goniometer of a Bruker D8 Quest diffractometer. The radiation was performed with Multilayer Mirror-monochromated Incoatec microfocus source (Mo-Kα, λ = 0.71073 Å). The structures were solved by direct method with SHELXT[53] and refined by full-matrix least-squares techniques against F^2 with SHELXL-2018/3[53]. The intensities were corrected for Lorentz and polarization effects. The non-hydrogen atoms were refined anisotropically. Hydrogen atoms were placed using AFIX instructions.

Table S2.1. Crystal data and structure refinement for **5-H$_4$**, **5**, **2a$^+$·SnCl$_3^-$**, and **2a$^\bullet$**.

compound	**5-H$_4$**	**5**	**2a$^+$·SnCl$_3^-$**	**2a$^\bullet$**
CCDC number	**2286092**	**2286093**	**2286094**	**2286095**
Molecular formula	$C_{40}H_{31}Cl_4NO$	$C_{40}H_{27}Cl_4NO$	$C_{48.50}H_{36}Cl_4NO_{0.50}Sn$	$C_{48}H_{34}N$
Formula weight	683.46	679.42	901.27	624.76
Temperature (K)	100	100	100	100
Wavelength (Å)	0.71073	0.71073	0.71073	0.71073
Crystal system	orthorhombic	monoclinic	triclinic	monoclinic
Space group	P n m a	P 1 21/n 1	P −1	P 1 21/c 1
Unit cell dimensions a (Å)	21.8286(5)	12.7918(5)	13.9134(19)	16.2682(8)
b (Å)	13.8827(3)	10.0666(4)	16.989(2)	20.2425(9)
c (Å)	10.5463(2)	24.5867(11)	16.986(2)	9.4245(5)
α (°)	90	90	77.545(5)	90
β (°)	90	103.2223(16)	76.754(5)	99.9512(19)
γ (°)	90	90	86.334(5)	90
Volume (Å^3)	3195.95(12)	3082.1(2)	3815.8(9)	3056.9(3)
Z	4	4	4	4
Density (calculated) (mg·m^{-3})	1.420	1.464	1.569	1.358
Absorption coefficient (mm^{-1})	0.406	0.421	0.989	0.078
F(000)	1416	1400	1824	1316
Crystal size (mm^3)	0.140 x 0.200 x 0.240	0.020 x 0.200 x 0.220	0.100 x 0.140 x 0.200	0.020 x 0.200 x 0.220
Theta range (°)	2.69 to 34.96	2.01 to 31.50	1.93 to 29.61	2.01 to 27.88
Index ranges	−33<=h<=35	−18<=h<=18	−19<=h<=19	−20<=h<=21
	−17<=k<=22	−14<=k<=14	−23<=k<=23	−26<=k<=26
	−16<=l<=12	−36<=l<=36	−23<=l<=23	−12<=l<=11
Reflections collected	38114	42736	142584	54075
Min. and max. transmission	0.9450, 0.9090	0.9920, 0.9130	0.9080, 0.8270	0.9980, 0.9830
Data / restraints / parameters	7214 / 153 / 269	10237 / 164 / 477	21467 / 0 / 1003	7289 / 0 / 448
Goodness-of-fit on F^2	1.033	1.030	1.052	1.014
Final *R* indices [$I > 2\sigma(I)$]	R_1 = 0.0427	R_1 = 0.0516	R_1 = 0.0630	R_1 = 0.0628
	wR_2 = 0.1039	wR_2 = 0.1205	wR_2 = 0.1331	wR_2 = 0.1357
R indices (all data) [$I > 2\sigma(I)$]	R_1 = 0.0598	R_1 = 0.0841	R_1 = 0.1393	R_1 = 0.1299
	wR_2 = 0.1130	wR_2 = 0.1360	wR_2 = 0.1674	wR_2 = 0.1712
Largest diff. peak and hole (e.Å^{-3})	0.574, −0.659	0.414, −0.540	2.272, −1.475	0.495, −0.277

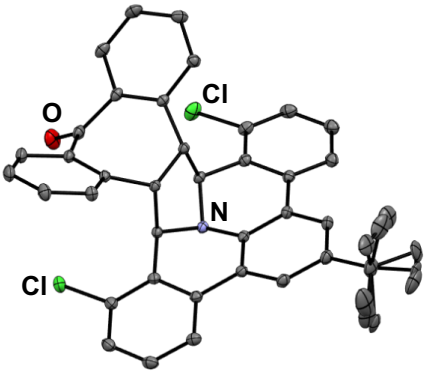

Figure S2.19. The X-ray structure of **5-H$_4$** with thermal ellipsoids of 50% probability. Hydrogen atoms are omitted for clarity.

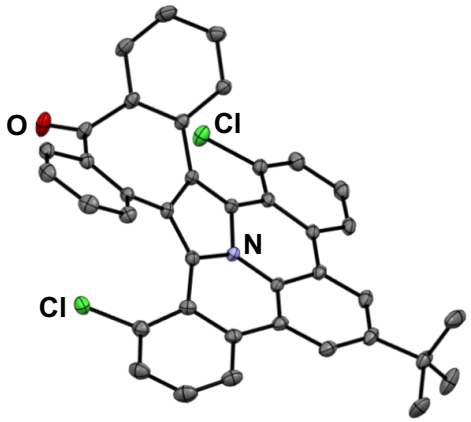

Figure S2.20. The X-ray structure of **5** with thermal ellipsoids of 50% probability. Hydrogen atoms are omitted for clarity.

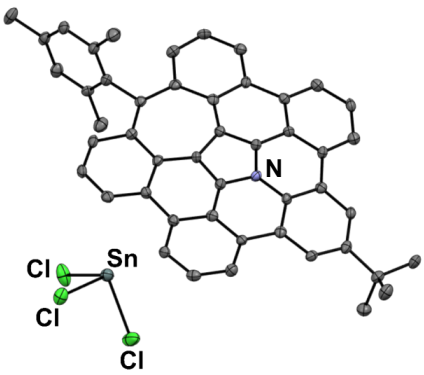

Figure S2.21. The X-ray structure of **2a$^+$·SnCl$_3^-$** with thermal ellipsoids of 50% probability. Hydrogen atoms are omitted for clarity.

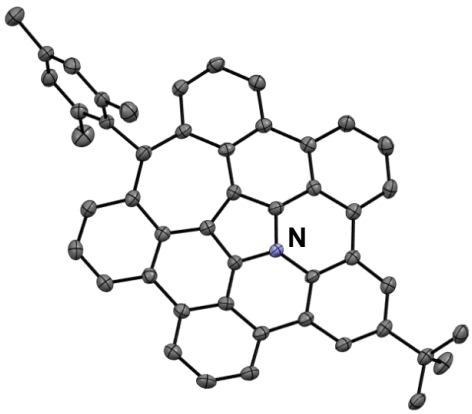

Figure S2.22. The X-ray structure of **2a**• with thermal ellipsoids of 50% probability. Hydrogen atoms are omitted for clarity.

5. Theoretical Calculations

Computations were performed using computing resources at High-Performance Center for Computational Science, Nanyang Technological University, Singapore. All the density functional theory (DFT) calculations were performed by using Gaussian 16 (revision A.03) program[54]. The molecular structures used for calculation and their compound numbers are shown in **Figure S2.23**. The geometries of closed-shell molecules **1**, **2b**$^+$, **2b**$^-$, **2c**$^+$, **2c**$^-$, Ⅰ, **II**, and Ⅳ in the singlet state were optimized with the RB3LYP[55] functional. The geometry optimization of radicals **2a**•, **2b**•, **2c**•, Ⅲ, Ⅴ, Ⅵ, Ⅶ, and Ⅷ was performed by using the broken-symmetry (BS) approach with the UB3LYP functional. The 6-31G(d,p) basis set[56] was used for structure optimization, vibrational frequency, while the 6-311+G(2d,p) basis set was used for time-dependent density functional theory (TD-DFT). Anisotropy of induced current density (ACID) plots were calculated by using the method developed by Herges[50] and applied the CSGT-RB3LYP/6-31G(d,p) level to the closed-shell molecules and the CSGT-UB3LYP/6-31G(d,p) level to the open-shell molecules. Nucleus-independent chemical shifts (NICS) values and the isochemical shielding surface (ICSS) plots were calculated at the GIAO-

RB3LYP/6-31G(d,p) method for closed-shell molecules and at the GIAO-UB3LYP/6-31G(d,p) method for open-shell molecules. The Multiwfn[47-49] package was used to generate the $ICSS(1)_{zz}$ plot.

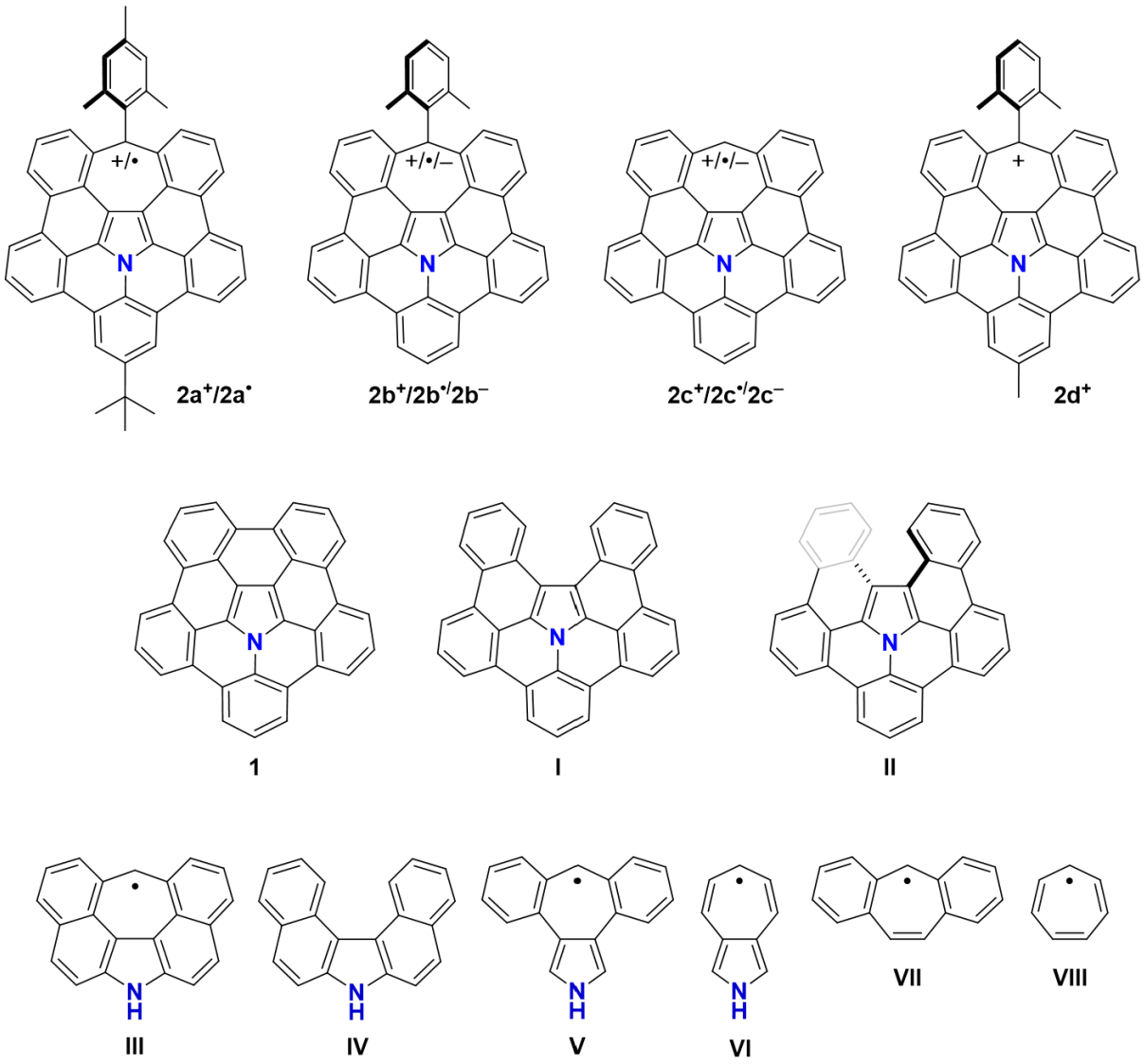

Figure S2.23. Compound names of the molecules used for theoretical calculations.

Note) The geometry of **I** is determined by removing the bridging CH group from **2c•** and manually attaching two hydrogen atoms, while the geometries of **II**–**VIII** were determined by structural optimization using the DFT methods.

5-1. Molecular Orbitals

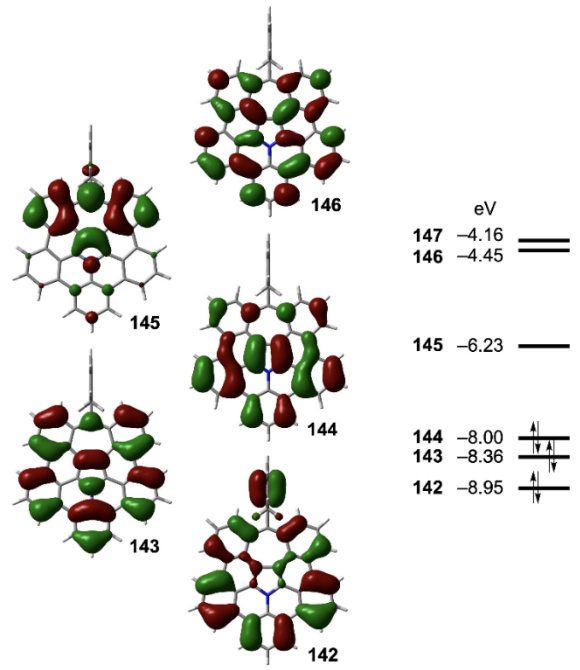

Figure S2.24. Kohn-Sham molecular orbitals of **2b**$^{+}$.

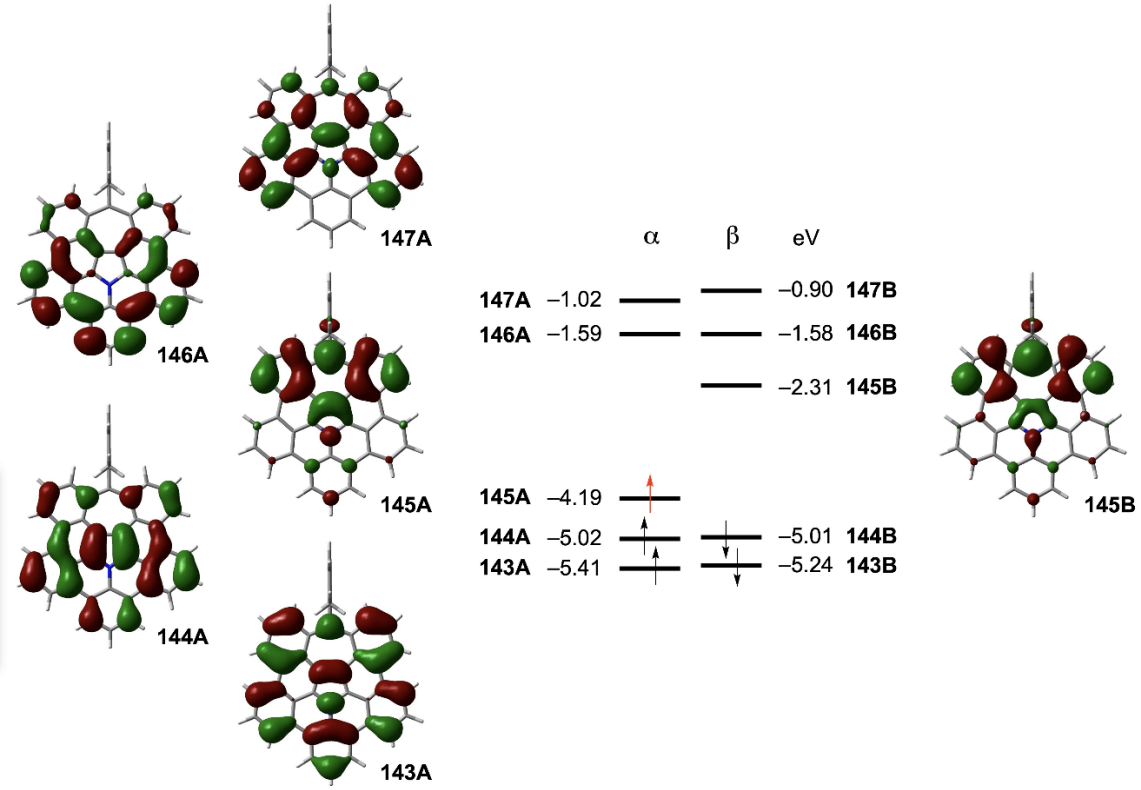

Figure S2.25. Kohn-Sham molecular orbitals of **2b**$^{\bullet}$.

5-2. Electrostatic Potential Map (ESP)

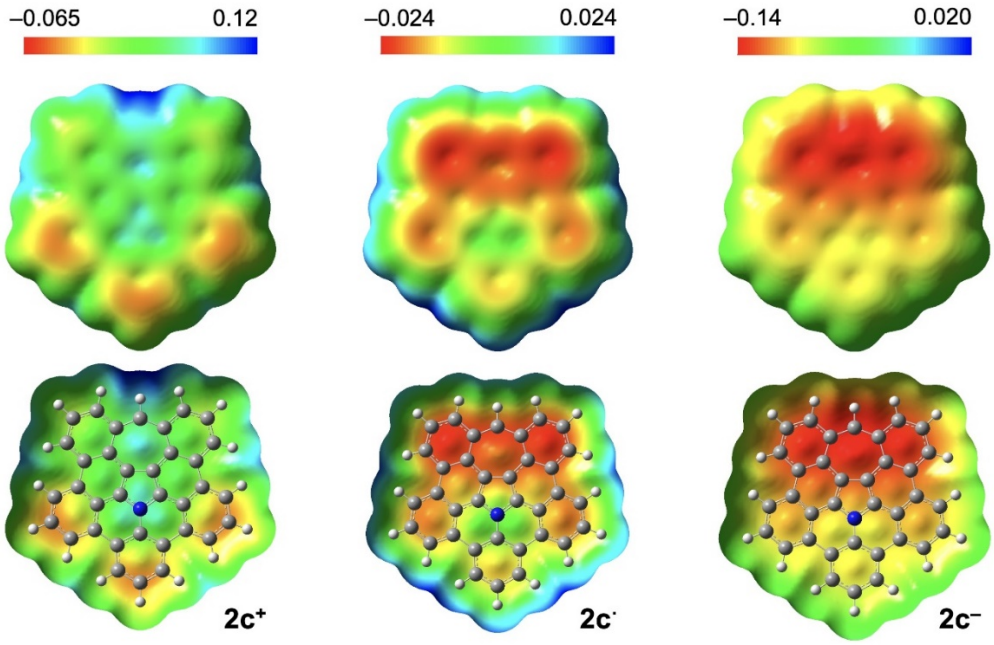

Figure S2.26. ESP map of **2c**$^{+}$ **2c**$^{\bullet}$, and **2c**$^{-}$.

5-3. Spin Density

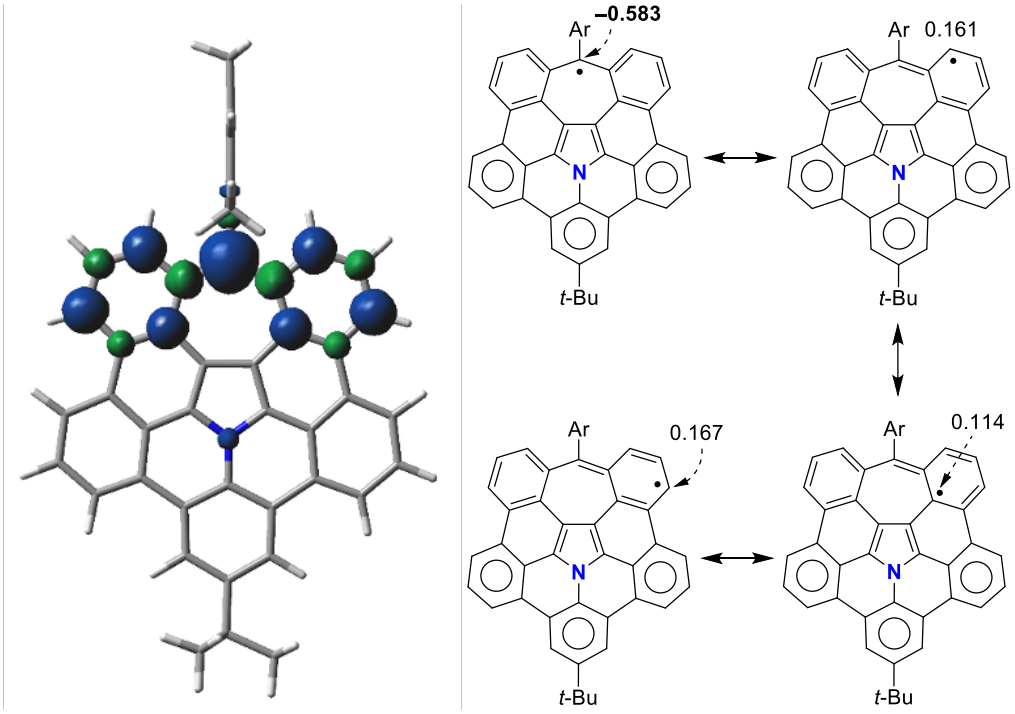

Figure S2.27. Spin density (isovalue = 0.0004) and major resonance structures of **2a**$^{\bullet}$. Numerals are calculated spin density.

5-4. NICS

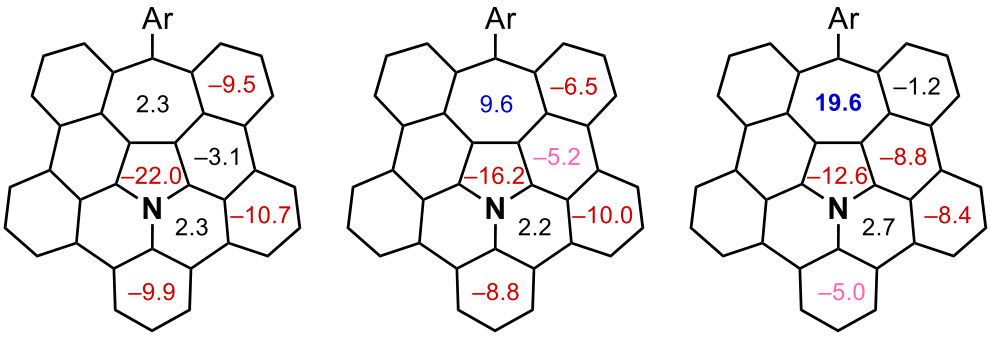

Figure S2.28. NICS(0) values of **2b**$^{+}$, **2b**$^{\bullet}$, and **2b**$^{-}$.

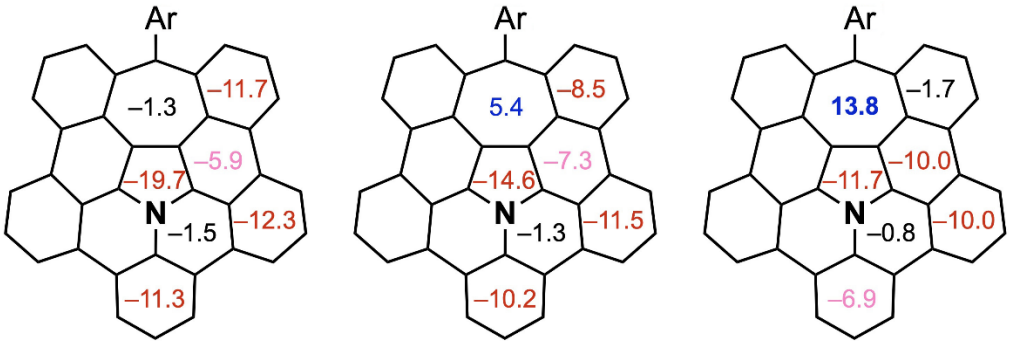

Figure S2.29. NICS(1) values of **2b**$^{+}$, **2b**$^{\bullet}$, and **2b**$^{-}$.

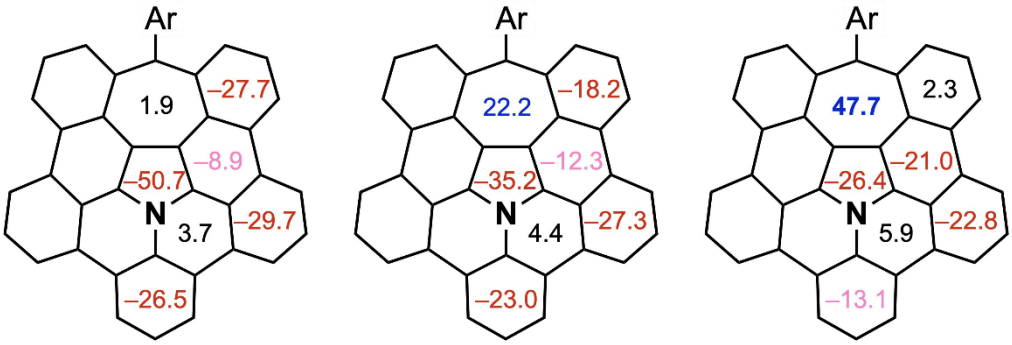

Figure S2.30. NICS(1)$_{zz}$ values of **2b**$^{+}$, **2b**$^{\bullet}$, and **2b**$^{-}$.

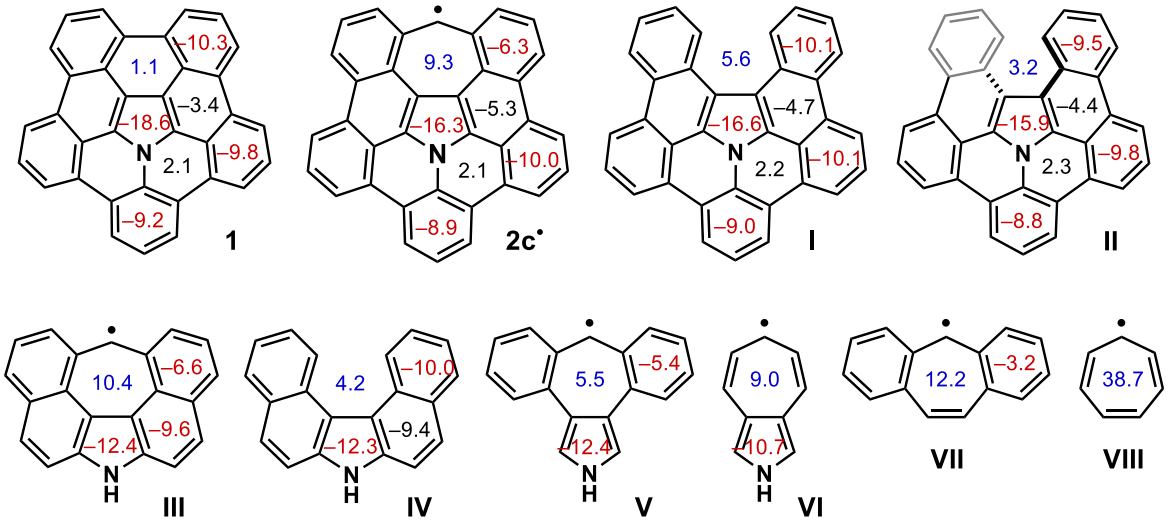

Figure S2.31. NICS(0) values of azacorannulene **1**, **2c•**, and fragmental molecules **I**–**VIII**.

Note) The value of the 7-membered ring in **2c•** (9.3) is higher than that in **I** (5.7), and the value in **III** (10.4) is higher than that in **IV** (4.2), indicating the bridging CH group in **2c•** contribute to enhance the shielding effect inside the 7-membered ring. On the other hand, the positive values of the 7-membered ring in **I** (5.7), **II** (3.2), and **IV** (4.2) indicate that even without the bridging CH group, there is a shielding effect by the adjacent aromatic rings.

5-5. TD-DFT

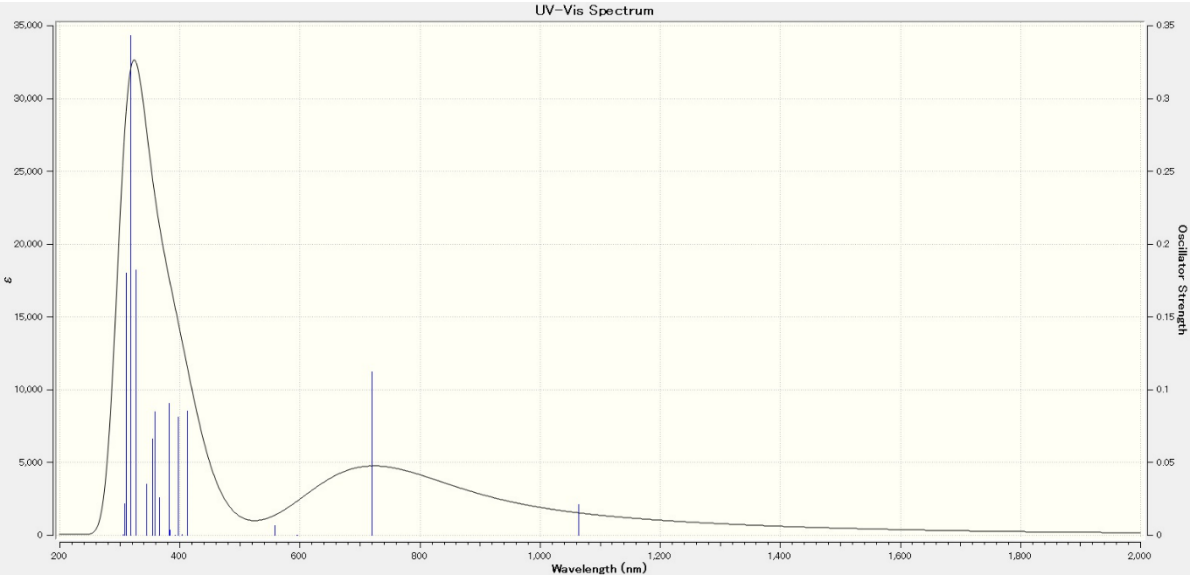

Figure S2.32. Simulated absorption spectrum of **2b**$^{+}$ calculated with B3LYP/6-311+G(2d,p).

Table S2.2. Selected wavelengths, oscillator strengths, major electronic transition of **2b**$^{+}$.

Excitation State	Wavelength (λ)	Oscillator Strengths (*f*)	Transitions
1	1063.97	0.0210	**144→145 (0.70341)**
2	719.49	0.1121	**143→145 (0.70131)**
3	596.24	0.0000	**140→145 (0.70500)**
4	594.66	0.0001	**141→145 (0.57798)** 142→145 (-0.40603)
5	558.16	0.0067	141→145 (0.40440) **142→145 (0.57230)**
6	411.68	0.0852	139→145 (0.37949) **144→146 (0.56600)** 144→147 (-0.11549)
8	397.29	0.0814	136→145 (0.10381) 138→145 (-0.39375) **139→145 (0.48871)** 144→146 (-0.27585) 144→147 (0.10273)
11	381.53	0.0904	136→145 (-0.14023) 138→145 (-0.30127) 139→145 (-0.17904) 143→148 (-0.12132) 144→146 (0.22288) **144→147 (0.53315)**
13	358.70	0.0849	**136→145 (0.67323)** 139→145 (-0.13320)

Table S2.3. TD-DFT calculations of **2b**$^+$ performed with various functionals and basis sets. The upper values present the wavelength of S_0–S_1 transition (nm) and the bottom values present wavelength of of S_0–S_2 transition (nm).

(A)

Basis set	Functional: B3LYP	B3LYP GD3BJ	B3LYP PCM (CH_2Cl_2)	B3LYP PCM (CH_3CN)
6-31G(d,p)	1038.65 703.33	---	---	---
6-311G(d,p)	1053.65 712.81	---	---	---
6-311+G(2d,p)	1063.97 719.49	1063.97 719.49	1040.54 718.24	1032.40 713.77
6-311++G(2d,2p)	1064.23 719.58	---	---	---
def2-SVP	1043.65 707.11	---	---	---
def2-TZVP	1061.84 717.58	---	---	---
cc-pVDZ	1048.71 710.02	---	---	---

Functional/Basis set // B3LYP/6-31G(d,p)

(B)

B3LYP	CAM-B3LYP	B3P86	B3PW91
1063.97 **719.49**	819.60 597.03	1060.01 717.63	1057.68 716.54
B97-1	B97D3	ωB97XD	
1050.39 711.97	1334.43 852.74	785.46 559.65	
M06	M06-2X	M06-HF	M08-HX
1002.68 689.57	849.53 592.00	712.02 505.39	849.27 596.00
MN15	O3LYP	PBE0	TPSSh
920.50 632.11	1147.53 763.90	1008.78 689.31	1144.40 763.21

Functional/6-311+G(2d,p) // B3LYP/6-31G(d,p)

Note) Structure of **2b**$^+$ was optimized with B3LYP/6-31G(d,p) and TD-DFT calculations were performed with the indicated functionals and basis sets.

	HF ratio	S0-S1	S1-S2
TPSSh	10	1144.40	763.21
O3LYP	11.6	1147.53	763.09
B3LYP	20	1063.97	719.49
B3BP86	20	1060.61	717.63
B3PW91	20	1057.68	716.54
B97-1	21	1050.39	711.97
PBE0	25	1008.78	689.31
M06	27	1002.68	689.57
MN15	44	920.50	632.11
M08-HX	52	849.27	596.00
M06-2X	54	849.53	592.00

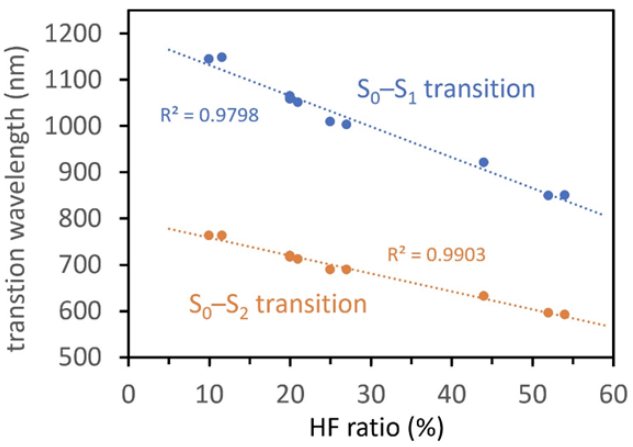

Figure S2.33. Correlation of S_0–S_1 (blue) and S_0–S_2 (orange) transition wavelengths (nm) and the ratio of Hartree-Fock (HF) exchange in the hybrid functionals used for TD-DFT calculations of **2b**$^+$.

Note) The simulated transitions are strongly correlated with the ratio of HF exchange in the hybrid functionals.

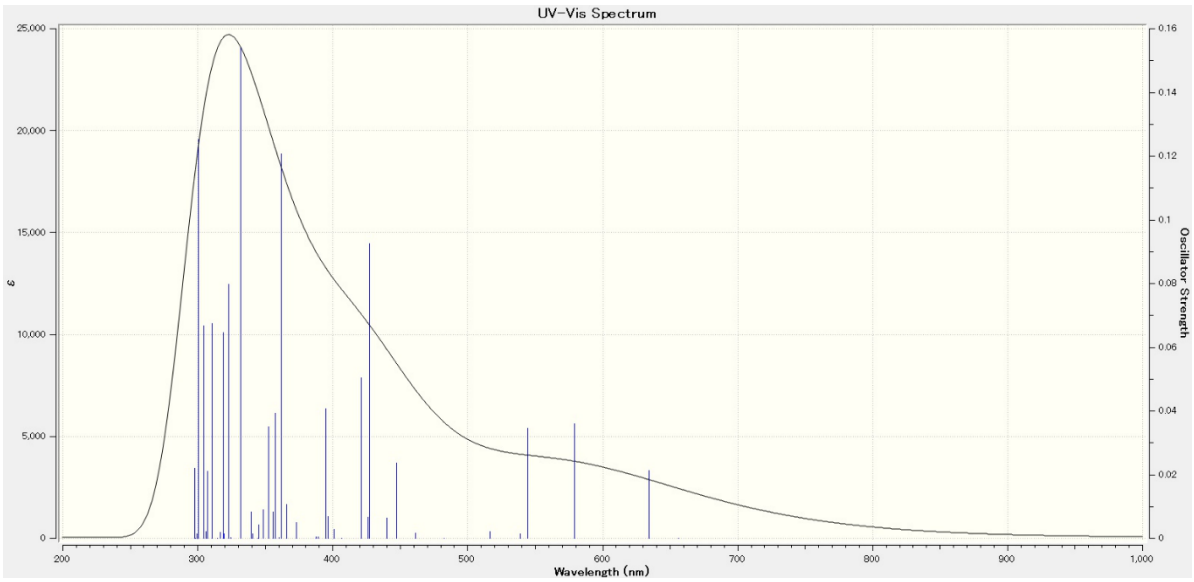

Figure S2.34. Simulated absorption spectrum of **2b•** calculated with B3LYP/6-311+G(2d,p).

Table S2.4. Selected wavelengths, oscillator strengths, major electronic transition of **2b•**.

Excitation State	Wavelength (λ)	Oscillator Strengths (*f*)	Transitions	
2	634.35	0.0212	**145A→146A (0.74186)** 145A→148A (0.27669)	143B→146B (0.12674) 144B→145B (-0.55793)
3	578.82	0.0360	142A→146A (-0.10194) 145A→146A (-0.14918) 145A→150A (-0.11332)	**143B→145B (0.92931)** 144B→146B (0.19396)
4	544.66	0.0345	143A→146A (-0.13655) 145A→146A (-0.19034) **145A→148A (0.86756)**	136B→145B (0.11687) 142B→145B (0.19688) 144B→145B (0.27595) 144B→147B (-0.12381)
9	447.09	0.0236	143A→150A (-0.11060) 144A→146A (0.54914) 144A→148A (-0.10118) 145A→150A (0.51661)	144B→146B (0.60295)
11	427.22	0.0926	142A→148A (0.11889) 143A→147A (-0.18856) 144A→146A (-0.24677) 144A→148A (-0.25838) 146A→149A (0.11355) 145A→150A (0.57558) 146A→158A (-0.10116)	138B→145B (-0.13020) 142B→146B (0.10822) 143B→150B (0.16887) 144B→146B (-0.41106) 144B→148B (-0.37143)
13	421.23	0.0236	142A→146A (-0.35035) 143A→147A (-0.17855) 143A→149A (0.22567) 144A→146A (0.40016) 144A→148A (-0.28546) 145A→147A (0.10437) 145A→150A (-0.38618)	137B→145B (-0.11220) 138B→145B (-0.13050) 142B→146B (0.33572) 142B→148B (-0.10173) 143B→145B (-0.11562) 143B→149B (-0.27788) 144B→148B (0.17047)
17	395.00	0.0926	**143A→146A (0.60056)** 144A→149A (-0.27428) 145A→151A (-0.39050)	143B→146B (0.46968) 144B→147B (-0.32970) 144B→149B (0.19624)

5-6. Cartesian Coordinates

2a•

C	-1.507870	2.384991	0.000002	C	4.818382	-0.003035	2.542992
C	-2.931184	2.521115	0.000001	C	4.818377	-0.003063	-2.542991
C	-3.768205	1.281590	0.000002	C	9.179125	-0.043867	-0.000004
C	-3.129997	0.016888	0.000002	C	-7.425914	-0.011585	0.000000
N	-1.767214	0.011702	0.000003	C	-8.052490	1.395826	-0.000007
C	-0.969341	1.107828	0.000003	C	-7.923771	-0.754539	1.262828
C	-0.553913	3.435958	0.000000	C	-7.923767	-0.754549	-1.262824
C	-1.107442	4.731152	-0.000002	H	-0.473473	5.611300	-0.000003
C	-2.492731	4.907524	-0.000001	H	-2.886492	5.919764	-0.000003
C	-3.401990	3.835783	0.000000	H	-4.466361	4.048935	0.000000
C	-3.776902	-1.247273	0.000001	H	-4.489885	-4.010352	-0.000007
C	-2.945826	-2.491964	-0.000001	H	-2.920895	-5.890732	-0.000010
C	-1.522110	-2.363506	0.000001	H	-0.506134	-5.595682	-0.000007
C	-0.976179	-1.089228	0.000003	H	-5.717539	2.173724	0.000001
C	-3.424224	-3.803527	-0.000005	H	-5.734555	-2.121323	-0.000001
C	-2.521307	-4.880803	-0.000007	H	4.716950	2.279383	-0.000013
C	-1.135221	-4.712031	-0.000005	H	3.956872	4.578201	-0.000013
C	-0.574315	-3.419922	0.000000	H	1.569339	5.149581	-0.000004
C	-5.171953	1.238989	0.000001	H	1.538896	-5.146163	0.000007
C	-5.882552	0.027533	0.000001	H	3.929668	-4.588737	0.000017
C	-5.175345	-1.191955	0.000000	H	4.703147	-2.294216	0.000016
C	0.361304	0.719097	0.000002	H	7.487061	-0.004159	-2.142393
C	0.356766	-0.708575	0.000002	H	7.487065	-0.004134	2.142388
C	1.347798	-1.717203	0.000002	H	5.523386	-0.004288	3.378646
C	1.358153	1.721818	0.000000	H	4.176510	0.878923	2.642250
C	2.756958	1.358540	-0.000002	H	4.170440	-0.880238	2.644849
C	3.651398	2.460117	-0.000008	H	4.170434	-0.880266	-2.644837
C	3.216070	3.783925	-0.000009	H	4.176505	0.878895	-2.642258
C	1.866091	4.106617	-0.000005	H	5.523378	-0.004325	-3.378648
C	0.892723	3.091212	-0.000001	H	9.590468	0.450115	-0.885511
C	0.874366	-3.083800	0.000002	H	9.590470	0.450125	0.885497
C	1.841707	-4.104946	0.000007	H	9.554997	-1.074896	0.000002
C	3.193539	-3.790119	0.000012	H	-7.768299	1.970230	-0.887766
C	3.636597	-2.468896	0.000011	H	-9.143684	1.310694	-0.000009
C	2.748693	-1.362055	0.000005	H	-7.768303	1.970236	0.887750
C	3.326414	-0.003479	0.000001	H	-7.556090	-1.783879	1.304425
C	4.839227	-0.008234	0.000001	H	-9.018748	-0.792830	1.275035
C	5.549132	-0.007937	-1.219876	H	-7.591415	-0.245088	2.173083
C	6.947964	-0.008089	-1.197271	H	-9.018745	-0.792842	-1.275032
C	7.668836	-0.011134	-0.000002	H	-7.591410	-0.245106	-2.173081
C	6.947967	-0.008076	1.197267	H	-7.556085	-1.783890	-1.304411
C	5.549133	-0.007923	1.219874				

2b+

C	-1.735071	-4.725089	0.000056	C	2.605486	3.756719	0.000056
C	-3.121209	-4.898327	0.000080	C	3.041989	2.446883	0.000043
C	-4.029151	-3.826241	0.000050	C	4.222536	0.000001	0.000007
C	-3.556943	-2.512026	-0.000013	C	4.915981	-0.000032	1.230516
C	-2.136581	-2.379166	-0.000050	C	6.315444	-0.000031	1.205123
C	-1.185059	-3.430161	-0.000011	C	7.013316	-0.000002	0.000028
C	-4.389309	-1.272404	-0.000019	C	6.315462	0.000029	-1.205078
C	-3.754266	-0.000001	-0.000048	C	4.915999	0.000033	-1.230492
N	-2.384123	-0.000001	-0.000095	C	4.184983	0.000083	-2.554119
C	-1.599439	-1.102544	-0.000096	C	4.184946	-0.000080	2.554134
C	-4.389310	1.272402	-0.000017	H	-1.104894	-5.607609	0.000097
C	-3.556945	2.512024	-0.000011	H	-3.515920	-5.909244	0.000133
C	-2.136582	2.379165	-0.000034	H	-5.092692	-4.039908	0.000084
C	-1.599439	1.102544	-0.000077	H	-6.368762	-2.144484	0.000041

C	-5.790802	-1.226858	0.000021	H	-7.547627	-0.000002	0.000069
C	-6.462560	-0.000002	0.000038	H	-6.368763	2.144480	0.000051
C	-5.790803	1.226855	0.000025	H	-5.092695	4.039905	0.000051
C	-4.029154	3.826239	0.000032	H	-3.515923	5.909243	0.000092
C	-3.121212	4.898325	0.000058	H	-1.104898	5.607609	0.000079
C	-1.735074	4.725088	0.000048	H	4.105751	-2.262051	-0.000022
C	-1.185061	3.430161	0.000003	H	3.336028	-4.558537	-0.000025
C	-0.263295	-0.720018	-0.000080	H	0.952568	-5.118619	-0.000025
C	-0.263295	0.720019	-0.000069	H	0.952564	5.118620	0.000048
C	0.726502	1.698736	-0.000023	H	3.336025	4.558540	0.000087
C	2.137353	1.340785	0.000002	H	4.105750	2.262054	0.000064
C	2.707982	0.000001	-0.000009	H	6.858374	-0.000055	2.145763
C	2.137354	-1.340782	-0.000026	H	8.098766	-0.000004	0.000036
C	0.726503	-1.698735	-0.000041	H	6.858406	0.000052	-2.145710
C	3.041991	-2.446880	-0.000022	H	4.892692	-0.000011	-3.385668
C	2.605488	-3.756716	-0.000025	H	3.543370	0.881187	-2.665029
C	1.240817	-4.073077	-0.000023	H	3.543173	-0.880880	-2.664995
C	0.261347	-3.081587	-0.000024	H	4.892644	0.000016	3.385692
C	0.261345	3.081588	0.000003	H	3.543334	-0.881184	2.665038
C	1.240814	4.073079	0.000037	H	3.543135	0.880884	2.665000

2b$^{\bullet}$

C	-1.736770	-4.722842	0.000002	C	2.587392	3.786359	0.000005
C	-3.122250	-4.897240	0.000007	C	3.025494	2.463618	0.000006
C	-4.029010	-3.823649	0.000008	C	4.220023	0.000003	0.000005
C	-3.554642	-2.510391	0.000007	C	4.925026	-0.000002	1.223889
C	-2.132211	-2.375697	0.000002	C	6.324946	-0.000006	1.204133
C	-1.180830	-3.428741	-0.000002	C	7.024893	-0.000004	0.000022
C	-4.390618	-1.271496	0.000008	C	6.324961	0.000002	-1.204097
C	-3.753140	-0.000002	0.000005	C	4.925041	0.000006	-1.223869
N	-2.389213	-0.000001	0.000002	C	4.189061	0.000007	-2.543994
C	-1.592969	-1.098726	0.000003	C	4.189033	0.000000	2.544006
C	-4.390620	1.271491	0.000003	H	-1.104256	-5.603992	0.000003
C	-3.554646	2.510387	-0.000002	H	-3.517803	-5.908716	0.000010
C	-2.132215	2.375695	-0.000002	H	-5.093983	-4.033676	0.000012
C	-1.592971	1.098725	0.000001	H	-6.368273	-2.145493	0.000015
C	-5.792728	-1.225565	0.000012	H	-7.552694	-0.000005	0.000016
C	-6.467041	-0.000005	0.000012	H	-6.368276	2.145484	0.000009
C	-5.792730	1.225557	0.000008	H	-5.093990	4.033669	-0.000013
C	-4.029017	3.823644	-0.000011	H	-3.517813	5.908712	-0.000026
C	-3.122258	4.897237	-0.000018	H	-1.104265	5.603992	-0.000024
C	-1.736778	4.722841	-0.000017	H	4.091517	-2.285839	-0.000036
C	-1.180836	3.428741	-0.000007	H	3.326325	-4.582317	-0.000048
C	-0.261306	-0.713852	0.000001	H	0.937218	-5.147543	-0.000036
C	-0.261307	0.713853	-0.000002	H	0.937209	5.147547	0.000000
C	0.733746	1.719145	-0.000003	H	3.326317	4.582324	0.000010
C	2.133575	1.359956	0.000000	H	4.091513	2.285847	0.000009
C	2.706605	0.000003	-0.000002	H	6.866949	-0.000012	2.146337
C	2.133577	-1.359951	-0.000013	H	8.111226	-0.000008	0.000029
C	0.733748	-1.719142	-0.000007	H	6.866974	0.000005	-2.146295
C	3.025499	-2.463611	-0.000027	H	4.891453	0.000047	-3.381836
C	2.587399	-3.786353	-0.000035	H	3.543965	0.879632	-2.642643
C	1.236707	-4.105415	-0.000026	H	3.544026	-0.879660	-2.642677
C	0.266054	-3.087422	-0.000011	H	4.891416	-0.000046	3.381855
C	0.266049	3.087425	-0.000004	H	3.543929	-0.879620	2.642647
C	1.236700	4.105419	0.000000	H	3.544004	0.879672	2.642683

2b^{-}

C	1.738197	4.721706	0.000007	C	-2.576021	-3.795128	0.000037
C	3.123266	4.898979	0.000013	C	-3.020995	-2.474098	0.000027

C	4.031691	3.825457	0.000004	C	-4.213108	0.000003	-0.000001
C	3.556117	2.511759	-0.000013	C	-4.932399	0.000023	1.217670
C	2.131498	2.374094	-0.000025	C	-6.333109	0.000021	1.203058
C	1.176718	3.427294	-0.000011	C	-7.036056	-0.000001	0.000003
C	4.393424	1.274214	-0.000012	C	-6.333112	-0.000022	-1.203054
C	3.750252	-0.000003	-0.000023	C	-4.932402	-0.000021	-1.217670
N	2.397097	-0.000001	-0.000046	C	-4.191640	-0.000046	-2.534268
C	1.591450	1.098545	-0.000042	C	-4.191633	0.000048	2.534266
C	4.393422	-1.274220	-0.000005	H	1.101805	5.600394	0.000019
C	3.556113	-2.511764	0.000001	H	3.518171	5.912074	0.000027
C	2.131493	-2.374096	-0.000011	H	5.097920	4.033815	0.000014
C	1.591448	-1.098546	-0.000035	H	6.369418	2.147334	0.000017
C	5.795014	1.225672	0.000008	H	7.558652	-0.000006	0.000034
C	6.472110	-0.000005	0.000019	H	6.369413	-2.147345	0.000028
C	5.795012	-1.225681	0.000015	H	5.097913	-4.033823	0.000036
C	4.031683	-3.825463	0.000026	H	3.518159	-5.912078	0.000060
C	3.123256	-4.898983	0.000041	H	1.101794	-5.600394	0.000053
C	1.738187	-4.721708	0.000036	H	-4.090043	2.309226	-0.000014
C	1.176711	-3.427294	0.000011	H	-3.322202	4.588164	-0.000010
C	0.260435	0.716255	-0.000031	H	-0.928898	5.172788	-0.000006
C	0.260434	-0.716254	-0.000026	H	-0.928908	-5.172784	0.000038
C	-0.738692	-1.728704	-0.000003	H	-3.322211	-4.588154	0.000052
C	-2.141701	-1.348186	0.000006	H	-4.090048	-2.309215	0.000037
C	-2.699281	0.000003	-0.000003	H	-6.874694	0.000036	2.147202
C	-2.141699	1.348192	-0.000009	H	-8.123786	-0.000003	0.000004
C	-0.738689	1.728708	-0.000016	H	-6.874700	-0.000039	-2.147197
C	-3.020991	2.474107	-0.000011	H	-4.890138	-0.000035	-3.378213
C	-2.576013	3.795135	-0.000009	H	-3.544274	-0.878936	-2.619890
C	-1.230124	4.131246	-0.000008	H	-3.544230	0.878811	-2.619901
C	-0.270078	3.095476	-0.000012	H	-4.890130	0.000034	3.378214
C	-0.270084	-3.095474	0.000011	H	-3.544270	0.878941	2.619888
C	-1.230132	-4.131241	0.000030	H	-3.544221	-0.878806	2.619896

2c$^+$

C	4.730935	-0.467598	0.000010	C	1.330954	3.372611	-0.000016
C	4.903265	-1.854574	0.000021	C	1.704083	1.972963	-0.000025
C	3.831623	-2.763377	0.000016	C	2.394615	4.318248	-0.000006
C	2.516123	-2.293039	-0.000005	C	3.712804	3.905150	-0.000002
C	2.384024	-0.872277	-0.000023	C	4.052487	2.539171	-0.000006
C	3.436937	0.082470	-0.000012	C	3.086736	1.529932	-0.000016
C	1.274838	-3.127755	-0.000001	C	-3.086736	1.529931	0.000000
C	0.000000	-2.495835	-0.000014	C	-4.052487	2.539171	0.000015
N	0.000000	-1.127315	-0.000041	C	-3.712804	3.905150	0.000016
C	1.103519	-0.343414	-0.000043	C	-2.394616	4.318248	0.000006
C	-1.274838	-3.127755	0.000006	H	5.612707	0.164095	0.000020
C	-2.516123	-2.293039	0.000007	H	5.914050	-2.249530	0.000037
C	-2.384024	-0.872277	-0.000010	H	4.046957	-3.826608	0.000030
C	-1.103519	-0.343414	-0.000036	H	2.144723	-5.108782	0.000035
C	1.228089	-4.529218	0.000024	H	0.000000	-6.284828	0.000057
C	0.000000	-5.199780	0.000038	H	-2.144723	-5.108782	0.000046
C	-1.228089	-4.529218	0.000031	H	-4.046957	-3.826608	0.000049
C	-3.831623	-2.763377	0.000034	H	-5.914050	-2.249530	0.000065
C	-4.903265	-1.854574	0.000044	H	-5.612707	0.164095	0.000046
C	-4.730935	-0.467598	0.000033	H	2.160986	5.378521	0.000000
C	-3.436937	0.082470	0.000006	H	4.506993	4.643764	0.000006
C	0.721184	0.990079	-0.000042	H	5.105151	2.276254	0.000000
C	-0.721184	0.990079	-0.000037	H	-5.105151	2.276254	0.000026
C	-1.704083	1.972963	-0.000017	H	-4.506994	4.643764	0.000028
C	-1.330954	3.372611	-0.000010	H	-2.160986	5.378521	0.000010
C	0.000000	3.884659	-0.000013	H	0.000000	4.973869	-0.000005

2c$^{\bullet}$

C	4.727536	-0.467664	0.000012	C	1.347692	3.373779	-0.000015
C	4.901623	-1.853782	0.000023	C	1.723048	1.984062	-0.000025
C	3.828617	-2.761734	0.000016	C	2.415588	4.300656	-0.000003
C	2.514142	-2.289479	-0.000007	C	3.745957	3.884599	0.000001
C	2.379783	-0.866574	-0.000026	C	4.087531	2.533500	-0.000003
C	3.434114	0.088149	-0.000012	C	3.091186	1.536044	-0.000015
C	1.273686	-3.127854	-0.000003	C	-3.091186	1.536044	0.000001
C	0.000000	-2.493175	-0.000019	C	-4.087531	2.533500	0.000017
N	0.000000	-1.130865	-0.000051	C	-3.745957	3.884599	0.000020
C	1.099370	-0.334898	-0.000049	C	-2.415588	4.300656	0.000008
C	-1.273686	-3.127854	0.000004	H	5.607694	0.166762	0.000024
C	-2.514142	-2.289479	0.000006	H	5.913102	-2.249341	0.000042
C	-2.379783	-0.866574	-0.000014	H	4.040436	-3.826415	0.000032
C	-1.099370	-0.334898	-0.000043	H	2.145758	-5.106849	0.000039
C	1.226601	-4.529971	0.000026	H	0.000000	-6.288995	0.000064
C	0.000000	-5.203341	0.000041	H	-2.145758	-5.106849	0.000051
C	-1.226601	-4.529971	0.000033	H	-4.040436	-3.826415	0.000051
C	-3.828617	-2.761734	0.000035	H	-5.913102	-2.249341	0.000070
C	-4.901623	-1.853782	0.000047	H	-5.607694	0.166762	0.000051
C	-4.727536	-0.467664	0.000035	H	2.189514	5.363527	0.000003
C	-3.434114	0.088149	0.000006	H	4.534651	4.631291	0.000010
C	0.714392	0.994262	-0.000043	H	5.136248	2.256399	0.000003
C	-0.714392	0.994262	-0.000039	H	-5.136248	2.256399	0.000029
C	-1.723048	1.984062	-0.000017	H	-4.534651	4.631291	0.000032
C	-1.347692	3.373779	-0.000009	H	-2.189514	5.363527	0.000013
C	0.000000	3.895337	-0.000014	H	0.000000	4.984230	-0.000009

2c^{-}

C	4.726351	-0.468644	0.000017	C	1.337275	3.386008	-0.000013
C	4.903617	-1.854098	0.000029	C	1.732340	1.992022	-0.000025
C	3.830375	-2.763772	0.000019	C	2.433107	4.295716	-0.000002
C	2.515537	-2.290165	-0.000009	C	3.759553	3.871545	0.000003
C	2.377844	-0.864839	-0.000030	C	4.117362	2.524064	-0.000001
C	3.432322	0.093043	-0.000011	C	3.100252	1.540956	-0.000014
C	1.276647	-3.129663	-0.000006	C	-3.100252	1.540956	0.000001
C	0.000000	-2.488315	-0.000025	C	-4.117362	2.524064	0.000020
N	0.000000	-1.137594	-0.000062	C	-3.759553	3.871545	0.000022
C	1.099308	-0.331575	-0.000058	C	-2.433107	4.295716	0.000009
C	-1.276647	-3.129663	0.000001	H	5.603935	0.169903	0.000032
C	-2.515537	-2.290165	0.000004	H	5.916792	-2.249124	0.000051
C	-2.377844	-0.864839	-0.000017	H	4.040271	-3.829833	0.000036
C	-1.099308	-0.331575	-0.000050	H	2.147777	-5.106669	0.000041
C	1.226696	-4.531062	0.000026	H	0.000000	-6.294313	0.000067
C	0.000000	-5.207714	0.000042	H	-2.147777	-5.106669	0.000053
C	-1.226696	-4.531062	0.000033	H	-4.040271	-3.829833	0.000056
C	-3.830375	-2.763772	0.000038	H	-5.916792	-2.249124	0.000079
C	-4.903617	-1.854098	0.000053	H	-5.603935	0.169903	0.000060
C	-4.726351	-0.468643	0.000040	H	2.218257	5.362385	0.000004
C	-3.432322	0.093043	0.000007	H	4.546562	4.624702	0.000012
C	0.717282	0.997523	-0.000047	H	5.164882	2.242708	0.000005
C	-0.717282	0.997523	-0.000043	H	-5.164881	2.242708	0.000032
C	-1.732340	1.992022	-0.000017	H	-4.546562	4.624702	0.000035
C	-1.337275	3.386008	-0.000008	H	-2.218257	5.362385	0.000014
C	0.000000	3.901435	-0.000013	H	0.000000	4.992160	-0.000007

1

C	0.953076	0.989157	0.699269	C	-1.534303	-0.568490	-4.748033

C	-0.360490	0.940365	1.114365	C	-0.170810	-0.362358	4.516937
N	-1.168340	0.935295	0.000000	C	-1.534303	-0.568490	4.748033
C	-0.360490	0.940365	-1.114365	C	-2.510005	-0.391721	3.752894
C	0.953076	0.989157	-0.699269	C	2.798123	-0.379643	3.552280
C	2.004049	0.475961	1.462495	C	4.036389	-0.568938	2.932494
C	1.706995	0.117919	2.816833	C	4.238693	-0.361635	1.557595
C	0.282443	0.111460	3.273004	C	4.238693	-0.361635	-1.557595
C	-0.765334	0.431864	2.342993	C	4.036389	-0.568938	-2.932494
C	-0.765334	0.431864	-2.342993	C	2.798123	-0.379643	-3.552280
C	0.282443	0.111460	-3.273004	H	-4.863798	-0.584333	2.142032
C	1.706995	0.117919	-2.816833	H	-6.023050	-0.864117	0.000000
C	2.004049	0.475961	-1.462495	H	-4.863798	-0.584333	-2.142032
C	-2.437875	0.414531	0.000000	H	-3.536891	-0.669199	-3.969247
C	-3.009460	0.102355	-1.269200	H	0.535612	-0.609238	-5.303480
C	-2.143798	0.092049	-2.493579	H	-1.846621	-0.938667	-5.720081
C	-2.143798	0.092049	2.493579	H	0.535612	-0.609238	5.303480
C	-3.009460	0.102355	1.269200	H	-1.846621	-0.938667	5.720081
C	3.206816	0.138843	-0.754850	H	-3.536891	-0.669199	3.969247
C	3.206816	0.138843	0.754850	H	2.685748	-0.659246	4.595447
C	-4.339143	-0.344315	1.223016	H	4.860668	-0.955976	3.524544
C	-4.992205	-0.523459	0.000000	H	5.196788	-0.635276	1.125999
C	-4.339143	-0.344315	-1.223016	H	5.196788	-0.635276	-1.125999
C	-2.510005	-0.391721	-3.752894	H	2.685748	-0.659246	-4.595447
C	-0.170810	-0.362358	-4.516937	H	4.860668	-0.955976	-3.524544

I

C	4.727536	-0.467664	0.000012	C	1.723048	1.984062	-0.000025
C	4.901623	-1.853782	0.000023	C	2.415588	4.300656	-0.000003
C	3.828617	-2.761734	0.000016	C	3.745957	3.884599	0.000001
C	2.514142	-2.289479	-0.000007	C	4.087531	2.533500	-0.000003
C	2.379783	-0.866574	-0.000026	C	3.091186	1.536044	-0.000015
C	3.434114	0.088149	-0.000012	C	-3.091186	1.536044	0.000001
C	1.273686	-3.127854	-0.000003	C	-4.087531	2.533500	0.000017
C	0.000000	-2.493175	-0.000019	C	-3.745957	3.884599	0.000020
N	0.000000	-1.130865	-0.000051	C	-2.415588	4.300656	0.000008
C	1.099370	-0.334898	-0.000049	H	5.607694	0.166762	0.000024
C	-1.273686	-3.127854	0.000004	H	5.913102	-2.249341	0.000042
C	-2.514142	-2.289479	0.000006	H	4.040436	-3.826415	0.000032
C	-2.379783	-0.866574	-0.000014	H	2.145758	-5.106849	0.000039
C	-1.099370	-0.334898	-0.000043	H	0.000000	-6.288995	0.000064
C	1.226601	-4.529971	0.000026	H	-2.145758	-5.106849	0.000051
C	0.000000	-5.203341	0.000041	H	-4.040436	-3.826415	0.000051
C	-1.226601	-4.529971	0.000033	H	-5.913102	-2.249341	0.000070
C	-3.828617	-2.761734	0.000035	H	-5.607694	0.166762	0.000051
C	-4.901623	-1.853782	0.000047	H	2.189514	5.363527	0.000003
C	-4.727536	-0.467664	0.000035	H	4.534651	4.631291	0.000010
C	-3.434114	0.088149	0.000006	H	5.136248	2.256399	0.000003
C	0.714392	0.994262	-0.000043	H	-5.136248	2.256399	0.000029
C	-0.714392	0.994262	-0.000039	H	-4.534651	4.631291	0.000032
C	-1.723048	1.984062	-0.000017	H	-2.189514	5.363527	0.000013
C	-1.347692	3.373779	-0.000009	H	-0.335988	3.763023	-0.000016
C	1.347692	3.373779	-0.000015	H	0.335988	3.763023	-0.000018

II

C	-0.734241	-1.189371	0.013660	C	3.477585	-0.151763	0.093730
N	0.000000	0.955223	0.000001	C	4.751665	0.437609	0.195249
C	-1.103799	0.158283	-0.010318	C	4.889293	1.822593	0.247579
C	-1.854516	-2.113406	0.120517	C	3.784631	2.682642	0.199104
C	-3.200522	-1.594164	0.020682	C	2.492227	2.162536	0.105295
C	-4.271506	-2.509961	0.091993	C	1.257373	2.980917	0.052540

C	-4.076639	-3.865264	0.295127	C	0.000000	2.328312	0.000000
C	-2.776075	-4.354886	0.467327	C	1.217893	4.383023	0.050354
C	-1.697551	-3.491089	0.385845	C	0.000001	5.063127	0.000000
C	-2.378292	0.739763	-0.062971	H	-5.287822	-2.142535	0.004452
C	-3.477585	-0.151762	-0.093730	H	-4.929494	-4.535135	0.346596
C	-4.751665	0.437610	-0.195249	H	-2.608820	-5.407501	0.675956
C	-4.889293	1.822594	-0.247579	H	-0.704594	-3.874754	0.572850
C	-3.784630	2.682643	-0.199104	H	-5.646183	-0.173449	-0.233838
C	-2.492227	2.162536	-0.105295	H	-5.884552	2.249947	-0.326136
C	-1.257373	2.980917	-0.052540	H	-3.948780	3.754238	-0.241184
C	-1.217893	4.383023	-0.050355	H	-2.140289	4.952463	-0.085942
C	0.734240	-1.189372	-0.013658	H	5.287822	-2.142535	-0.004456
C	1.103799	0.158283	0.010319	H	4.929493	-4.535136	-0.346599
C	1.854516	-2.113406	-0.120516	H	2.608819	-5.407502	-0.675955
C	3.200522	-1.594164	-0.020683	H	0.704593	-3.874755	-0.572847
C	4.271505	-2.509961	-0.091995	H	5.646183	-0.173450	0.233839
C	4.076639	-3.865265	-0.295129	H	5.884553	2.249946	0.326137
C	2.776074	-4.354886	-0.467326	H	3.948781	3.754238	0.241184
C	1.697550	-3.491089	-0.385843	H	2.140290	4.952462	0.085941
C	2.378292	0.739763	0.062971	H	0.000001	6.148719	-0.000001

III

C	2.484040	2.527932	-0.000001	C	-4.068643	-0.858127	0.000008
N	-0.000001	2.946715	-0.000011	C	-3.725652	-2.197442	-0.000006
C	1.127836	2.147883	-0.000008	C	-2.381468	-2.579837	-0.000012
C	3.422196	1.524348	0.000006	C	-1.323414	-1.644827	-0.000002
C	-2.484043	2.527930	0.000002	C	0.000002	-2.183225	-0.000008
C	-1.127839	2.147882	-0.000009	H	2.775951	3.573953	0.000000
C	-3.422199	1.524346	0.000014	H	-0.000002	3.953575	-0.000016
C	0.719766	0.798998	-0.000002	H	4.479198	1.774808	0.000006
C	-0.719768	0.798997	-0.000003	H	-2.775955	3.573951	-0.000003
C	-1.680775	-0.243646	0.000007	H	-4.479200	1.774803	0.000014
C	1.680775	-0.243644	0.000003	H	2.132331	-3.637306	0.000015
C	1.323418	-1.644826	0.000003	H	4.499199	-2.959738	0.000014
C	2.381472	-2.579835	0.000003	H	5.111307	-0.553038	-0.000002
C	3.725654	-2.197441	0.000003	H	-5.111307	-0.553041	0.000020
C	4.068644	-0.858125	0.000002	H	-4.499194	-2.959743	-0.000012
C	3.061481	0.140792	0.000003	H	-2.132328	-3.637308	-0.000023
C	-3.061482	0.140789	0.000011	H	0.000002	-3.271455	-0.000021

IV

C	2.449810	2.405057	-0.281479	C	-4.184341	-0.881978	0.098772
N	0.000000	2.769004	0.000000	C	-3.947861	-2.202710	-0.214424
C	1.118121	1.973564	-0.104962	C	-2.635205	-2.612772	-0.522598
C	3.429390	1.449900	-0.344868	C	-1.583874	-1.719816	-0.454520
C	-2.449810	2.405057	0.281479	H	2.680864	3.462272	-0.374998
C	-1.118121	1.973564	0.104962	H	0.000000	3.775927	-0.000001
C	-3.429390	1.449900	0.344868	H	4.464932	1.738365	-0.501027
C	0.728591	0.616889	-0.028279	H	-2.680864	3.462272	0.374998
C	-0.728591	0.616889	0.028279	H	-4.464932	1.738365	0.501026
C	-1.776650	-0.368523	-0.067628	H	0.597475	-2.049335	0.749548
C	1.776650	-0.368523	0.067628	H	2.447183	-3.637008	0.831749
C	1.583874	-1.719816	0.454520	H	4.767217	-2.914006	0.255395
C	2.635205	-2.612772	0.522598	H	5.197396	-0.537099	-0.290566
C	3.947861	-2.202710	0.214424	H	-5.197396	-0.537099	0.290565
C	4.184341	-0.881978	-0.098772	H	-4.767217	-2.914006	-0.255395
C	3.131673	0.066611	-0.148456	H	-2.447183	-3.637008	-0.831749
C	-3.131673	0.066611	0.148456	H	-0.597475	-2.049335	-0.749548

V

C	-1.312946	-1.168740	0.200758	C	1.118313	2.621462	0.203449
C	0.000000	-1.679635	0.434188	N	0.000000	3.402011	0.300595
C	1.312946	-1.168740	0.200758	C	-1.118313	2.621462	0.203449
C	1.667699	0.187509	-0.093291	H	0.000000	-2.734286	0.701776
C	0.723435	1.301987	0.031152	H	2.104272	-3.157786	0.477500
C	-0.723435	1.301987	0.031153	H	4.439584	-2.587582	-0.051860
C	-1.667699	0.187509	-0.093291	H	5.014997	-0.237106	-0.705288
C	2.363637	-2.132341	0.228485	H	3.262530	1.481355	-0.725080
C	3.674590	-1.817071	-0.074053	H	-3.262530	1.481355	-0.725080
C	3.997982	-0.502082	-0.432544	H	-5.014997	-0.237106	-0.705288
C	3.001808	0.468092	-0.437110	H	-4.439584	-2.587582	-0.051860
C	-3.001808	0.468092	-0.437110	H	-2.104272	-3.157786	0.477500
C	-3.997982	-0.502082	-0.432544	H	2.102978	3.050074	0.302171
C	-3.674590	-1.817071	-0.074053	H	0.000000	4.394324	0.471900
C	-2.363637	-2.132341	0.228485	H	-2.102978	3.050074	0.302172

VI

C	-1.936521	1.277051	-0.000002	C	1.855426	-1.123550	-0.000001
C	-0.602682	1.619174	-0.000002	H	-2.632210	2.114752	-0.000004
C	0.528925	0.727220	0.000004	H	-0.363560	2.680406	-0.000002
C	0.528925	-0.727220	0.000004	H	-0.363560	-2.680406	-0.000002
C	-0.602682	-1.619174	-0.000002	H	-2.632210	-2.114752	-0.000004
C	-1.936521	-1.277051	-0.000002	H	-3.632366	0.000000	0.000021
C	-2.545362	0.000000	0.000002	H	2.284655	2.114557	0.000016
C	1.855426	1.123550	-0.000002	H	3.653939	0.000000	0.000005
N	2.647292	0.000000	-0.000004	H	2.284655	-2.114557	0.000016

VII

C	1.311692	-0.630157	0.000006	C	3.717362	-1.158887	-0.000007
C	0.000000	-1.188981	0.000014	C	2.391218	-1.557190	0.000000
C	-1.311692	-0.630157	0.000006	H	0.000000	-2.276856	0.000031
C	-1.646695	0.766251	0.000001	H	-1.135215	2.835611	0.000015
C	-0.676498	1.848393	0.000008	H	1.135215	2.835611	0.000015
C	0.676498	1.848393	0.000009	H	-2.152347	-2.617076	0.000004
C	1.646695	0.766251	0.000002	H	-4.505735	-1.905942	-0.000008
C	-2.391218	-1.557190	0.000001	H	-5.069346	0.532778	-0.000017
C	-3.717362	-1.158887	-0.000007	H	-3.242770	2.197421	-0.000010
C	-4.034804	0.204600	-0.000011	H	3.242770	2.197421	-0.000009
C	-3.002466	1.137421	-0.000007	H	5.069346	0.532778	-0.000016
C	3.002466	1.137421	-0.000006	H	4.505735	-1.905942	-0.000009
C	4.034804	0.204600	-0.000011	H	2.152347	-2.617076	0.000002

VIII

C	-1.184990	-1.095021	0.000001	H	-1.993298	-1.825712	0.000002
C	0.086610	-1.623258	-0.000001	H	0.166791	-2.706781	-0.000004
C	1.344459	-0.903283	0.000000	H	2.232284	-1.532600	0.000004
C	1.558806	0.440054	0.000000	H	2.598386	0.761839	0.000004
C	0.587452	1.515711	-0.000001	H	1.000830	2.520485	-0.000004
C	-0.785382	1.409402	0.000001	H	-1.326177	2.355348	0.000002
C	-1.606914	0.256388	-0.000001	H	-2.679069	0.427461	0.000003

5-7. Vibronic Spectra Calculations

All calculations were done with TURBOMOLE[57].

Geometry Optimizations: Ground state equilibrium structures were optimized using DFT, equilibrium structures for S_1 and S_2 were computed by TD-DFT. Both calculations employed the PBE0 hybrid approximation to the exchange-correlation[58,59] and the def2-SVP[60,61] basis set. The resolution of identity[62,63] approximation and dispersion correction[64,65] was used. Excited state gradients and energies were computed using the Langrangian formualtion of TD-DFT[66,67], as implemented in TURBOMOLE. Ground and excited state frequencies were computed using the aoforce and Num-Force modules, respectively[68].

Second-Order Approximate Coupled Cluster (CC2): Ground and excited state energies for the (TD)DFT equilibrium structures were computed using the CC2 within the resolution of identity method[69,70]. Calculations employed the def2-TZVP basis set.

Vibronic spectra calculations: Vibronic spectra calculations employed the RADLESS module of TURBOMOLE[71,72], which has been shown to reproduce the experimentally observed vibronic envelope structure in various rigid molecules[73,74]. (TD)DFT optimized structures and vibrational frequencies were used. Vibronic absorption spectra were computed for the $S_0 \rightarrow S_1$ and $S_0 \rightarrow S_2$ separately, and then superimposed to yield the overall absorption spectrum.

Results: Cartesian coordinates ground and excited state equilibrium structures are given in **Table S2.5**. Vibrational frequencies for all electronic states are given in **Tables S2.6–S2.11**. Spectra were computed using two different lifetimes: Using a lifetime $\tau = 400$ au yields good agreement with the experimentally observed envelope of the absorption spectrum. The lifetime of 100000 au allows to resolve the individual vibronic transitions. Vibronic spectra were calculated using a (TD)DFT structures and vibrational frequencies (**Figure S2.35**). In addition, vibronic spectra were calculated using a mixed (TD)DFT/CC2 approach, in which structures

and vibrational frequencies computed by (TD)DFT (PBE0/def2-SVP) were used in combination with the adiabatic excitation energies computed by CC2 (**Figure S2.36**). With respect to the lowest three absorption bands, the mixed approach is slightly more accurate than the pure (TD)DFT approach (**Table S2.12**), underestimating the peak positions between 0.10 and 0.14 eV, whereas (TD)DFT overestimates the position by 0.18–0.19 eV. The CC2 excitation energies are slightly more accurate of the previously determined overall accuracy of this method, which has been found to be within a mean absolute error of 0.21 eV with respect to experimental adiabatic excitation energies[75].

Table S2.5. Cartesian coordinates (Å) of the ground and excited state equilibrium structures of **2d**$^{+}$ computed by (TD)PBE0/def2-SVP and used in vibronic spectra calculations.

	S_0 structure			S_1 structure			S_2 structure		
C	-1.7190092	-4.7166057	0.0000444	-1.6717228	-4.6899350	0.0000453	-1.6718911	-4.7223596	0.0000437
C	-3.1039454	-4.8891912	0.0000675	-3.0678480	-4.8654390	0.0000660	-3.0537258	-4.8982942	0.0000677
C	-4.0111850	-3.8187490	0.0000445	-3.9814934	-3.8076978	0.0000427	-3.9603946	-3.8252842	0.0000469
C	-3.5389406	-2.5058438	-0.0000044	-3.5110237	-2.4912855	-0.0000042	-3.4901770	-2.5059730	-0.0000024
C	-2.1217637	-2.3756369	-0.0000315	-2.0833463	-2.3580747	-0.0000299	-2.0747420	-2.3724897	-0.0000309
C	-1.1699002	-3.4232086	-0.0000060	-1.1235723	-3.4079071	-0.0000028	-1.1196279	-3.4202452	-0.0000053
C	-4.3675395	-1.2697883	-0.0000105	-4.3409922	-1.2658037	-0.0000100	-4.3236785	-1.2788812	-0.0000079
C	-3.7325140	0.0000042	-0.0000352	-3.7082060	-0.0000004	-0.0000354	-3.6828229	-0.0000024	-0.0000334
N	-2.3685882	-0.0000140	-0.0000681	-2.3476815	-0.0000005	-0.0000716	-2.3352735	0.0000031	-0.0000690
C	-1.5878974	-1.0977598	-0.0000653	-1.5557326	-1.0893188	-0.0000622	-1.5408304	-1.0966010	-0.0000663
C	-4.3675411	1.2697798	-0.0000130	-4.3409923	1.2658011	-0.0000117	-4.3236815	1.2788789	-0.0000101
C	-3.5389467	2.5058480	-0.0000090	-3.5110250	2.4912802	-0.0000068	-3.4901701	2.5059793	-0.0000063
C	-2.1217545	2.3756149	-0.0000294	-2.0833479	2.3580762	-0.0000248	-2.0747730	2.3725045	-0.0000281
C	-1.5879094	1.0977873	-0.0000636	-1.5557318	1.0893181	-0.0000586	-1.5407844	1.0965719	-0.0000639
C	-5.7673560	-1.2252771	0.0000219	-5.7462858	-1.2230562	0.0000247	-5.7212032	-1.2289826	0.0000240
C	-6.4386770	-0.0000044	0.0000343	-6.4207769	-0.0000036	0.0000377	-6.3900166	-0.0000025	0.0000357
C	-5.7673553	1.2252779	0.0000205	-5.7462867	1.2230549	0.0000230	-5.7212023	1.2289795	0.0000227
C	-4.0111863	3.8187447	0.0000308	-3.9814948	3.8077001	0.0000305	-3.9604018	3.8252688	0.0000341
C	-3.1039504	4.8891910	0.0000535	-3.0678520	4.8654329	0.0000536	-3.0537156	4.8982994	0.0000557
C	-1.7190089	4.7166026	0.0000423	-1.6717247	4.6899392	0.0000443	-1.6719070	4.7223559	0.0000437
C	-1.1699039	3.4232155	0.0000013	-1.1235732	3.4079029	0.0000062	-1.1196143	3.4202489	0.0000031
C	-0.2528044	-0.7175923	-0.0000601	-0.2010127	-0.6953804	-0.0000509	-0.2130873	-0.7131092	-0.0000592
C	-0.2527985	0.7175877	-0.0000586	-0.2010124	0.6953816	-0.0000481	-0.2131323	0.7131143	-0.0000574
C	0.7349319	1.6979237	-0.0000219	0.7939643	1.7109227	-0.0000149	0.7777749	1.7144392	-0.0000206
C	2.1393013	1.3380676	-0.0000008	2.1840369	1.3478115	0.0000029	2.1689354	1.3511326	0.0000003
C	2.7014224	0.0000008	-0.0000097	2.7535267	0.0000015	-0.0000079	2.7416849	0.0000037	-0.0000090
C	2.1393028	-1.3380660	-0.0000237	2.1840365	-1.3478086	-0.0000189	2.1689363	-1.3511338	-0.0000204
C	0.7349338	-1.6979191	-0.0000349	0.7939663	-1.7109230	-0.0000284	0.7777630	-1.7144361	-0.0000327
C	3.0492756	-2.4355340	-0.0000217	3.0816082	-2.4475483	-0.0000195	3.0625062	-2.4456648	-0.0000174
C	2.6164940	-3.7458995	-0.0000214	2.6446418	-3.7659505	-0.0000188	2.6321442	-3.7798627	-0.0000153
C	1.2530877	-4.0641007	-0.0000168	1.2911209	-4.0844145	-0.0000116	1.2900352	-4.1019828	-0.0000109
C	0.2716191	-3.0748224	-0.0000200	0.3281804	-3.0636743	-0.0000162	0.3099108	-3.0781549	-0.0000175
C	0.2716213	3.0748190	0.0000023	0.3281810	3.0636795	0.0000066	0.3099000	3.0781571	0.0000042
C	1.2530847	4.0641034	0.0000374	1.2911186	4.0844118	0.0000401	1.2900329	4.1019836	0.0000410
C	2.6164926	3.7458997	0.0000532	2.6446391	3.7659551	0.0000544	2.6321440	3.7798643	0.0000564
C	3.0492740	2.4355385	0.0000362	3.0816077	2.4475498	0.0000375	3.0625050	2.4456686	0.0000379
C	4.2025917	0.0000012	0.0000045	4.2521388	0.0000017	0.0000051	4.2397437	0.0000010	0.0000049
C	4.8877176	-0.0000298	1.2302135	4.9447416	-0.0000304	1.2268404	4.9321993	-0.0000307	1.2278808
C	6.2854635	-0.0000283	1.2060624	6.3427247	-0.0000298	1.2057098	6.3302760	-0.0000293	1.2059853
C	6.9803646	-0.0000012	0.0000266	7.0383155	-0.0000010	0.0000276	7.0254714	-0.0000011	0.0000278
C	6.2854827	0.0000273	-1.2060202	6.3427440	0.0000288	-1.2056656	6.3302959	0.0000286	-1.2059410
C	4.8877371	0.0000316	-1.2301935	4.9447614	0.0000325	-1.2268186	4.9322194	0.0000325	-1.2278593
C	4.1345225	0.0000804	-2.5294532	4.1903996	0.0000785	-2.5252404	4.1788394	0.0000803	-2.5272078
C	4.1344828	-0.0000773	2.5294617	4.1903594	-0.0000760	2.5252502	4.1787987	-0.0000771	2.5272174
H	-1.0842856	-5.6043357	0.0000727	-1.0400566	-5.5790864	0.0000744	-1.0332816	-5.6067880	0.0000699
H	-3.5012790	-5.9065042	0.0001115	-3.4572676	-5.8860926	0.0001066	-3.4518150	-5.9149665	0.0001100
H	-5.0816105	-4.0326032	0.0000711	-5.0503185	-4.0271367	0.0000674	-5.0310259	-4.0388907	0.0000751
H	-6.3470736	-2.1497398	0.0000406	-6.3242129	-2.1488236	0.0000452	-6.3060048	-2.1502907	0.0000428
H	-7.5306304	-0.0000022	0.0000612	-7.5123506	-0.0000024	0.0000646	-7.4820132	-0.0000021	0.0000613
H	-6.3470755	2.1497360	0.0000394	-6.3242151	2.1488195	0.0000430	-6.3060062	2.1502878	0.0000415
H	-5.0816148	4.0326014	0.0000489	-5.0503207	4.0271332	0.0000467	-5.0310276	4.0388884	0.0000529
H	-3.5012828	5.9065028	0.0000869	-3.4572717	5.8860917	0.0000845	-3.4518188	5.9149640	0.0000885
H	-1.0842884	5.6043374	0.0000697	-1.0400603	5.5790845	0.0000713	-1.0332826	5.6067900	0.0000695
H	4.1203770	-2.2417463	-0.0000199	4.1540960	-2.2585410	-0.0000208	4.1357308	-2.2564156	-0.0000169
H	3.3536197	-4.5511028	-0.0000220	3.3859125	-4.5678511	-0.0000201	3.3814665	-4.5738595	-0.0000153
H	0.9640613	-5.1166279	-0.0000127	0.9914145	-5.1325766	-0.0000098	0.9917181	-5.1507054	-0.0000063
H	0.9640589	5.1166280	0.0000556	0.9914120	5.1325800	0.0000557	0.9917150	5.1507066	0.0000587
H	3.3536170	4.5511050	0.0000824	3.3859100	4.5678539	0.0000811	3.3814635	4.5738617	0.0000858
H	4.1203756	2.2417491	0.0000546	4.1540947	2.2585453	0.0000539	4.1357298	2.2564184	0.0000554
H	6.8328357	-0.0000499	2.1519962	6.8899040	-0.0000519	2.1519445	6.8781608	-0.0000514	2.1519810
H	8.0726360	-0.0000023	0.0000353	8.1307031	-0.0000023	0.0000365	8.1178139	-0.0000022	0.0000368
H	6.8328698	0.0000481	-2.1519453	6.8899386	0.0000499	-2.1518916	6.8781960	0.0000497	-2.1519278
H	4.8201079	0.0000023	-3.3870062	4.8737934	0.0000117	-3.3850670	4.8630551	0.0000057	-3.3864067
H	3.4838974	0.8848451	-2.6181883	3.5382945	0.8841617	-2.6096572	3.5262735	0.8835659	-2.6132385
H	3.4837228	-0.8845575	-2.6181643	3.5381410	-0.8838925	-2.6096395	3.5261049	-0.8832819	-2.6132148
H	4.8200552	0.0000022	3.3870251	4.8737397	-0.0000083	3.3850876	4.8630010	-0.0000013	3.3864270
H	3.4838569	-0.8848424	2.6181882	3.5382534	-0.8841595	2.6096577	3.5262317	-0.8835630	2.6132394
H	3.4836816	0.8845604	2.6181619	3.5380991	0.8838946	2.6096386	3.5260626	0.8832850	2.6132133

Table S2.6. Ground state vibrational frequencies of **2d**$^{+}$, computed using PBE0/def2-SVP.

mode	symmetry	wave number cm**(-1)	IR intensity km/mol	mode	symmetry	wave number cm**(-1)	IR intensity km/mol
7	a	23.63	0.07626	70	a	747.85	3.40757
8	a	32.86	0.00000	71	a	758.67	10.23035
9	a	36.12	2.90428	72	a	781.63	28.85653
10	a	59.36	0.00480	73	a	782.23	0.00003
11	a	61.78	0.24272	74	a	784.12	89.51370
12	a	65.82	0.00000	75	a	786.14	0.95290
13	a	101.86	0.05245	76	a	798.55	27.50161
14	a	118.85	0.73077	77	a	802.30	13.64202
15	a	120.11	0.00000	78	a	816.50	0.00000
16	a	140.28	0.03158	79	a	818.36	0.32109
17	a	144.48	0.00000	80	a	818.83	3.49454
18	a	157.33	0.00000	81	a	827.48	43.71979
19	a	161.65	0.11004	82	a	840.74	4.74444
20	a	174.22	0.47672	83	a	842.72	0.00000
21	a	204.54	0.06936	84	a	843.28	0.29798
22	a	205.26	0.00000	85	a	870.38	0.69007
23	a	239.11	0.00000	86	a	879.02	12.83857
24	a	242.25	0.00000	87	a	911.55	0.00000
25	a	245.44	0.05577	88	a	912.24	0.40578
26	a	257.97	0.34001	89	a	930.91	0.00000
27	a	265.56	1.65655	90	a	943.42	1.76013
28	a	268.04	5.00923	91	a	948.50	0.00000
29	a	297.68	0.21268	92	a	951.32	0.12753
30	a	312.41	0.02105	93	a	952.98	0.00000
31	a	316.24	0.05000	94	a	957.13	21.59272
32	a	324.75	0.00000	95	a	957.54	63.97796
33	a	338.13	2.00938	96	a	980.29	0.00000
34	a	347.26	0.01978	97	a	980.69	0.53357
35	a	357.37	1.07341	98	a	992.76	5.19981
36	a	369.81	3.52803	99	a	1000.78	0.00383
37	a	372.26	0.00000	100	a	1004.80	4.84291
38	a	386.36	0.16349	101	a	1020.89	0.18889
39	a	401.12	0.86346	102	a	1021.25	0.00946
40	a	435.59	0.00073	103	a	1021.77	0.00000
41	a	442.80	12.32607	104	a	1022.54	0.45508
42	a	470.80	0.01309	105	a	1031.85	0.00000
43	a	492.33	0.05328	106	a	1032.15	0.00395
44	a	493.62	0.00000	107	a	1050.34	0.41770
45	a	500.16	0.28332	108	a	1051.88	0.00000
46	a	501.95	0.00000	109	a	1060.85	26.30023
47	a	527.53	0.00000	110	a	1060.89	0.21406
48	a	530.05	0.10265	111	a	1082.66	1.48885
49	a	537.57	11.74903	112	a	1096.20	2.66334
50	a	542.03	1.39714	113	a	1101.87	9.11066
51	a	548.29	1.00116	114	a	1108.46	0.14033
52	a	549.19	0.32326	115	a	1123.54	5.08477
53	a	550.11	3.65725	116	a	1133.42	5.31369
54	a	560.49	0.00000	117	a	1135.48	32.83137
55	a	561.33	0.02020	118	a	1147.67	0.55011
56	a	566.26	11.11236	119	a	1163.70	23.96786
57	a	597.90	11.13998	120	a	1182.42	113.36186
58	a	608.96	0.23463	121	a	1191.11	2.27834
59	a	609.53	0.00000	122	a	1201.51	123.75625
60	a	623.77	1.00463	123	a	1205.14	8.36378
61	a	633.24	0.02064	124	a	1211.32	26.35058
62	a	666.19	4.81499	125	a	1212.65	8.46050
63	a	678.13	0.22780	126	a	1218.71	41.04701
64	a	689.88	0.00642	127	a	1242.26	69.62622
65	a	699.71	0.00000	128	a	1254.30	40.68947
66	a	711.93	5.85908	129	a	1257.31	136.27422
67	a	714.37	0.57678	130	a	1267.60	19.96828
68	a	726.37	0.00000	131	a	1269.26	13.44499
69	a	728.53	9.36103	132	a	1274.88	0.00040

Table S2.7. Ground state vibrational frequencies of **2d**$^{+}$, computed using PBE0/def2-SVP (continuation from **Table S2.6**).

mode	symmetry	wave number cm**(-1)	IR intensity km/mol	mode	symmetry	wave number cm**(-1)	IR intensity km/mol
133	a	1284.78	42.59988	169	a	1638.92	63.82233
134	a	1295.07	0.69574	170	a	1642.12	0.01682
135	a	1303.51	6.70437	171	a	1647.22	0.64813
136	a	1304.81	20.78541	172	a	1647.98	48.01436
137	a	1330.22	28.83249	173	a	1656.16	30.46645
138	a	1356.18	88.41500	174	a	1662.89	5.63451
139	a	1361.59	14.43762	175	a	1666.40	65.85504
140	a	1365.32	0.52202	176	a	1676.74	5.27735
141	a	1381.64	1.49942	177	a	1680.65	3.44076
142	a	1383.17	25.74382	178	a	1700.38	353.44314
143	a	1398.25	3.40662	179	a	1741.30	11.97157
144	a	1398.25	39.82413	180	a	1749.04	11.90014
145	a	1401.69	0.22184	181	a	3053.00	11.61439
146	a	1402.93	17.90039	182	a	3053.50	5.81098
147	a	1416.81	51.03066	183	a	3133.10	0.00001
148	a	1421.23	237.07943	184	a	3133.39	8.48378
149	a	1431.92	0.02822	185	a	3174.44	4.88253
150	a	1439.27	1.78711	186	a	3174.53	11.50636
151	a	1453.11	49.81512	187	a	3206.34	0.06529
152	a	1459.07	17.43587	188	a	3212.74	2.97133
153	a	1459.20	0.00016	189	a	3216.69	0.00828
154	a	1459.54	6.36941	190	a	3216.74	0.12557
155	a	1466.48	86.05613	191	a	3220.72	0.57242
156	a	1480.96	23.22757	192	a	3223.74	0.00021
157	a	1499.93	8.13844	193	a	3223.83	2.39710
158	a	1503.06	16.16028	194	a	3227.86	0.41272
159	a	1505.18	1.19569	195	a	3228.39	0.09078
160	a	1506.94	3.73622	196	a	3229.88	3.79288
161	a	1516.33	26.70569	197	a	3233.29	0.05779
162	a	1529.62	26.77666	198	a	3235.67	0.51757
163	a	1555.55	1.90943	199	a	3236.36	1.09758
164	a	1584.80	72.53196	200	a	3238.87	0.02764
165	a	1597.64	2.99796	201	a	3238.96	2.03112
166	a	1604.52	100.70485	202	a	3240.80	1.47086
167	a	1614.64	25.90894	203	a	3262.16	3.41430
168	a	1623.01	2.99502	204	a	3262.68	8.97522

Table S2.8. S_1 vibrational frequencies of **2d**$^+$, computed using TDPBE0/def2-SVP.

mode	symmetry	wave number cm**(-1)	IR intensity km/mol	mode	symmetry	wave number cm**(-1)	IR intensity km/mol
7	a	34.99	0.20127	70	a	733.91	0.00000
8	a	61.03	0.00000	71	a	758.74	0.01590
9	a	65.71	1.89812	72	a	784.43	15.39777
10	a	78.97	0.00000	73	a	795.19	0.02998
11	a	79.80	0.00924	74	a	797.23	23.36701
12	a	82.01	0.02274	75	a	805.25	0.00000
13	a	112.54	0.00699	76	a	817.74	0.02311
14	a	128.53	0.04614	77	a	818.27	4.70629
15	a	151.29	0.00000	78	a	820.28	6.36334
16	a	156.60	0.02996	79	a	824.54	16.79568
17	a	160.18	0.00448	80	a	824.80	0.00001
18	a	171.44	0.00000	81	a	837.21	123.22091
19	a	210.33	0.02036	82	a	840.19	1.28588
20	a	214.78	0.00000	83	a	840.49	1.26853
21	a	231.47	0.00000	84	a	853.53	0.00000
22	a	233.30	0.21776	85	a	873.49	3.23318
23	a	258.93	1.04201	86	a	881.60	0.34673
24	a	260.65	0.17624	87	a	909.93	0.00000
25	a	266.80	2.00664	88	a	911.01	0.38775
26	a	269.90	0.00000	89	a	938.45	4.68744
27	a	270.68	0.00000	90	a	944.80	0.00000
28	a	276.56	4.27575	91	a	957.39	8.01640
29	a	299.35	3.94155	92	a	964.74	0.00000
30	a	313.78	3.04170	93	a	965.95	0.05221
31	a	316.11	2.53768	94	a	969.30	0.00000
32	a	335.72	0.00000	95	a	969.74	0.00064
33	a	336.27	0.03530	96	a	973.36	0.00000
34	a	346.65	0.00121	97	a	978.84	25.73978
35	a	358.99	0.24782	98	a	990.53	3.56811
36	a	375.16	5.23703	99	a	1001.25	0.25939
37	a	380.66	0.08944	100	a	1003.98	4.33003
38	a	398.24	0.22410	101	a	1029.44	0.93143
39	a	401.30	0.00000	102	a	1034.59	0.00298
40	a	437.42	0.00793	103	a	1038.72	0.00195
41	a	449.42	0.48210	104	a	1038.86	1.26726
42	a	470.70	0.13375	105	a	1039.97	0.00017
43	a	498.10	0.00000	106	a	1040.05	0.04507
44	a	500.22	0.96919	107	a	1055.16	8.37126
45	a	500.43	0.16406	108	a	1055.73	0.00001
46	a	522.82	0.00000	109	a	1060.22	0.24348
47	a	524.52	0.08851	110	a	1061.22	3.13062
48	a	539.70	0.38276	111	a	1079.83	4.01209
49	a	541.53	1.05053	112	a	1090.37	1.23328
50	a	547.02	0.00000	113	a	1103.81	0.33850
51	a	549.34	1.06958	114	a	1106.91	3.53920
52	a	551.56	0.34158	115	a	1123.53	9.63432
53	a	555.26	3.38465	116	a	1132.59	0.31607
54	a	566.54	13.75034	117	a	1138.69	18.63881
55	a	568.19	0.01156	118	a	1150.29	21.73319
56	a	574.46	0.00000	119	a	1167.49	2.92857
57	a	602.45	0.02725	120	a	1190.07	1.10124
58	a	610.30	1.17155	121	a	1193.69	6.00609
59	a	616.68	0.00000	122	a	1198.73	5.40229
60	a	624.48	1.84995	123	a	1207.37	0.12211
61	a	632.34	0.32890	124	a	1215.03	20.72908
62	a	670.03	4.05545	125	a	1215.78	3.44805
63	a	676.09	0.00511	126	a	1218.40	46.19112
64	a	689.14	3.05461	127	a	1241.05	0.34863
65	a	708.91	0.00000	128	a	1249.92	4.85107
66	a	713.84	2.15615	129	a	1255.75	0.02484
67	a	718.83	0.07876	130	a	1272.43	18.54203
68	a	722.25	0.00448	131	a	1272.45	0.46924
69	a	730.77	5.31868	132	a	1285.63	9.79249

Table S2.9. S_1 vibrational frequencies of **2d**$^+$, computed using TDPBE0/def2-SVP (continuation from Table **S2.8**).

mode	symmetry	wave number cm**(-1)	IR intensity km/mol	mode	symmetry	wave number cm**(-1)	IR intensity km/mol
133	a	1292.96	16.24369	169	a	1618.37	6.42745
134	a	1293.45	0.62601	170	a	1634.32	0.39490
135	a	1303.81	1.46573	171	a	1634.61	79.45058
136	a	1314.21	1.45000	172	a	1648.03	17.61548
137	a	1331.13	18.99264	173	a	1653.60	29.99460
138	a	1352.99	19.62117	174	a	1655.54	79.63441
139	a	1356.06	0.08448	175	a	1662.86	4.33850
140	a	1372.07	0.35145	176	a	1678.68	2.23008
141	a	1378.45	24.73062	177	a	1696.10	284.33178
142	a	1395.15	3.56824	178	a	1706.45	298.30136
143	a	1395.55	2.11609	179	a	1756.24	19.21024
144	a	1396.85	5.17799	180	a	1852.25	1044.93482
145	a	1399.77	1.80459	181	a	3053.66	19.23526
146	a	1410.25	65.37296	182	a	3054.13	4.02244
147	a	1413.97	20.54597	183	a	3134.49	0.00002
148	a	1417.10	0.36953	184	a	3134.74	6.48378
149	a	1428.18	150.95175	185	a	3171.36	11.08282
150	a	1442.82	25.34029	186	a	3171.55	8.12215
151	a	1448.22	18.63537	187	a	3205.63	0.26579
152	a	1448.44	0.00058	188	a	3211.67	4.70671
153	a	1452.62	94.14646	189	a	3221.47	0.20855
154	a	1453.92	6.93154	190	a	3221.55	0.03792
155	a	1468.06	54.17895	191	a	3223.21	1.22555
156	a	1476.20	3.07324	192	a	3223.46	0.44420
157	a	1492.35	68.86258	193	a	3226.08	0.15440
158	a	1494.42	0.07652	194	a	3229.51	6.43964
159	a	1506.80	0.12805	195	a	3234.26	0.24681
160	a	1513.87	11.42748	196	a	3237.18	0.32602
161	a	1519.73	31.16981	197	a	3238.84	0.15804
162	a	1535.51	2.06288	198	a	3241.42	0.00137
163	a	1539.68	2.73571	199	a	3242.57	0.08481
164	a	1576.22	46.98106	200	a	3245.53	0.19082
165	a	1587.56	2.81215	201	a	3246.92	0.77367
166	a	1598.75	9.20651	202	a	3247.61	2.12678
167	a	1613.14	41.30982	203	a	3257.68	2.27607
168	a	1616.98	129.62601	204	a	3263.81	0.79652

Table S2.10. S_2 vibrational frequencies of **2d**$^+$, computed using TDPBE0/def2-SVP.

mode	symmetry	wave number cm**(-1)	IR intensity km/mol	mode	symmetry	wave number cm**(-1)	IR intensity km/mol
7	a	29.36	0.02155	70	a	728.52	5.37236
8	a	39.43	0.00021	71	a	756.21	0.27080
9	a	44.09	3.64925	72	a	769.70	0.00009
10	a	59.50	0.40725	73	a	771.07	80.88733
11	a	64.26	0.26899	74	a	786.08	44.43167
12	a	65.30	0.00001	75	a	794.10	35.97013
13	a	106.03	0.02299	76	a	796.98	0.09630
14	a	119.33	0.00387	77	a	798.76	14.41467
15	a	127.91	0.00001	78	a	814.48	0.00007
16	a	146.39	0.15289	79	a	815.22	17.42187
17	a	150.16	0.00004	80	a	819.16	0.42114
18	a	159.73	0.00027	81	a	822.33	52.43937
19	a	193.91	0.00001	82	a	839.10	0.00004
20	a	205.56	0.00551	83	a	840.78	14.76661
21	a	213.65	0.00001	84	a	842.62	0.34753
22	a	221.22	0.59425	85	a	865.02	1.15051
23	a	240.31	0.00010	86	a	880.96	5.63176
24	a	243.95	0.41513	87	a	911.91	0.00004
25	a	255.03	0.00035	88	a	915.67	0.00041
26	a	255.36	40.15039	89	a	930.39	0.00001
27	a	265.41	0.14824	90	a	938.62	2.11403
28	a	274.14	4.56262	91	a	948.99	0.00000
29	a	303.04	0.96459	92	a	954.30	0.28171
30	a	313.80	1.50558	93	a	955.08	0.00009
31	a	315.66	1.51882	94	a	955.87	11.67641
32	a	323.02	0.00002	95	a	961.76	0.00001
33	a	336.13	0.17969	96	a	965.40	1.11934
34	a	351.97	0.01006	97	a	975.29	46.13148
35	a	356.81	0.46235	98	a	988.77	1.14650
36	a	371.20	6.27191	99	a	1001.99	1.97682
37	a	373.54	0.00000	100	a	1002.91	2.47490
38	a	387.32	0.10797	101	a	1019.53	0.17611
39	a	400.20	0.53126	102	a	1019.81	0.02549
40	a	436.68	0.14453	103	a	1020.32	0.00004
41	a	443.58	51.29537	104	a	1021.02	0.12652
42	a	470.77	0.70967	105	a	1023.02	0.00000
43	a	488.33	0.00000	106	a	1025.36	0.05631
44	a	496.05	0.01592	107	a	1053.00	0.03728
45	a	503.26	5.39119	108	a	1053.23	0.00000
46	a	516.74	0.00001	109	a	1057.65	2.61567
47	a	527.33	0.02269	110	a	1058.51	0.07649
48	a	534.70	1.21399	111	a	1078.48	0.00425
49	a	535.45	0.00017	112	a	1096.05	26.06846
50	a	537.32	3.71620	113	a	1100.29	0.48080
51	a	546.47	2.47153	114	a	1107.03	0.81384
52	a	548.19	6.02547	115	a	1118.72	136.50334
53	a	550.53	7.41399	116	a	1123.78	6.62254
54	a	552.67	0.00002	117	a	1144.03	50.01775
55	a	564.22	0.54186	118	a	1144.33	4.15487
56	a	565.68	15.87790	119	a	1155.39	14.94131
57	a	593.41	102.79130	120	a	1187.70	205.00888
58	a	608.81	0.00048	121	a	1193.37	1.86779
59	a	609.42	23.89299	122	a	1194.27	5.56843
60	a	620.40	17.44048	123	a	1200.68	405.55322
61	a	630.23	0.01196	124	a	1206.55	37.69786
62	a	666.44	2.00245	125	a	1216.89	22.78177
63	a	675.93	3.31271	126	a	1218.68	0.25579
64	a	687.94	15.15989	127	a	1239.73	431.17554
65	a	701.13	129.11573	128	a	1253.61	61.80712
66	a	704.31	0.00004	129	a	1254.20	103.77724
67	a	711.43	0.99933	130	a	1271.78	1.00495
68	a	716.76	0.11465	131	a	1272.63	0.46665
69	a	722.05	0.00002	132	a	1276.91	22.85073

Table S2.11. S_2 vibrational frequencies of **2d**$^+$, computed using TDPBE0/def2-SVP (continuation from **Table S2.10**).

mode	symmetry	wave number cm**(-1)	IR intensity km/mol	mode	symmetry	wave number cm**(-1)	IR intensity km/mol
133	a	1288.41	138.44449	169	a	1622.35	203.27011
134	a	1293.76	0.62268	170	a	1627.34	85.43326
135	a	1300.30	0.81670	171	a	1630.24	34.48174
136	a	1319.87	15.55137	172	a	1645.09	14.73150
137	a	1331.68	5.09346	173	a	1647.44	3.86072
138	a	1353.43	26.59499	174	a	1660.89	4.39104
139	a	1371.67	0.18428	175	a	1664.38	9.76458
140	a	1373.31	0.40695	176	a	1677.58	6.16299
141	a	1381.83	7.04127	177	a	1679.42	9.82825
142	a	1389.64	465.55994	178	a	1731.25	332.78552
143	a	1396.06	3.31853	179	a	1754.08	28.95154
144	a	1397.85	24.55391	180	a	1773.95	9.29133
145	a	1400.58	2.06106	181	a	3055.01	16.37877
146	a	1402.08	235.42385	182	a	3055.31	4.24342
147	a	1421.74	51.83746	183	a	3134.85	0.00005
148	a	1422.71	248.67418	184	a	3135.00	5.76989
149	a	1435.55	34.89187	185	a	3171.63	10.58396
150	a	1442.34	6.00208	186	a	3171.64	6.57046
151	a	1448.06	27.56353	187	a	3205.01	0.15383
152	a	1448.38	0.00163	188	a	3210.50	4.09559
153	a	1453.45	87.17021	189	a	3221.39	0.73979
154	a	1453.92	15.81657	190	a	3222.13	0.01926
155	a	1454.79	6.15754	191	a	3223.52	0.00184
156	a	1479.31	24.35882	192	a	3226.36	14.36322
157	a	1489.20	9.94450	193	a	3226.61	0.60236
158	a	1495.50	25.68189	194	a	3229.71	5.89206
159	a	1495.78	132.41826	195	a	3232.04	0.27973
160	a	1504.52	0.53531	196	a	3233.72	0.30349
161	a	1518.28	30.03866	197	a	3236.83	0.53203
162	a	1530.35	24.90834	198	a	3240.98	0.04583
163	a	1551.27	18.57867	199	a	3241.71	9.67187
164	a	1567.89	30.99842	200	a	3243.19	0.03277
165	a	1573.99	98.04748	201	a	3247.58	2.85686
166	a	1587.66	90.52366	202	a	3248.75	7.25673
167	a	1598.79	174.19386	203	a	3251.22	0.00084
168	a	1607.63	269.99813	204	a	3258.20	16.87657

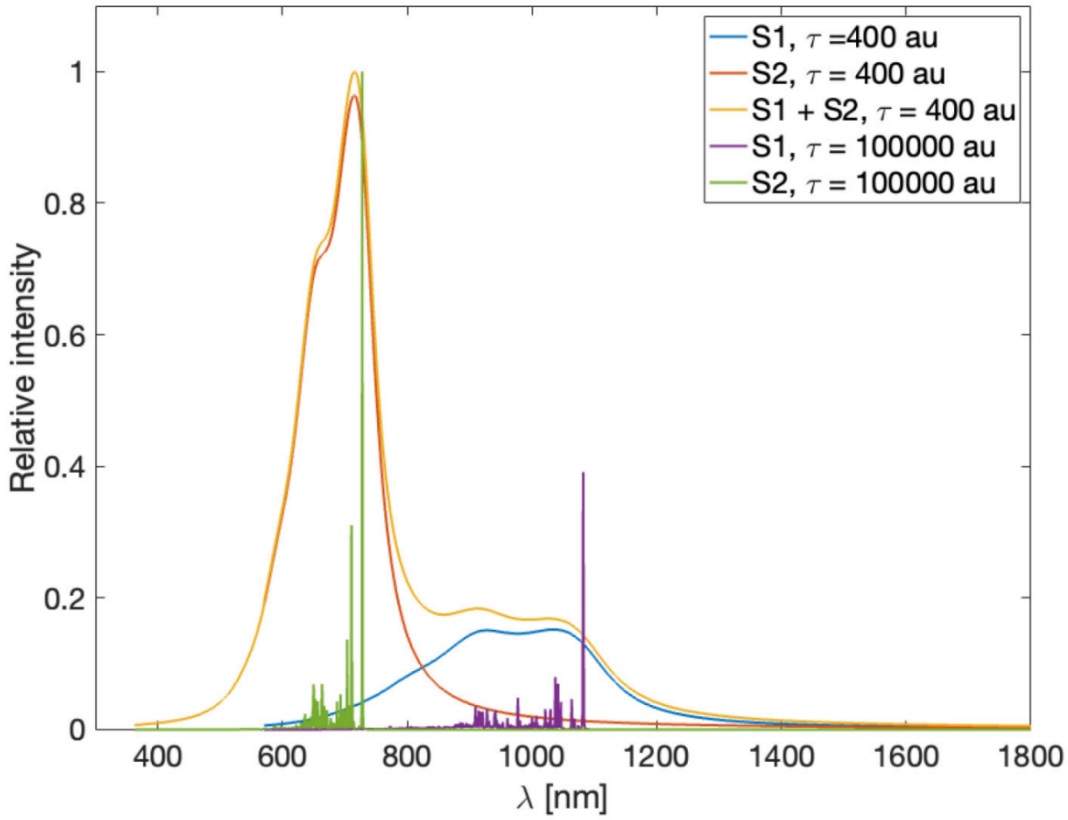

Figure S2.35. Vibronic absorption spectrum of **2d**$^+$ computed by the pure TDDFT approach. τ denotes the lifetime used in the calculations.

Table S2.12. Assignment of the lowest three absorption bands of **2d**$^+$ and comparison between the peak positions of experiment and calculations.

Experiment (nm)	1210	1051	803
TDPBE0/def2-SVP (nm)	1339	1153	881
deviation wrt. exp (eV)	0.1826	0.1798	0.1900
CC2/def2-TZVP (nm)	1027	912	715
deviation wrt. exp (eV)	−0.0987	−0.1044	−0.1367
Assignment	$S_1 \leftarrow S_0$	$S_1 \leftarrow S_0$	$S_2 \leftarrow S_0$

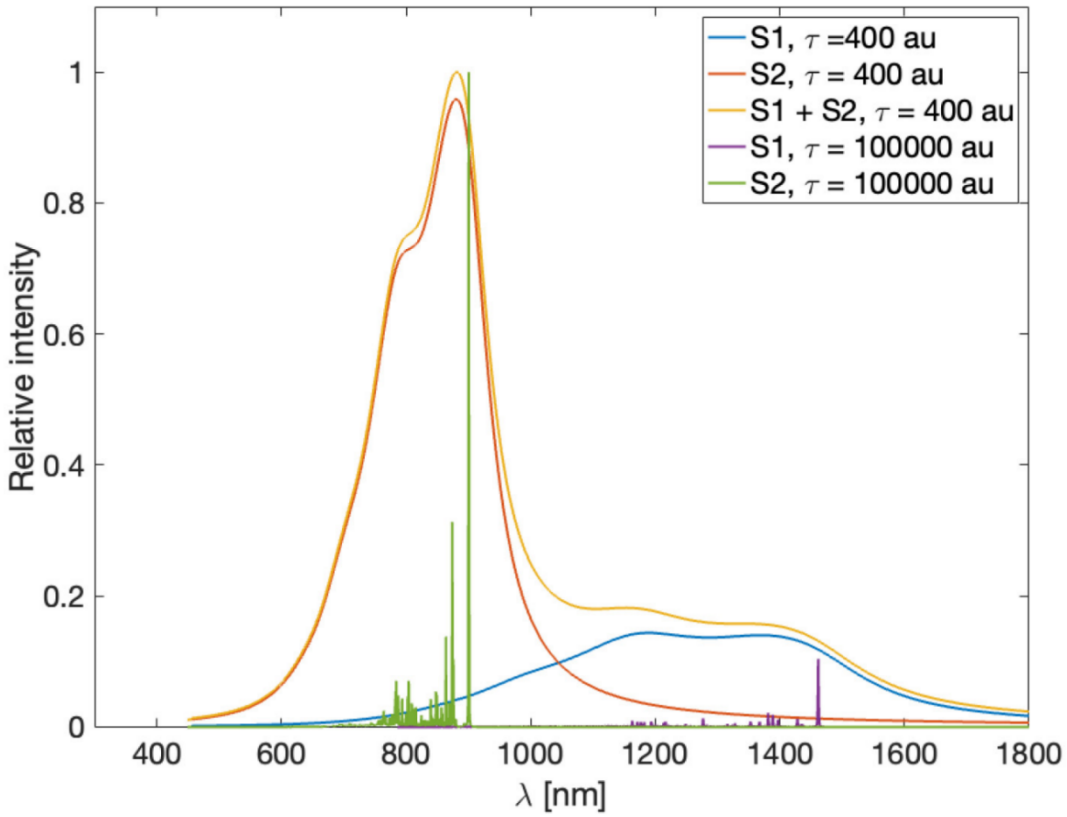

Figure S2.36. Vibronic absorption spectrum of **2d**$^{+}$ computed by the mixed TDDFT/CC2 approach. τ denotes the lifetime used in the calculations.

References

1. Merling, G. *Chem. Ber*. **1891**, *24*, 3108–3126.

2. von E Doering, W., Knox, L. H. *J. Am. Chem. Soc*. **1954**, *76*, 3203–3206.

3. Komatsu, K. *Chem. Rec*. **2015**, *15*, 160–174.

4. Kitaigorodskii, A., Struchkov, Y., Khotsyanova, T., Vol'pin, M., Kursanov, D. *Bull. Acad. Sci. USSR* **1960**, *9*, 32–36.

5. Grnowitz, S., Pedaja, P. *Tetrahedron* **1978**, *34*, 587–590.

6. Saha, P. K. *et al*. *Nat. Chem.* **2023**, *15*, 516–525.

7. Borstelmann, J., Bergner, J., Rominger, F., Kivala, M. *Angew. Chem. Int. Ed*. **2023**, *62*, e202312740.

8. Lyons, D. J. M., Crocker, R. D, Blümel, M., Nguyen, T. V. *Angew. Chem. Int. Ed.* **2017**, *56*, 1466–1484.

9. Zahra, F. T., Saeed, A., Mumtaz, K., Albericio, F. *Molecules* **2023**, *28*, 4095.

10. Wang, Z., Xing, Y., Shao, H., Lu, P., Weber, W. P. *Org. Lett*. **2005**, *7*, 87–90.

11. Wang, X. *et al*. *Macromolecules* **2009**, *42*, 5534–5544.

12. Ruggiero, A. *et al*. *Tetrahedron* **2009**, *65*, 9690–9693.

13. Murai, M., Amir, E., Amira, R. J., Hawker, C. J. *Chem. Sci*. **2012**, *3*, 2721–2725.

14. Wang, F. *et al*. *J. Mater. Chem*. **2012**, *22*, 10448–10451.

15. Asai, K., Fukazawa, A., Yamaguchi, S. *Chem. Eur. J*. **2016**, *22*, 17571–17575.

16. Asai, K., Fukazawa, A., Yamaguchi, S. *Angew. Chem. Int. Ed*. **2017**, *56*, 6848–6852.

17. Lyons, D. J. M., Crocker, R. D., Nguyen, T. V. *Chem. Eur. J.* **2018**, *24*, 10959–10965.

18. Harrison, A. G., Honnen, L. R., Dauben, H. J., Lossing, F. P. *J. Am. Chem. Soc*. **1960**, *82*, 5593–5598.

19. Stakhursky, V. L., Sioutis, I., Tarczay, G., Miller, T. A. *J. Chem. Phys.* **2008**, *128*, 084310.

20. Sioutis, I., Stakhursky, V. L., Tarczay, G., Miller, T. A. *J. Chem. Phys*. **2008**, *128*, 084311.

21. Vincow, G. in *Aromaticity, Pseudo-aromaticity, and Anti-aromaticity* (Eds.: E. D. Bergmann, B. Pullman), Academic Press, New York, 1971, pp. 336–347.

22. Wiberg, K. B. *Chem. Rev*. **2001**, *101*, 1317−1331.

23. Allen, A. D., Tidwell, T. T. *Chem. Rev*. **2001**, *101*, 1333−1348.

24. Tsipis, A. C. *Phys. Chem. Chem. Phys*. **2009**, *11*, 8244−8261.

25. Nishiuchi, T. *et al*. *Chem. Asian J*. **2019**, *14*, 1830–1836.

26. Moshniaha, L. *et al*. *J. Am. Chem. Soc*. **2020**, *142*, 3626–3635.

27. Ito, S., Tokimaru, Y., Nozaki, K. *Angew. Chem. Int. Ed*. **2015**, *54*, 7256–7260.

28. Yokoi, H. *et al*. *Nat. Commun.* **2015**, *6*, 8215.

29. Li, Q.-Q. *et al*. *Angew. Chem. Int. Ed.* **2022**, *61*, e202112638.

30. Borissov, A. *et al*. *Chem. Rev*. **2022**, *122*, 565–788.

31. Kise, K., Tanaka, T. *Heterocycles* **2022**, *104*, 1373–1413.

32. According to the International Union of Pure and Applied Chemistry (IUPAC) nomenclature, "homo" is an affix used to denote a ring expansion by inclusion of a methylene group into a ring-sector. See: H. A. Favre, W. H. Powell, *Nomenclature of Organic Chemistry*, The Royal Society of Chemistry, London, **2013**.

33. The parent homocorannulene molecule has not yet been synthesized. See: J. D. Walsh, PhD Thesis, Memorial University of Newfoundland: Canada, **2016**.

34. Wang, W. *et al*. *Angew. Chem. Int. Ed*. **2023**, *62*, e202218176.

35. Bricks, J. L., Kachkovskii, A. D., Slominskii, Y. L., Gerasov, A. O., Popov, S. V. *Dyes Pigments* **2015**, *121*, 238–255.

36. Koçak, R., Daştan, A. *Beilstein J. Org. Chem*. **2021**, *17*, 719–729.

37. Cramer, E. K., Lash, T. D. *J. Org. Chem*. **2022**, *87*, 952–962.

38. Deposition numbers 2286092 (for **5-H$_4$**), 2286093 (for **5**), 2286094 (for **2 a**$^+ \cdot$ **SnCl$_3$**$^-$) and 2286095 (for **2 a**·) contain the supplementary crystallographic data for this paper. These data are provided free of charge by the joint Cambridge Crystallographic Data Centre and Fachinformationszentrum Karlsruhe Access Structures service.

39. Krygowski, T. M., Cyrański, M. K. *Chem. Rev*. **2001**, *101*, 1385–1420.

40. Yamamoto, H. M., Yamaura, J.-I., Kato, R. *J. Mater. Chem*. **1998**, *8*, 289–294.

41. Narita, M. *et al*. *Bull. Chem. Soc. Jpn.* **2019**, *92*, 1867–1873.

42. Zhu, C., Shoyama, K., Würthner, F. *Angew. Chem. Int. Ed*. **2020**, *59*, 21505–21509.

43. Horii, K. *et al*. *J. Am. Chem. Soc.* **2022**, *144*, 3370–3375.

44. Franzke, Y. J. *et al*. *J. Chem. Theory Comput*. **2023**, *19*, 6859–6890.

45. Tapavicza, E., Furche, F., Sundholm, D. *J. Chem. Theory Comput*. **2016**, *12*, 5058–5066.

46. We have investigated solvent-dependence (**Figure S2.14**), concentration-dependence (**Figure S2.15**), anion-dependence (**Figure S2.16**), and stability in air (**Figure S2.17**) of the absorption spectra of **2 a**$^{+}$.

47. Klod, S., Kleinpeter, E. *J. Chem. Soc. Perkin Trans. 2* **2001**, 1893–1898.

48. Lu, T., Chen, F. *J. Comput. Chem*. **2012**, *33*, 580–592.

49. Liu, Z., Lu, T., Chen, Q. *Carbon* **2020**, *165*, 468–475.

50. Geuenich, D., Hess, K., Köhler, F., Herges, R. *Chem. Rev.* **2005**, *105*, 3758–3772.

51. Tokimaru, Y., Ito, S., Nozaki, K. *Angew. Chem. Int. Ed*. **2018**, *57*, 9818–9822.

52. Reichardt, C. *Chem. Rev*. **1994**, *94*, 2319–2358.

53. Sheldrick, G. M. University of Göttingen: Göttingen, Germany, **2014**.

54. Frisch, M. J. *et al*. *Gaussian 16, Revision A.03*, Gaussian, Inc., Wallingford CT, **2016**.

55. (a) Becke, A. D. *J. Chem. Phys*. **1993**, *98*, 5648–5652. (b) Lee, C., Yang, W., Parr, R. G. *Phys. Rev. B* **1998**, *37*, 785–789.

56. (a) Hehre, W. J., Ditchfield, R., Pople, J. A. *J. Chem. Phys*. **1972**, *56*, 2257–2261. (b) Ditchfield, R., Hehre, W. J., Pople, J. A. *J. Chem. Phys.* **1971**, *54*, 724–728.

57. TURBOMOLE V7.3 2018, a development of University of Karlsruhe and Forschungszentrum Karlsruhe GmbH, TURBOMOLE GmbH, since 2007; available from http://www.turbomole.com.

58. Perdew, J. P., Burke, K., Ernzerhof, M. *Phys. Rev. Lett*. **1996**, *77*, 3865.

59. Perdew, J. P., Ernzerhof, M., Burke, K. *J. Chem. Phys*. **1996**, *105*, 9982–9985.

60. Schäfer, A., Horn, H., Ahlrichs, R. *J. Chem. Phys*. **1992**, *97*, 2571–2577.

61. Weigend, F., Ahlrichs, R. *Phys. Chem. Chem. Phys*. **2005**, *7*, 3297–3305.

62. Weigend, F. *Phys. Chem. Chem. Phys*. **2006**, *8*, 1057–1065.

63. Sierka, M., Hogekamp, A., Ahlrichs, R. *J. Chem. Phys.* **2003**, *118*, 9136–9148.

64. Grimme, S. *J. Comput. Chem.* **2004**, *25*, 1463–1473.

65. Grimme, S. *J. Comput. Chem*. **2006**, *27*, 1787–1799.

66. Furche, F. *J. Chem. Phys*. **2001**, *114*, 5982–5992.

67. Furche, F., Ahlrichs, R. *J. Chem. Phys.* **2002**, *117*, 7433–7447.

68. Deglmann, P., Furche, F., Ahlrichs, R. *Chem. Phys. Lett*. **2002**, *362*, 511–518.

69. Hättig, C., Weigend, F. *J. Chem. Phys.* **2000**, *113*, 5154–5161.

70. Hättig, C., Köhn, A. *J. Chem. Phys*. **2002**, *117*, 6939–6951.

71. Tapavicza, E. *J. Phys. Chem. Lett*. **2019**, *10*, 6003–6009.

72. Begušić, T., Tapavicza, E., Vaníček, J. *J. Chem. Theory Comput.* **2022**, *18*, 3065–3074.

73. de Queiroz, T. B. *et al*. *J. Chem. Phys*. **2021**, *154*, 044106.

74. Benkyi, I., Tapavicza, E., Fliegl, H., Sundholm, D. *Phys. Chem. Chem. Phys*. **2019**, *21*, 21094–21103.

75. Send, R., Kühn, M., Furche, F. *J. Chem. Theory Comput*. **2011**, *7*, 2376–2386.

Chapter 3. Azapentabenzodihomocorannulene: Synthesis and Properties as Polycyclic Aromatic Heptagonal Diradicaloid

Abstract

Polycyclic aromatic diradical(oid) molecules are attracting significant attention because of their unique magnetic and electronic properties as well as their applications as functional materials. While diradical(oid) molecules bearing five-membered rings have been extensively investigated, those bearing seven-membered rings are relatively fewer. Herein, we report the synthesis of azapentabenzodihomocorannu-lene dication and diradical molecules. The synthesis was achieved through an mechanochemical $C(sp^2)$–H/$C(sp^3)$–H coupling in the presence of sodium as a key reaction. Electron spin resonance studies revealed that the neutral azapentabenzodihomocorannulene adopts a singlet diradical (diradicaloid) ground state with a small singlet–triplet energy gap of 2.1 kcal/mol. The electronic and optical properties were investigated both experimentally and theoretically to elucidate their aromatic character.

3.1. Introduction

Non-alternant polycyclic aromatic molecules[1] can be synthesized by substituting the hexagonal rings of parent alternant aromatic molecules with odd-membered rings such as pentagons and heptagons. The resulting non-alternant aromatic molecules have molecular structures with positive and negative curvature[2] and distinct molecular orbitals and orbital coefficients, leading to physicochemical properties which are not observed in their alternant counterparts, such as induced dipole moments,[3] small excitation energies[4], antiaromatic characters[5], and anti-Kasha emission properties[6]. A significant feature of introducing non-alternant structures into polycyclic aromatic frameworks is the introduction of open-shell nature, leading to the formation of mono- and multiradical(oid) molecules[7]. In particular,

polycyclic aromatic diradical(oid)s have garnered attention due to their potential applications such as organic electronics[8] and nonlinear optics[9]. The introduction of pentagon rings has proven effective in forming diradical(oid) species[10,11], while the incorporation of seven-membered rings remains less explored (**Figure 3.1A**)[12]. In the seminal reports in the 1960s and 1970s, Cava[13] and Michl[14] investigated the reactivity of a heptagonal diradicaloid intermediate **A**, observing that **A** underwent various radical-mediated reactions. The introduction of a seven-membered ring together with a pentagon ring is another way to create diradicaloid species such as isoelectronic pentacene **B**[15]. A fused pentagon/heptagon, so-called azulene, was also used to form cyclohepta[*def*]fluorene (**C**)[16] and its π-extended analogue **C'**[17], demonstrating the versatility of the method.

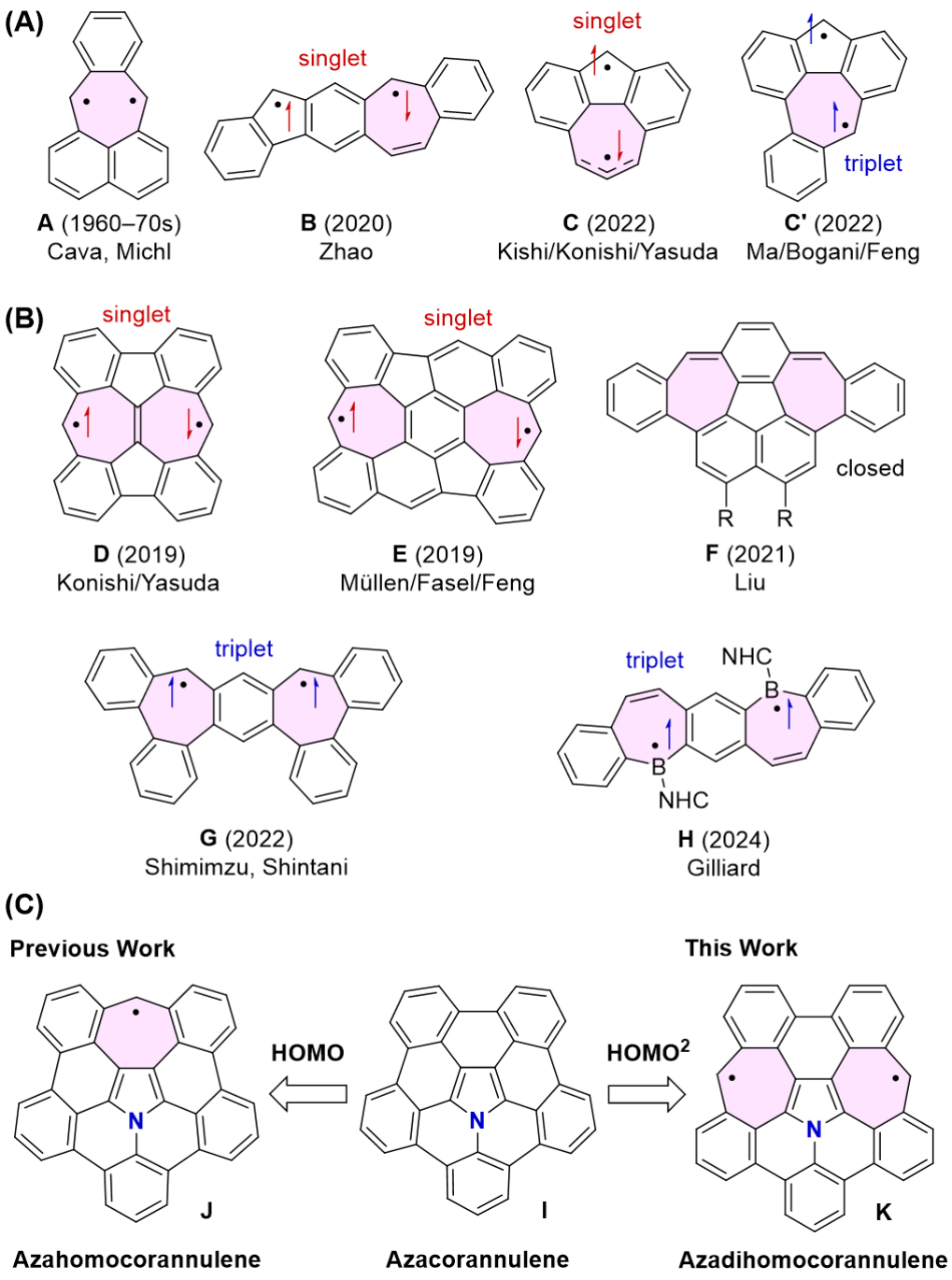

Figure 3.1. (**A**) Precedented examples of polycyclic aromatic diradical(oid) molecules bearing a heptagon ring. (**B**) Precedented examples of polycyclic aromatic diradical(oid) molecules bearing two heptagon rings. (**C**) Azacorannulene **I** and azahomocorannulene **J** reported in our previous paper and azadihomocoranulene **K** in this work.

The introduction of two heptagon rings is another powerful method for creating diradical molecules (**Figure 3.1B**). Konishi and Yasuda reported π-extended heptalene **D**[18], while Müllen, Fasel, and Feng reported two azulene-embedded nanographenes **E**[19]. These molecules show singlet diradical character in a ground state. Liu reported π-extended dihomocorannulene **F** that adopts a closed-shell structure in the ground state[20]. In contrast, π-extended dicyclohepta[*a*,*d*]benzene **G** reported by Shimizu and Shintani exhibits a triplet ground state[21], which could be due to the *m*-quinodimethane-type structure known as typical a triplet diradical species[22]. Despite these advances, there are few examples of heteroatom-embedded heptagon diradicals, as one example **H** was demonstrated by Gilliard, et al[23].

We have been interested in the introduction of heteroatoms into polycyclic aromatic molecules, as the modification can lead to distinct electronic structures and physicochemical properties that differ significantly from those of pure hydrocarbon molecules[24]. In the context, we previously reported azacorannulene **I** as the first example of a heteroatom-embedded corannulene molecule (**Figure 3.1C**)[25]. Building on this research, we achieved the synthesis of azahomocorannulenyl radical **J** through the homo-type π-extension of **I**[26], which offers a rare example of polycyclic aromatic tropyl radical species. Thus, what would happen if **I** is subject to homo-type π-extension twice, which poses our next challenge. In this work, we present the synthesis and properties of azadihomocorannulene **K**, a nitrogen-embedded polycyclic aromatic diradicaloid species that has two heptagon rings within its framework. The distinct structural and electronic features of azadihomocorannulene make it a significant addition to the family of polycyclic aromatic diradical(oid)s, paving the way for their further explorations and applications. This is particularly noteworthy as little is known about the impact of introducing heteroatoms into non-alternant polycyclic aromatic molecules.

3.2. Results and discussion

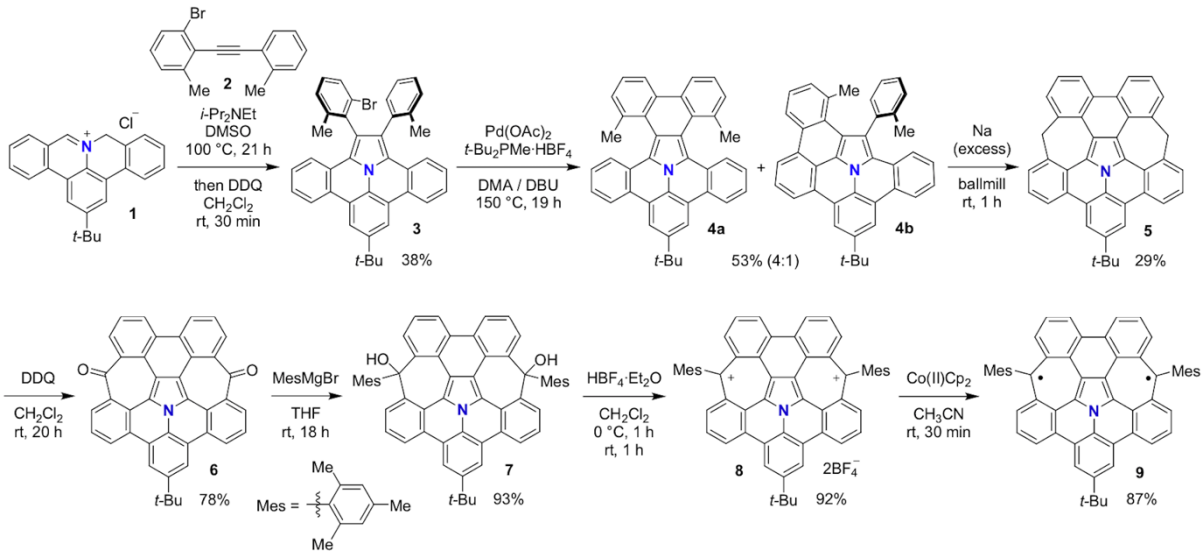

Scheme 3.1. Synthesis of Azadihomocorannulene Dication **8** and Diradical **9**.

As shown in **Scheme 3.1**, the synthesis of azadihomocorannulene commenced with a 1,3-dipolar cycloaddition reaction of diarylacetylene **2** and the azomethine ylide generated from iminium salt **1**. This was followed by a dehydrogenation reaction with 2,3-dichloro-5,6-dicyano-*p*-benzoquinone (DDQ), leading to the formation of π-extended pyrrole **4** in a 38% yield. The subsequent palladium-catalyzed intramolecular cyclization produced a mixture of cyclized products, **4a** and **4b**, with a total yield of 83%. Following this, we performed mechanochemical intramolecular cyclization via a ball-mill in the presence of sodium to form cyclized compound **5**, which bears two 7-membered rings, in 29% yield. Notably, this reaction is a relatively rare example of a transition-metal-free direct C–H/C–H coupling reaction between sp^2 and sp^3 carbon atoms[27,28]. Subsequently, an oxidation reaction was conducted using DDQ to produce diketone **6** in 78% yield. Treatment of **6** with an excess of mesitylmagnesium bromide in the presence of cerium(III) chloride yielded diol **7** in 93% yield and the crystal structure showed the molecule has a distorted structure due to the steric effect of mesitylene groups (**Figure S3.12**). The dihydroxylation, employing tetrafluoroboric acid

diethyl ether complex, yielded dication **8**. Finally, a two-electron reduction of **8** using cobaltocene in acetonitrile was conducted to obtain compound **9** as a black solid.

Single crystals of dication **8** suitable for X-ray diffraction analysis were obtained by slow evaporation of its solution in dichloromethane and benzene under an argon atmosphere. The dication molecules crystalized in the triclinic space group $P\bar{1}$ and a single unit cell contains two ionic pairs, including a solvent molecule of benzene (**Figure 3.2 and S3.14**). The main p-core of **8** adopts a twisted structure with an approximate C_2 symmetry and features mesityl substituents with an averaged dihedral angle of 77°, which is likely due to the interaction between the mesityl groups and the vacant p-orbitals at the ipso position. The observed bond lengths, ranging from 1.407 to 1.448 Å, indicate no significant bond alternation in the heptagon rings. HOMA analysis show the heptagon rings have an averaged value of 0.546 (mean) (**Figure S3.17**), suggesting it may have weak 6π aromaticity. In contrast, single crystals of diradicaloid **9** were obtained by slow evaporation of its solution in dichloromethane and benzene under argon atmosphere at −20 °C to form the tetragonal space group $I4/m$. A unit cell of **9** contains eight molecules and the residue solvents of dichloromethane and water (**Figure S3.16**). Each of the four molecules of **9** aggregates to form a square-shaped with the residual solvent molecules filling the vacant space. No significant intermolecular π-π interactions were observed in the packing structure. The main p-core of **9** forms a slightly wavy structure with C_s symmetry and is more planar than **8**. The dihedral angle of the core and mesityl substituents was determined to be 87°, larger than that of **8**, indicating minimal electronic perturbation by the mesityl groups. Upon conversion from **8** to **9**, their bond lengths do not change significantly, with deviations up to 0.035 Å, likely due to the rigid structures of both **8** and **9**.

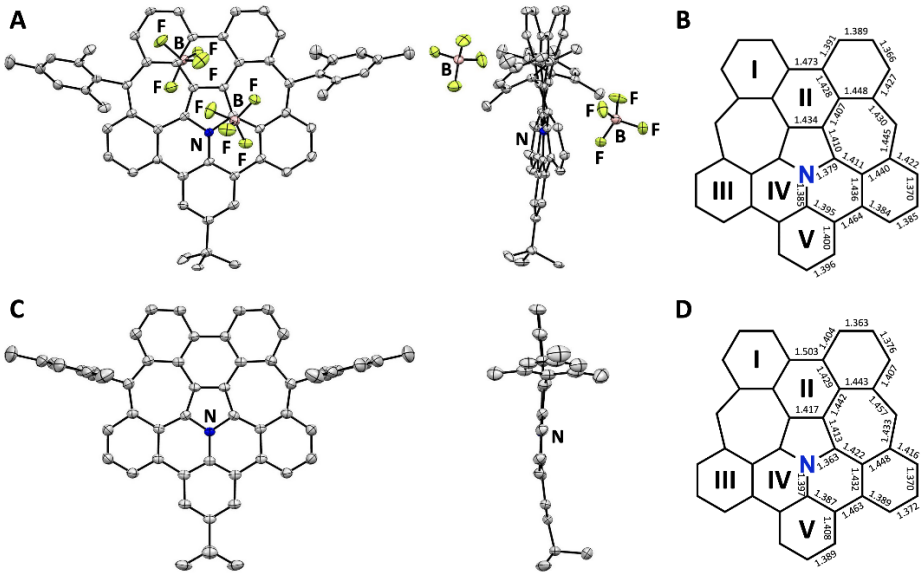

Figure 3.2. (**A**) ORTEP structures and (**B**) mean bond lengths (Å) of dication **8**. (**C**) ORTEP structures and (**D**) bond lengths of diradical **9**.

Density functional theory (DFT) calculation (**Table S3.2**) at the CASSCF(2,2)/6-31G(d) level of theory revealed that the diradical character (*y*) of compound **9** was estimated to be 0.83, which suggested that **9** would have an open-shell nature. To investigate the radical character of **9** experimentally, therefore, ESR measurements of **9** were conducted both in solution and in the frozen state. The ESR spectrum in toluene solution shown in **Figure S3.18** revealed a signal split into five components, indicative of the presence of two interacting radicals, which suggests the presence of a triplet species. The spectrum of $\Delta M_s = \pm 1$ in frozen *o*-terphenyl (**Figure S3.19**) showed small signals around 317 and 338 mT, attributed to the "*z*" component of the triplet signal, although the spectrum was likely affected by the presence of a prominent monoradical impurity, leading to overlapping "x, y" tensors. Further analysis revealed the forbidden transition signals of $\Delta M_s = \pm 2$, which exhibit a tensor approximately half the magnitude of $\Delta M_s = \pm 1$, to indicate an |E| value close to 0 (**Figure 3.3B**). These results clearly indicate the presence of triplet diradical species. Based on these findings, spin–spin distances were calculated using the point dipole approximation, resulting in an estimated |D|

value of approximately 11 mT and an average spin–spin distance of 6.32 Å. This spin–spin distance value is close to the 6.19 Å distance determined by averaging the distance between the heptagon centers (4.645 Å) and the distance of ipso carbons (7.740 Å) of the 7-membered rings in the X-ray structure (**Figure S3.21**). Variable-temperature ESR measurements in frozen *o*-terphenyl (**Figure 3.3A** and **Figure S3.19**) showed that the signals were weakened progressively as the temperature decreased. This trend implies that the molecule predominantly exists in the singlet state at lower temperatures, with triplet species appearing at higher temperatures. To explore the temperature dependence of the signal decay, the Bleany-Bowers equation was employed, focusing on the $\Delta M_s = \pm 2$ forbidden transition signals. The fitting yielded a J/k value of −1063 K and a corresponding ΔE_{S-T} of −2.1 kcal/mol. These values are consistent with the value of −1.3 kcal/mol obtained by DFT calculation at the UB3LYP/6-31G(d,p) level of theory (**Table S3.3**). Due to this small ΔE_{S-T} gap, diradicaloid **9** is easily activated to the triplet state, and no ^{1}H NMR signal of **9** was observed even at low temperatures of −80 °C in dichloromethane.

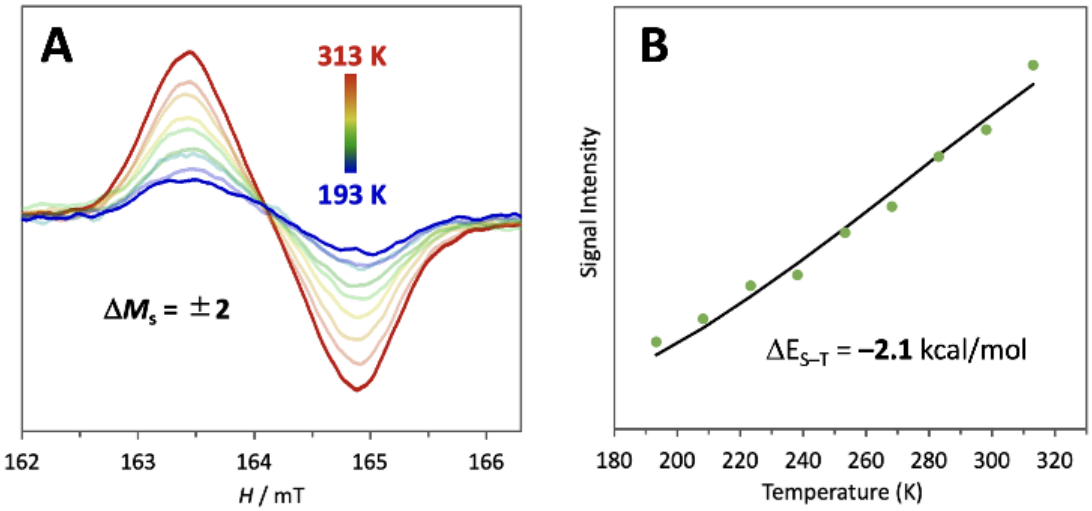

Figure 3.3. (**A**) Variable-temperature ESR spectra of **9** in *o*-terphenyl. (**B**) Variable-temperature ESR spectra of **9** in toluene.

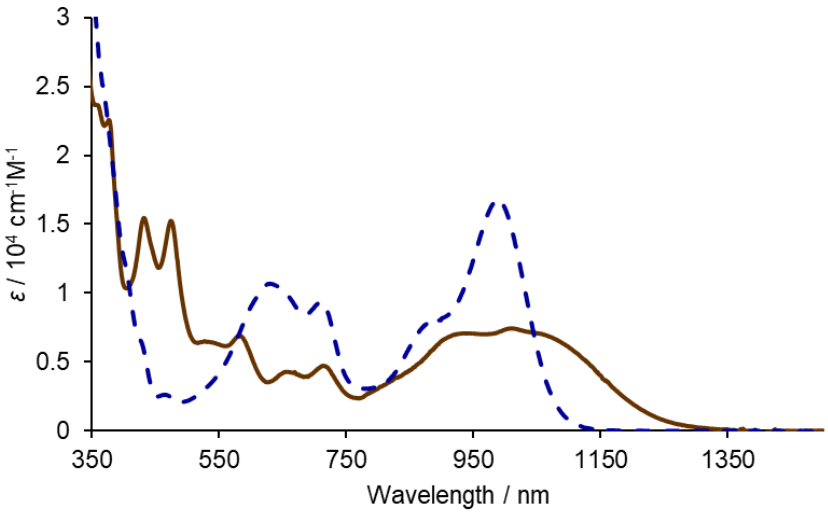

Figure 3.4. UV-visible absorption spectra of **8** (1.0×10^{-4} M :blue) and **9** (5.3×10^{-5} M :brown) in dichloromethane.

A characteristics of open-shell diradicaloid molecules is its small HOMO−LUMO gap. In order to reveal it, the photophysical properties of dication **8** and diradicaloid **9** were investigated. A solution of **8** in dichloromethane, exhibiting a dark blue color, showed a sharp peak at 1000 nm (**Figure 3.4**). This is attributed to the HOMO–LUMO transition (λ = 863 nm, f = 0.146), as determined by TD-DFT calculations at the B3LYP/6-311+G(2d,p) level (**Figure S3.27** and **Table S3.4**). The absorption spectrum of **9** displays a deep brown color and a broad band in the near-infrared region from 800 nm to 1300 nm, which is also consistent with the HOMO–LUMO transition (λ = 1121 and 1034 nm, f = 0.005 and 0.062; **Figure S3.28** and **Table S3.5**). The absorption in the near-infrared region is an indication of its diradicaloid character[29]. The narrow HOMO–LUMO gap of diradicaloid **9** is also supported by the electrochemical measurement. The cyclic voltammogram of **9** in dichloromethane showed three reversible and one irreversible redox wave (E_2^{ox} = +0.09 V, E_1^{ox} = −0.56 V, E_1^{red} = −1.64 V, and $E_2^{red,pc}$ = −1.91 V vs Fc/Fc^+) (**Figure 3.5**). The HOMO–LUMO gap from the cyclic voltaammogram was calculated to be 1.08 eV.

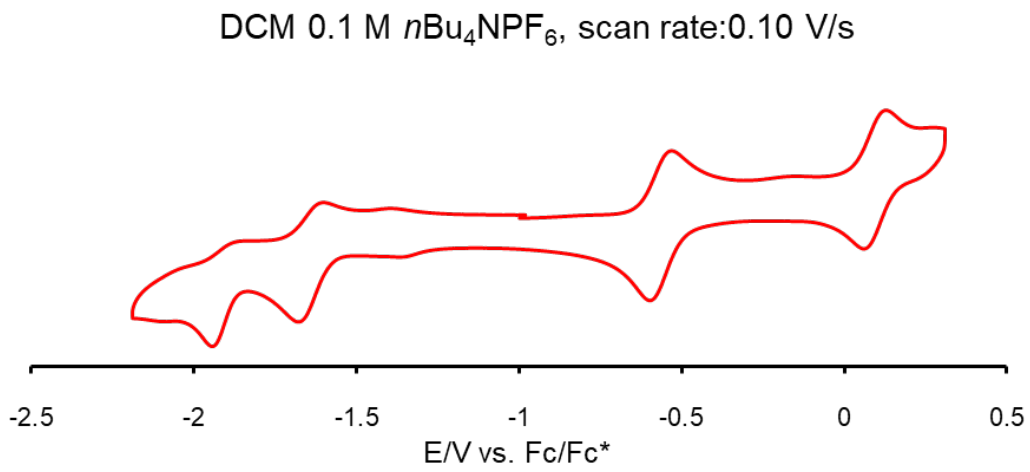

Figure 3.5. Cyclic voltammogram of **9·** measured in dichloromethane with 0.10 M Bu_4NPF_6 at a scan rate of 100 mV/s.

To gain further insight into aromaticity, the Nucleus-Independent Chemical Shifts (NICS) values (**Figure 3.6A**) of dication **8** and diradical **9** were calculated at the (U)B3LYP/6-31g(d,p) level of theory, using the molecular structures where *t*-butyl and mesityl substituents of **8** and **9** were replaced by hydrogen atoms. The NICS(1)zz values of **8** indicate significant shielding effects on the pyrrole ring (−39.4 ppm) and the peripheral five benzene rings (from −26.1 to −31.3 ppm). These trends are similar to those observed in other azacorannulene derivatives[30]. On the other hand, the NICS(1)zz values of **9** suggest that the heptagon rings have a positive value of +15.6 ppm, which falls within the non-aromatic region. This value is comparable to those of compound **F** (+13.5)[20] and compound **G** (+10.5)[21], and lower than azahomocorannulene **L** (+22.2)[26]. A significant difference of NICS values upon conversion from **8** to **9** was observed in hexagon ring **II**, which changes from −4.55 to −34.7, and hexagon ring **III**, which changes from −31.3 to −12.3. This indicates the contribution of the resonance structure of **9-quino** in **Figure 3.6B** to some extent. The overall resonance structures of diradical **9** are depicted in **Figure 3.6B**, where both of **9-dirad** with 6 Clar benzene rings and **9-quino** with 2 Clar benzene rings contribute to the resonance.

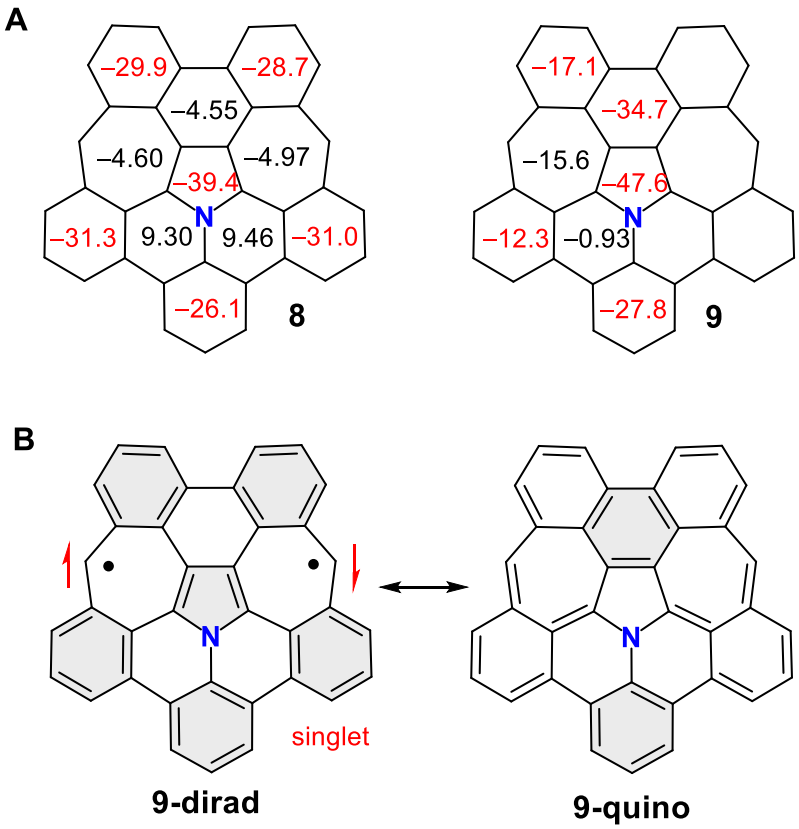

Figure 3.6. (**A**) NICS(1)zz values of **8** (left) and **9** (right). (**B**) Resonance structures of **9**. Gray ring color indicates Clar structures with 6π electrons.

3.3. Conclusion

In conclusion, we synthesized azapentabenzodihomocorannulene derivatives, dication **8** and diradicaloid **9**. The key step in the synthesis of these molecules was the mechanochemical intramolecular cyclization of molecule **4** in the presence of sodium, efficiently connecting C(sp^2) and C(sp^3) in a single step via C-H activation. The neutral molecule **9** was obtained through the one-electron reduction of dication **8**. X-ray diffraction analysis revealed notable differences in planarity between **8** and **9**. ESR measurements and DFT calculations revealed that **9** adopts a singlet diradical (diradicaloid) ground state with small ΔE_{S-T} gap. The findings from this study highlight the effectiveness of homo-type π-extension in designing polycyclic

aromatic diradicaloid molecules and provide valuable insights into the topological features of non-alternant aromatic molecules.

3.4. Experimental section

1. Experimental section

General: All reactions were conducted under an argon atmosphere using Schlenk techniques. Thin-layer chromatography (TLC) was performed on glass plates pre-coated with silica gel that was impregnated with fluorescent indicators (Merck, #1.05715.0001). For column chromatography on silica gel, the method described by Still, et al.[31] was employed, utilizing silica gel 60N (spherical, neutral) purchased from W. R. Grace, Ltd.

Instrumentation: NMR spectra were measured by JEOL JNM-ECZL-500, Bruker Avance 400 and Bruker Avance III 400 NMR spectrometers. Proton chemical shifts are referenced to tetramethylsilane (δ = 0.00), or the residual signal of chloroform-*d* (δ = 7.26) and dichloromethane-d_2 (δ = 5.32). Carbon chemical shifts are referenced to tetramethylsilane (δ = 0.00) or the carbon resonance of chloroform-*d* (δ = 77.2) and dichloromethane-d_2 (δ = 54.0). Preparative high-pressure liquid chromatography (HPLC) was carried out using a LaboACE (Japan Analytical Industry Co. Ltd.) equipped with JAIGEL-2HR columns (Japan Analytical Industry; 20 mm i.d. × 600 mm) by eluting with chloroform at 8.0 mL/min or with a Buckyprep column (Nacalai, Co. Ltd.; 20 mm i.d. × 250 mm) by eluting with toluene at 8.0 mL/min, both at room temperature. High-resolution mass spectra (HRMS) were obtained with a Waters Q-Tof Premier mass spectrometer using the electrospray ionization time-of-flight (ESI-TOF) method and JEOL JMS-S3000 SpiralTOF mass spectrometer employing the matrix-assisted laser desorption/ionization time-of-flight (MALDI-TOF) method. Melting temperatures and decomposition temperatures were recorded on an OptiMelt MPA-100 apparatus. Infrared (IR) spectra were recorded with a PerkinElmer FTIR spectrum 100, utilizing an attenuated total

reflection (ATR) sampling accessary. Electron spin resonance (ESR) spectra were measured using a JEOL JES-X310 spectrometer and g-value was determined by the Mn^{2+}/MgO solid as a standard. Ultraviolet–visible (UV–vis) absorption spectra were taken on a Shimadzu UV-3600 spectrometer. Electrochemical analyses were conducted using a Biologic SP-50 electrochemical analyzer. Cyclic voltammetry was performed with a glassy carbon working electrode and a platinum counter electrode in dichloromethane containing 0.1 M Bu_4NPF_6 as a supporting electrolyte. The experiments employed an $Ag/AgNO_3$ reference electrode. Electrochemical experiments were done under argon atmosphere at room temperature.

Materials: The following reagents were purchased from the indicated suppliers and used as received: *N,N*-diisopropylethylamine (*i*-Pr_2NEt; TCI), 2,3-dichloro-5,6-dicyano-*p*-benzoquinone (DDQ; Fluorochem), palladium(II) diacetate ($Pd(OAc)_2$; Sigma), di-*t*-butyl(methyl)phosphonium tetrafluoroborate (*t*-$Bu_2PMe{\cdot}HBF_4$; Sigma), 1,8-diazabicyclo[5.4.0]undec-7-ene (DBU, Sigma), sodium (Na, Sigma), tin(II) chloride ($SnCl_2$; Sigma), cobaltocene ($CoCp_2$; Sigma), and tetrafluoroboric acid diethyl ether complex ($HBF_4{\cdot}Et_2O$; 51–57 wt% solution in diethyl ether; Sigma). Cerium(III) trichloride ($CeCl_3$) was prepared by heating cerium(III) trichloride heptahydrate ($CeCl_3{\cdot}7H_2O$; Sigma) for 24 h at 200 °C under vacuum. Mesitylmagnesium bromide (MesMgBr) was prepared from bromomesitylene and magnesium using a standard method and titrated before use. Anhydrous toluene, tetrahydrofuran (THF), dichloromethane (CH_2Cl_2), dimethylacetamide (DMA), and acetonitrile (CH_3CN) were purchased from Sigma. Anhydrous dimethyl sulfoxide (DMSO) was purchased from Alfa Aesar. The following reagents were prepared according to literature procedures: 1-Ethynyl-2-methylbenzene[32], 1-bromo-2-iodo-3-methylbenzene[33], 2-*t*-butyl-8*H*-isoquinolino[4,3,2-*de*]phenanthridinium chloride (**1**)[34].

1-Bromo-3-methyl-2-(*o*-tolylethynyl)benzene (2)

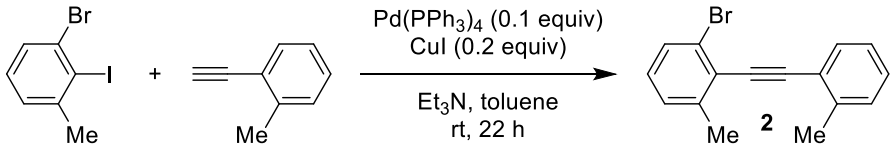

To a solution of 1-bromo-2-iodo-3-methylbenzene (1.19 g, 4.00 mmol), tetrakis(triphenylphosphine) palladium ($Pd(PPh_3)_4$, 0.46 g, 0.40 mmol) in triethylamine (7.5 mL) and toluene (15 mL) was added copper iodide (CuI, 0.15 g, 0.79 mmol) and then 1-ethynyl-2-methylbenzene (0.47 g, 4.05 mmol) under argon atmosphere. The mixture was stirred for 22 h at room temperature. After the volatile matters were evaporated, the residue was extracted with dichloromethane. The combined organic phases were washed with water and brine, and dried over sodium sulfate (Na_2SO_4). After filtration, the filtrate was concentrated under reduced pressure to obtain brown oil. The crude product was purified by silica gel column chromatography using hexane as eluent to yield compound **2** as colorless solids (0.95 g, 3.3 mmol, 83%).

mp 55–58 °C; R_f 0.35 (hexane); IR (neat) cm^{-1} 3071, 3052, 2921, 2214, 1950, 1934, 1860, 1664, 1551, 1488, 1448, 1377, 1175, 1128, 1104, 1069, 1040, 989, 942, 857, 836, 770, 751; ^1H NMR (400 MHz, CD_2Cl_2, 300 K) δ 7.56 (d, J = 7.5 Hz, 1H), 7.47 (d, J = 8.0 Hz, 1H), 7.27 (d, J = 4.1 Hz, 2H), 7.24–7.16 (m, 2H), 7.09 (t, J = 7.8 Hz, 1H), 2.57 (s, 6H). ^{13}C NMR (101 MHz, CD_2Cl_2, 300 K) δ 143.0, 140.8, 132.4, 130.1, 130.0, 129.3, 129.1, 128.7, 126.0, 125.9, 125.7, 123.3, 97.7, 91.2, 53.8, 22.1, 21.3; HRMS (ESI) *m*/*z* calcd for $C_{16}H_{12}Br$ $[M+H]^+$ 285.0279, found 285.0268.

1,3-Dipolar Cycloaddition of Azomethine Ylide with Alkyne 2

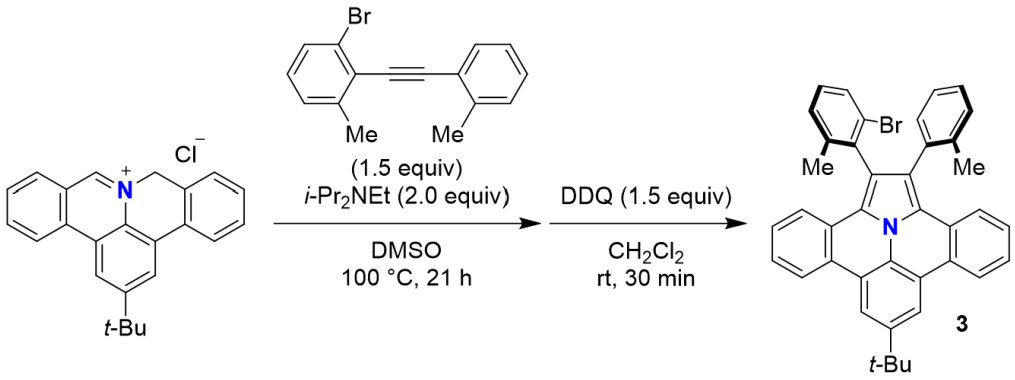

To a solution of iminium salt **1** (144 mg, 0.40 mmol) and alkyne **2** (171 mg, 0.60 mmol) in DMSO (6 mL) was added *N*,*N*-diisopropyl(ethyl)amine (136 µL, 0.80 mmol), and the mixture was stirred for 21 h at 100 °C. The solution was cooled to room temperature and diluted with toluene. The combined organic phases were washed with water three times and dried over sodium sulfate (Na_2SO_4). After filtration, the filtrate was concentrated under reduced pressure to obtain brown oil. The crude mixture was passed through a pad of silica gel with dichloromethane. After evaporation of volatile matters, the crude mixture was dissolved in dichloromethane (5 mL). The resulting mixture was added DDQ (136 mg, 0.60 mmol) and stirred for 30 minutes at room temperature. The reaction mixture was diluted with dichloromethane and quenched with saturated sodium bicarbonate ($NaHCO_3$) solution. The solution was extracted with dichloromethane and dried over sodium sulfate (Na_2SO_4). After filtration, the filtrate was concentrated under reduced pressure to obtain black oil. The crude product was purified by silica gel column chromatography using a mixed solvent of dichloromethane and hexane (1/9, v/v) as eluent to yield pyrrole **3** as a yellow solid (91 mg, 0.15 mmol, 38%).

R_f 0.43 (dichloromethane:hexane = 1:5); mp 252–254 °C; IR (neat) cm^{-1} 2959, 1942, 1610, 1572, 1477, 1437, 1417, 1380, 1361, 1291, 1251, 1171, 1121, 1042, 963, 943, 892, 864, 841, 757, 729; ^1H NMR (400 MHz, $CDCl_3$, 300 K) For major isomer, δ 8.43 (s, 2H), 8.39 (dd, J = 8.1, 3.3 Hz, 2H), 7.56 (t, J = 4.8 Hz, 1H), 7.50 (d, J = 7.7 Hz, 1H), 7.46 (d, J = 8.4 Hz, 1H),

7.40 (t, J = 7.5 Hz, 1H) 7.28–7.16 (m, 6H), 7.12–7.08 (m, 3H), 2.16 (s, 3H), 1.9 (s, 3H), 1.58 (s, 9H). For minor isomer, δ 8.43 (s, 2H), 8.39 (dd, J = 8.1, 3.3 Hz, 2H), 7.46–7.37 (m, 4H), 7.29–7.16 (m, 6H), 7.13–7.03 (m, 3H), 2.26 (s, 3H), 2.21 (s, 3H), 1.58 (s, 9H). ^{13}C NMR (101 MHz, $CDCl_3$, 300 K) δ 146.25, 141.26, 140.40, 138.79, 137.34, 136.81, 136.77, 135.14, 135.03, 131.17, 130.35, 130.31, 130.22, 130.08, 129.89, 128.95, 128.83, 128.77, 128.57, 128.51, 128.25, 128.01, 127.31, 127.19, 126.89, 126.19, 125.97, 125.87, 125.67, 125.25, 122.97, 122.94, 122.65, 122.62, 122.43, 122.35, 122.31, 121.33, 121.29, 120.51, 120.31, 120.23, 120.07, 117.47, 117.42, 35.29, 31.86, 21.66, 21.22, 20.51, 19.82; HRMS (ESI) m/z calcd for $C_{40}H_{32}NBr$ $[M+H]^+$ 606.1796, found 606.1823.

Palladium-Catalyzed Intramolecular Cyclization of 3

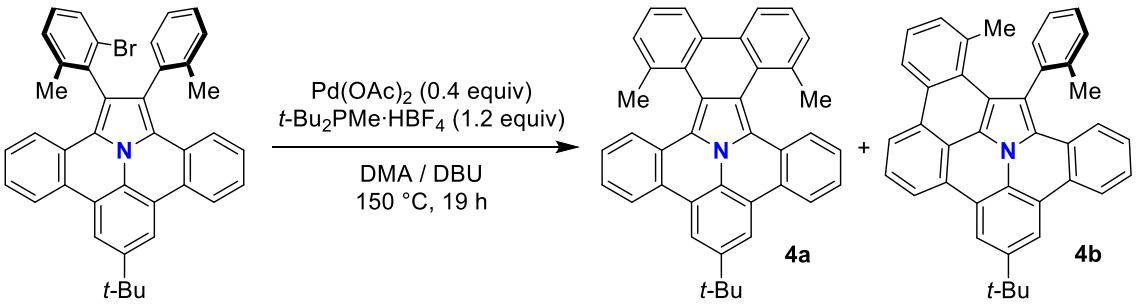

To a mixture of compound **3** (93 mg, 0.15 mmol), palladium(II) diacetate (14 mg, 0.06 mmol), and t-$Bu_2PMe{\cdot}HBF_4$ (45 mg, 0.18 mmol) in a Schlenk tube were added DBU (1.0 mL) and DMA (4.0 mL) via a syringe. The solution was degassed by a repeated freeze-pump-thaw method three times. The solution was stirred for 19 h at 150 °C. The solution was cooled to room temperature and diluted with toluene. The organic phase was washed with water three times and dried over sodium sulfate. After filtration, the filtrate was concentrated under reduced pressure to obtain orange oil. The crude product was purified by preparative HPLC with JAI-GEL columns. The collected fraction was evaporated to yield the mixture products in the ratio of 4:1 as a yellow solid (40 mg, 0.08 mmol, 53%); R_f: 0.44 (dichloromethane:hexane = 1:5).

Mechanochemical Cyclization of 4

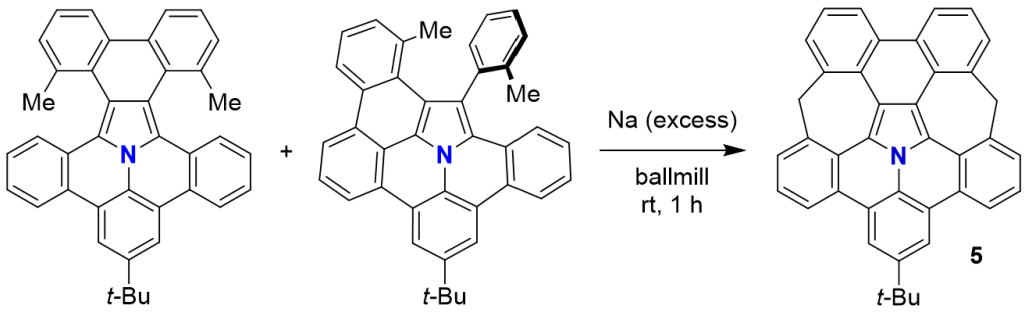

To a 10-mL stainless steel jar was placed compound **4** (10 mg), sodium (10 mg, 0.43 mmol) and a stainless steel ball. The jar was closed and set to 30 Hz of milling for 1 hour. After opening the jar, the reaction mixture was collected with dichloromethane and filtered (*Caution: At the 10-mg scale, the sodium residue spontaneously deactivates during the mechanochemical reaction. However, since the sodium residue is potentially flammable, so it is strongly recommended to carefully quench the reaction with alcohol/water under inert atmosphere and extract the products with organic solvents*). The solution was concentrated under reduced pressure to obtain brown solids. The crude was passed through a pad of silica gel with dichloromethane. After the evaporation of volatile matters, the crude product was purified by preparative HPLC with JAI-GEL columns. The collected fraction was evaporated to yield the product **5** as an orange solid (2.9 mg, 5.6 μmol, 29%).

R_f 0.38 (dichloromethane:hexane = 1:5); mp 283–285 °C (decomp); IR (neat) cm^{-1} 3069, 3031, 2951, 1906, 1608, 1578, 1476, 1459, 1435, 1413, 1349, 1303, 1285, 1249, 1188, 1095, 1078, 947, 863, 815, 799, 783, 761, 755, 740; ^{1}H NMR (400 MHz, CD_2Cl_2, 300 K) δ 8.50–8.48 (s, 2H), 8.45 (dd, J = 6.4 Hz, J = 2.8 Hz, 2H), 8.38 (d, J = 7.9 Hz, 2H), 7.66 (d, J = 7.1 Hz, 2H), 7.64–7.57 (m, 6H), 4.49 (s, 4H), 1.58 (s, 9H). ^{13}C NMR (101 MHz, CD_2Cl_2, 300 K) δ ^{13}C NMR (101 MHz, CD_2Cl_2) δ 148.0, 134.6, 132.8, 129.8, 129.3, 129.1, 128.3, 128.1, 127.6, 127.2, 126.8, 126.3, 122.8, 122.1, 121.2, 121.1, 118.5, 118.3, 44.2, 35.7, 31.9; HRMS (ESI) *m*/*z* calcd for $C_{40}H_{27}N$ $[M+H]^+$ 522.2222, found 522.2238.

Oxidative Carbonylation of 5

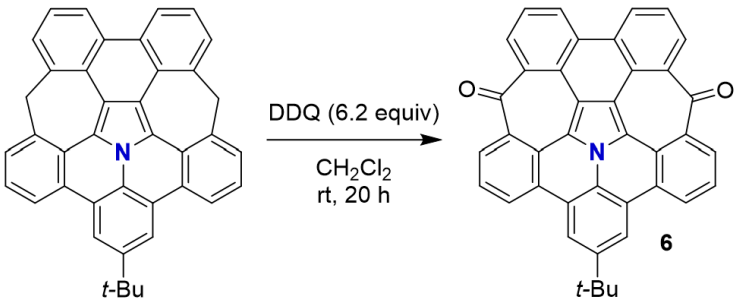

A solution of DDQ (90 mg, 0.40 mmol) and compound **5** (34 mg, 0.065 mmol) in dichloromethane (8 mL) was stirred for 20 h at room temperature to gradually afford orange precipitate. The solution was cooled to room temperature and poured into ethyl acetate. The precipitate was collected by filtration and washed with ethyl acetate and hexane to obtain diketone **6** (28 mg, 0.051 mmol, 78%) orange solid.

R_f 0.41 (dichloromethane:hexane = 1:2); mp 391–393 °C (decomp); IR (neat) cm^{-1} 3053, 2950, 2901, 2867, 1619, 1606, 1572, 1560, 1548, 1526, 1476, 1447, 1436, 1408, 1310, 1278, 1253, 1205, 1163, 1085, 992, 918, 862, 824, 800, 747, 730; ^{1}H NMR (500 MHz, CD_2Cl_2/CS_2, 300 K) δ 8.91 (d, J = 6.8 Hz, 2H), 8.76 (d, J = 6.7 Hz, 2H), 8.56 (d, J = 8.0 Hz, 2H), 8.54 (s, 2H), 8.49 (d, J = 7.4 Hz), 7.85–7.75 (m, 4H), 1.63 (s, 9H); ^{13}C NMR (Note: Clear ^{13}C NMR signals were not obtained due to poor solubility of compound **6**); HRMS (MALDI-TOF MS) m/z calcd for $C_{40}H_{23}NO_2$ $[M]^+$ 549.1723, found 549.1726.

Addition of Mesityl Grignard Reagent to Diketone 6

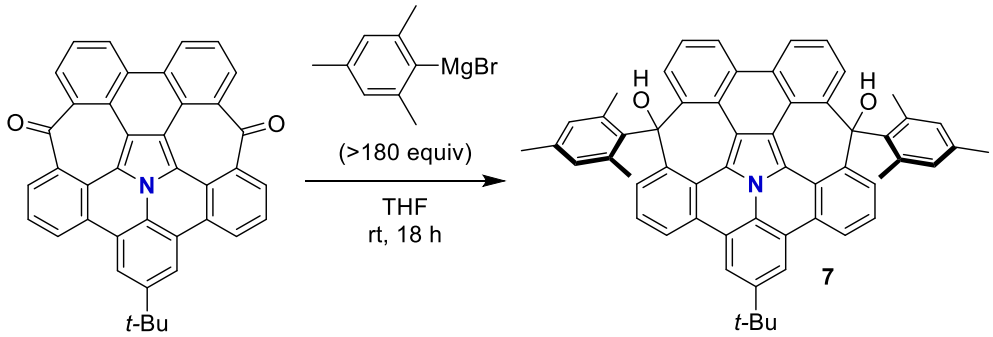

To a mixture of diketone **6** (24 mg, 0.044 mmol) in a 25-mL Schlenk tube was added mesitylmagnesium bromide (2.0 M solution in THF, 4.0 mL, 8.0 mmol) at 0 °C. The reaction mixture was stirred for 18 h at room temperature. The reaction mixture was quenched with an aqueous solution of ammonium chloride and extracted with dichloromethane three times. The combined organic phases were washed with water and brine, and dried over sodium sulfate. After filtration, the volatile matters were removed under reduced pressure to obtain brown oil. The crude mixture was purified by preparative HPLC with a buckyprep column with toluene. The collected fraction was evaporated to yield compound **7** as a yellow solid (32 mg, 0.041 mmol, 93%).

R_f 0.40 (dichloromethane:hexane = 3:1); mp 242–254 °C (decomp); IR (neat) cm^{-1} 3570, 3443, 2958, 1937, 1611, 1573, 1553, 1476, 1442, 1412, 1377, 1286, 1263, 1165, 1123, 1034, 1017, 953, 926, 845, 778, 737; ^1H NMR (500 MHz, $CDCl_3$, 300 K) δ 8.51 (d, J = 7.9 Hz, 2H), 8.41 (br, 2H), 8.37 (s, 2H), 8.31 (d, J = 7.4 Hz, 2H), 7.69 (t, J = 7.3 Hz, 2H), 7.64 (t, J = 7.3 Hz, 2H), 6.27 (br, 4H), 2.72 (s, 2H), 1.95 (s, 6H), 1.56 (s, 9H), 1.37 (br, 12H). ^{13}C NMR (126 MHz, $CDCl_3$, 300 K) δ 147.2, 139.4, 138.4, 137.6, 135.7, 131.9, 128.4, 126.9, 126.8, 126.7, 126.5, 126.4, 124.7, 124.0, 122.4, 122.3, 121.5, 121.0, 118.3, 117.8, 35.4, 31.8, 22.7, 20.6; HRMS (ESI) m/z calcd for $C_{58}H_{47}NO_2$ $[M+H]^+$ 790.3685, found 790.3649.

Dehydroxylation of Diol 7

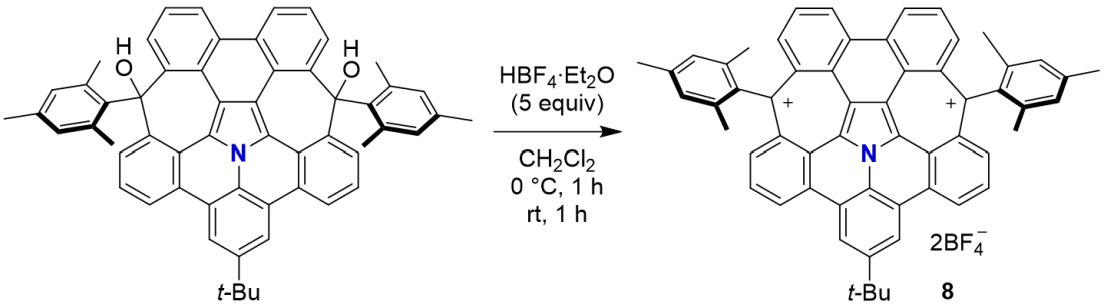

To a solution of diol **7** (5.1 mg, 6.5 μmol) in dichloromethane (1.0 mL) in a 10 mL Schlenk tube was added tetrafluoroboric acid diethyl ether complex (51–57 wt% solution in diethyl ether, 8.9 μL, 32 μmol) at 0 °C. The reaction mixture was stirred for 1 h at 0 °C and warmed to room temperature gradually. After additional strring for 1 h, diethyl ether was added to the solution to obtain dark blue precipitation. The precipitates were collected by filtration and washed with diethyl ether and hexane to obtain dication **8** as a dark blue solid (5.6 mg, 6.0 μmol, 92%).

IR (neat); cm^{-1} 2955, 2915, 1610, 1586, 1540, 1498, 1446, 1412, 1377, 1343, 1295, 1260, 1231, 1187, 1027, 940, 852, 828, 751, 681; ^1H NMR (500 MHz, CD_2Cl_2 with CF_3SO_3H (0.06%), 300 K) δ 9.94 (d, J = 7.6 Hz, 2H), 9.76 (d, J = 7.7 Hz, 2H), 9.09 (s, 2H), 8.85 (d, J = 8.7 Hz, 2H), 8.82 (d, J = 8.7 Hz, 2H), 8.58 (t, J = 8.2 Hz, 2H), 8.53 (t, J = 8.2 Hz, 2H), 7.34 (s, 4H), 2.60 (s, 6H), 1.84 (s, 12H), 1.75 (s, 9H). ^{13}C NMR (126 MHz, CD_2Cl_2 with CF_3SO_3H (0.06%), 300 K) δ 185.1, 154.2, 142.2, 141.9, 140.3, 140.2, 139.3, 136.3, 136.1, 135.9, 135.7, 134.7, 133.4, 133.3, 132.3, 132.2, 131.7, 131.1, 130.2, 128.0, 124.7, 123.6, 123.4, 122.8, 120.2, 117.7, 115.2, 36.7, 31.7, 21.5, 19.9; HRMS (MALDI-TOF MS) *m*/*z* calcd for $C_{58}H_{45}N$ $[M]^+$ 755.3547, found 755.3552.

Reduction of Dication 8

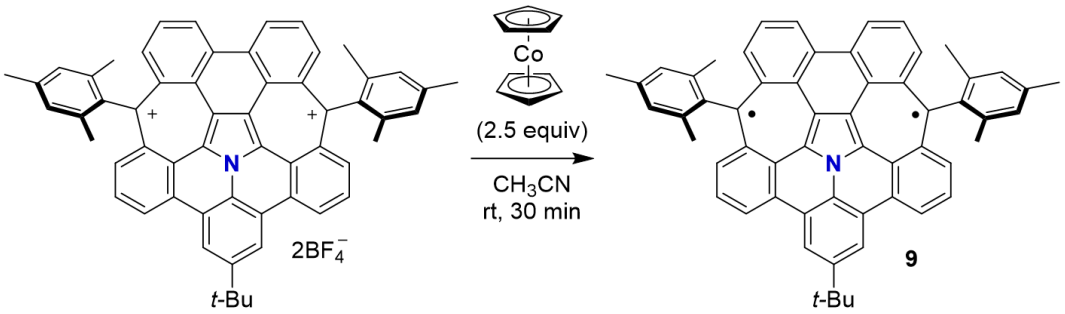

To a solution of **8** (5.6 mg, 6.0 μmol) in acetonitrile (2.5 mL) in a vial was added a solution of cobaltocene (2.9 mg, 15 μmol) in acetonitrile (2.5 mL). The mixture was stirred in the glove box for 0.5 h at room temperature to afford dark brown precipitates. The precipitates were collected by filtration and washed with acetonitrile and hexane to obtain **9** (3.9 mg, 5.2 μmol, 87%).

IR (neat); cm^{-1} 2955, 2918, 2851, 1741, 1607, 1579, 1547, 1492, 1427, 1373, 1357, 1258, 1213, 1177, 1107, 1004, 926, 908, 849, 799, 782, 728; HRMS (MALDI-TOF MS) *m*/*z* calcd for $C_{58}H_{45}N$ $[M]^+$ 755.3547, found 755.3574.

2. NMR Spectra

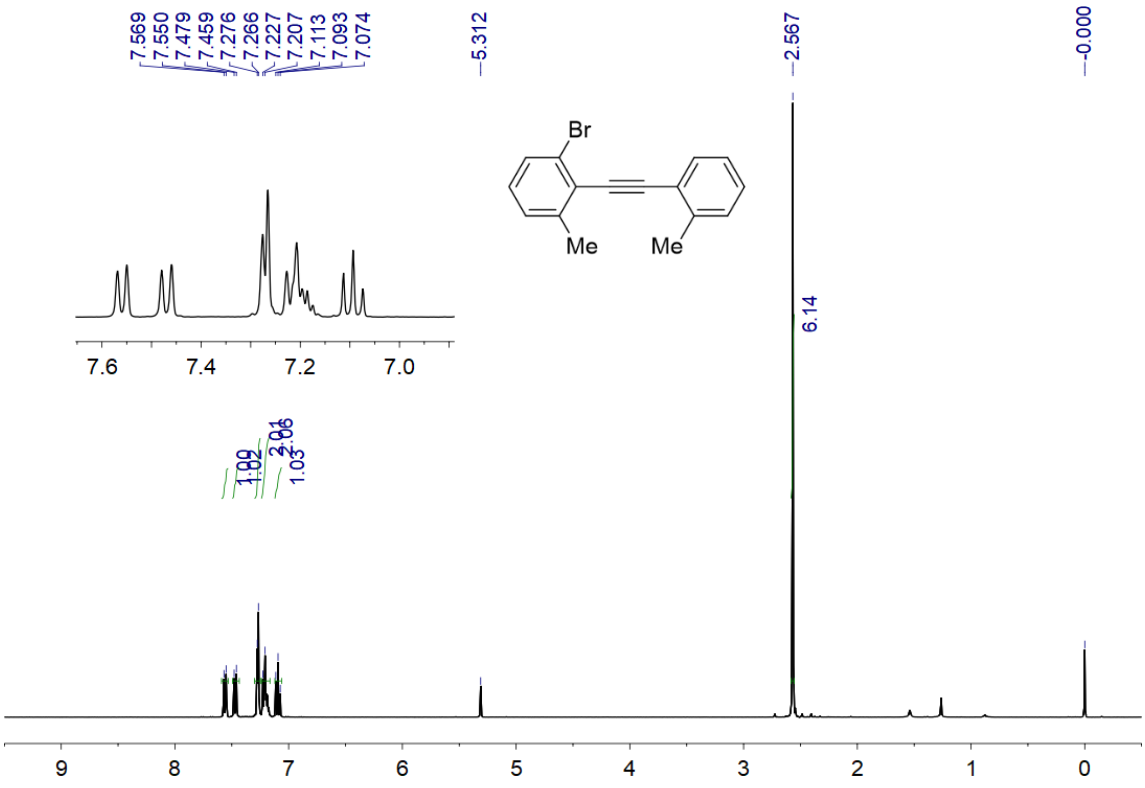

Figure S3.1. ^{1}H NMR spectrum of **2** (400 MHz, CD_2Cl_2, 300 K).

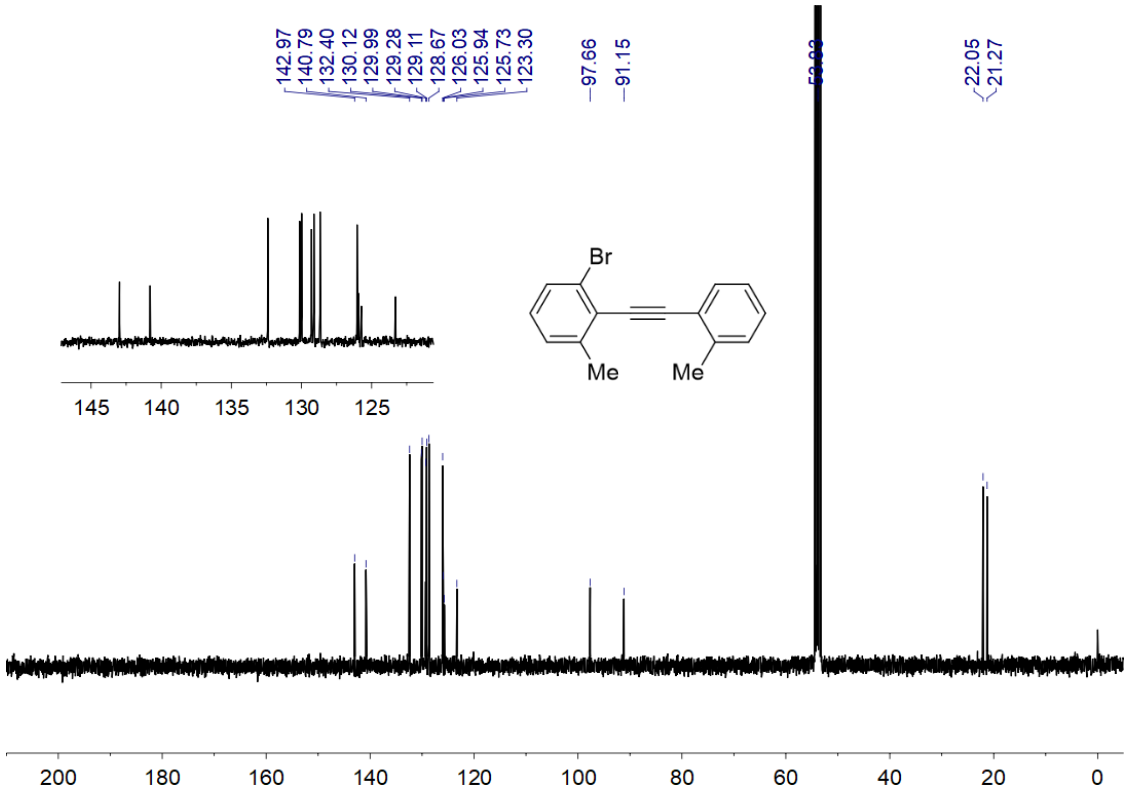

Figure S3.2. ^{13}C NMR spectrum of **2** (101 MHz, CD_2Cl_2, 300 K).

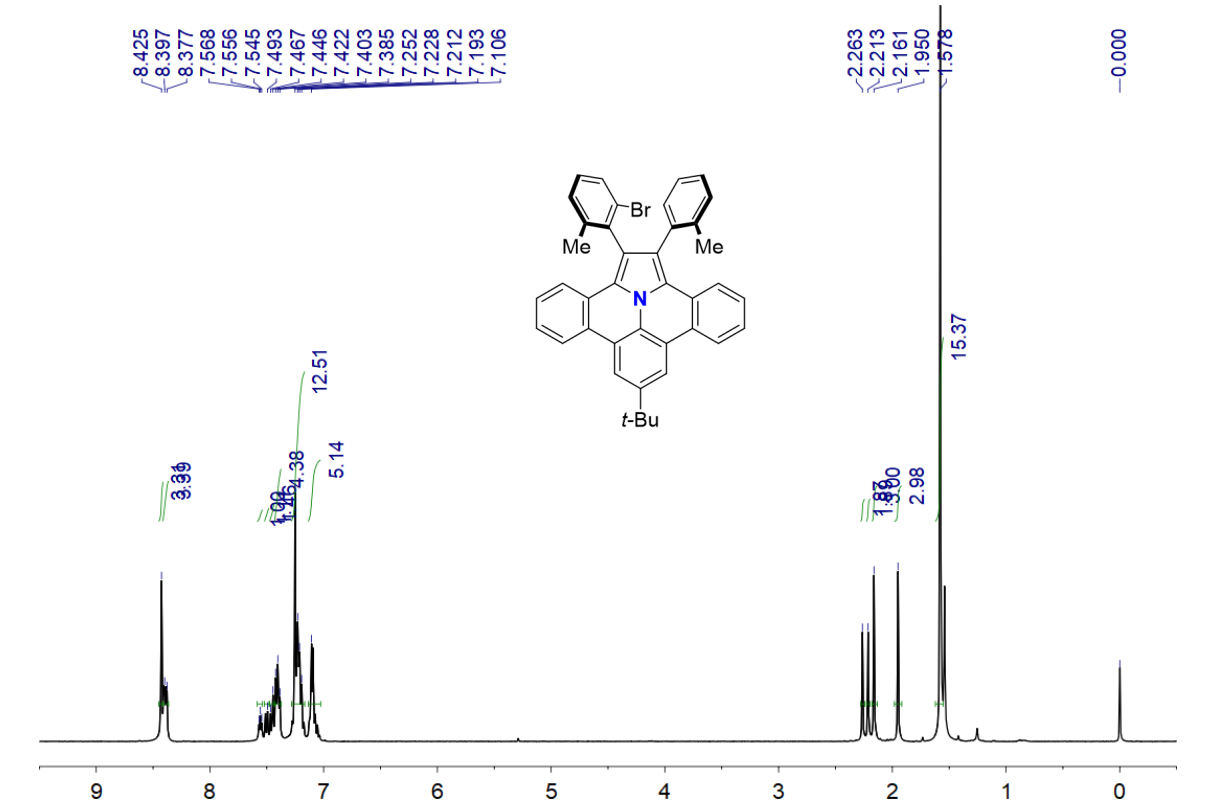

Figure S3.3. ^{1}H NMR spectrum of **3** (400 MHz, $CDCl_3$, 300 K).

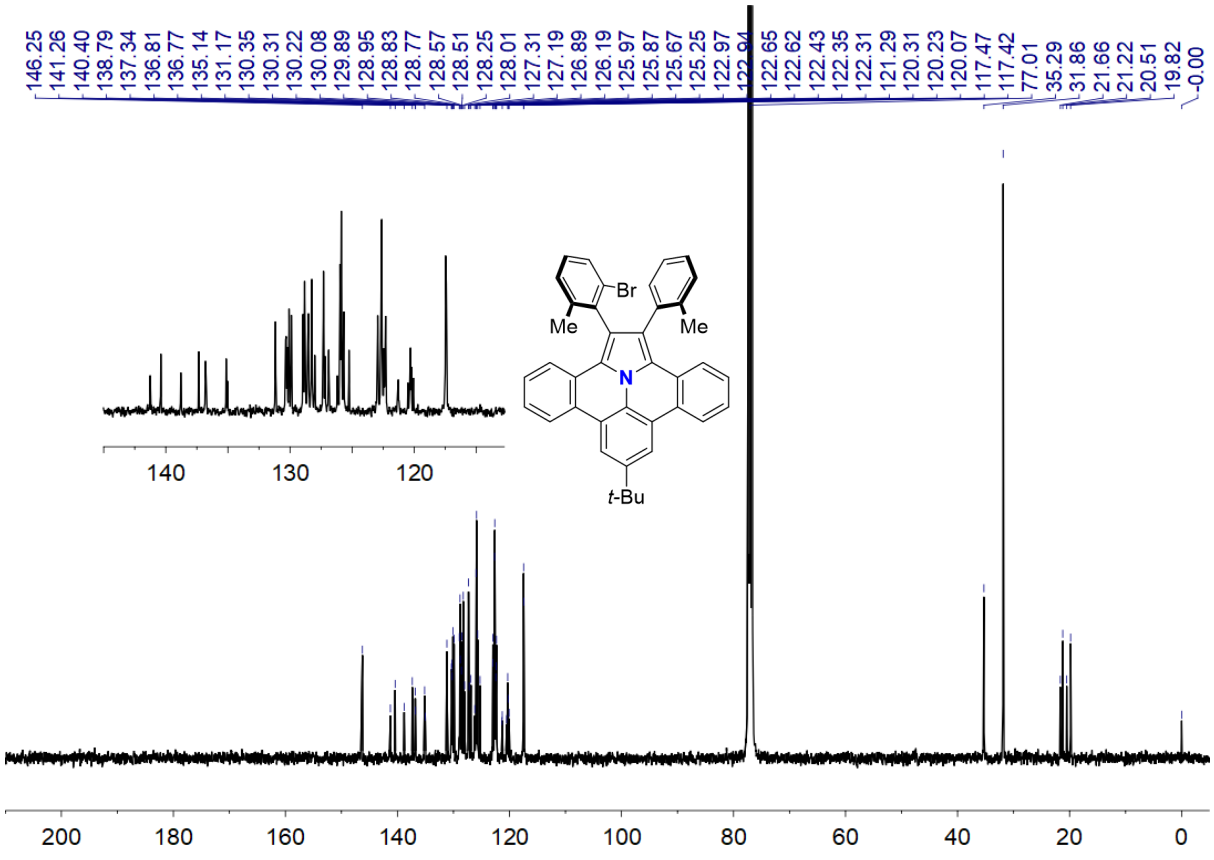

Figure S3.4. ^{13}C NMR spectrum of **3** (101 MHz, $CDCl_3$, 300 K).

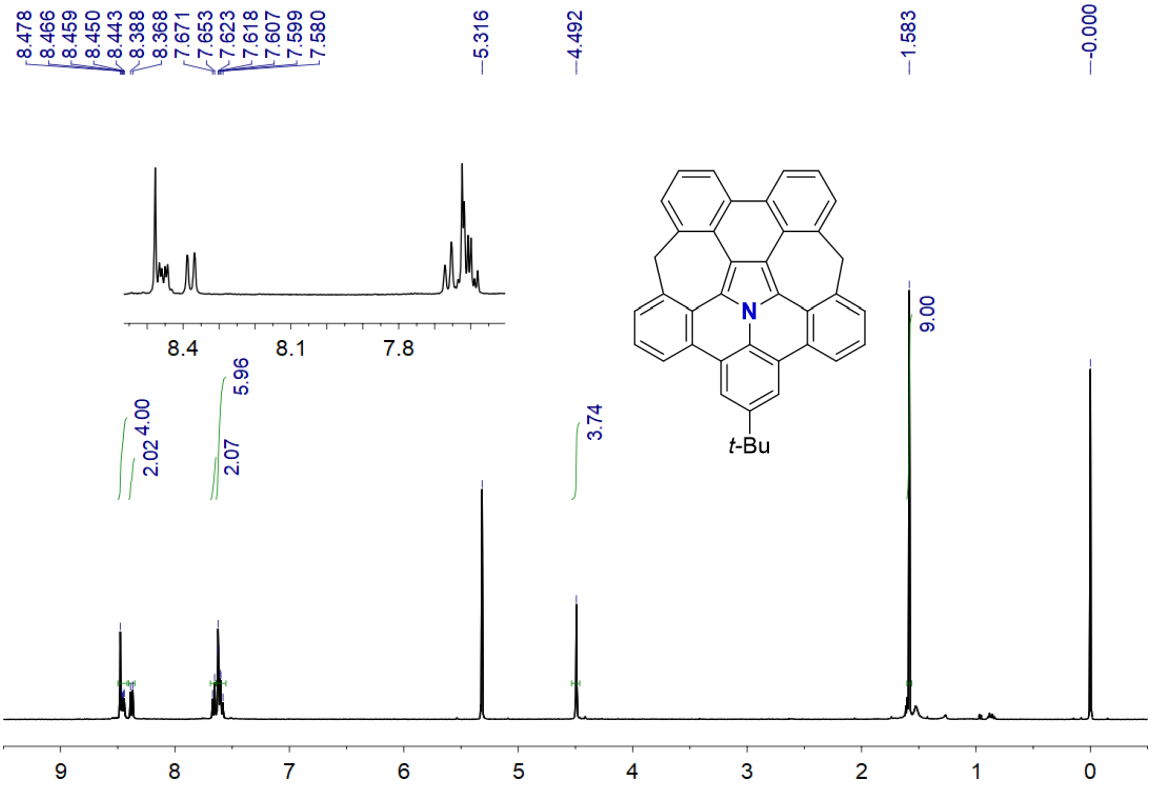

Figure S3.5. ^{1}H NMR spectrum of **5** (400 MHz, CD_2Cl_2, 300 K).

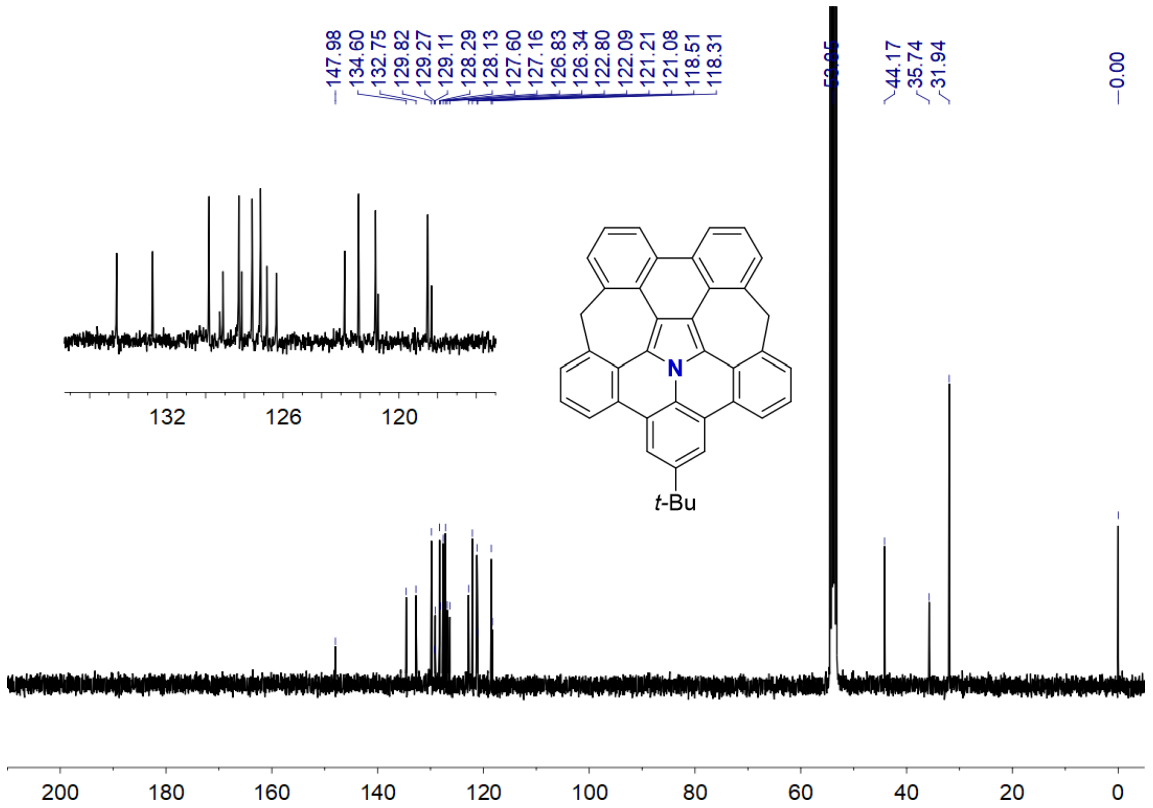

Figure S3.6. ^{13}C NMR spectrum of **5** (101 MHz, CD_2Cl_2, 300 K).

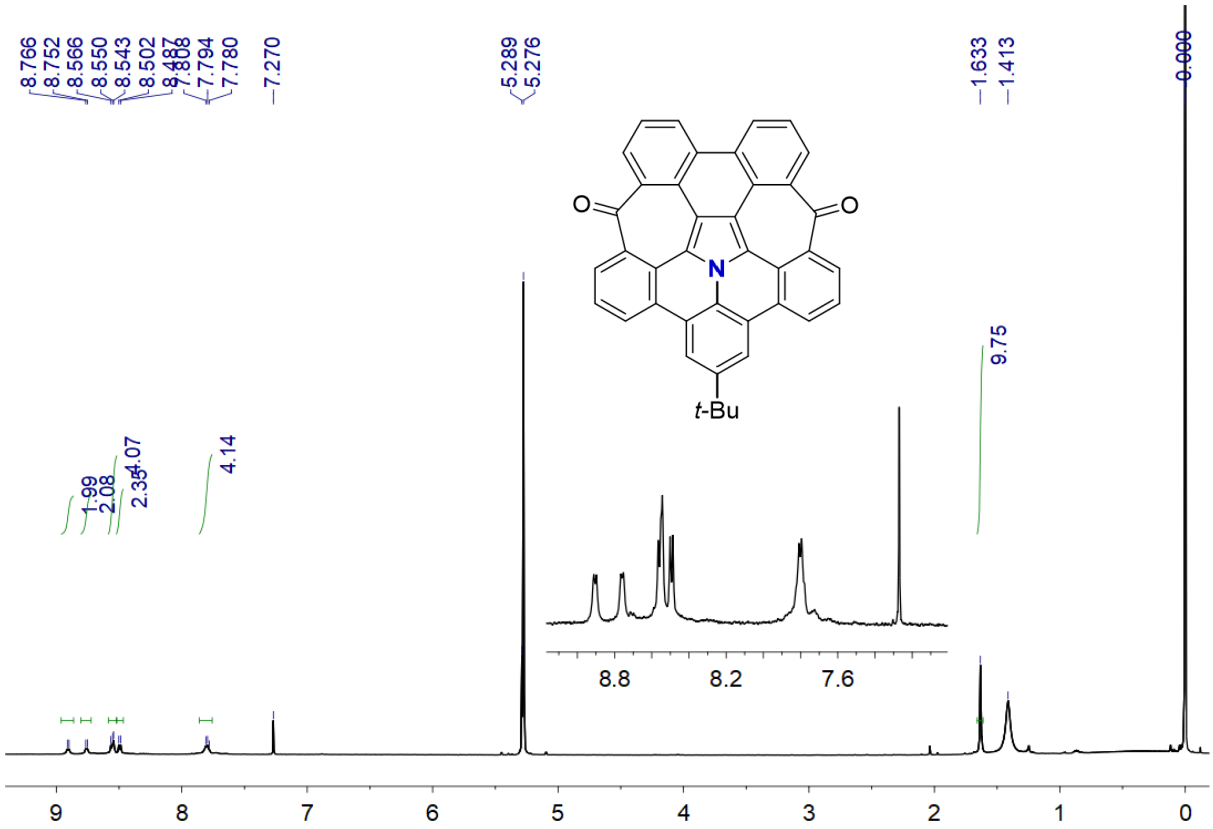

Figure S3.7. ^{1}H NMR spectrum of **6** (500 MHz, CD_2Cl_2/CS_2, 300 K).

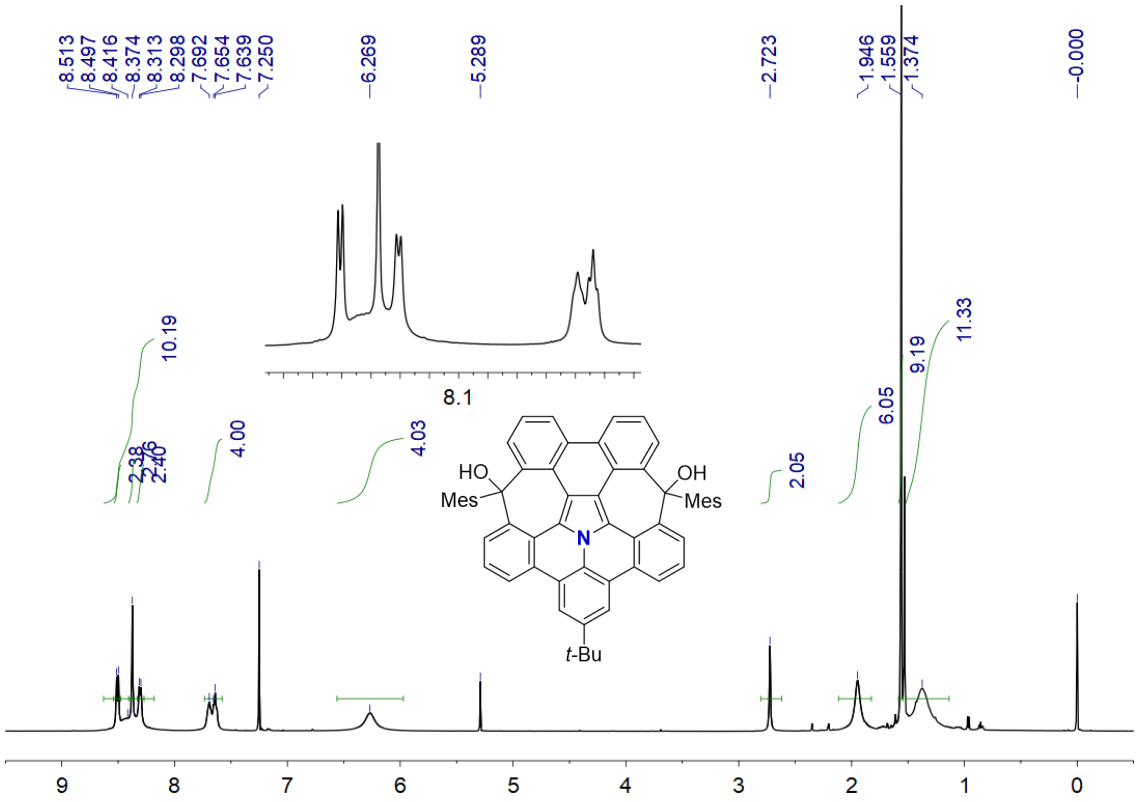

Figure S3.8. ^{1}H NMR spectrum of **7** (500 MHz, $CDCl_3$, 300 K).

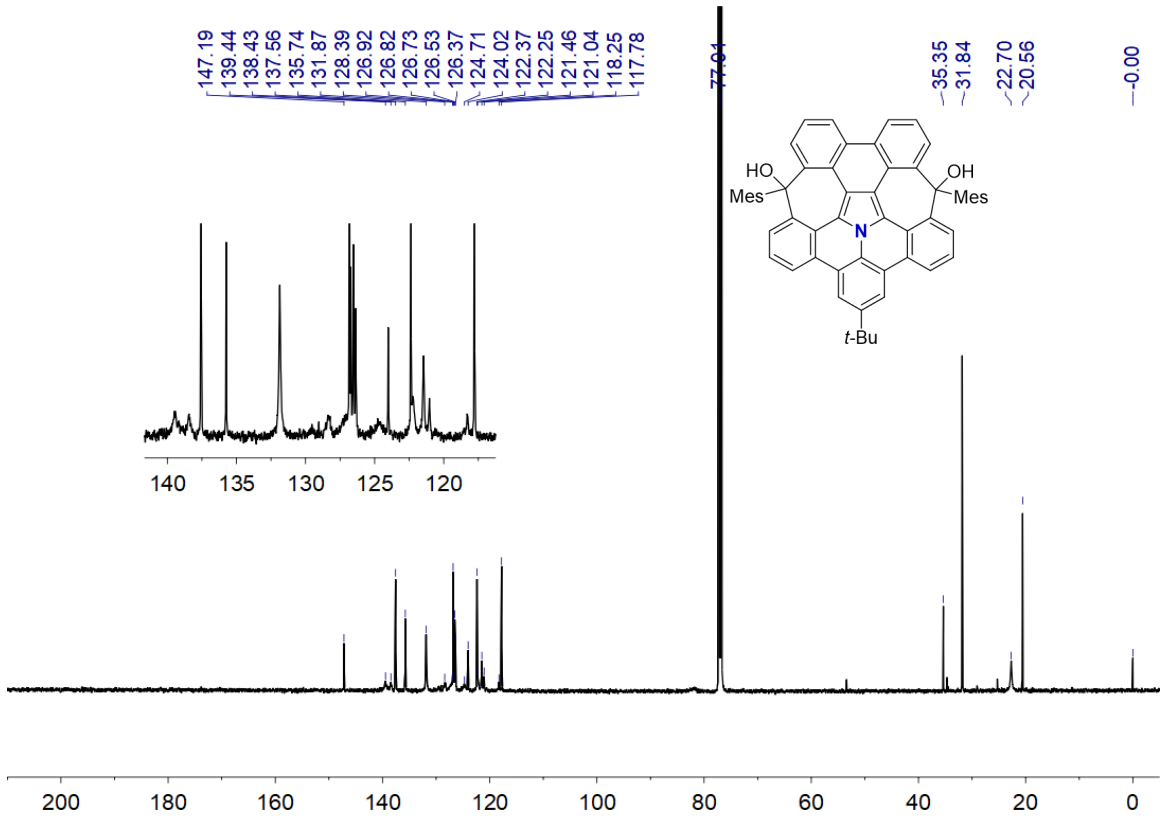

Figure S3.9. ^{13}C NMR spectrum of **7** (126 MHz, $CDCl_3$, 300 K).

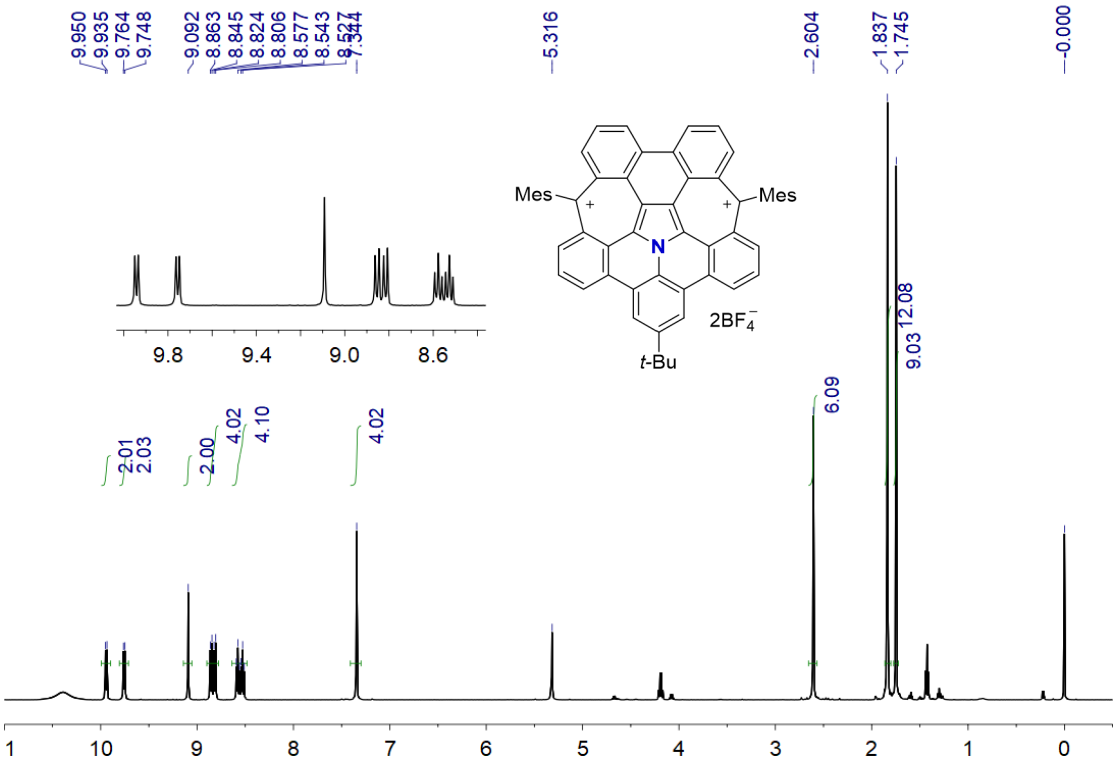

Figure S3.10. ^{1}H NMR spectrum of **8** (500 MHz, CD_2Cl_2 with CF_3SO_3H (0.06%), 300 K).

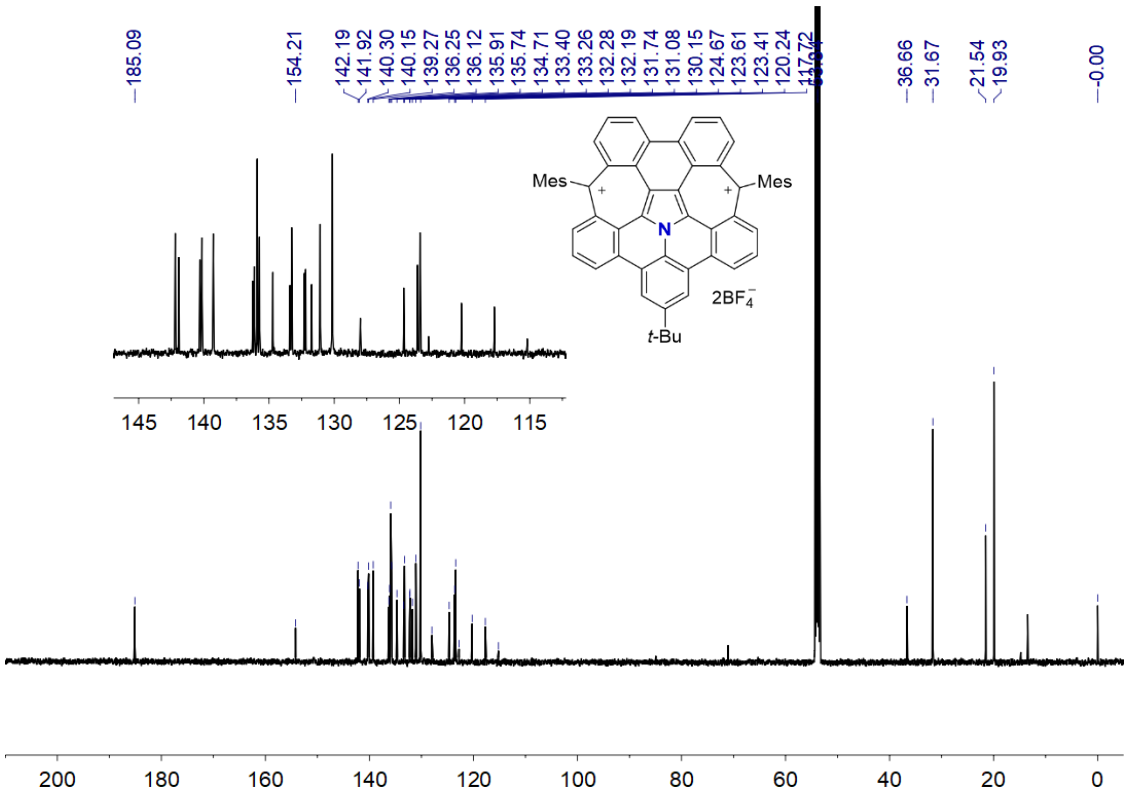

Figure S3.11. ^{13}C NMR spectrum of **8** (126 MHz, CD_2Cl_2 with CF_3SO_3H (0.06%), 300 K).

3. X-Ray Crystallographic Data

Single crystals suitable for X-ray analysis of **7** were obtained by slow evaporation of solvent from their solution in dichloromethane at room temperature, those of **8** were obtained by slow evaporation of its solution in dichloromethane and benzene under argon atmosphere at room temperature, and those of **9** were obtained by slow evaporation of its solution in dichloromethane and benzene under argon atmosphere at −20 °C. A single crystal was mounted on a loop-type mount with mineral oil with mineral oil and transferred to the goniometer of a Bruker D8 Quest diffractometer. Data collection was performed using Multilayer Mirror-monochromated Incoatec microfocus source (Mo-Kα, λ= 0.71073 Å). The obtained structures were solved using the direct method with SHELXT[35] and refined by full-matrix least-squares techniques against F^2 with SHELXL-2018/3[35]. Intensity data were corrected for applying Lorentz and polarization effects. Non-hydrogen atoms were refined anisotropically, while hydrogen atoms were placed using AFIX instructions.

Table S3.1. Crystal data for **7**, **8**, and **9**.

compound	**7**	**8**	**9**
Molecular formula	$C_{59}H_{49.67}Cl_2NO_{2.33}$	$C_{67}H_{54}B_2F_8N$	$C_{58.16}H_{45.74}Cl_{0.32}NO_{0.21}$
Formula weight	880.89	1046.73	773.21
Temperature (K)	100	100	100
Wavelength (Å)	0.71073	0.71073	0.71073
Crystal system	trigonal	triclinic	tetragonal
Space group	R -3	P -1	I 4/m
Unit cell dimensions a (Å)	23.1687(7)	13.6666(7)	17.5490(6)
b (Å)	23.1687(7)	14.0957(8)	17.5490(6)
c (Å)	42.9367(18)	15.8075(8)	26.9301(12)
α (°)	90	114.9734(17)	90
β (°)	90	103.5523(18)	90
γ (°)	120	99.4973(18)	90
Volume ($Å^3$)	19960.1(15)	2560.4(2)	8293.6(7)
Z	18	2	8
Density (calculated) ($mg \cdot m^{-3}$)	1.319	1.358	1.239
Absorption coefficient (mm^{-1})	0.195	0.098	0.091
F(000)	8340	1090	3270
Crystal size (mm^3)	0.020 x 0.160 x 0.180	0.040 x 0.200 x 0.220	0.010 x 0.020 x 0.180
Theta range (°)	2.15 to 25.68	1.94 to 25.00	2.32 to 25.37
Index ranges	−26<=h<=28	−16<=h<=16	−21<=h<=21
	−28<=k<=26	−16<=k<=16	−16<=k<=21
	−52<=l<=52	−17<=l<=18	−32<=l<=32
Reflections collected	57214	52509	35950
Min. and max. transmission	0.9660, 0.9960	0.9790, 0.9960	0.9840, 0.9990
Data / restraints / parameters	8448 / 163 / 635	9006 / 1442 / 960	3896 / 811 / 452
Goodness-of-fit on F^2	1.036	1.029	1.061
Final *R* indices [$I > 2\sigma(I)$]	R_1 = 0.0729	R_1 = 0.0522	R_1 = 0.0672
	wR_2 = 0.1806	wR_2 = 0.1228	wR_2 = 0.1746
R indices (all data) [$I > 2\sigma(I)$]	R_1 = 0.1231	R_1 = 0.0748	R_1 = 0.1262
	wR_2 = 0.2122	wR_2 = 0.1383	wR_2 = 0.2159
Largest diff. peak and hole ($e.Å^{-3}$)	0.697, −0.945	0.897, −0.381	0.841, −0.294

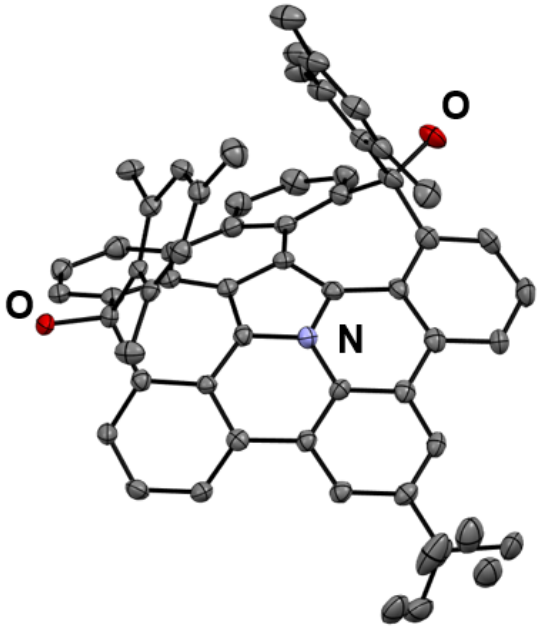

Figure S3.12. The X-ray structure of **7** with thermal ellipsoids of 50% probability. Hydrogen atoms are omitted for clarity.

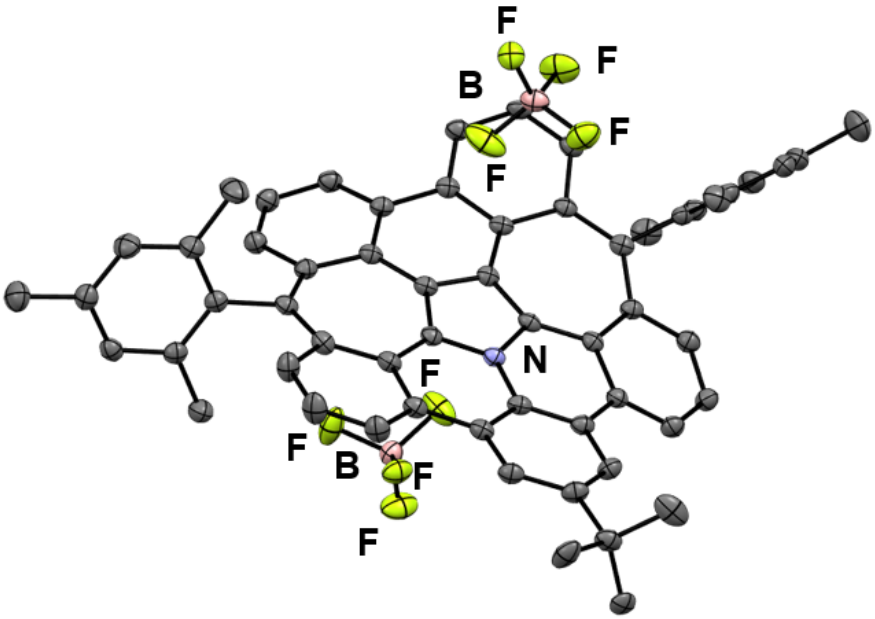

Figure S3.13. The X-ray structures of **8** with thermal ellipsoids of 50% probability.

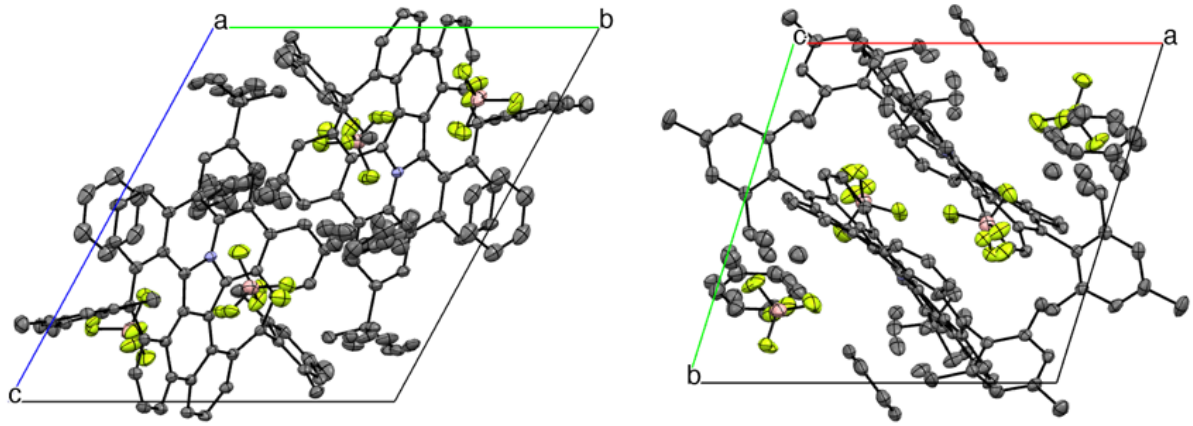

Figure S3.14. Packing structures of **8** with thermal ellipsoids of 50% probability. Left: view from the *a*-axis. Right: view from the *c*-axis.

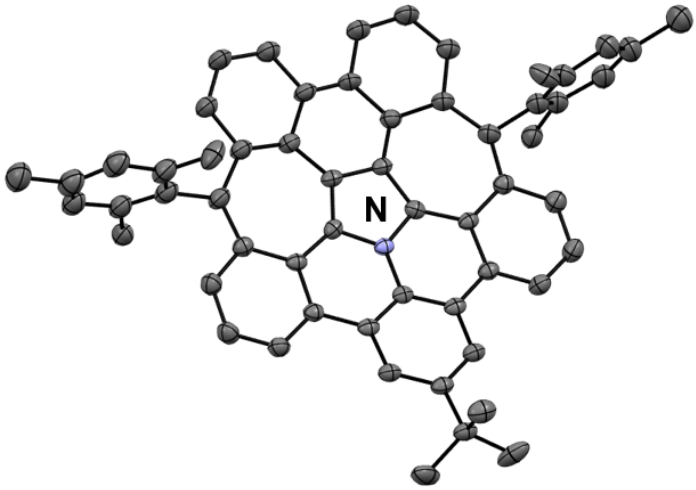

Figure S3.15. The X-ray structure of **9** with thermal ellipsoids of 50% probability.

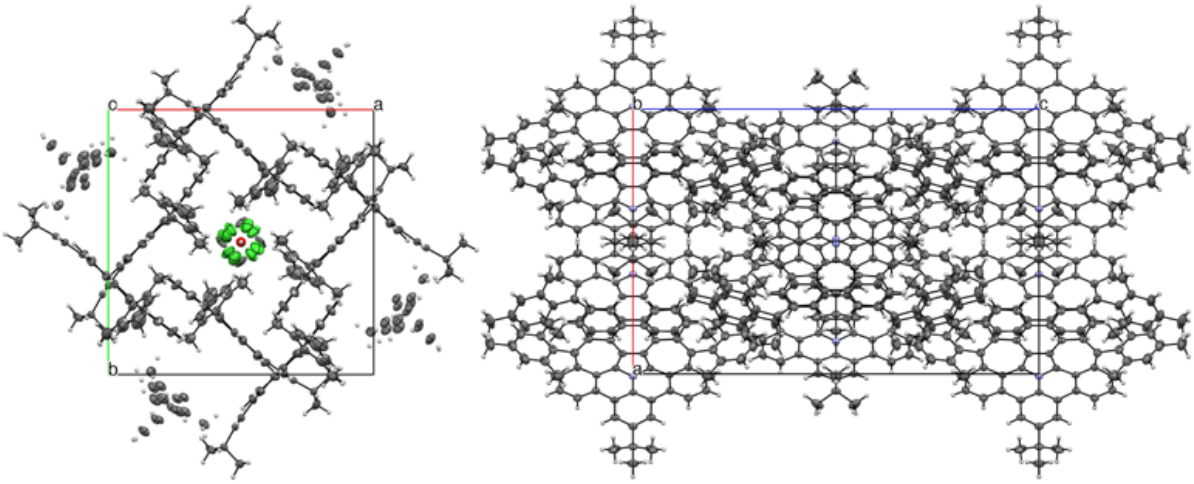

Figure S3.16. Packing structures of **9** with thermal ellipsoids of 50% probability. Left: view from the *c*-axis. Right: view from the *b*-axis.

HOMA Analysis

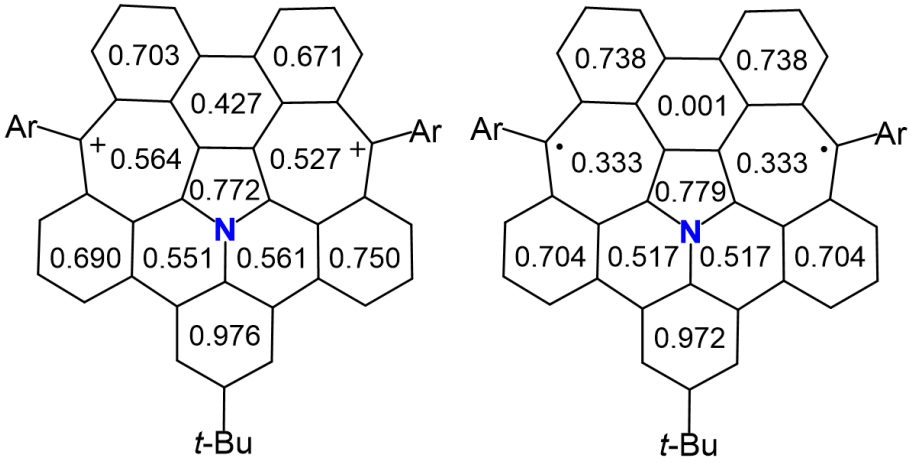

Figure S3.17. Harmonic oscillator model of aromaticity (HOMA) of **8** and **9**.

4. ESR measurements

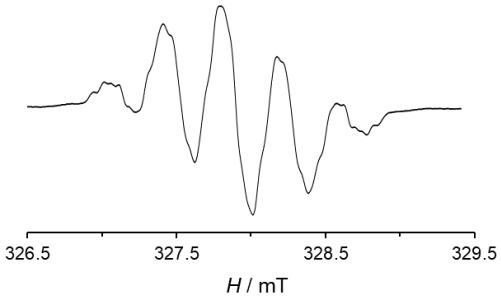

Figure S3.18. ESR spectrum of **9** in toluene at 300 K.

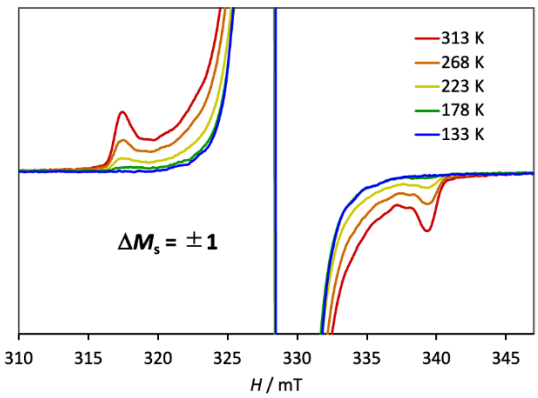

Figure S3.19. ESR spectra for the $\Delta M_S = \pm 1$ transition of **9** in a glassy *o*-terphenyl at 133–313 K.

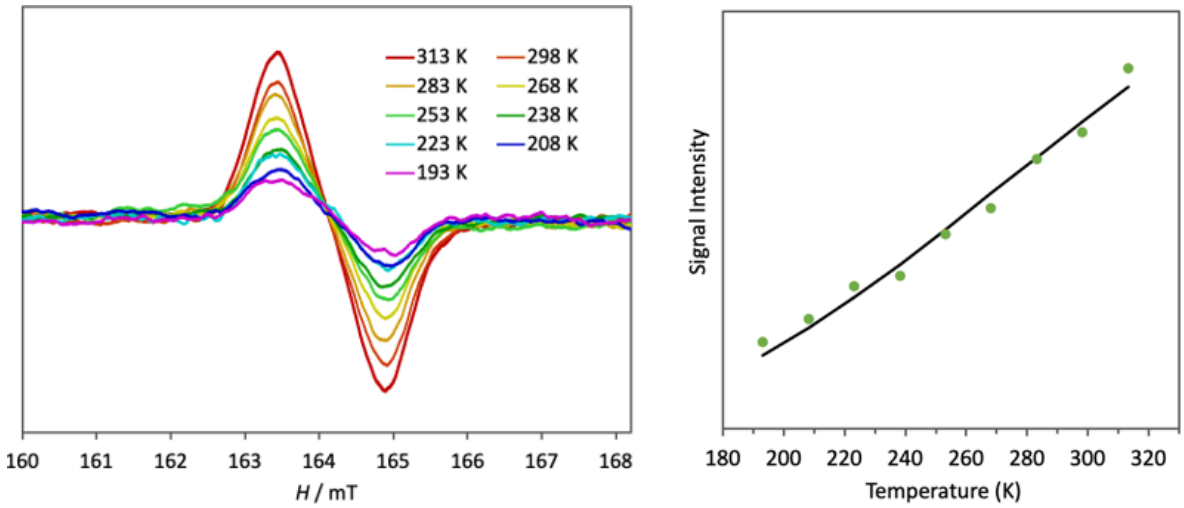

Figrue S3.20. (A) ESR spectra for the $\Delta M_S = \pm 2$ forbidden transition of **9** in a glassy *o*-terphenyl at 133–313 K. (B) Change in ESR signal intensity with temperature and the Bleaney-Bowers fit. The estimated ΔE_{S-T} value is −1063 K.

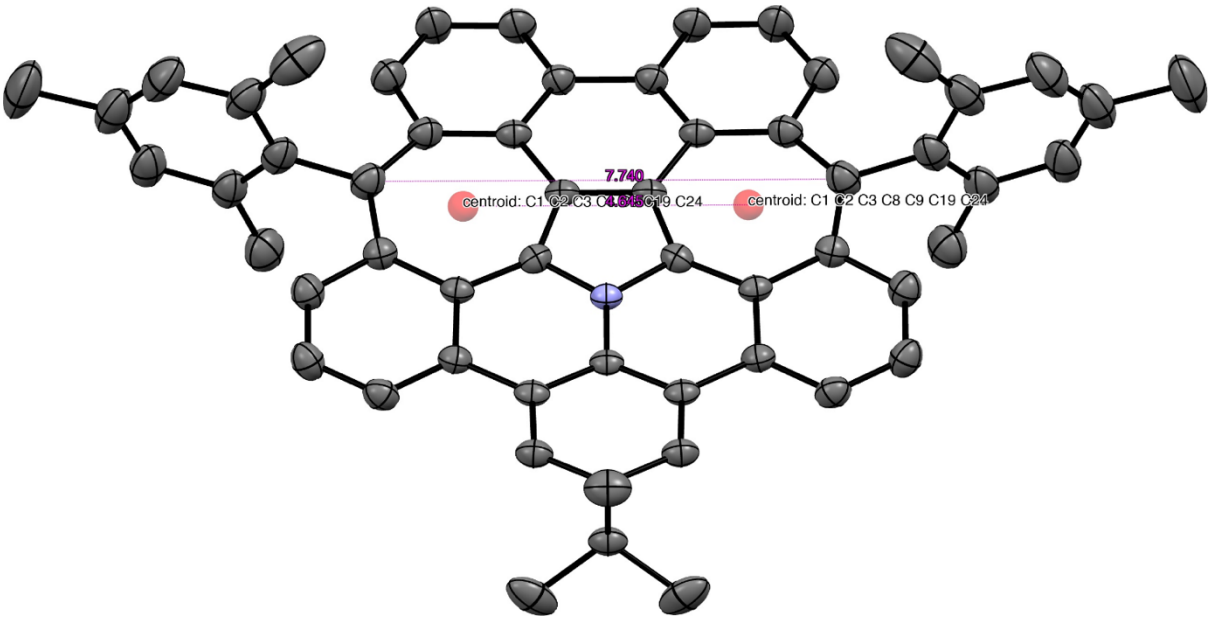

Figure S3.21. Distances between the centers of heptagon rings (4.645 Å), and the ipso carbons of the heptagon rings (7.740 Å).

5. Theoretical Calculations

Theoretical calculations were performed using computing resources at High-Performance Center for Computational Science, Nanyang Technological University, Singapore. Density functional theory (DFT) calculations were performed by using Gaussian 16 (revision C.01) program[36]. The geometries molecules **8a** and **9a** were optimized with the (U)B3LYP[37] functional. The corrections of dispersion were calculated using the Grimme's D3 version. Open-shell molecules were calculated using unrestricted broken symmetry (BS) approach. The 6-31G(d,p) basis set[38] was used for structure optimization, vibrational frequency, while the 6-311+G(2d,p) basis set was used for time-dependent density functional theory (TD-DFT). Anisotropy of induced current density (ACID) plots were calculated by using the method developed by Herges[39]. The geometries of **8b** and **9b** for aromaticity evaluation were taken from X-ray crystal analysis, which were replaced mesitylene and *tert*-butyl groups to hydrogen atoms and optimized only hydrogen atoms positions at the (U)B3LYP/6-31G(d,p) level. This evaluation was applied the CSGT-RB3LYP/6-31G(d,p) level to the closed-shell molecules and the CSGT-UB3LYP/6-31G(d,p) level to the open-shell molecules. Nucleus-independent chemical shifts (NICS) values were calculated at the GIAO-RB3LYP/6-31G(d,p) method for closed-shell molecules and at the GIAO-UB3LYP/6-31G(d,p) method for open-shell molecules.

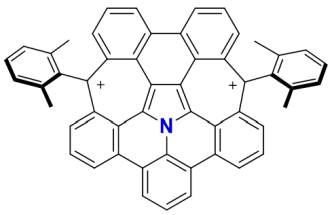

8a

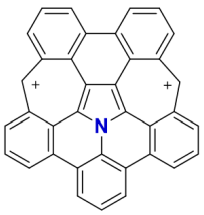

8b

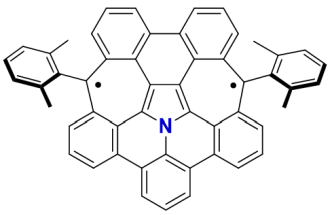

9a

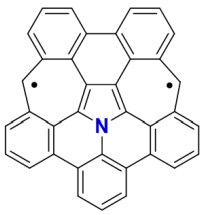

9b

5-1. Diradical Index (y_0)

Table S3.2. Calculated Diradical Index (y_0) of **9a**

Functional / Basis Set	y_0
CASSCF(2,2)/6-31G(d)	0.830
UB3LYP-D3/6-31G(d,p)	0.724

5-2. Singlet–Triplet Energy Gap

Table S3.3. Singlet–Triplet Energy Gaps (ΔE_{S-T}) of **9a**

ΔE_{S-T} (+ZPE)[a] / kJ mol^{-1}	**−5.50**
Singlet (+ZPE) / Hartree	−2055.708003
$<S^2>$ = 0.988	
Triplet (+ZPE) / Hartree	−2055.705909
$<S^2>$ = 2.050	

a) Geometry optimizations of **9a** were performed at the UB3LYP-D3/6-31G(d,p) level.

5-3. Spin Density

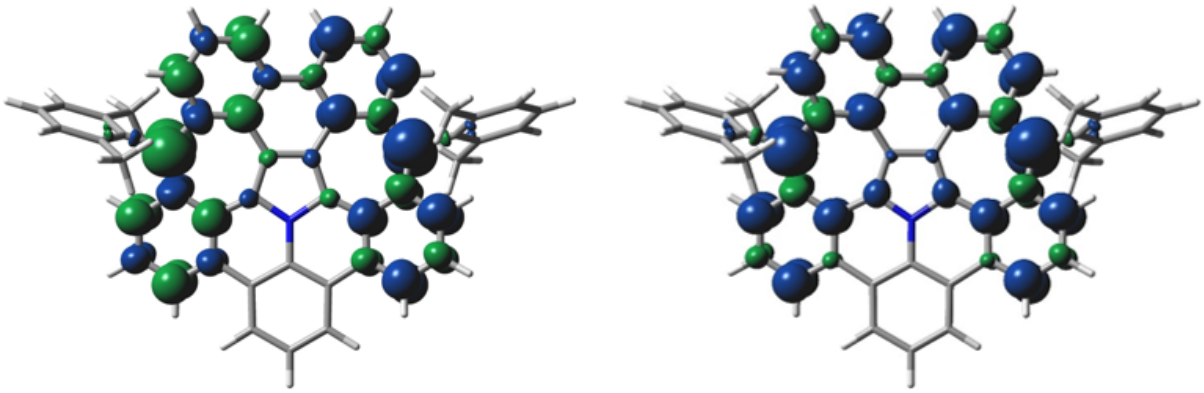

Figure S3.22. Spin density (isovalue = 0.003) of **9a**. (left: singlet, right: triplet).

5-4. Molecular Orbitals

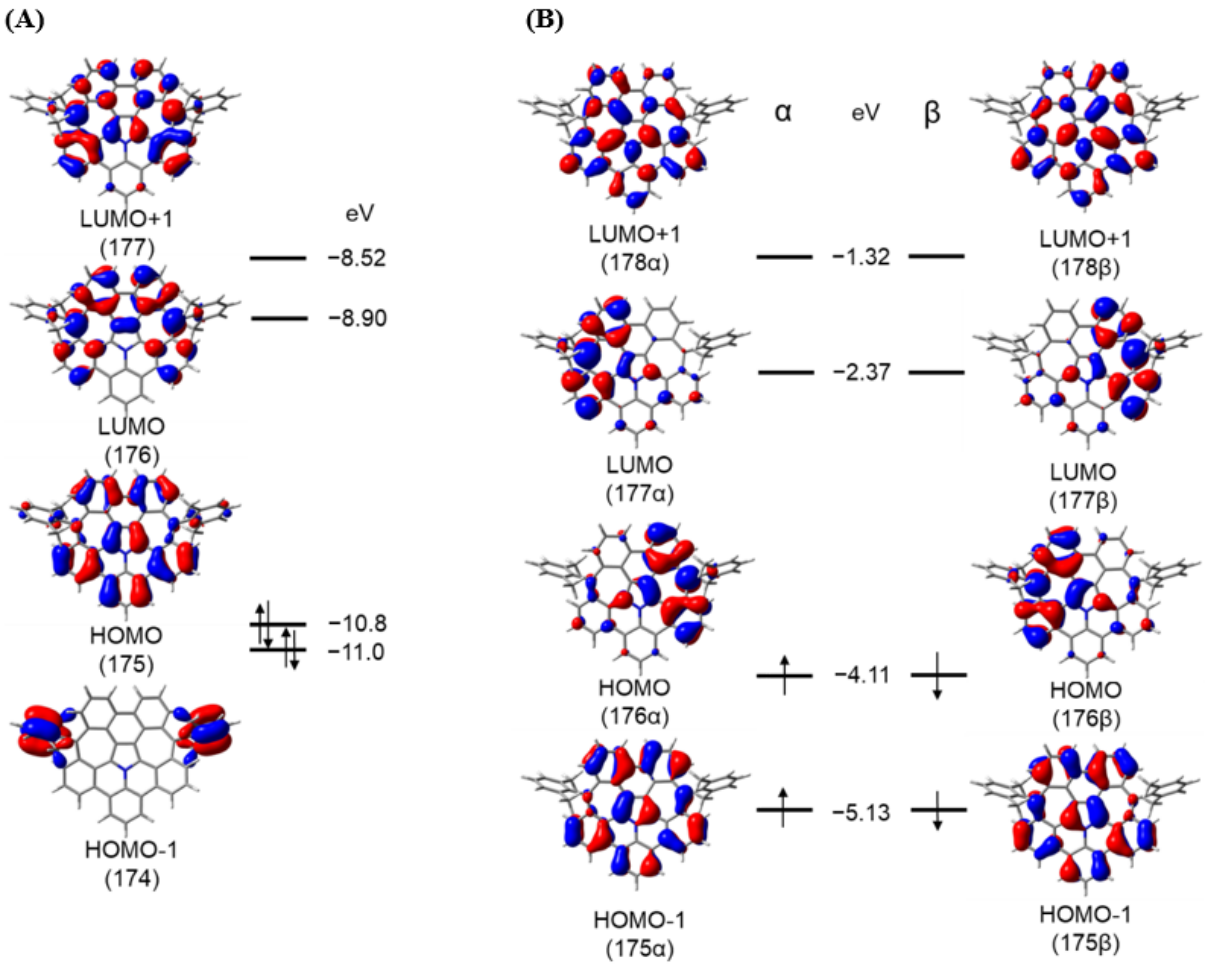

Figure S3.23. Kohn-Sham molecular orbitals of (A) **8a** and (B) **9a**.

5-5. ACID

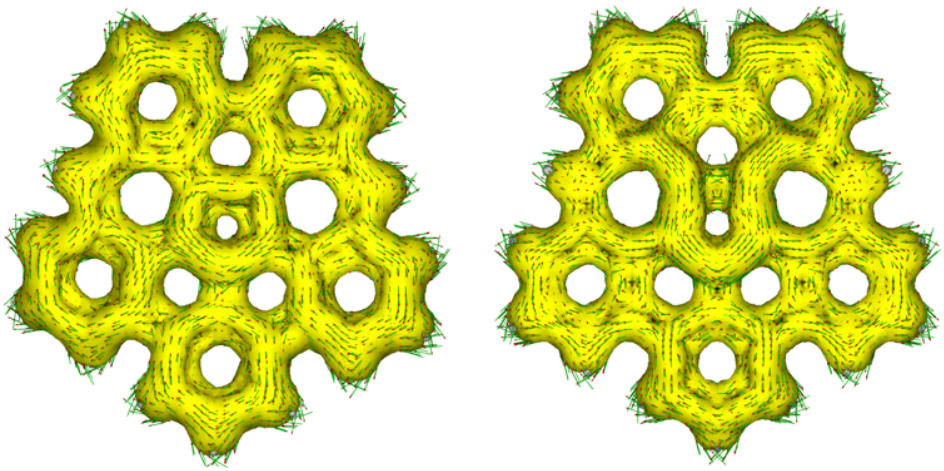

Figure S3.24. ACID plots (Isovalue = 0.03) of **8b** (left) and **9b** (right).

5-6. NICS

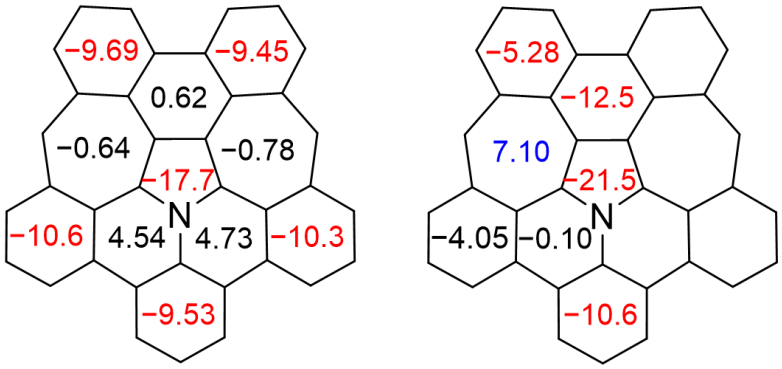

Figure S3.25. NICS(0) values of **8b** (left),and **9b** (right).

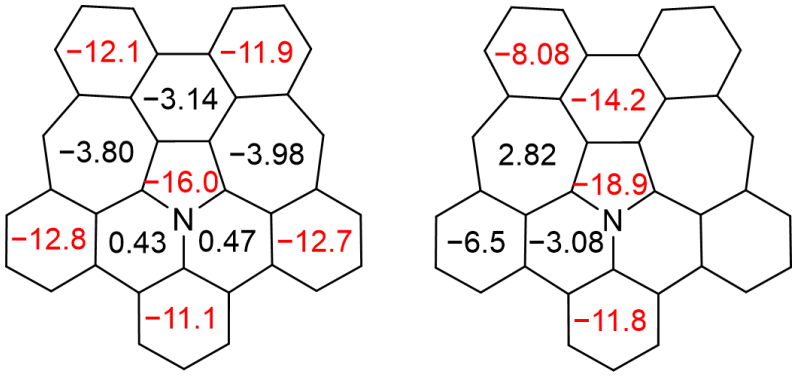

Figure S3.26. NICS(1)$_{average}$ values of **8b** (left),and **9b** (right).

5-7. TD-DFT

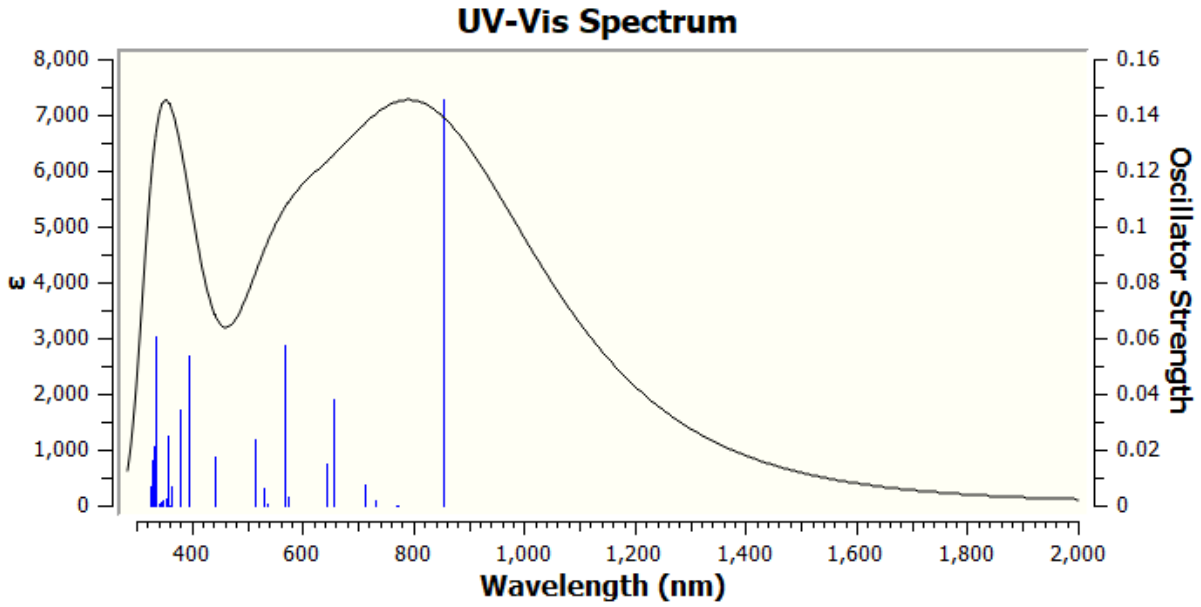

Figure S3.27. Simulated UV-visible absorption spectrum of **8a**.

Table S3.4. Selected wavelengths, oscillator strengths, major electronic transition of **8a**.

Excitation State	Wavelength (λ)	Oscillator Strengths (*f*)	Transitions
1	863.14	0.1459	**175→176 (0.69585)**
2	782.00	0.0003	173→177 (0.24925) **174→176 (0.66080)**
3	781.03	0.0000	**173→176 (0.65989)** 174→177 (0.25136)
4	743.59	0.0017	170→176 (-0.11369) 171→177 (-0.23034) **172→176 (0.63475)** 175→177 (0.16538)
5	724.14	0.0077	**171→176 (0.63951)** 172→177 (-0.27637)
6	667.18	0.0382	172→176 (-0.15528) **175→177 (0.68235)**
10	579.61	0.0576	169→176 (-0.11189) 170→177 (0.31909) 171→176 (0.20972) **172→177 (0.56312)** 173→177 (-0.10198)
13	529.07	0.0240	**169→176 (0.64218)** 170→177 (0.27565)
15	410.51	0.0536	165→176 (-0.15370) **175→178 (0.65954)**

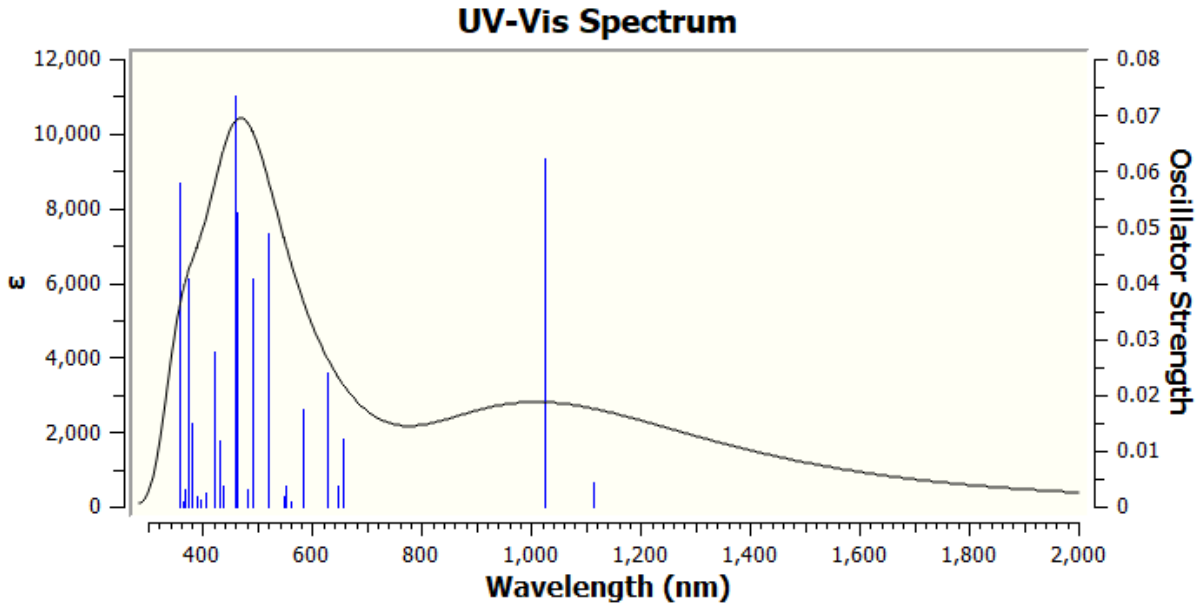

Figure S3.28. Simulated UV-visible absorption spectrum of **9a**.

Table S3.5. Selected wavelengths, oscillator strengths, major electronic transition of **9a**.

Excitation State	Wavelength (λ)	Oscillator Strengths (*f*)	Transitions	
1	1121.29	0.0045	**176A→177A (0.69691)**	**176B→177B (-0.69691)**
2	1034.20	0.0623	**176A→177A (0.69535)**	**176B→177B (0.69535)**
3	667.36	0.0121	**176A→178A (0.58668)** 176A→180A (0.32955)	**176B→178B (0.58668)** 176B→180B (0.32955)
5	638.65	0.0241	**175A→177A (0.56384)** 176A→178A (0.27105) 176A→180A (0.24049)	**175B→177B (-0.56384)** 176B→178B (-0.27105) 176B→180B (-0.24049)
6	596.06	0.0174	174A→177A (-0.15895) **175A→177A (0.62944)** 176A→179A (-0.21097) 176A→181A (-0.13576)	174B→177B (0.15895) **175B→177B (0.62944)** 176B→179B (-0.21097) 176B→181B (-0.13576)
10	533.24	0.0488	173A→177A (0.11193) 174A→177A (0.23737) 175A→177A (0.11871) 176A→178A (0.35541) 176A→179A (-0.17682) **176A→180A (-0.47326)** 176A→182A (0.10420)	173B→177B (0.11193) 174B→177B (0.23737) 175B→177B (-0.11871) 176B→178B (-0.35541) 176B→179B (0.17682) **176B→180B (0.47326)** 176B→182B (-0.10420)
11	504.41	0.0407	173A→177A (0.20653) 174A→177A (0.20513) 176A→180A (0.24458) **176A→181A (0.42625)** 176A→182A (0.36505)	173B→177B (0.20653) 174B→177B (0.20513) 176B→180B (-0.24458) **176B→181B (-0.42625)** 176B→182B (-0.36505)
14	476.81	0.0527	174A→177A (0.17336) 175A→177A (0.13217) 175A→178A (0.15001) 176A→178A (-0.10329) **176A→181A (0.61618)**	174B→177B (-0.17336) 175B→177B (0.13217) 175B→178B (-0.15001) 176B→178B (-0.10329) **176B→181B (0.61618)**

5-8. Cartesian Coordinates

9a singlet

C	-2.422455	1.584881	0.216690	C	-5.118037	-1.744231	2.346080
C	-2.451994	3.010250	0.361746	C	-5.383074	-0.203453	-2.468828
C	-1.228349	3.794491	0.174663	C	5.303110	-0.990009	0.063685
C	0.000000	3.125311	-0.000002	C	6.038998	-0.813210	1.253255
N	0.000000	1.741989	-0.000001	C	7.378481	-1.216101	1.289633
C	-1.148690	0.961202	0.048688	C	7.985248	-1.779314	0.168692
C	1.228350	3.794491	-0.174667	C	7.252754	-1.948249	-1.004921
C	2.451995	3.010249	-0.361747	C	5.909868	-1.562002	-1.073678
C	2.422456	1.584880	-0.216691	C	5.118051	-1.744222	-2.346077
C	1.148690	0.961202	-0.048691	C	5.383060	-0.203462	2.468838
C	-1.198969	5.197921	0.153171	H	-2.116303	5.764484	0.247651
C	0.000000	5.884173	-0.000005	H	2.116304	5.764484	-0.247661
C	1.198970	5.197921	-0.153179	H	3.661608	4.732521	-0.848328
C	3.646663	3.661809	-0.692050	H	5.736469	3.438097	-1.145371
C	4.817766	2.935346	-0.858992	H	5.756762	1.040772	-0.764968
C	4.822459	1.569716	-0.649900	H	-5.756760	1.040773	0.764977
C	3.658425	0.830406	-0.289563	H	-5.736465	3.438098	1.145381
C	-3.658424	0.830407	0.289565	H	-3.661605	4.732522	0.848331
C	-4.822457	1.569717	0.649906	H	-0.757377	-4.905550	-0.627129
C	-4.817763	2.935347	0.858998	H	-3.174331	-4.963800	-1.090924
C	-3.646660	3.661810	0.692053	H	-4.528602	-2.961085	-0.815088
C	-0.714513	-0.378975	0.013438	H	4.528600	-2.961090	0.815077
C	0.714513	-0.378975	-0.013443	H	3.174328	-4.963806	1.090900
C	1.477622	-1.592084	0.101522	H	0.757374	-4.905554	0.627102
C	0.719605	-2.794790	0.147688	H	-7.947364	-1.085738	-2.206524
C	-0.719607	-2.794789	-0.147703	H	-7.724897	-2.385251	1.880970
C	-1.477623	-1.592082	-0.101531	H	-4.692857	-0.793309	2.685175
C	-1.345164	-4.005087	-0.504027	H	-4.277690	-2.429400	2.190389
C	-2.701773	-4.038937	-0.774072	H	-5.742698	-2.145749	3.148303
C	-3.466737	-2.892050	-0.630684	H	-5.068643	0.827066	-2.270329
C	-2.912691	-1.639814	-0.256080	H	-6.063745	-0.193790	-3.324180
C	2.912690	-1.639816	0.256073	H	-4.483311	-0.760322	-2.751830
C	3.466735	-2.892054	0.630672	H	7.947352	-1.085743	2.206545
C	2.701770	-4.038942	0.774053	H	7.724909	-2.385242	-1.880956
C	1.345162	-4.005090	0.504007	H	5.742716	-2.145737	-3.148299
C	-3.855613	-0.564909	-0.011420	H	4.277703	-2.429392	-2.190393
C	3.855613	-0.564911	0.011421	H	4.692872	-0.793298	-2.685171
C	-5.303110	-0.990008	-0.063678	H	5.068628	0.827057	2.270341
C	-6.039005	-0.813206	-1.253244	H	4.483296	-0.760334	2.751834
C	-7.378488	-1.216098	-1.289615	H	6.063726	-0.193800	3.324194
C	-7.985248	-1.779316	-0.168673	H	-9.026527	-2.086003	-0.209463
C	-7.252748	-1.948255	1.004934	H	9.026527	-2.086000	0.209486
C	-5.909861	-1.562007	1.073686	H	0.000000	6.969724	-0.000007

9a Triplet

C	-2.422034	1.577605	0.244881	C	-5.168502	-1.772031	2.326398
C	-2.446301	2.997843	0.398201	C	-5.334788	-0.162642	-2.470369
C	-1.225808	3.782237	0.194084	C	5.304689	-0.982661	0.075381
C	0.000000	3.113114	-0.000003	C	6.018372	-0.780300	1.274207
N	0.000000	1.729907	-0.000002	C	7.361976	-1.165730	1.338024
C	-1.147605	0.948925	0.057872	C	7.994215	-1.736329	0.235103
C	1.225808	3.782237	-0.194092	C	7.283470	-1.930574	-0.947987
C	2.446302	2.997843	-0.398204	C	5.937276	-1.562245	-1.044086
C	2.422035	1.577605	-0.244885	C	5.168525	-1.772025	-2.326389
C	1.147606	0.948925	-0.057878	C	5.334765	-0.162648	2.470383
C	-1.196643	5.185914	0.172622	H	-2.112436	5.752487	0.281301
C	-0.000001	5.871867	-0.000008	H	2.112434	5.752488	-0.281317

C	1.196642	5.185914	-0.172635	H	3.648638	4.719799	-0.916769
C	3.638935	3.650257	-0.751867	H	5.719851	3.424798	-1.231884
C	4.804604	2.925442	-0.929115	H	5.745911	1.028611	-0.823746
C	4.811986	1.557765	-0.705730	H	-5.745907	1.028609	0.823759
C	3.655033	0.826135	-0.326781	H	-5.719846	3.424796	1.231896
C	-3.655032	0.826135	0.326783	H	-3.648635	4.719799	0.916771
C	-4.811983	1.557764	0.705738	H	-0.758931	-4.910055	-0.636955
C	-4.804601	2.925440	0.929122	H	-3.180970	-4.970079	-1.079464
C	-3.638932	3.650257	0.751869	H	-4.534544	-2.968956	-0.791894
C	-0.716865	-0.388826	0.019689	H	4.534542	-2.968963	0.791875
C	0.716865	-0.388826	-0.019698	H	3.180967	-4.970088	1.079428
C	1.479068	-1.601217	0.089289	H	0.758929	-4.910060	0.636917
C	0.721205	-2.803838	0.143291	H	-7.913928	-1.015732	-2.262217
C	-0.721206	-2.803837	-0.143314	H	-7.775471	-2.373350	1.810106
C	-1.479068	-1.601216	-0.089303	H	-4.730867	-0.832723	2.681671
C	-1.347424	-4.011293	-0.503406	H	-4.338883	-2.471427	2.176442
C	-2.707456	-4.045815	-0.762328	H	-5.812745	-2.169662	3.114947
C	-3.471876	-2.900715	-0.611484	H	-5.007116	0.859566	-2.251237
C	-2.915755	-1.647410	-0.237316	H	-6.002307	-0.128905	-3.335408
C	2.915754	-1.647413	0.237304	H	-4.439798	-0.729428	-2.748759
C	3.471874	-2.900720	0.611464	H	7.913908	-1.015735	2.262252
C	2.707454	-4.045821	0.762298	H	7.775490	-2.373343	-1.810075
C	1.347422	-4.011297	0.503375	H	5.812774	-2.169656	-3.114933
C	-3.854642	-0.572847	0.005129	H	4.338903	-2.471420	-2.176442
C	3.854642	-0.572848	-0.005129	H	4.730894	-0.832716	-2.681666
C	-5.304690	-0.982662	-0.075369	H	5.007092	0.859559	2.251249
C	-6.018384	-0.780298	-1.274189	H	4.439775	-0.729437	2.748765
C	-7.361988	-1.165729	-1.337995	H	6.002277	-0.128910	3.335427
C	-7.994216	-1.736331	-0.235069	H	-9.038440	-2.029101	-0.297130
C	-7.283460	-1.930578	0.948014	H	9.038439	-2.029098	0.297172
C	-5.937266	-1.562248	1.044101	H	-0.000001	6.957452	-0.000010

9b

C	0.108124	-0.356741	1.153416	C	0.108124	-0.356741	-1.153416
C	0.123200	0.984472	0.708262	C	0.123200	0.984472	-0.708262
C	0.247709	2.208205	1.432681	C	0.247709	2.208205	-1.432681
C	0.037051	3.370466	0.627471	C	0.037051	3.370466	-0.627471
C	-0.135788	4.611220	1.271101	C	-0.135788	4.611220	-1.271101
H	-0.203922	5.553922	0.772680	H	-0.203922	5.553922	-0.772680
C	-0.205831	4.677652	2.631071	C	-0.205831	4.677652	-2.631071
H	-0.328526	5.643477	3.115568	H	-0.328526	5.643477	-3.115568
C	-0.179046	3.541168	3.406658	C	-0.179046	3.541168	-3.406658
H	-0.290261	3.621937	4.484688	H	-0.290261	3.621937	-4.484688
C	-0.007130	2.261938	2.846512	C	-0.007130	2.261938	-2.846512
C	0.149585	1.169964	3.807916	C	0.149585	1.169964	-3.807916
C	0.072695	-0.259373	3.675689	C	0.072695	-0.259373	-3.675689
C	0.059684	-1.040903	4.856844	C	0.059684	-1.040903	-4.856844
H	0.050981	-0.506488	5.803809	H	0.050981	-0.506488	-5.803809
C	0.098084	-2.411083	4.863307	C	0.098084	-2.411083	-4.863307
H	0.118249	-2.944712	5.808948	H	0.118249	-2.944712	-5.808948
C	0.090889	-3.100612	3.677574	C	0.090889	-3.100612	-3.677574
H	0.124205	-4.181730	3.696849	H	0.124205	-4.181730	-3.696849
C	0.056849	-2.421725	2.466259	C	0.056849	-2.421725	-2.466259
C	0.095753	-0.990718	2.425863	C	0.095753	-0.990718	-2.425863
C	-0.041094	-3.181994	1.220203	C	-0.041094	-3.181994	-1.220203
C	0.017626	-2.525420	0.000000	C	-0.264388	-4.569729	-1.187617
C	-0.264388	-4.569729	1.187617	H	-0.374229	-5.109989	-2.119578
H	-0.374229	-5.109989	2.119578	H	0.134329	1.508572	-4.840962
C	-0.397636	-5.277551	0.000000	H	0.134329	1.508572	4.840962
N	0.105227	-1.130743	0.000000	H	-0.594341	-6.343462	0.000000

8a

C	-2.409333	1.566569	0.246628	C	-5.065503	-1.995016	2.259326
C	-2.440497	2.993229	0.406338	C	-5.415347	0.052345	-2.396718
C	-1.226361	3.789555	0.192864	C	5.294474	-0.989059	0.072834
C	0.000000	3.126932	0.000000	C	6.043215	-0.672264	1.228408
N	0.000000	1.742195	0.000000	C	7.380647	-1.076847	1.277146
C	-1.143759	0.962737	0.052425	C	7.966299	-1.749968	0.206329
C	1.226361	3.789554	-0.192865	C	7.216185	-2.042006	-0.931766
C	2.440497	2.993229	-0.406338	C	5.868223	-1.681221	-1.017660
C	2.409333	1.566568	-0.246628	C	5.065508	-1.995013	-2.259325
C	1.143759	0.962737	-0.052425	C	5.415342	0.052342	2.396722
C	-1.199131	5.191803	0.171796	H	-2.111720	5.763662	0.281612
C	0.000000	5.876736	-0.000002	H	2.111720	5.763662	-0.281616
C	1.199131	5.191803	-0.171800	H	3.655068	4.678805	-0.970603
C	3.630725	3.610054	-0.798877	H	5.691788	3.367527	-1.366503
C	4.791245	2.872225	-1.020758	H	5.715408	0.964613	-0.944572
C	4.798080	1.512488	-0.790000	H	-5.715407	0.964613	0.944576
C	3.640945	0.804734	-0.354423	H	-5.691787	3.367528	1.366505
C	-3.640945	0.804735	0.354424	H	-3.655068	4.678806	0.970602
C	-4.798080	1.512489	0.790002	H	-0.765758	-4.874748	-0.683820
C	-4.791244	2.872225	1.020759	H	-3.157172	-4.915524	-1.240078
C	-3.630724	3.610055	0.798877	H	-4.522813	-2.908458	-0.965319
C	-0.718067	-0.385532	0.009446	H	4.522812	-2.908461	0.965314
C	0.718066	-0.385532	-0.009447	H	3.157170	-4.915528	1.240067
C	1.474297	-1.572602	0.115854	H	0.765757	-4.874750	0.683810
C	0.717349	-2.785523	0.160730	H	-7.966373	-0.858774	-2.164910
C	-0.717349	-2.785522	-0.160735	H	-7.679201	-2.557763	1.767458
C	-1.474297	-1.572602	-0.115857	H	-4.587504	-1.098552	2.670213
C	-1.345855	-3.967546	-0.561209	H	-4.270471	-2.720108	2.052909
C	-2.704571	-3.997798	-0.881591	H	-5.701760	-2.417249	3.039048
C	-3.468219	-2.861242	-0.737814	H	-5.123350	1.073533	-2.127376
C	-2.913335	-1.619988	-0.297902	H	-6.111272	0.119238	-3.234731
C	2.913335	-1.619989	0.297900	H	-4.514206	-0.459159	-2.753578
C	3.468218	-2.861244	0.737809	H	7.966369	-0.858775	2.164917
C	2.704570	-3.997800	0.881583	H	7.679206	-2.557758	-1.767453
C	1.345854	-3.967548	0.561202	H	5.701767	-2.417245	-3.039047
C	-3.850264	-0.575709	-0.006135	H	4.270477	-2.720106	-2.052911
C	3.850264	-0.575709	0.006136	H	4.587509	-1.098549	-2.670212
C	-5.294474	-0.989059	-0.072832	H	5.123345	1.073531	2.127380
C	-6.043217	-0.672263	-1.228403	H	4.514201	-0.459162	2.753580
C	-7.380649	-1.076847	-1.277140	H	6.111265	0.119235	3.234736
C	-7.966299	-1.749970	-0.206322	H	-9.008763	-2.046767	-0.258374
C	-7.216183	-2.042009	0.931771	H	9.008764	-2.046765	0.258382
C	-5.868220	-1.681223	1.017663	H	0.000000	6.961126	-0.000003

8b

C	0.419466	1.129580	0.005144	H	0.702092	5.751803	-0.327309
C	-0.943597	0.768478	-0.001790	C	0.404570	3.630094	-0.059939
C	-1.012166	-0.661782	-0.075193	C	1.095939	2.365551	-0.073334
C	0.311097	-1.145107	-0.031849	C	-0.979880	3.874885	0.254456
C	0.851665	-2.439444	0.126134	C	-2.078514	2.981804	0.442121
C	0.047165	-3.632143	0.145587	C	-3.301393	3.566582	0.885690
C	0.676109	-4.822630	0.593056	H	-3.301608	4.619869	1.149310
H	0.081931	-5.730023	0.643185	C	-4.466845	2.851326	0.949111
C	2.001595	-4.863690	0.948182	H	-5.376502	3.326416	1.299972
H	2.433446	-5.785657	1.322319	C	-4.493054	1.523269	0.543587
C	2.803349	-3.741252	0.775667	H	-5.435407	0.993201	0.604571
H	3.858636	-3.808159	1.011578	C	-3.340603	0.863298	0.145294
C	2.265575	-2.543345	0.336590	C	-2.092607	1.563558	0.164546
C	3.118597	-1.376115	0.104047	C	-3.400291	-0.562624	-0.221397
C	2.522423	-0.117021	-0.009601	C	-4.618989	-1.129587	-0.595255

C	3.247990	1.060524	-0.175835	H	-5.516640	-0.526461	-0.644981
C	4.635951	0.933219	-0.325812	C	-4.698311	-2.462811	-0.981594
H	5.247923	1.812742	-0.482712	H	-5.649902	-2.870075	-1.306450
C	5.274524	-0.305810	-0.298645	C	-3.592140	-3.258285	-0.960717
C	4.506318	-1.446732	-0.049469	H	-3.680102	-4.306052	-1.232029
H	5.002589	-2.409938	-0.021229	C	-2.318807	-2.781583	-0.524996
C	2.526063	2.332856	-0.225847	C	-2.221174	-1.361381	-0.238181
C	3.212458	3.513855	-0.444459	C	-1.312901	-3.764449	-0.339404
H	4.286348	3.506236	-0.576870	N	1.139285	-0.040708	0.003392
C	2.549686	4.724225	-0.506250	H	-1.634315	-4.790499	-0.495959
H	3.106826	5.635715	-0.695473	H	-1.228084	4.926291	0.370570
C	1.197770	4.785867	-0.312848	H	6.345562	-0.379537	-0.442981

References

1. (a) Tobe, Y. *Chem. Rec.* **2015**, *15*, 86. (b) Tobe, Y. *Top. Curr. Chem.* **2018**, *376*, 12. (c) Konishi, A., Yasuda. M. *Chem. Lett.* **2021**, *50*, 195–212. (d) Konishi, A., Yasuda, M. *Adv. Phys. Org. Chem.* **2021**, *55*, 17–40.

2. (a) Stuparu, M. C. *Acc. Chem. Res.* **2021**, *54*, 2858–2870. (b) Chaolumen, Stepek, C., Yamada, K. E., Ito, H., Itami, K. *Angew. Chem. Int. Ed.* **2021**, *60*, 23508−23532.

3. (a) Pitt, D. A., Petro, A. J., Smyth, C. P. *J. Am. Chem. Soc*. **1957**, *79*, 5633– 5634. (b) Anderson, A. G., Jr., Steckler, B. M. *J. Am. Chem. Soc*. **1959**, *81*, 4941– 4946. (c) Tobler, H. J., Bauder, A., Günthard, H. H. *J. Mol. Spec-trosc*. **1965**, *18*, 239– 246. (d) Yang, X. *et al*. *Chem. Sci*. **2016**, *7*, 6176−6181. (e) Konishi, A., Morinaga, A., Yasuda, M. *Chem.-Eur. J.* **2018**, *24*, 8548−8552. (f) Liu, P. *et al*. *J. Am. Chem. Soc*. **2021**, *143*, 5314−5318.

4. (a) Zou, Y. *et al*. *J. Am. Chem. Soc*. **2019**, *141*, 7266–7270. (b) Tanaka, Y., Fukui, N., Shinokubo, H. *Nat Commun* **2020**, *11*, 3873.

5. (a) Majzik, Z. *et al*. *Nat. Commun.* **2018**, *9*, 1198. (b) Xu, T. *et al*. *J. Am. Chem. Soc.* **2021**, *143*, 20562–20568. (c) Xu, T. *et al*. *Angew. Chem. Int. Ed.* **2023**, *62*, e202304937. (d) Mizuno, Y. *et al*. *J. Am. Chem. Soc.* **2023**, *145*, 20595–20609. (e) Warren, G. I., Zocchi, L. J., Zakharov, L. N., Haley, M. M. *Chem. Eur. J.* **2023**, *29*, e202301153.

6. (a) Demchenko, A. P., Tomin, V. I., Chou, P.-T. *Chem. Rev.* **2017**, *117*, 13353–13381. (b) Xin, H., Hou, B., Gao, X. *Acc. Chem. Res.* **2021**, *54*, 1737–1753. (c) Dunlop, D., Ludvíková, L., Banerjee, A., Ottosson, H., Slanina, T. *J. Am. Chem. Soc.* **2023**, *145*, 21569–21575.

7. (a) Abe, M. *Chem. Rev.* **2013**, *113*, 7011–7088. (b) Zeng, Z. *et al*. *Chem. Soc. Rev.* **2015**, *44*, 6578–6595. (c) Das, S., Wu, J. *Phys. Sci. Rev.* **2017**, *2*, 20160109. (d) Kubo, T. *Pure Appl. Chem.* **2023**, *95*, 363–375. (e) Ishigaki, Y., Harimoto, T., Shimajiri, T., Suzuki, T. *Chem. Rev.* **2023**, *123*, 13952–13965.

8. Hu, X., Wang, W., Wang, D., Zheng, Y. *J. Mater. Chem. C* **2018**, *6*, 11232–11242.

9. Nakano, M. *Chem. Rec.* **2017**, *17*, 27–62.

10. (a) Frederickson, C. K., Rose, B. D., Haley, M. M. *Acc. Chem. Res.* **2017**, *50*, 977−987. (b) Gopalakrishna, T. Y., Zeng, W., Lu, X., Wu, J. *Chem. Commun.* **2018**, *54*, 2186–2199. (c) Dressler, J. J., Haley, M. M. *J. Phys. Org. Chem.* **2020**, *33*, e4114.

11. (a) Kang, H.-W. *et al*. *Nature Commun.* **2023**, *14*, 5248. (b) Yuan, L. *et al*. *Angew. Chem. Int. Ed.* **2023**, *62*, e202314982. (c) Mishra, S. *et al*. *Nature Chem.* **2024**, *16*, 755–761.

12. Fei, Y., Liu, J. *Adv. Sci.* **2022**, *9*, 2201000.

13. (a) Cava, M. P., Schlessinger, R. H. *J. Am. Chem. Soc.* **1963**, *85*, 835–836. (b) Cava, M. P., Schlessinger, R. H. *Tetrahedron* **1965**, *21*, 3051. (c) Cava, M. P., Schlessinger, R. H. *Tetrahedron* **1965**, *21*, 3065. (d) Cava, M. P., Schlessinger, R. H. *Tetrahedron* **1965**, *21*, 3073.

14. (a) Kolc, J., Michl, J. *J. Am. Chem. Soc.* **1970**, *92*, 4147–4148. (b) Kolc, J., Michl, J. *J. Am. Chem. Soc.* **1970**, *92*, 4148–4150. (c) Kolc, J., Michl, J. *J. Am. Chem. Soc.* **1973**, *95*, 7391–7401.

15. Fu, X. *et al*. *Chem. Sci.* **2020**, *11*, 5565–5571.

16. Horii, K. *et al*. *J. Am. Chem. Soc.* **2022**, *144*, 3370−3375.

17. Wu, F. *et al*. *Angew. Chem. Int. Ed.* **2022**, *61*, e202202170.

18. Konishi, A. *et al*. *J. Am. Chem. Soc.* **2019**, *141*, 10165−10170.

19. Liu, J. *et al*. *J. Am. Chem. Soc.* **2019**, *141*, 12011−12020.

20. Fei, Y. *et al*. *J. Am. Chem. Soc.* **2021**, *143*, 2353–2360.

21. Shimizu, A. *et al*. *Angew. Chem. Int. Ed.* **2022**, *61*, e202205729.

22. Shimizu, A., Arikawa, S., Morikoshi, T., Shintani, R. *Pure Appl. Chem.* **2023**, *95*, 401–412.

23. Hollister, K. K. *et al*. *J. Am. Chem. Soc.* **2024**, *146*, 6506−6515.

24. (a) Stępień, M., Gońka, E., Żyła, M., Sprutta, N. *Chem. Rev.* **2017**, *117*, 3479–3716. (b) Borissov, A. *et al*. *Chem. Rev.* **2022**, *122*, 565–788.

25. Ito, S., Tokimaru, Y., Nozaki, K. *Angew. Chem. Int. Ed.* **2015**, *54*, 7256–7260.

26. Hamamoto, Y., Ochiai, K., Li, Y., Tapavicza, E., Ito, S. *Angew. Chem. Int. Ed.* **2024**, *63*, e202319022.

27. (a) Narayan, R., Matcha, K., Antonchick, A. P. *Chem. Eur. J.* **2015**, *21*, 14678–14685. (b) Pulis, A. P., Procter, D. J. *Angew. Chem. Int. Ed.* **2016**, *55*, 9842–9860. (c) Yanagi, T., Nogi, K., Yorimitsu, H. *Tetrahedron Lett.* **2018**, *59*, 2951–2959. (d) Tian, T., Li, Z., Li, C.-J. *Green Chem.* **2021**, *23*, 6789–6862. (e) Ghosh, A., Pyne, P., Ghosh, S., Majumder, S., Hajra, A. *Green Chem.* **2022**, *24*, 3056–3080.

28. Zhang, Y.-F. *et al*. *Org. Biomol. Chem.* **2023**, *21*, 8284–8288.

29. Bendikov, M. *et al*. *J. Am. Chem. Soc.* **2004**, *126*, 7416−7417.

30. (a) Li, Q.-Q. *et al*. *Angew. Chem. Int. Ed.* **2022**, *61*, e202112638. (b) Nakamura, K. *et al*. *Precision Chem.* **2023**, *1*, 29–33.

31. Still, W. C., Kahn, M., Mitra, A. *J. Org. Chem.* **1978**, *43*, 2923–2925.

32. Biletskyi, B., Kong, L., Tenaglia, A., Clavier, H. *Adv. Synth. Catal.* **2021**, *363*, 2578–2585.

33. Jančařík, A. *et al*. *Angew. Chem. Int. Ed.* **2013**, *52*, 9970–9975.

34. Ito, S., Tokimaru, Y. Nozaki, K. *Chem. Commun.* **2015**, *51*, 221–224.

35. Sheldrick, G. M. University of Göttingen: Göttingen, Germany, **2018**.

36. Gaussian 16, Revision C.01, M. J. Frisch. *et al*. Gaussian, Inc., Wallingford CT, 2019.

37. (a) Becke, A. D., *J. Chem. Phys.* **1993**, *98*, 5648–5652. (b) Lee, C., Yang, W., Parr, R. G. *Phys. Rev. B* **1998**, *37*, 785–789.

38. (a) Hehre., W. J., Ditchfield, R., Pople, J. A. *J. Chem. Phys.* **1972**, *56*, 2257–2261. (b) Ditchfield, R., Hehre, W. J., Pople, J. A. *J. Chem. Phys.* **1971**, *54*, 724–728.

39. Geuenich, D., Hess, K., Köhler, F., Herges, R. *Chem. Rev*. **2005**, *105*, 3758–3772.

Chapter 4. Diazapentabenzocorannulenium: A Hydrophilic/Biophilic Cationic Buckybowl

Abstract

Polycyclic aromatic molecules are promising functional materials for a wide range of applications, especially in organic electronics. However, their largely hydrophobic nature has impeded further applications. As such, imparting high solubility/hydrophilicity to polycyclic aromatic molecules leads to a breakthrough in this research field. Herein, we report the synthesis of diazapentabenzocorannulenium, a cationic nitrogen-embedded buckybowl bearing a central imidazolium core, by a bottom-up strategy from polycyclic aromatic azomethine ylide. X-ray crystallography analyses have revealed a bowl-shaped molecular structure that is capable of forming charge-segregated one-dimensional columns by bowl-in-bowl packing. In addition to its fluorescence capabilities and high dispersibility in water, the molecule was found to selectively localize in the mitochondria of various tumor cells, showing potential as viable mitochondria-selective fluorescent probes.

4.1. Introduction

Polycyclic aromatic molecules are one of the most important class of organic molecules owing to their widespread applications in various scientific fields.[1,2,3,4,5] The significant progress and application of polycyclic aromatic molecules in material sciences, especially in organic electronics, are mainly based on their intrinsic hydrophobic properties. [6,7] In order to further extend possible applications, for example in biological or medicinal research, the development of highly-soluble/hydrophilic molecules is desirable. [8,9] The most conventional method to achieve water-soluble polycyclic aromatic molecules is to add hydrophilic substituents at their peripheral positions (**Figure 4.1a**)[10,11,12,13,14,15,16]. However, the method

may not be ideal in terms of step economy as it requires some additional steps for functionalization. It is therefore essential to develop more efficient methods in introducing hydrophilicity to polycyclic aromatic molecules by other methods than introducing hydrophilic substituents. A possible solution would be to change the framework of polycyclic aromatic molecules. Firstly, the introduction of curvature to planar framework would be an efficient method to change the degree of intermolecular interaction and aggregation, resulting in higher solubility (yellow in **Figure 4.1b**) [17,18,19,20]. Secondly, adding positive or negative charges into polycyclic aromatic molecules will increase ionic solvation potentials, which lead to better solvation of ions (red in **Figure 4.1b**)[21]. Lastly, introducing heteroatoms will help improve molecular polarity and increase affinity with polar solvents (blue in **Figure 4.1b**)[20, 22 , 23 , 24 , 25 , 26]. Although these three concepts themselves are not new, with such modifications, polycyclic aromatic molecules can be conferred higher solubility and hydrophilic functions required for biological and supramolecular applications.

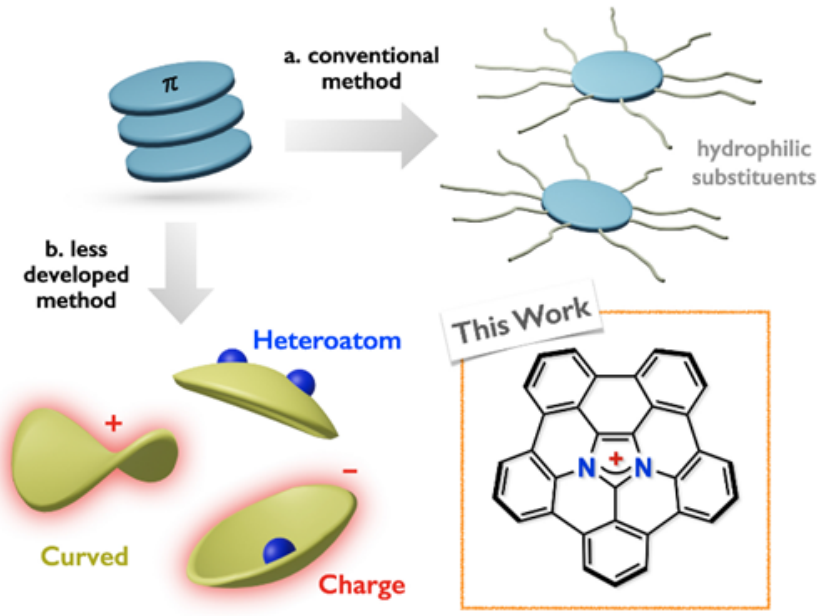

Figure 4.1. a) A conventional method to increase solubility/hydrophilicity to polycyclic aromatic molecules: introduction of hydrophilic substituents. b) Less developed methods: introduction of curvature, charge, and heteroatoms to polycyclic aromatic molecules.

Considering the abovementioned factors, cationic curved polycyclic aromatic molecules have attracted much attention as they will have physical and chemical properties different from neutral planar molecules. An effective method in generating cationic curved polycyclic aromatic molecules is chemical oxidation of neutral molecules using external oxidants[27,28,29,30,31]. However in this work, we have adopted a different approach in generating cationic curved polycyclic aromatic molecules via introducing intrinsically stable cationic functionality into polycyclic aromatic structures[32,33,34]. Herein, we utilized imidazolium, which is an important structural motif for functional organic materials such as ionic liquids[35,36,37] and N-heterocyclic carbene precursors [38, 39, 40]. Despite its potential utility and application, imidazolium-containing polycyclic aromatic molecules are limited[41,42]. Here we report the synthesis of diazapentabenzocorannulenium, a cationic bowl-shaped polycyclic aromatic molecule bearing multiple internal nitrogen atoms. This molecule exhibits fluorescence and high solubility in various solvents including water. In addition, the molecule selectively localized at the mitochondria of tumor cells, showing potential as mitochondrial fluorescent probes.

4.2. Results and discussion

As shown in **Scheme 4.1**, the synthesis of diazapentabenzocorannulenium **4** started with 1,3-dipolar cycloaddition of 6-chlorophenathridine **1** and polycyclic aromatic azomethine ylide prepared from iminium salt **2**, which proceeds via a nitrilium salt intermediate generated at high temperature under basic conditions[43,44]. The subsequent dehydrogenation took place spontaneously to form fused imidazolium salt **3**, the structure of which was confirmed by X-ray crystallography analysis (**Figure S4.8**). The access to diazapentabenzocorannulenium **4a** was accomplished by palladium-catalyzed intramolecular cyclization, where the use of triphenyl phosphine and potassium carbonate is essential to obtain

a higher yield of **4a**, although the reaction produced a lot of side products that could not be identified. Unfortunately, as **4a** resisted all attempts at crystallization, an anion exchange reaction of **4a** was attempted with silver hexafluoroantimonate ($AgSbF_6$) in methanol to obtain the corresponding hexafluoroantimonate salt **4b**.

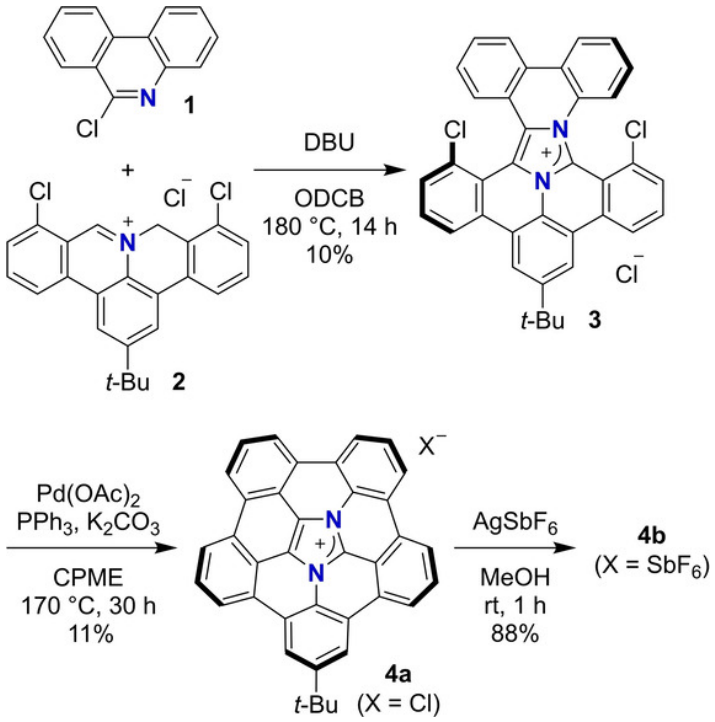

Scheme 4.1. Synthesis of diazapentabenzocorannulenium **4**.

Single crystals of **4b** suitable for X-ray crystallography analysis were obtained by slow diffusion of 1,3-difluorobenzene to a solution of **4b** in methanol under argon at room temperature. It crystallized in monoclinic space group $P2_1/c$ and composed of four ionic pairs of **4b** including solvent molecules. The X-ray diffraction analysis elucidated that **4b** has a bowl-shaped structure with bowl depths of 0.97–1.43 Å (**Figure 4.2a**). This bowl depth value is larger than the other closed-shell cationic buckybowls reported in literature, such as "hydrazinobuckybowl" (ca. 0.7 Å)[28] and BN-substituted triangulene (0.07–0.25 Å)[34]. On the other hand, these values are ca. 0.4 Å shorter than the parent azapentabenzocorannulene (1.38–1.73 Å)[45]. This shallower bowl depth is attributed to shorter C−N bonds than C−C bonds. The

bowl inversion energy was determined by density functional theory (DFT) calculation at the B3LYP/6-311+G(2d,p) level of theory to be 8.5 kcal mol^{-1}, which is lower than the azapentabenzocorannulene (17.0 kcal mol^{-1}) (**Figure S4.14**).

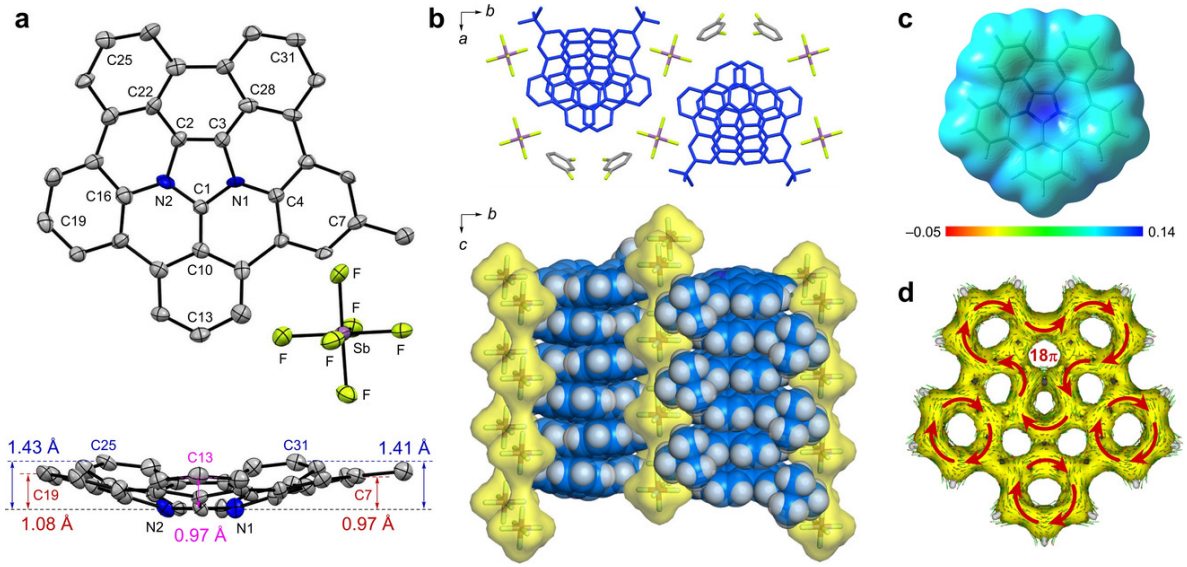

Figure 4.2. a) ORTEP structure of **4b** with thermal ellipsoids at 50 % probability. The hydrogen atoms and the methyl groups of *tert*-butyl group are omitted for clarity. b) Packing structure of **4b**. c) Electrostatic potential map of **4**. d) ACID plot of **4**.

Another notable feature of **4b** in the crystal structure is the formation of charge-segregated one-dimensional columns along to the *c* axis by intermolecular bowl-in-bowl interaction (**Figure 4.2b**). This indicates that the intermolecular concave-to-convex interaction is more favorable than the intermolecular repulsion between positive charges over the entire molecule. Each molecule in the column is shifted by about 82° so that the *tert*-butyl groups can fill the vacant space complementarily with 1,3-difluorobenzene and the counterion species. The intermolecular stacking distance of 3.54 Å is closer than neutral azapentabenzocorannulene (3.69 Å)[45]. Meanwhile, the central imidazolium rings are "slipped stacked" with 29.8° degrees (**Figure S4.11**), in contrast to azapentabenzocorannulene core being overlapped[45]. The electrostatic potential map shown in **Figure 4.2c** indicates that this may be attributed to

interaction between the relatively positive imidazolium core and the relatively negative benzene rings. The adjacent columns were concave-to-convex π-stacking with dipoles in opposite directions in order to cancel overall dipole moments. It is worth noting that the formation of charge-segregated column by heteroatom-containing polycyclic aromatic molecules has been reported, but most examples have planar or quasi-planar structures,[31,46,47,48] Therefore, this molecule is one of the rare examples of cationic buckybowls forming highly ordered charge-segregated one-dimensional columns[49], which are expected to be applied as charge-transfer materials with high carrier density[50].

The aromaticity of **4** was evaluated by nucleus-independent chemical shift (NICS) analysis and the anisotropy of the induced current density (ACID) using DFT calculations at the B3LYP/6-311+G(2d,p) level of theory. The imidazolium ring and the peripheral five benzene rings show NICS(0) values of −14.9 ppm and −7.6 to −8.0 ppm, respectively (**Figure S4.20**), suggesting that the aromatic contribution in the central imidazolium ring and the outer five benzene rings is significant, which is similar to azapentabenzocorannulene[45]. The ACID plot also supports the presence of 6π conjugation on the imidazolium and five benzene rings, while another clockwise ring current in the 18π ring including the central imidazolium and three peripheral benzenes is also observed as a minor contribution (**Figure 4.2d**).

During our experimental investigation, imidazolium salt **4a** possessing a chloride ion was found to exhibit high solubility in common polar reagents such as acetonitrile, dimethylsulfoxide, and methanol, whereas **4b** possessing a hexafluoroantimonate ion shows much lower solubility. Moreover, **4a** also gave a clear yellow "solution" in water despite the absence of hydrophilic substituents. As such, further investigations were performed to elucidate the phenomenon in water. Dynamic light scattering (DLS) (**Figure 4.3d**) revealed the presence of **4a** nanostructures in water with an average size of 38 nm. Transmission electron microscope (TEM) images further confirmed a uniform spherical morphology (**Figure 4.3a, b**) with a size

distribution (36.7±3.0 nm; **Figure 4.3c**) matching that of the DLS data. These results have revealed that **4a** is highly dispersed in water to give a visually clear and transparent suspension. This was also supported by the Tyndall effect observed from **4a** in water (**Figure 4.3d**).

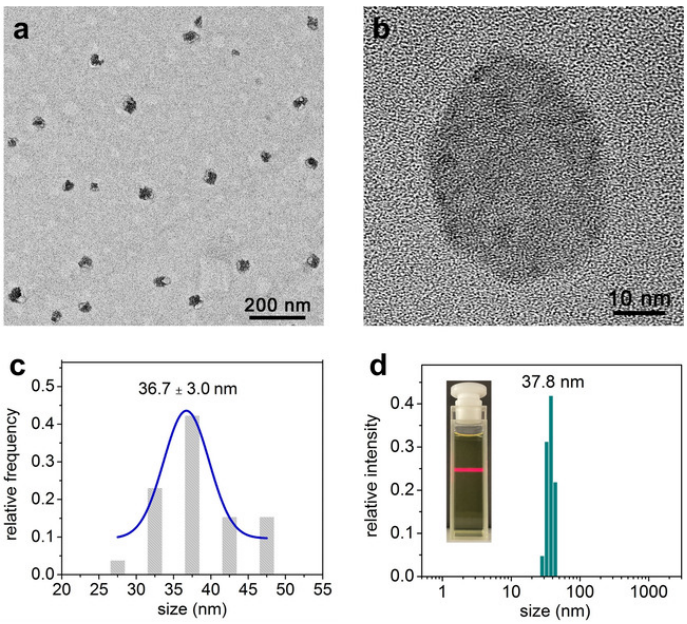

Figure 4.3. a) Low magnification TEM image of **4a**. b) High magnification TEM image of **4a**. c) Size distribution of **4a** determined by TEM analysis. d) Size distribution of **4a** in aqueous suspension determined by DLS analysis. Inset: photo of aqueous suspension of **4a** irradiated with red laser.

To study the fluorescence capabilities of **4a**, the absorption and emission spectra in dichloromethane and water were obtained. As shown in **Figure 4.4a**, a solution of **4a** in dichloromethane exhibits broad absorption at λ = 300–500 nm with discrete major peaks at 352, 441 nm, which are slightly lower than those of the azapentabenzocorannulene (395 and 466 nm)[45]. In contrast, its aqueous suspension showed broaden absorption bands with peaks at 339 and 447 nm. The lower intensity could be attributed to the formation of nanoparticles in water, which is known to be a common phenomenon[51,52,53]. To assign the absorption bands in the absorption spectra, time-dependent DFT calculations were performed at the B3LYP/6-

311+G(2d,p) level of theory. The low band at 441 nm is attributed to the transition from HOMO (−8.68 eV) to LUMO (−5.33 eV) (**Figure 4.4b**) with an oscillator strength of 0.1464 (Table S3). The HOMO of **4** is mainly delocalized at the side of the 18π conjugation including the central imidazolium core. In contrast, the LUMO is localized centered at C1 to the benzene ring at its tip. A noteworthy feature in the fluorescence spectra is solvatofluorchromic behavior: the emission of **4a** in dichloromethane and water appeared at 491 and 511 nm, respectively, with fluorescent quantum yields of 12 % and 6 %. The aqueous suspension exhibited obvious red shift compared with dichloromethane solution. Considering the polarity of organic solvents does not affect the emission wavelengths (**Figure S4.12**), this difference would be attributed to the aggregation of **4a** in water.

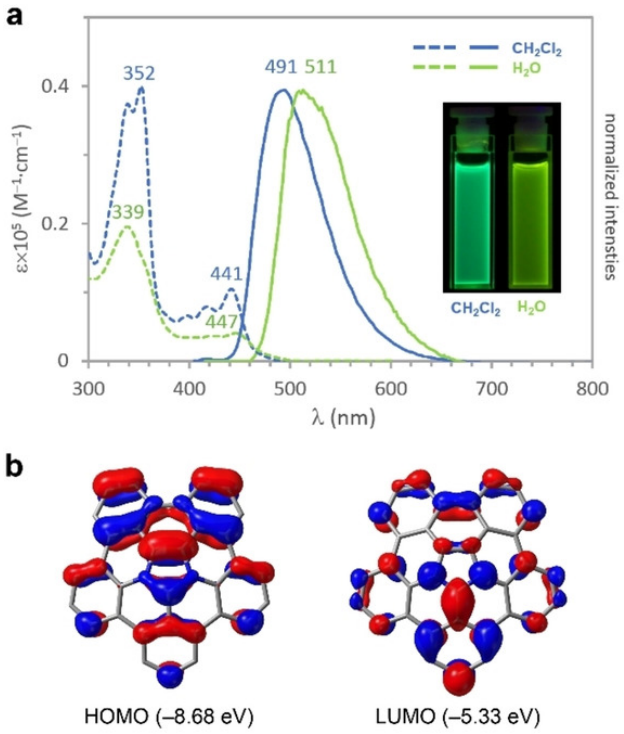

Figure 4.4. a) UV-visible absorption and normalized emission spectra (excited with 400 nm) of **4a** (2.0×10^{-5} M) in dichloromethane (CH_2Cl_2) and water (H_2O). b) HOMO and LUMO of **4** (iso value=0.030).

The fluorescent properties and high dispersibility of **4a** in water motivated us to further investigate its potential biological applications. We first assessed the biocompatibility of imidazolium **4a** with a resazurin based toxicology assay kit. HeLa, HCT116, and MDA-MB-231 cells were incubated with **4a** for 24 h. The incubation did not cause any drastic effect on the viabilities of the various treated cell lines, indicating relatively low toxicity of **4a** (**Figure S4.24**). Subsequently, HeLa cells incubated with **4a** were co-stained with CellMask™ Deep Red Plasma (**Figure 4.5a**). Fluorescence emission of **4a** upon excitation at 488 nm was observed inside the cytoplasm, which clearly indicates the successful cellular uptake of **4a** after 2 h incubation.

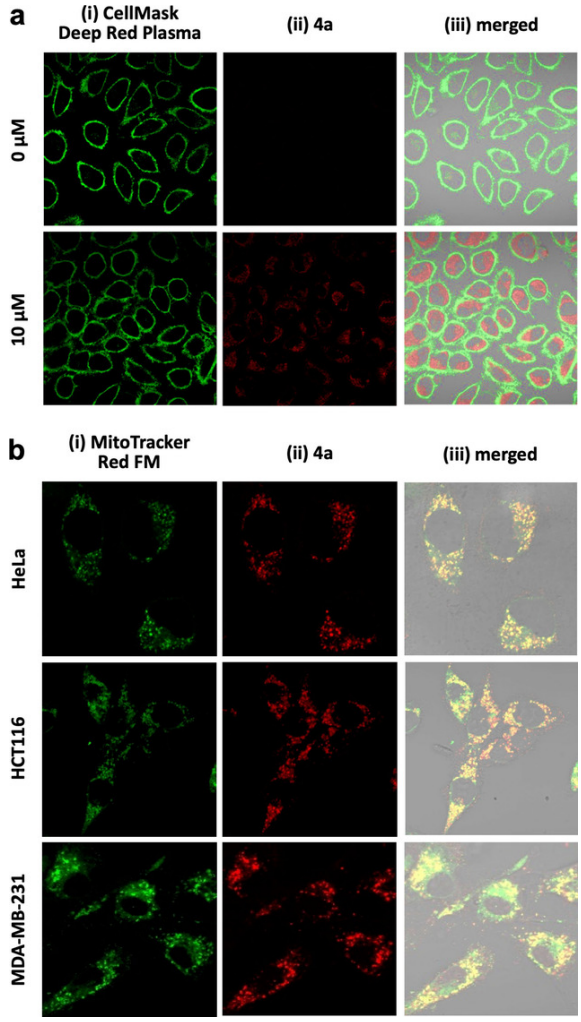

Figure 4.5. a) Confocal fluorescence images of HeLa cells stained with CellMask Deep Red Plasma (5 µg mL^{-1}) and **4a** (0–10 µM). Images of (i) CellMask Deep Red Plasma (excited with

640 nm laser) and (ii) **4 a** (excited with 488 nm laser). (iii) Merged bright field images of CellMask Deep Red Plasma and **4 a**. b) Confocal fluorescence images of HeLa (row 1), HCT116 (row 2), and MDA-MB-231 (row 3) cells. Images of (i) MitoTracker Red FM (1.0 nM, excited with 561 nm laser), (ii) **4 a** (excited with 488 nm laser). (iii) Merged bright field images of MitoTracker and **4 a**.

Upon confirming successful cellular uptake, we hypothesized that the unique cationic core present in **4 a** might confer it certain specific subcellular localization properties, particularly in the mitochondria due to possible affinity with its negative membrane potential (−160 to −180 mV)[32,33,54]. In order to further confirm this, HeLa, HCT116, and MDA-MB-231 cells incubated with **4 a** were co-stained with MitoTracker™ Red FM to observe the extent of possible co-localization. As shown in **Figure 4.5b**, the merged confocal images of MitoTracker™ Red FM and **4 a** showed significant overlap for all the tested cell lines. These results have confirmed that **4 a** mainly accumulates in the mitochondria upon cellular uptake. The high selectivity could be explained by an appropriate balance of lipophilicity and cationic nature of **4 a**. Lipophilicity of **4 a** was determined via a shake-flask method [55] with a log *P* value of 1.15±0.05 (**Table S4.10**). This indicates that **4 a** possesses good lipophilicity to pass through membranes. Given its positive charge, as shown in the electrostatic potential map in **Figure 4.2c**, the cationic nature of **4** plays an important role in its selective mitochondrial accumulation. Compared to conventional small molecule mitochondrial targeting strategies, our polycyclic aromatic molecule does not require further lipophilic and cationic conjugations to confer it efficient mitochondrial targeting properties. Therefore, our molecule could be potentially used as a mitochondria-selective fluorescent probe to complement the known probes[56].

4.3. Conclusion

In conclusion, we have designed and synthesized diazapentabenzocorannulenium **4** by 1,3-dipolar cycloaddition of polycyclic aromatic azomethine ylide and 6-chlorophenathridine, followed by palladium-catalyzed intramolecular cyclization. In the crystal state, the obtained buckybowl exhibits a bowl-shaped structure and forms charge-segregated one-dimensional columns by bowl-in-bowl interaction. Despite the lack of hydrophilic substituents, the molecule shows high water dispersibility and biocompatibility, and thus was applied as a fluorescent cellular probe: **4 a** was selectively introduced into the mitochondria of tumor cells. The present study provides an excellent polycyclic aromatic molecular platform which could be utilized for a wide range of applications in material and biological sciences.

4.4. Experimental section

1. Experimental section

General: Reactions were carried out under nitrogen atmosphere using standard Schlenk techniques. Thin-layer chromatography (TLC) was performed using glass plates pre-coated with silica gel impregnated with a fluorescent indicator (Merck, #1.15685.0001).

Instrumentation: NMR spectra were recorded on Bruker AV 800 (^{1}H: 800 MHz and ^{13}C: 200 MHz) and AV 400 (^{1}H: 400 MHz and ^{13}C: 100 MHz) NMR spectrometers. Chemical shift values for protons are referenced to the signal of tetramethylsilane (δ 0.00), the residual signal of chloroform-*d* (δ 7.26) chemical shift values for carbons are referenced to the signal of tetramethylsilane (δ 0.00) or the carbon resonance of chloroform-*d* (δ 77.2). High-resolution mass (HRMS) spectra were taken on a Waters Q-Tof Premier mass spectrometer with the electron spray ionization time-of-flight (ESI-TOF) method. Infrared (IR) spectra were recorded on a Shimadzu FTIR-8400 spectrometer with an attenuated total reflection (ATR) system.

Ultraviolet–visible (UV–vis) absorption spectra were recorded on a Shimadzu UV-3100 spectrometer. Fluorescence spectra were recorded on a JASCO FP-8500 Spectrofluorometer. Quantum yields were determined by a relative method with quinine sulfate as standard. Melting temperatures and decomposition temperatures were recorded on an OptiMelt MPA-100 apparatus. Dynamic light scattering (DLS) size distribution was measured on a Malvern Zetasizer Nano. Transmission electron microscopy (TEM) image was recorded by a JEOL JEM 1400 TEM microscope.

Materials: The following reagents were purchased from the indicated suppliers and used as received: 1,2-dichlorobenzene (TCI), 1,8-diazabicyclo[5.4.0]undec-7-ene (DBU; Sigma), potassium carbonate (TCI), palladium(II) acetate (Sigma), triphenylphosphine (Sigma). Cyclopentyl methyl ether (Alfa Aesar) was pre-dried over activated 4 Å molecular sieves and heated to reflux over calcium hydride under nitrogen atmosphere, collected by distillation and stored under argon in a Schlenk flask. Silica gel (Davisil, 60 Å, 40–63 micron) was purchased from Sigma-Aldrich. The following reagents were prepared according to literature procedures: 2-*t*-butyl-8-hydroisoquinolino[4,3,2-*de*]phenanthridin-9-ium chloride [57], 6-chlorophenanthridine[58]. In vitro toxicology assay kit (TOX8, resazurin based) was purchased from Sigma-Aldrich. Dulbecco's modified Eagle medium (Gibco), foetal bovine serum (Hyclone), penicillin−streptomycin, trypsin−EDTA, CellMask™ deep red plasma membrane stain and MitoTracker™ Red FM were purchased from Life Technologies Holdings. Human uterus adenocarcinoma HeLa, human colorectal carcinoma HCT116 and human breast adenocarcinoma MDA-MB-231 were purchased from ATCC.

11-*tert*-butyl-6,16-dichloroimidazolo[4',3':1,2]isoquinolino[4,3,2-*de*:1',5'-*f*']diphenathridinium chloride (3):

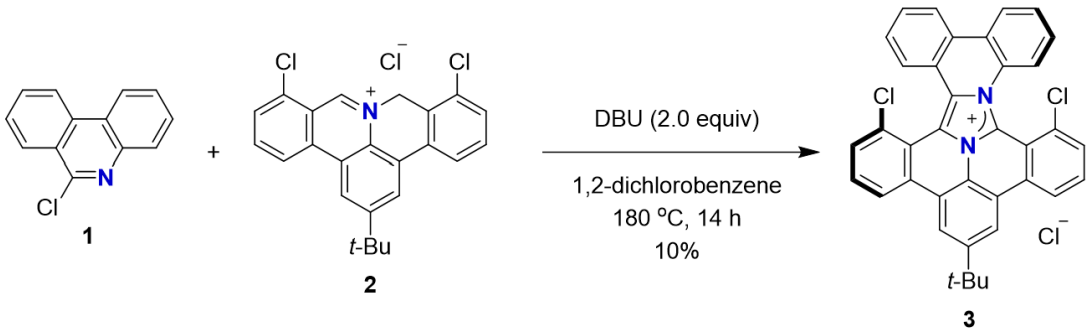

In a 25-mL Schlenk tube were added 6-chlorophenanthridine **1** (128 mg, 0.60 mmol) and iminium salt **2** (0.20 mmol). The tube was evacuated and refilled with argon for three times. After adding 1,2-dichlorobenzene (3.0 mL) and DBU (60 μL, 0.40 mmol), the reaction mixture was stirred for 14 hours at 180 °C (oil bath temperature). The reaction mixture was cooled to room temperature and directly purified by silica gel column chromatography to yield **3** as a brown solid (12.1 mg, 0.020 mmol, 10%). R_f: 0.3 (with dichloromethane:methanol = 10:1); Φ 0.16 (in dichloromethane); mp 330–335 °C (decomp); IR (neat); cm^{-1} 3649, 3365, 3066, 2955, 2924, 2858, 1718, 1589, 1560, 1487, 1460, 1438, 1365, 1253, 1205, 1133, 1063, 887, 809, 782, 750, 728, 688, 678; ^{1}H NMR (400 MHz, $CDCl_3$, 300 K) δ 9.07 (d, J = 8.4 Hz, 1H), 8.86 (s, 1H), 8.76 (s, 1H), 8.73 (d, J = 8.0 Hz, 1H), 8.47 (d, J = 8.0 Hz, 1H), 8.45 (d, J = 8.0 Hz, 1H), 8.29 (t, J = 8.0 Hz, 1H), 7.98 (t, J = 8.0 Hz, 1H), 7.95–7.83 (m, 5H), 7.78 (t, J = 7.6 Hz, 1H), 7.67 (t, J = 7.6 Hz, 1H), 7.60 (t, J = 7.4 Hz, 1H), 1.64 (s, 9H); ^{13}C NMR (100 MHz, $CDCl_3$, 300 K) δ 153.8, 135.2, 134.7, 132.8, 132.8, 132.6, 132.5, 132,3, 132.3, 132.0, 131.7, 130.2, 129.6, 129.5, 128.7, 127.7, 127.7, 127.6, 125.4, 124.7, 123.8, 123.7, 123.6, 123.5, 123.3, 122.9, 122.5, 122.2, 121.7, 120.4, 118.7, 116.9, 116.5, 36.3, 31.7 (3C); HRMS (ESI) *m*/*z* calcd for $C_{37}H_{25}Cl_2N_2$ $[M-Cl]^+$ 567.1395, found 567.1392.

8-*tert*-butyl-3a^2,6b^2-diazadibenzo[*fg,ij*]benzo[5,6]acenaphtho[4,3,2,1,8,7-*pqrstuv*]pentaphenium chloride (4a):

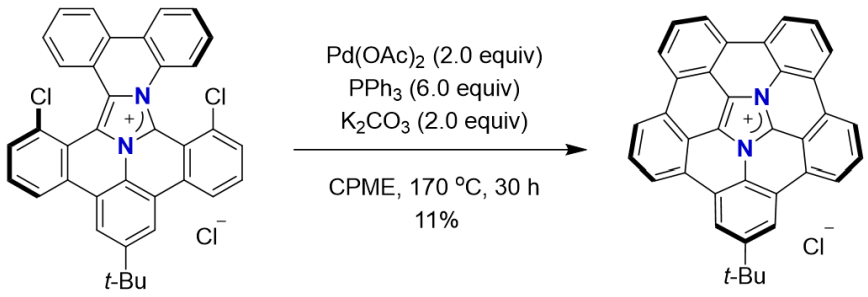

In a 25-mL Schlenk tube placed with imidazolium salt **3** (18 mg, 30 μmol) and a magnetic stirring bar were added palladium(II) acetate (13.4 mg, 60 μmol), triphenylphosphine (46.9 mg, 180 μmol) and potassium carbonate (8.2 mg, 60 μmol). Then, cyclopentyl methyl ether was added into the mixture. The reaction mixture was stirred for 30 hours at 170 °C (oil bath temperature). After cooling to room temperature and dilution with dichloromethane (30 mL), the mixture was extracted with water (20 mL) four times. The aqueous phases were filtered with filter paper and the filtrate was extracted with dichloromethane (20 mL) for six times. The combined organic phases were dried over sodium sulfate. After filtration and evaporation, the crude product was purified by silica gel column chromatography to yield **4a** as a yellow solid (1.7 mg, 3.2 μmol, 11%). R_f: 0.3 (with dichloromethane:methanol = 10:1); Φ 0.12 (in dichloromethane); mp 280–285 °C (decomp); IR (neat); cm^{-1} 3066, 3063, 2956, 2925, 2864, 1978, 1634, 1565, 1524, 1466, 1394, 1378, 1241, 1134, 1083, 878, 789, 764, 750, 731, 657; ^{1}H NMR (800 MHz, CD_2Cl_2, 300 K) δ 8.74 (d, J = 7.2 Hz, 1H), 8.71 (d, J = 7.2 Hz, 1H), 8.68–8.60 (m, 5H), 8.55 (d, J = 7.2 Hz, 1H), 8.46 (d, J = 7.2 Hz, 1H), 8.42–8.34 (m, 2H), 8.06 (t, J = 7.2 Hz, 1H), 8.04–7.98 (m, 2H), 1.64 (s, 9H); ^{13}C NMR (200 MHz, CD_2Cl_2, 300 K) δ 153.7, 138.7, 135.1, 132.2, 132.1, 132.1, 130.6, 130.6, 130.1, 129.4, 129.0, 128.7, 128.1, 128.0, 128.0, 127.3, 126.8, 126.7, 126.6, 126.4, 125.8, 125.6, 125.3, 125.3, 125.0, 124.3, 124.2, 123.8, 122.5,

122.2, 122.0, 121.9, 115.6, 36.7, 32.0 (3C); HRMS (ESI) *m*/*z* calcd for $C_{37}H_{23}N_2$ $[M-Cl]^+$ 495.1861, found 495.1858.

8-*tert*-butyl-3a^2,6b^2-diazadibenzo[*fg,ij*]benzo[5,6]acenaphtho[4,3,2,1,8,7-*pqrstuv*]pentaphenium hexafluoroantimonate (4b):

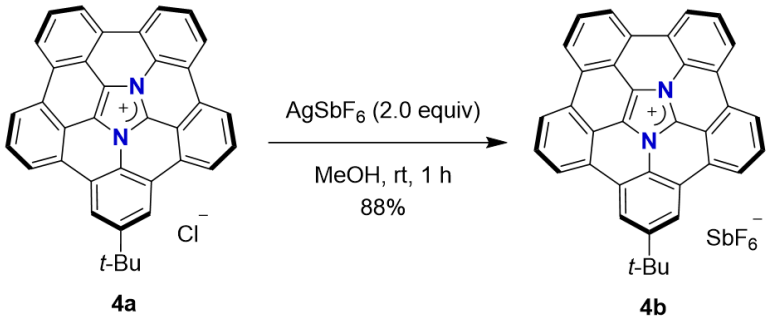

In a 25-mL Schlenk tube placed with imidazolium salt **4a** (3.2 mg, 6.0 μmol) and a magnetic stirring bar was added methanol (1.5 mL) to completely dissolve the solids. A solution of silver hexafluoroantimonate (4.2 mg, 12 μmol) in methanol (3.0 mL) was added dropwise into the above reaction mixture. After stirring at room temperature for 1 hour, the solvent was removed under vacuum. The crude residue was purified by silica gel column chromatography to yield **4b** as a yellow solid (3.9 mg, 5.3 μmol, 88%). R_f: 0.3 (with dichloromethane:methanol = 10:1); Φ 0.14 (in dichloromethane); mp 275–282 °C (decomp); IR (neat); cm^{-1} 3079, 2955, 2920, 2852, 1633, 1564, 1464, 1394, 1379, 1258, 1240, 1091, 1029, 973, 883, 817, 788, 764, 749, 732, 652; ^{1}H NMR (800 MHz, acetone-d_6, 300 K) δ 9.14 (d, *J* = 8.0 Hz, 1H), 9.04-8.97 (m, 5H), 8.94 (d, *J* = 8.0 Hz, 1H), 8.90 (d, *J* = 8.8 Hz, 1H), 8.88 (d, *J* = 8.0 Hz, 1H), 8.75 (d, *J* = 7.2 Hz, 1H), 8.46 (t, *J* = 8.0 Hz, 1H), 8.20-8.15 (m, 2H), 8.14 (t, *J* = 8.0 Hz, 1H), 1.67 (s, 9H); ^{13}C NMR (200 MHz, acetone-d_6, 300 K) δ 153.7, 141.7, 135.1, 133.1, 132.9, 132.8, 131.6, 130.8, 130.7, 130.6, 130.1, 130.0, 129.9, 129.7, 129.4, 128.0, 127.6, 127.3, 127.2, 127.1, 126.7, 126.6, 126.4, 126.2, 125.9, 125.6, 125.0, 124.8, 124.4, 123.5, 123.4, 123.2, 117.1, 37.1, 32.0 (3C); HRMS (ESI) *m*/*z* calcd for $C_{37}H_{23}N_2$ $[M-SbF_6]^+$ 495.1861, found 495.1856.

General Methods for Cell Culture

All cells were grown in Dulbecco's modified eagle medium supplemented with 10% foetal bovine serum at 5% CO_2 and 37 °C.

General Methods for Confocal Live-Cell Imaging

HeLa, HCT116 and MDA-MB-231 were seeded in μ-slide 8 well (ibidi GmbH, Germany) with complete medium for 24 hours at 5% CO_2 and 37 °C. The medium was subsequently replaced with fresh medium containing **4a** at the different required concentrations for 2 hours. Thereafter, cells were washed with phosphate buffered saline (PBS) three times before incubation with either CellMask Deep Red (5 μg/mL) for 10 minutes or MitoTracker Red FM (1 nM) for 1 hour. Cells were washed with PBS three times again before live-cell imaging was performed with a confocal laser scanning microscope (Carl Zeiss LSM800) (**4a**: λ_{ex} = 488 nm; CellMask Deep Red: λ_{ex} = 640 nm, λ_{em} = 678/25 nm; MitoTracker Red FM: λ_{ex} = 561 nm, λ_{em} = 644/25 nm).

Cell Viability Test

HeLa, HCT116 and MDA-MB-231 were seeded in 96-well plates at a density of 1×10^4 cells per well for 24 hours at 5% CO_2 and 37 °C. The medium was subsequently replaced with fresh medium containing **4a** at the different required concentrations for a further 24 hours. TOX8 solution (0.3 mg/ml) was added to the wells and the plate was incubated for another 4 hours. The fluorescence at 590 nm was measured upon excitation at 560 nm with a microplate reader (Tecan Infinite M200).

2. NMR Spectra

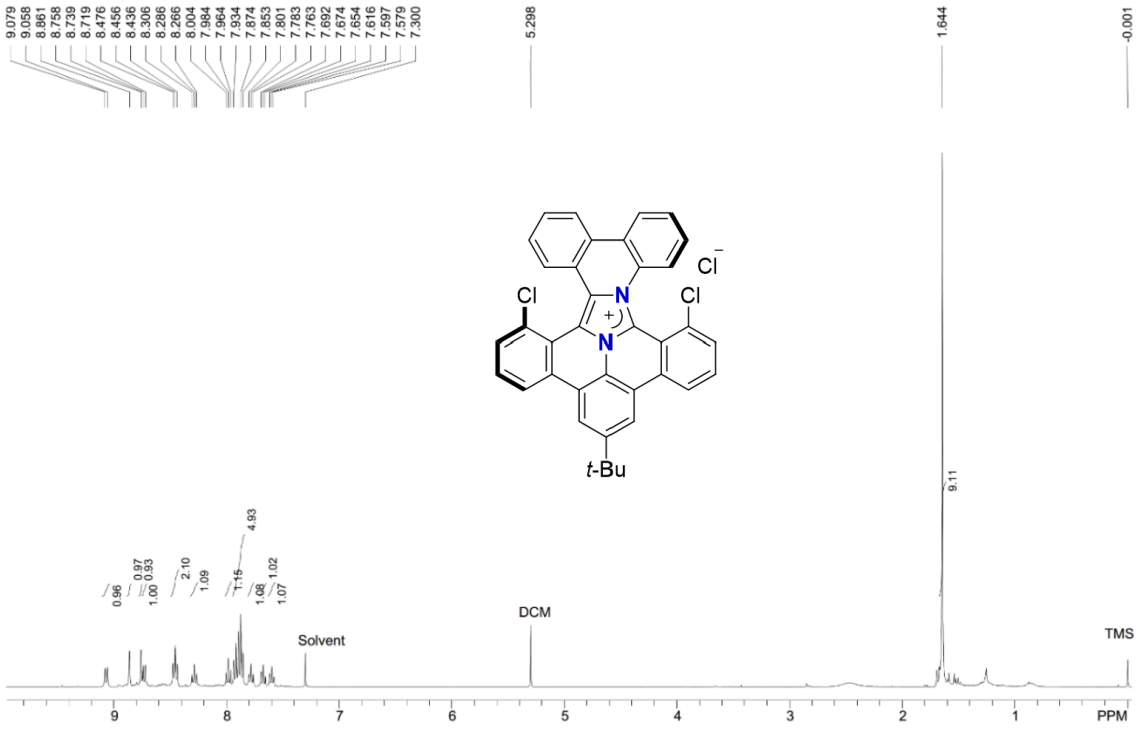

Figure S4.1. ^{1}H NMR spectrum of **3** (400 MHz, $CDCl_3$, 300 K).

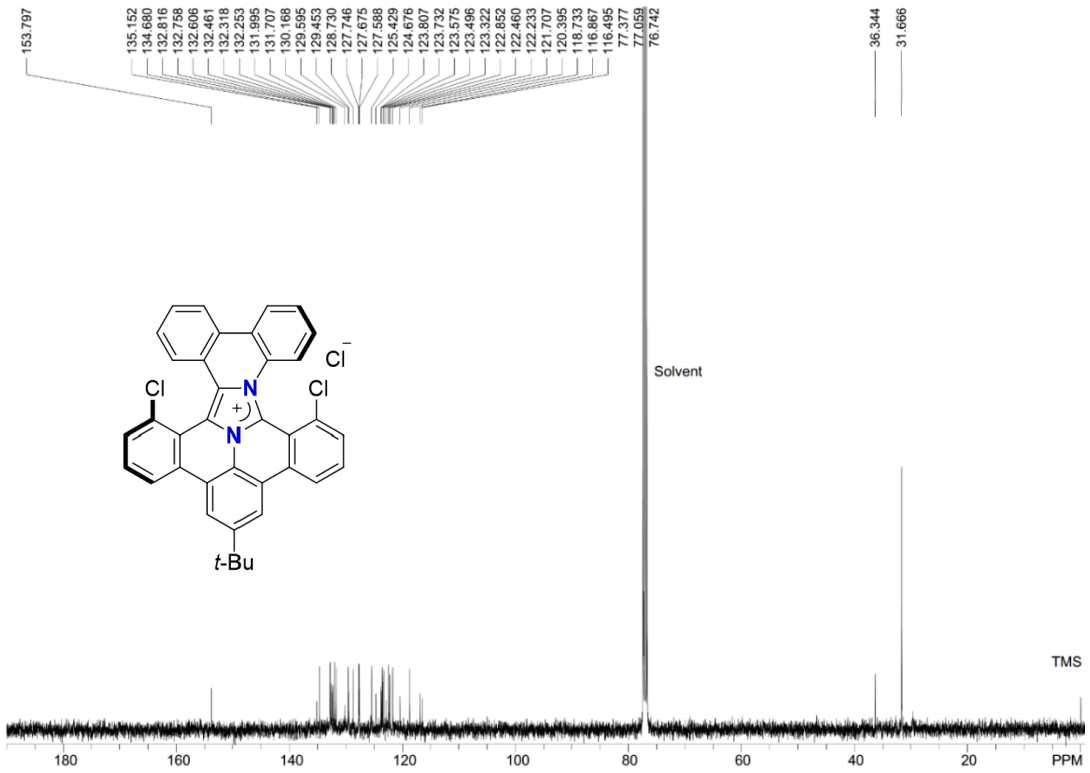

Figure S4.2. ^{13}C NMR spectrum of **3** (100 MHz, $CDCl_3$, 300 K).

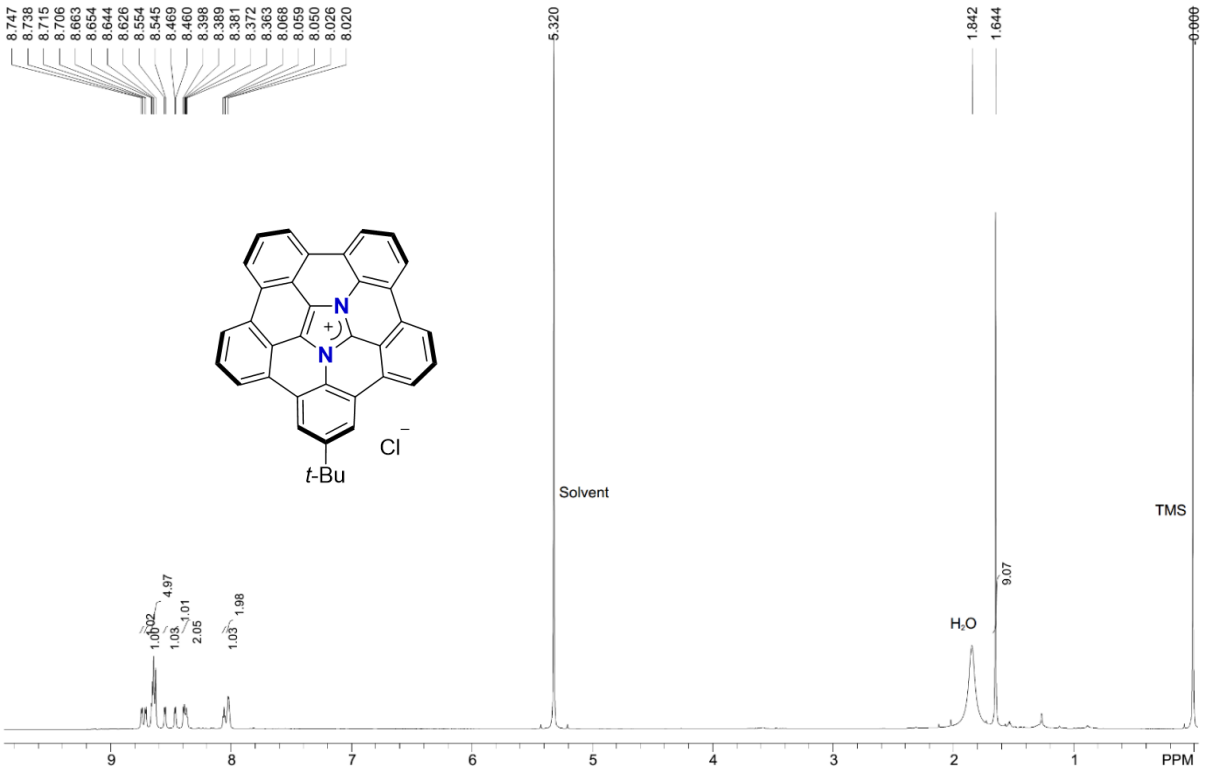

Figure S4.3. ^{1}H NMR spectrum of **4a** (800 MHz, CD_2Cl_2, 300 K).

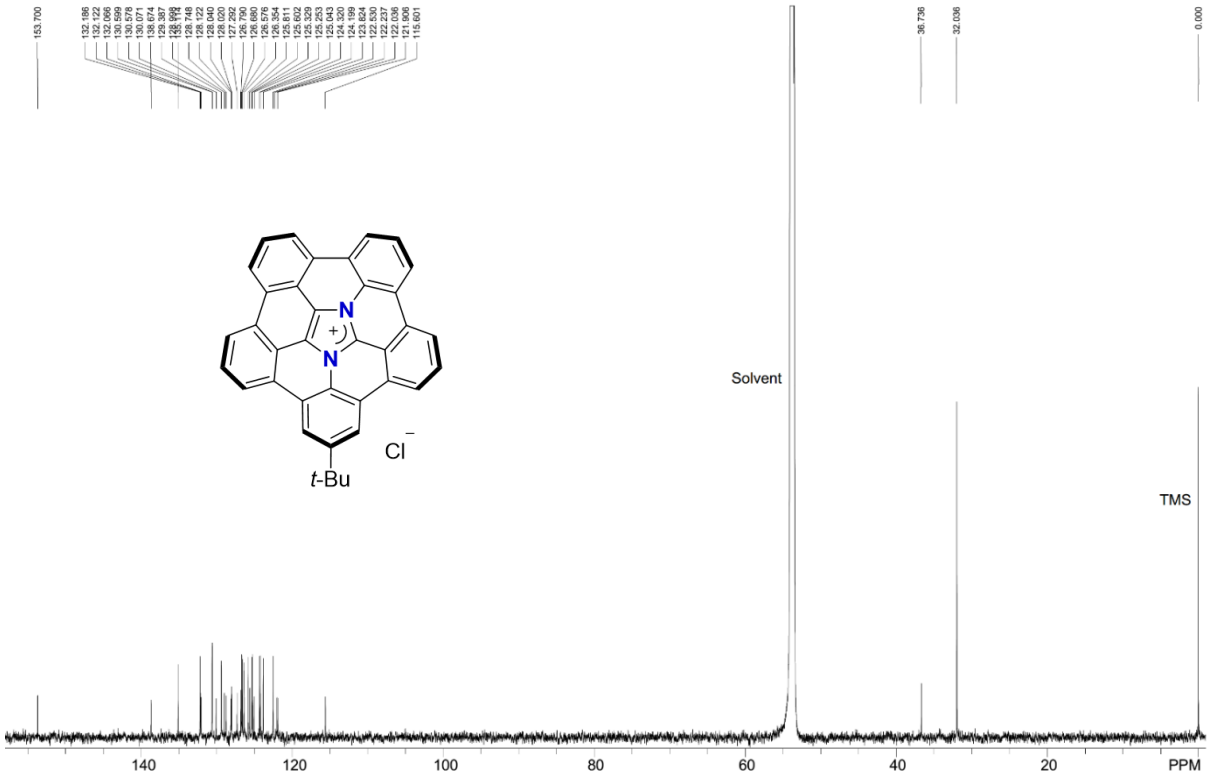

Figure S2.4. ^{13}C NMR spectrum of **4a** (200 MHz, CD_2Cl_2, 300 K).

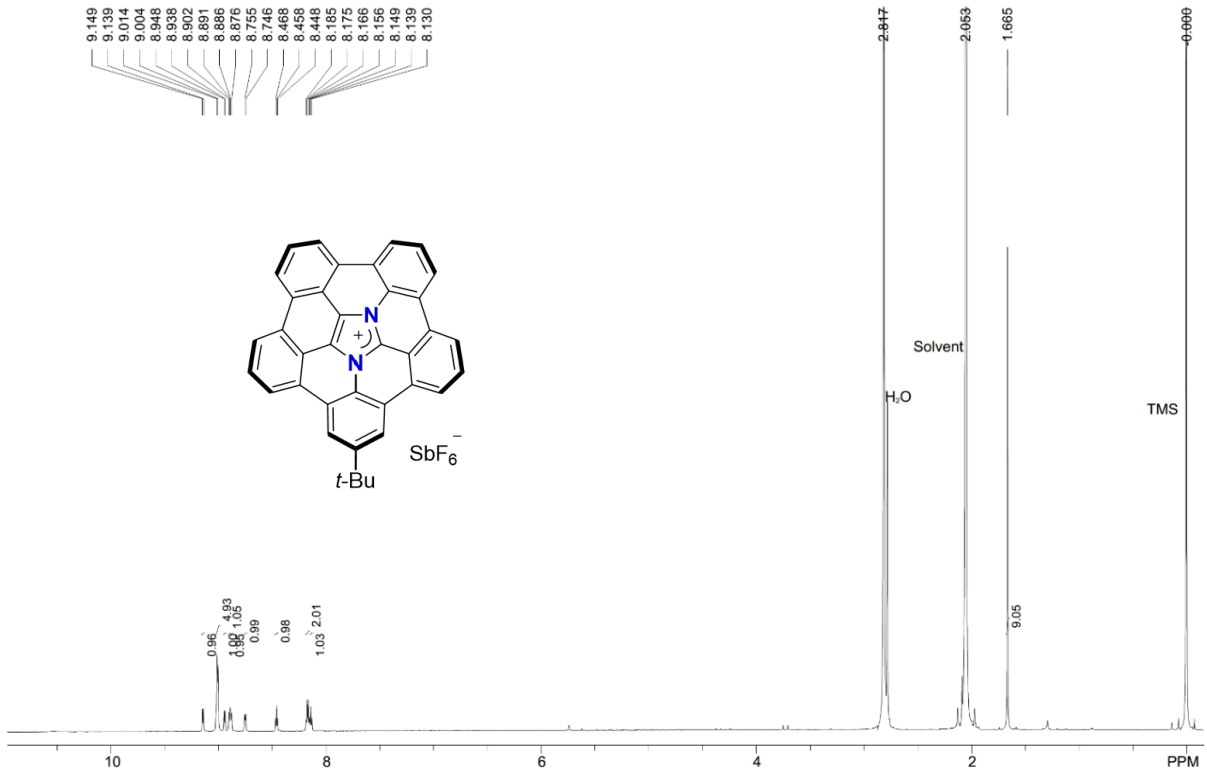

Figure S4.5. ^{1}H NMR spectrum of **4b** (800 MHz, acetone-d_6, 300 K).

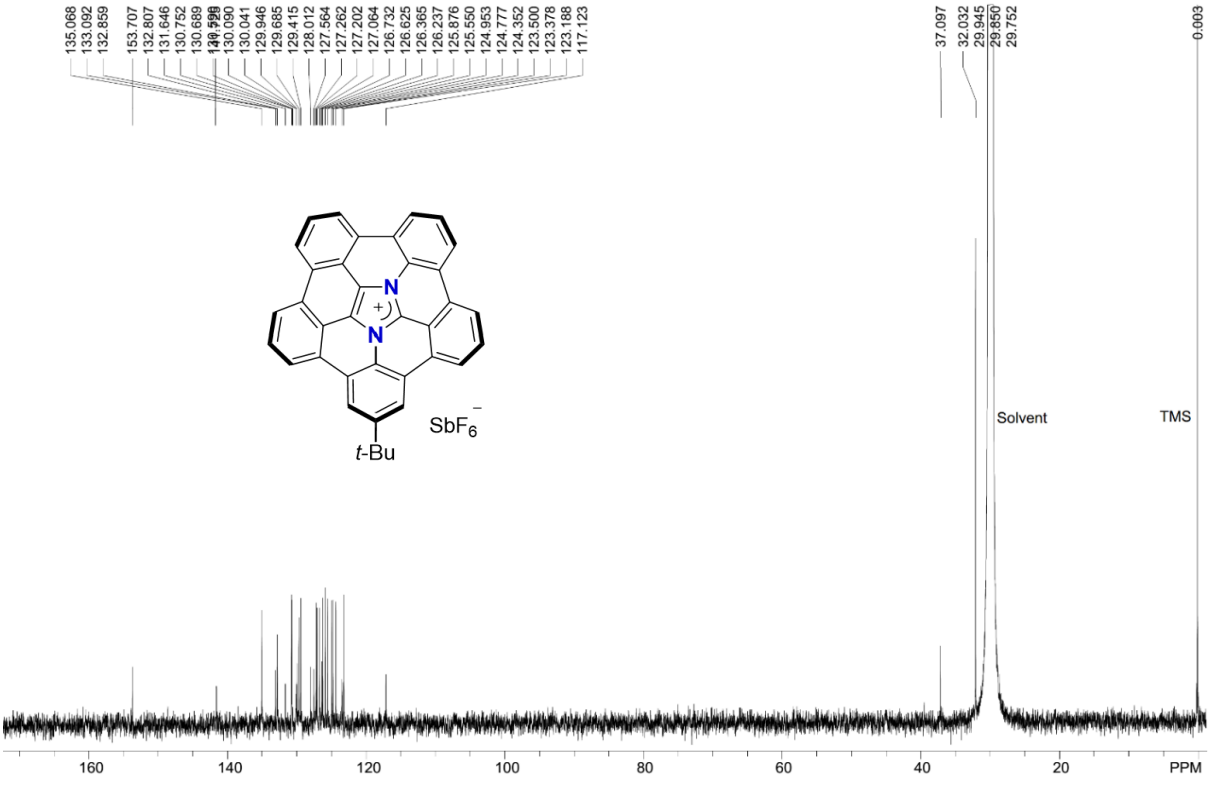

Figure S4.6. ^{13}C NMR spectrum of **4b** (200 MHz, acetone-d_6, 300 K).

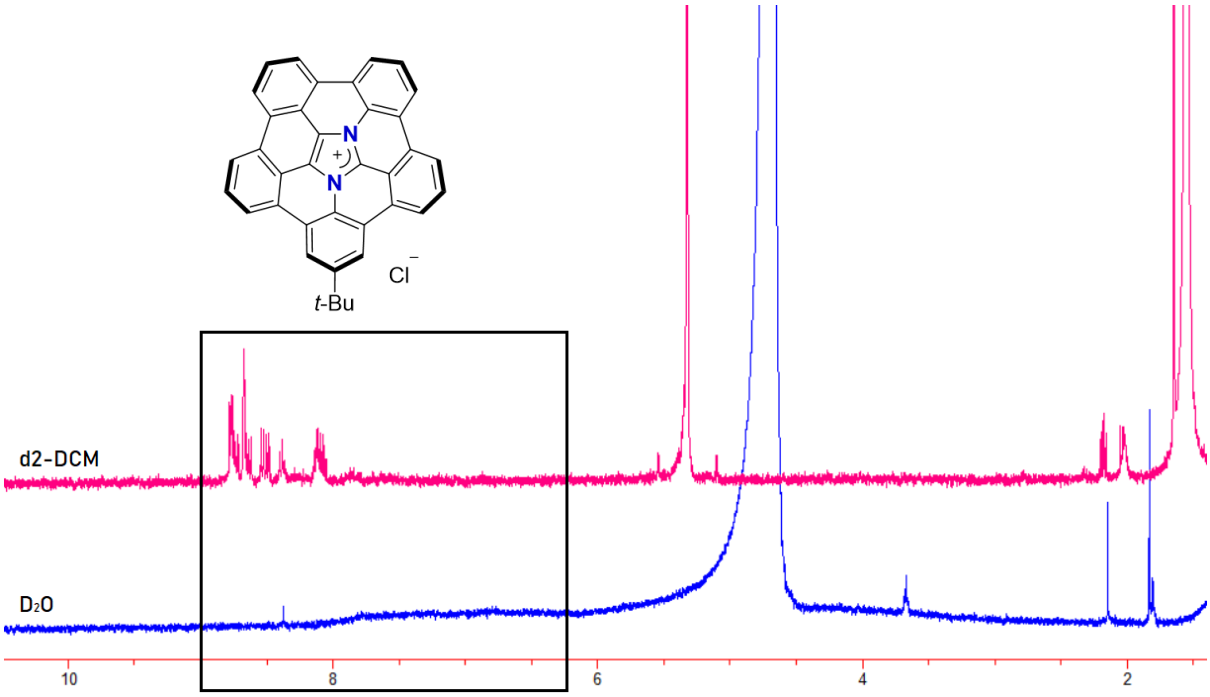

Figure S4.7. ^{1}H NMR of **4a** in CD_2Cl_2 and D_2O.

Note: The NMR signals are not clearly observed in water, which suggests that **4a** aggregates in water to form nanoparticles.

3. X-Ray Crystallographic Data

Single crystals suitable for X-ray analysis for **3** were obtained by slow diffusion of hexane to a solution of **3** in chloroform, and for **4b** was obtained by slow diffusion of 1,3-difluorobenzne to a solution of **4b** in methanol under argon at room temperature. A single crystal was mounted with mineral oil on a loop-type mount and transferred to the goniometer of a Bruker D8 Quest diffractometer. The radiation was performed with Multilayer Mirror-monochromated Incoatec microfocus source (λ = 0.71073 Å). The structures were solved by direct method with SHELXT[59] and refined by full-matrix least-squares techniques against F^2 with SHELXL-2018/3[59]. The intensities were corrected for Lorentz and polarization effects. The non-hydrogen atoms were refined anisotropically. Hydrogen atoms were placed using AFIX instructions.

Table S4.1. Crystal data and structure refinement for **3** and **4b**.

compound	**3**	**4b**
CCDC number	2101558	2101559
Molecular formula	$C_{37}H_{25}Cl_3N_2$ $CHCl_3$	$C_{37}H_{23}N_2 \cdot SbF_6 \cdot C_6H_4F_2$
Formula weight	723.31	485.41
Temperature (K)	100	100
Wavelength (Å)	0.71073	1.54178
Crystal system	triclinic	monoclinic
Space group	*P*1	$P2_1/c$
Unit cell dimensions a (Å)	10.4281(5)	16.9508(11)
b (Å)	12.9323(6)	27.7194(18)
c (Å)	13.2877(7)	7.0883(5)
α (°)	71.519(2)	90
β (°)	79.538(2)	101.674(5)
γ (°)	78.364(2)	90
Volume (Å^3)	1651.22(14)	3261.7(4)
Z	2	4
Density (calculated) (mg·m^{-3})	1.455	1.722
Absorption cosfficient (mm^{-1})	0.552	7.446
F(000)	740	1688
Crystal size (mm^3)	0.060 x 0.140 x 0.260	0.008 x 0.010 x 0.12
Theta range (°)	1.63 to 33.73	1.59 to 68.27
Index ranges	–16<=h<=16 -20<=k<=16 -20<=l<=18	–20<=h<=18 -32<=k<=29 -8<=l<=8
Reflections collected	36854	18497
Min. and max. transmission	0.8700, 0.9680	0.4690, 0.9430
Data / restraints / parameters	13160 / 0 / 418	5879 / 537 / 491
Goodness-of-fit on F^2	1.044	1.044
Final *R* indices [$I > 2\sigma(I)$]	R_1 = 0.0591 wR_2 = 0.1414	R_1 = 0.0807 wR_2 = 0.1884
R indices (all data) [$I > 2\sigma(I)$]	R_1 = 0.1051 wR_2 = 0.1684	R_1 = 0.1294 wR_2 = 0.2246
Largest diff. peak and hole (e.Å^{-3})	0.830, -0.674	0.961, -1.722

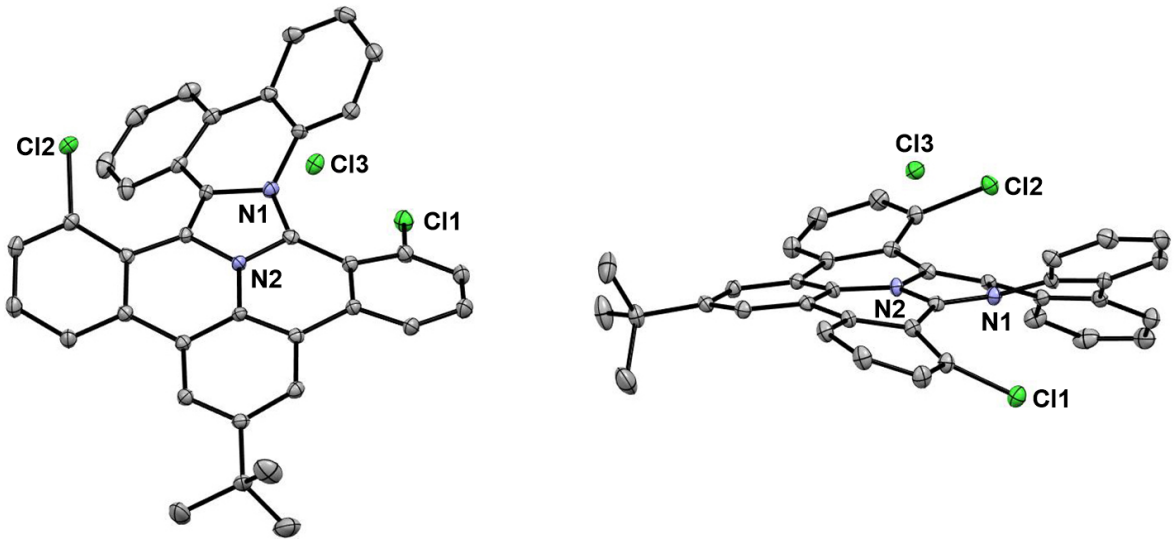

Figure S4.8. X-ray structures of **3** with thermal ellipsoids of 50% probability. Solvent molecules and hydrogen atoms were omitted for clarity.

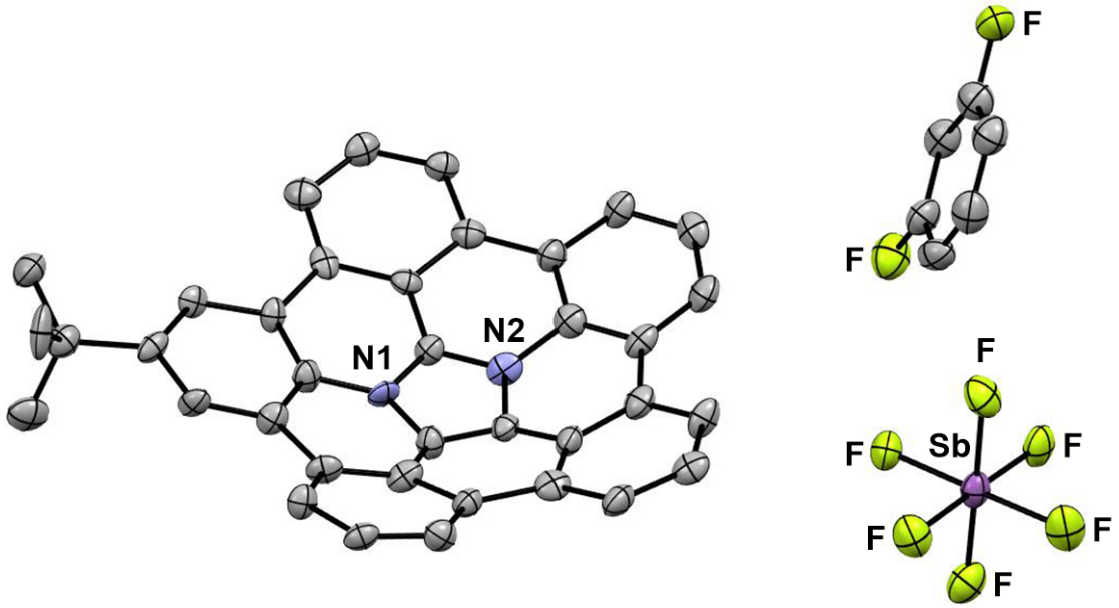

Figure S4.9. The X-ray structure of **4b** with thermal ellipsoids of 50% probability. Solvent molecules and hydrogen atoms were omitted for clarity.

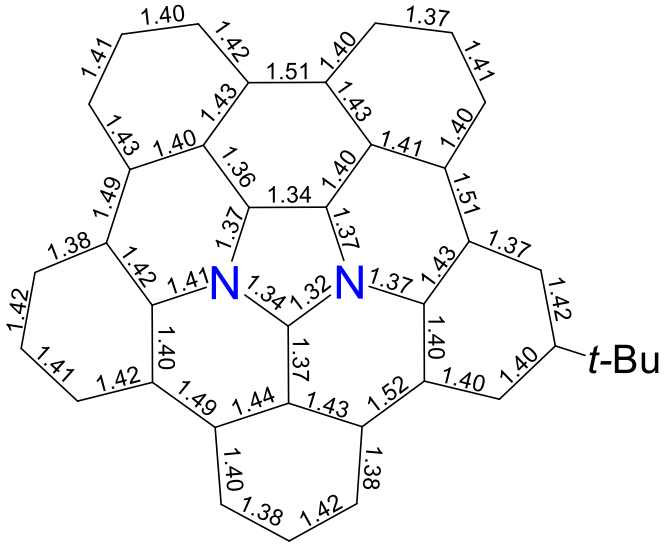

Figure S4.10. Bond lengths (Å) of **4b** determined by X-ray analysis.

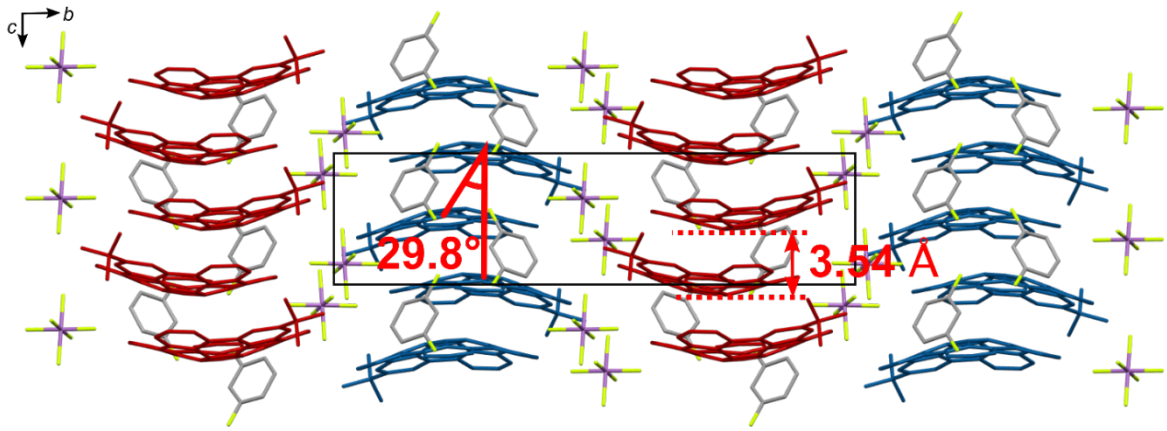

Figure S4.11. Packing structure of **4b** along *a*-axis.

4. Optical Properties

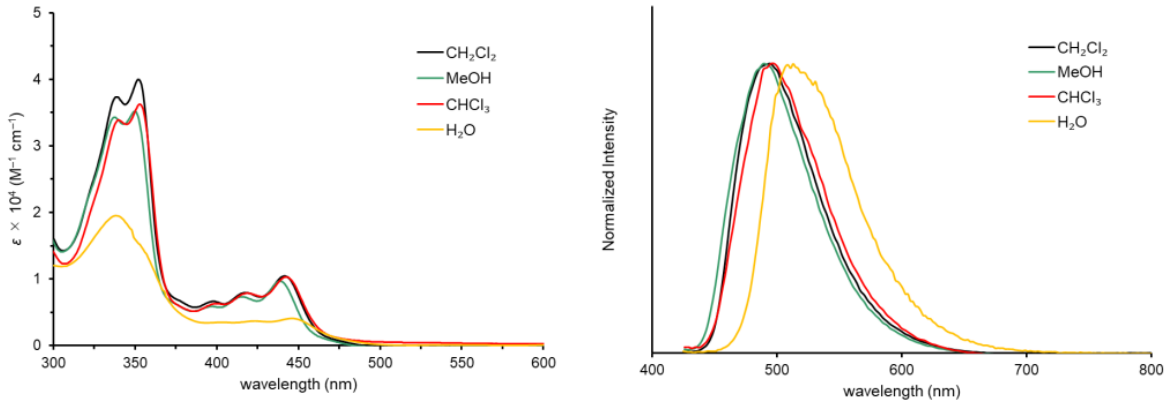

Figure S4.12. UV–vis absorption (left; 2.0×10^{-5} M) and emission (right; 6.0×10^{-5} M; excited with 400 nm) spectra of **4a** in different solvents.

Note: The absorption intensity in water is much lower than those in the other organic solvents. This could be attributed to the formation of nanoparticles in water, which in general leads to lower absorption intensity.

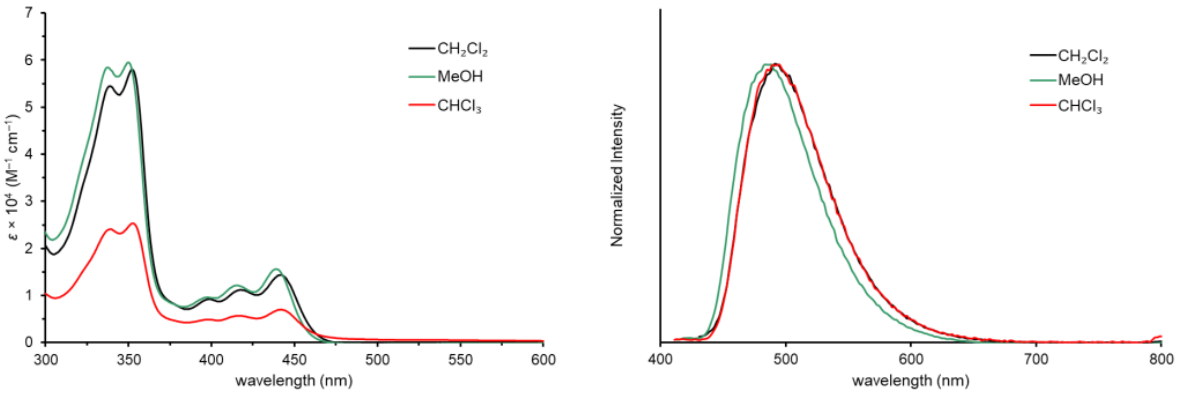

Figure S4.13. UV–vis absorption (left; 1.0×10^{-5} M) and emission (right; 9.1×10^{-6} M; excited with 400 nm) spectra of **4b** in different solvents.

Note: The absorption intensity in chloroform is lower than that in dichloromethane and methanol, which is consistent with the experimental observation that the solubility of **4b** in chloroform is lower than those in the other solvents. These results suggest that the lower degree

of solvation in the case of chloroform leads to lower absorption intensity. The solubility of **4b** in water is very low.

5. Theoretical Calculations

The computations were performed using workstation at High-Performance Center for Computational Science, Nanyang Technological University, Singapore. All the calculations were performed by using Gaussian 16 (revision A.03) program[60] by the B3LYP method[61] with the 6-311+G(2d,p) basis set[62] for structure optimization, vibrational frequency, time-dependent density functional theory (TD-DFT), NICS, and ACID calculations. The geometries of **4** and **5** were optimized under *Cs* symmetry constraint. The geometries of ***t*-Bu-4** were optimized under C_1 symmetry constraint. The geometries of **TS_{bowl}(4)** and **TS_{bowl}(*t*-Bu-4)** were optimized without symmetry assumption. Each transition state structure was optimized without any symmetry assumptions and IRC calculations were also performed to check the transition states. The *tert*-butyl substituent is replaced by a hydrogen atom.

Table S4.2. Energies determined by DFT calculation at the 6-311+G(2d,p) level.

structure	*E* (Hartree)	*E+ZPE* (Hartree)	*H* (Hartree)	*G* (Hartree)
4	–1376.263830	–1375.883149	–1375.861726	–1375.929626
TS_{bowl}(4)	–1376.249887	–1375.870052	–1375.849018	–1375.916098
***t*-Bu-4**	–1533.564436	–1533.072245	–1533.045058	–1533.125328
TS_{bowl}(*t*-Bu-4)	–1533.549592	–1533.058221	–1533.031426	–1533.110828
5	–1359.815005	–1359.436006	–1359.414643	–1359.482299

5-1. Bowl Inversion of 4

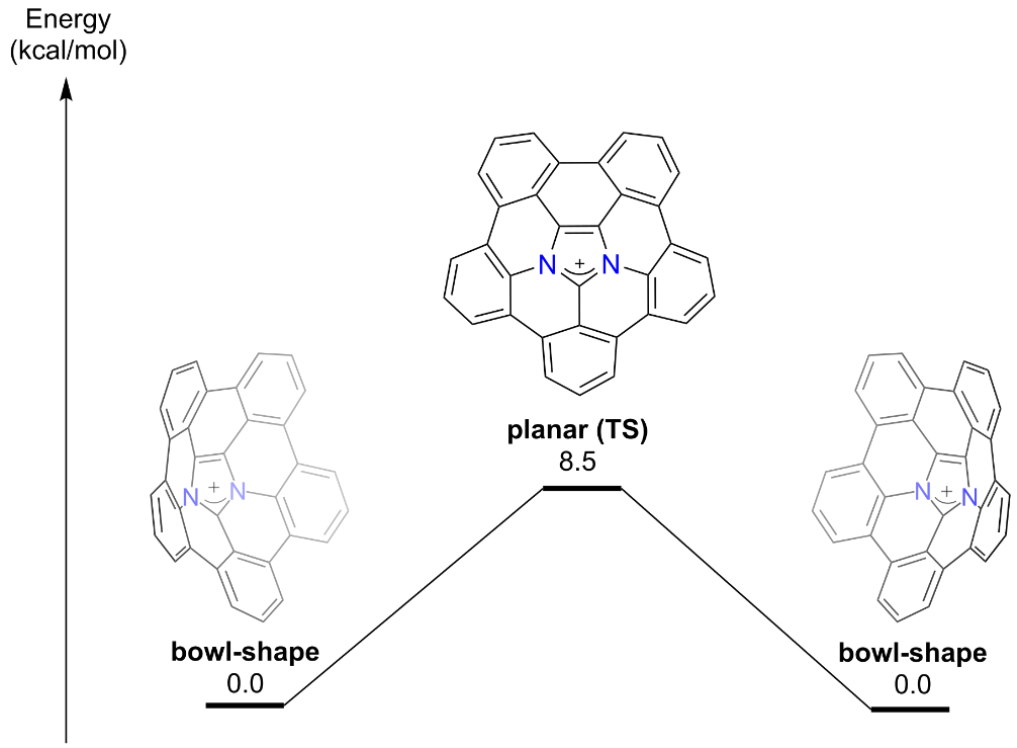

Figure S4.14. Energy diagram of bowl inversion for **4** through $\mathbf{Ts_{bowl}(4)}$. Values (kcal/mol) are relative Gibbs free energies (ΔG) at 298.15 K and 1 atm.

5-2. Bond Lengths

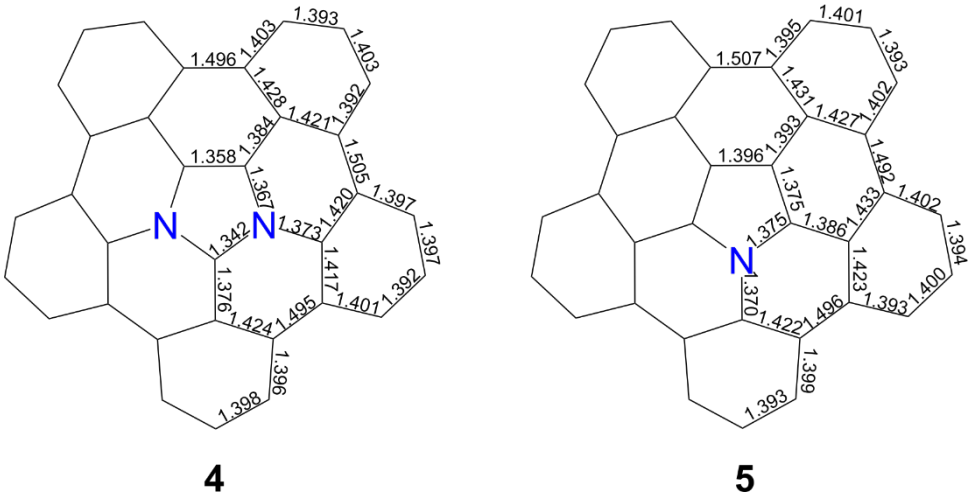

Figure S4.15. Bond lengths (Å) of **4** and azapentabenzocorannulene (**5**).

5-3. Dipole Moments

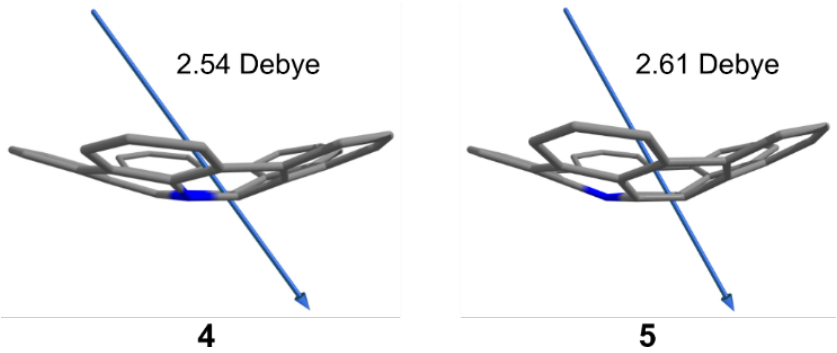

Figure S4.16. Dipole moments of **4** and **5**.

5-4. Molecular Orbitals

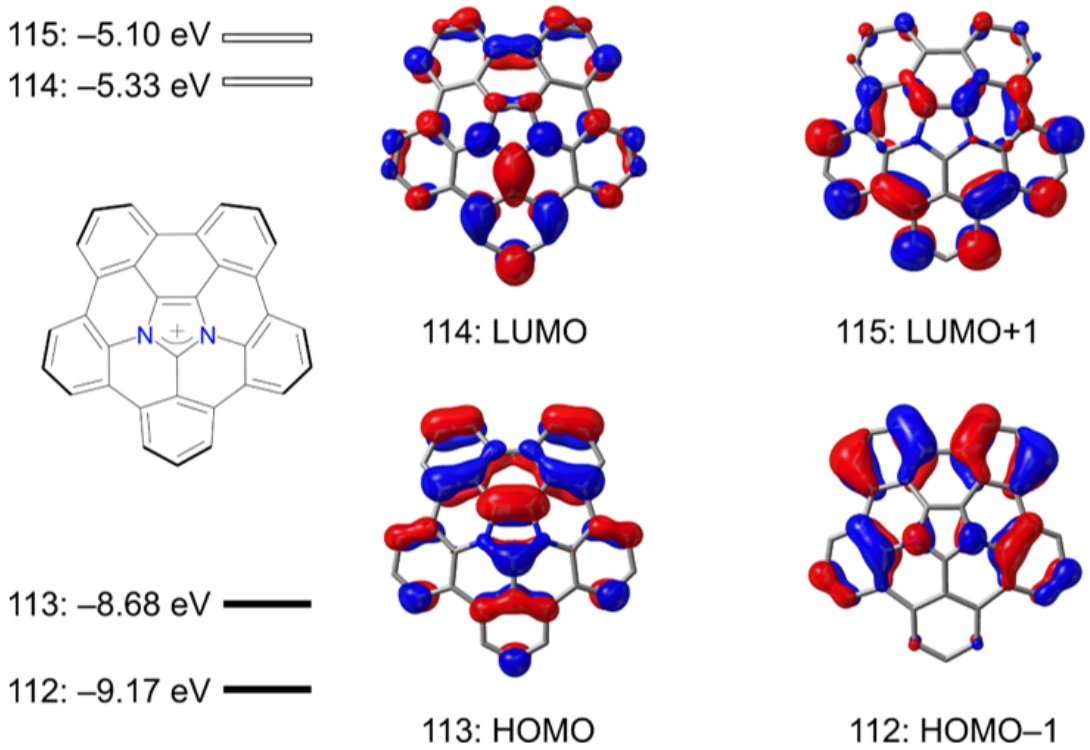

Figure S4.17. Kohn-Sham molecular orbitals of **4**. For each MO, the view from the convex surface of the molecule.

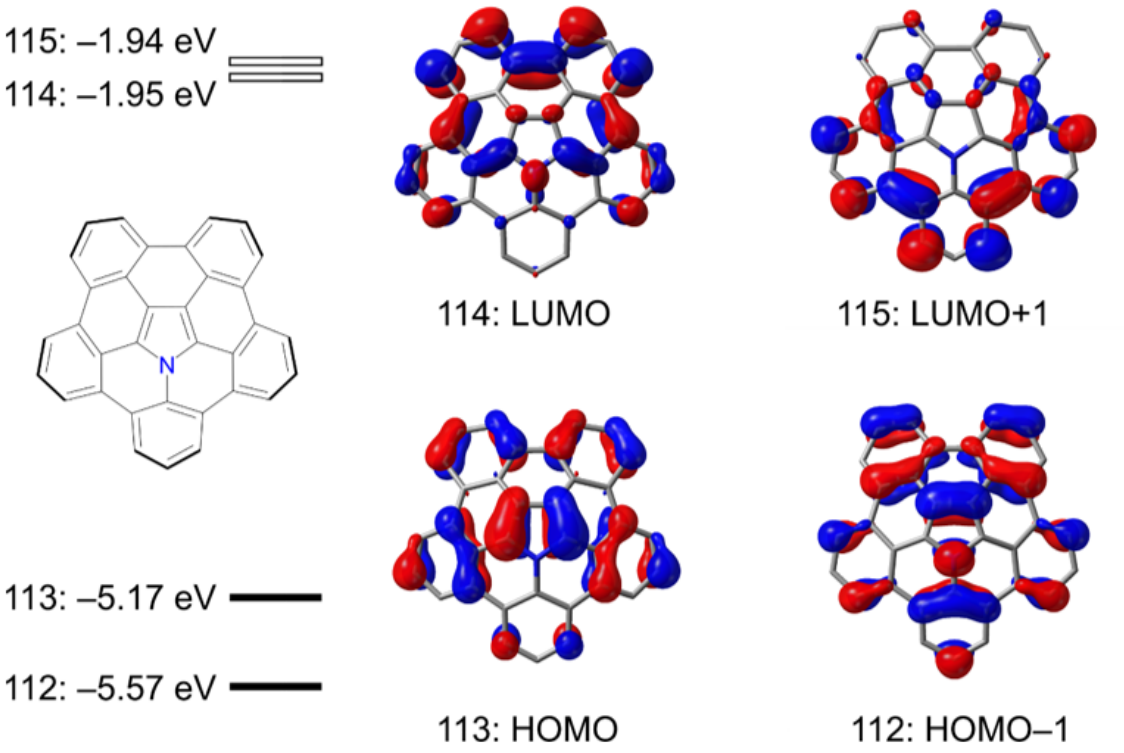

Figure S4.18. Kohn-Sham molecular orbitals of **5**. For each MO, the view from the convex surface of the molecule.

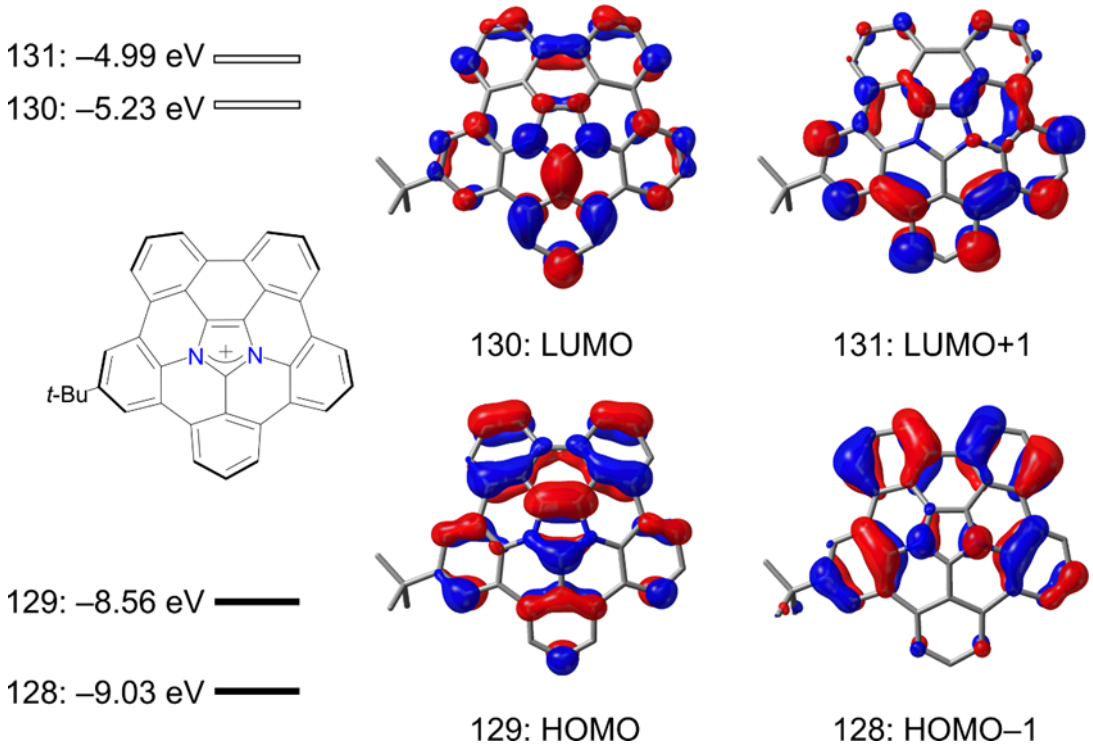

Figure S4.19. Kohn-Sham molecular orbitals of ***t*-Bu-4**. For each MO, the view from the convex surface of the molecule.

5-5. NICS Calculation

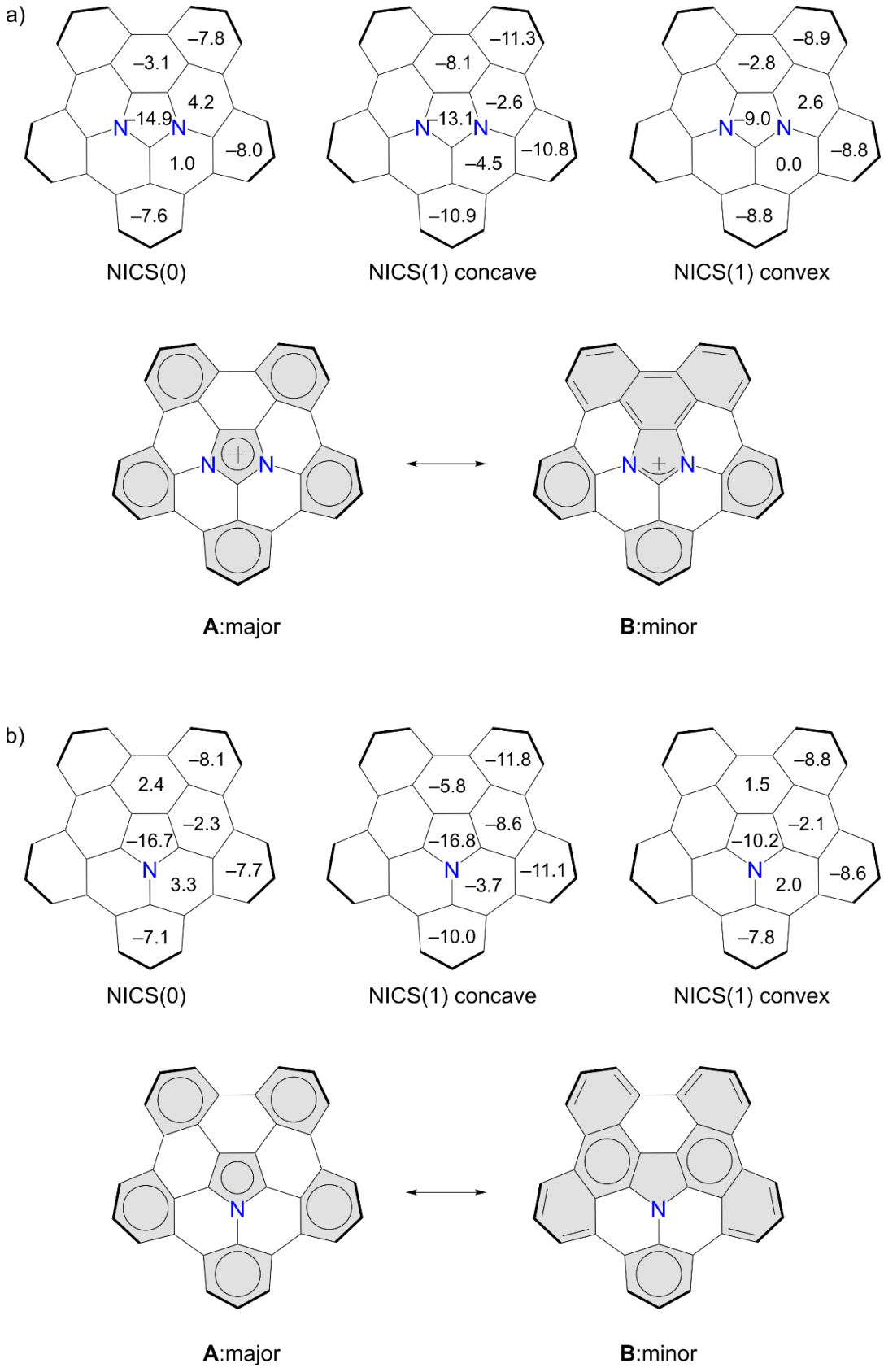

Figure S4.20. NICS values of (a) **4** and (b) **5**.

5-6. ACID Plots

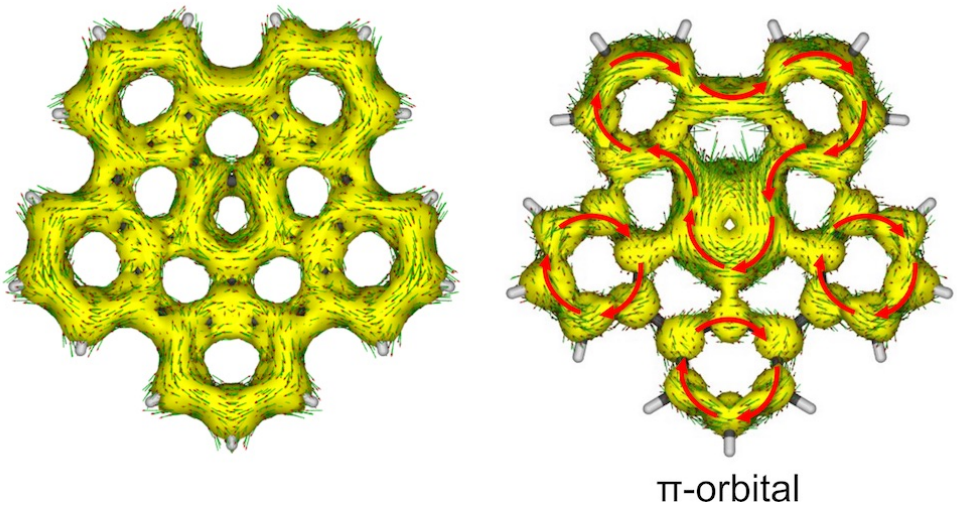

Figure S4.21. ACID plots of **4**. The concave surface of the molecule is shown.

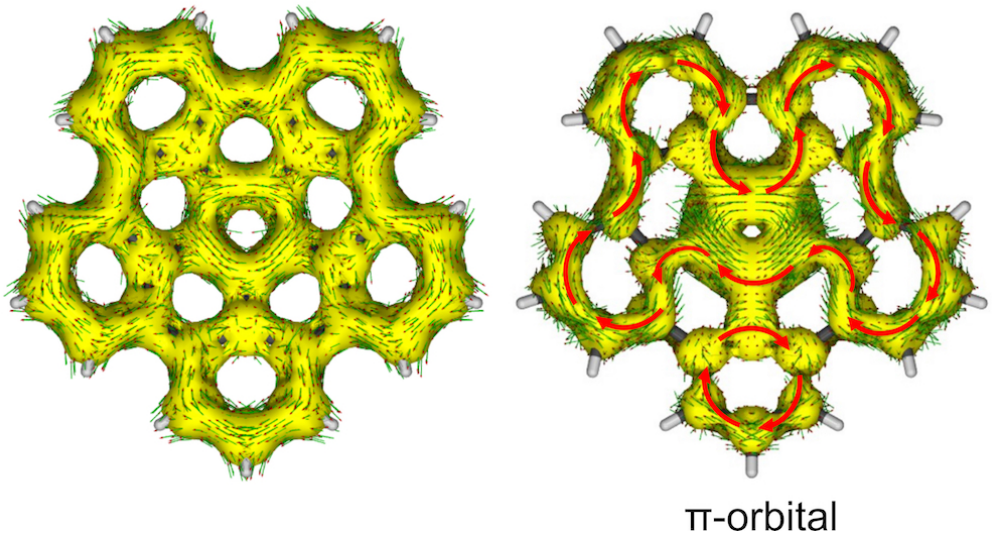

Figure S4.22. ACID plots of **5**. The concave surface of the molecule is shown.

5-7. TD-DFT Calculations

Table S4.3. Selected wavelengths, oscillator strengths, major electronic transition of **4**.

Wavelength (λ)	Oscillator Strengths (*f*)	Transitions
429.12	0.1464	112→115 (–0.16522) 113→114 (0.67299)
408.32	0.0344	111→114 (0.21113) 112→114 (0.24488) 113→115 (0.62501)
369.59	0.0005	112→115 (–0.12352) 113→116 (0.66997) 113→117 (–0.14114)
366.20	0.0637	111→114 (–0.23055) 112→114 (0.60409) 113→115 (–0.15851) 113→118 (0.22001)
348.54	0.1528	111→114 (0.58276) 112→116 (0.12396) 113→115 (–0.23588) 113→118 (0.23990)
346.45	0.0253	111→115 (0.18732) 112→115 (0.17987) 112→118 (–0.10187) 113→116 (0.13655) 113→117 (0.61933)
341.79	0.2176	112→115 (0.63721) 113→114 (0.15874) 113→117 (–0.19858)
333.52	0.2045	111→114 (–0.16996) 112→114 (–0.21557) 112→116 (0.11955) 113→115 (0.13897) 113→118 (0.57639) 113→119 (0.18133)
315.58	0.0493	108→114 (–0.12423) 111→115 (0.64512) 111→118 (0.10300) 112→118 (0.11127) 113→117 (–0.15671)
313.30	0.0001	111→116 (0.24090) 112→116 (0.54107) 113→119 (–0.32516)

Note) 111: HOMO−2, 112: HOMO−1, 113: HOMO, 114: LUMO, 115: LUMO+1, 116: LUMO+2, 117: LUMO+3, 118: LUMO+4

5-8. Cartesian Coordinates

Table S4.4. Cartesian Coordinates (Å) for **4**

atom	x	y	z	atom	x	y	z
C	0.851039000	0.942685000	0.678924000	C	-0.503196000	-5.000253000	0.000000000
C	0.851039000	0.942685000	-0.678924000	C	-0.330657000	4.252698000	-1.566544000
N	0.818562000	-0.361360000	-1.087281000	C	-0.518704000	4.047704000	-2.931816000
C	0.772813000	-1.145925000	0.000000000	C	-0.349159000	2.801840000	-3.553212000
N	0.818562000	-0.361360000	1.087281000	C	-0.330657000	4.252698000	1.566544000
C	0.414453000	2.001211000	1.456044000	C	-0.518704000	4.047704000	2.931816000
C	0.115569000	3.204714000	0.748025000	C	-0.349159000	2.801840000	3.553212000
C	0.115569000	3.204714000	-0.748025000	C	-0.292298000	-0.179797000	4.515462000
C	0.414453000	2.001211000	-1.456044000	C	-0.465328000	-1.544888000	4.757914000
C	0.356150000	-2.457735000	0.000000000	C	-0.315131000	-2.508836000	3.765060000
C	0.078843000	-3.028203000	1.274872000	H	-0.506931000	0.523102000	-5.309729000
C	0.091530000	-2.139265000	2.476660000	H	-0.776180000	-1.860243000	-5.745834000
C	0.376715000	-0.759057000	2.325221000	H	-0.541887000	-3.541585000	-3.994650000
C	0.376715000	-0.759057000	-2.325221000	H	-0.567235000	-4.903584000	-2.138638000
C	0.091530000	-2.139265000	-2.476660000	H	-0.567235000	-4.903584000	2.138638000
C	0.078843000	-3.028203000	-1.274872000	H	-0.826143000	-6.033978000	0.000000000
C	0.107048000	1.714516000	-2.813598000	H	-0.568407000	5.222373000	-1.148424000
C	0.114638000	0.277336000	-3.260212000	H	-0.867455000	4.877515000	-3.533852000
C	0.114638000	0.277336000	3.260212000	H	-0.610987000	2.701803000	-4.598673000
C	0.107048000	1.714516000	2.813598000	H	-0.568407000	5.222373000	1.148424000
C	-0.292298000	-0.179797000	-4.515462000	H	-0.867455000	4.877515000	3.533852000
C	-0.465328000	-1.544888000	-4.757914000	H	-0.610987000	2.701803000	4.598673000
C	-0.315131000	-2.508836000	-3.765060000	H	-0.506931000	0.523102000	5.309729000
C	-0.337737000	-4.359513000	-1.231901000	H	-0.541887000	-3.541585000	3.994650000
C	-0.337737000	-4.359513000	1.231901000	H	-0.776180000	-1.860243000	5.745834000

Table S4.5. Cartesian Coordinates (Å) for the transition state of bowl inversion of **4** (**TS_{bowl}(4)**)

atom	x	y	z	atom	x	y	z
C	3.087480000	1.299355000	0.000022000	C	-4.162635000	3.020242000	0.000110000
C	4.483525000	1.245418000	0.000020000	C	-2.025572000	1.476005000	-0.000100000
C	5.132399000	0.000000000	0.000019000	C	-2.025572000	-1.476004000	-0.000101000
C	4.483525000	-1.245418000	0.000020000	C	-2.902445000	3.650566000	0.000119000
C	3.087480000	-1.299356000	0.000022000	C	-2.902445000	-3.650565000	0.000117000
C	2.494528000	0.000000000	0.000027000	C	-1.746397000	-2.871974000	0.000001000
C	1.136179000	0.000000000	-0.000005000	C	-0.928096000	0.670325000	-0.000154000
C	2.183850000	2.522831000	0.000037000	C	-1.746396000	2.871974000	0.000002000
C	2.183849000	-2.522831000	0.000037000	C	-0.928096000	-0.670325000	-0.000155000
C	0.771684000	2.358405000	0.000013000	N	0.355209000	-1.072838000	-0.000049000
C	-0.280743000	3.321209000	0.000008000	H	5.085736000	2.145107000	0.000047000
C	0.208400000	4.630117000	-0.000018000	H	5.085735000	-2.145108000	0.000047000

C	1.590393000	4.874093000	-0.000013000	H	-0.468684000	5.474937000	-0.000068000
C	2.564683000	3.871881000	0.000020000	H	1.922174000	5.904757000	-0.000045000
C	2.564682000	-3.871882000	0.000022000	H	3.609151000	4.156297000	0.000031000
C	1.590392000	-4.874094000	-0.000011000	H	3.609151000	-4.156298000	0.000033000
C	0.208399000	-4.630117000	-0.000016000	H	1.922173000	-5.904758000	-0.000041000
C	-0.280744000	-3.321209000	0.000007000	H	-0.468685000	-5.474937000	-0.000065000
C	0.771683000	-2.358405000	0.000011000	H	-2.864264000	4.732843000	0.000203000
N	0.355209000	1.072838000	-0.000046000	H	-2.864265000	-4.732843000	0.000201000
C	-3.267690000	-0.762270000	-0.000091000	H	6.215485000	-0.000001000	0.000039000
C	-3.267690000	0.762270000	-0.000091000	H	-5.039067000	-3.656522000	0.000186000
C	-4.367176000	1.634538000	0.000002000	H	-5.384109000	-1.261925000	-0.000010000
C	-4.367176000	-1.634537000	0.000001000	H	-5.384109000	1.261926000	-0.000008000
C	-4.162636000	-3.020241000	0.000107000	H	-5.039066000	3.656523000	0.000189000

Table S4.6. Cartesian Coordinates (Å) for ***t*-Bu-4**

atom	x	y	z	atom	x	y	z
C	-0.586902000	1.109091000	-0.955619000	C	1.633449000	3.772235000	0.113703000
C	-1.872987000	0.680612000	-0.868158000	C	3.476238000	1.244941000	-0.064606000
N	-1.846776000	-0.685954000	-0.838115000	C	4.182639000	0.039952000	0.071758000
C	-0.566255000	-1.087032000	-0.880086000	C	3.496708000	-1.179034000	-0.043804000
N	0.211338000	0.000553000	-0.978985000	C	5.687473000	0.016630000	0.398982000
C	-0.151976000	2.356183000	-0.541017000	C	6.432413000	-0.751222000	-0.716336000
C	-1.179926000	3.274605000	-0.167631000	C	5.911518000	-0.692349000	1.753529000
C	-2.596649000	2.803634000	-0.072346000	C	6.290851000	1.427910000	0.492119000
C	-2.910177000	1.439242000	-0.354407000	H	-6.027440000	-1.178243000	0.790553000
C	-0.122142000	-2.329346000	-0.484268000	H	-5.669735000	-3.577003000	1.039658000
C	1.283200000	-2.465027000	-0.295272000	H	-3.497802000	-4.618145000	0.655306000
C	2.139595000	-1.239805000	-0.368014000	H	-1.313538000	-5.320341000	0.539556000
C	1.536766000	0.015318000	-0.622125000	H	2.734207000	-3.967016000	0.267537000
C	-2.861221000	-1.453240000	-0.320328000	H	1.085124000	-5.715203000	0.643745000
C	-2.548858000	-2.809529000	-0.051616000	H	-3.561067000	4.590705000	0.685810000
C	-1.129698000	-3.272362000	-0.133364000	H	-5.690864000	3.511920000	1.132335000
C	-4.083552000	0.739052000	0.036380000	H	-6.032915000	1.111653000	0.895204000
C	-4.054353000	-0.765306000	0.026601000	H	-1.388914000	5.312297000	0.541888000
C	2.117297000	1.283542000	-0.390499000	H	0.998868000	5.734523000	0.683477000
C	1.244902000	2.508823000	-0.322889000	H	2.672373000	4.005160000	0.308325000
C	-5.069470000	-1.594815000	0.508100000	H	3.992388000	2.176190000	0.113666000
C	-4.856291000	-2.966070000	0.669308000	H	4.031254000	-2.098829000	0.149787000
C	-3.622843000	-3.566529000	0.433569000	H	6.296391000	-0.267459000	-1.686145000
C	-0.641832000	-4.519399000	0.260040000	H	7.502458000	-0.777551000	-0.499729000
C	1.689198000	-3.739246000	0.103490000	H	6.089154000	-1.783571000	-0.804908000
C	0.737110000	-4.736564000	0.336988000	H	5.391711000	-0.172295000	2.561360000
C	-3.669490000	3.539369000	0.452207000	H	6.976769000	-0.708217000	1.993438000
C	-4.884750000	2.914712000	0.724645000	H	5.564054000	-1.726971000	1.740718000

C	-5.093315000	1.536895000	0.566738000	H	6.182096000	1.983630000	-0.442211000
C	-0.704287000	4.524963000	0.253807000	H	7.358990000	1.350237000	0.700851000
C	0.665599000	4.758928000	0.351933000	H	5.846600000	2.013744000	1.300401000

Table S4.7. Cartesian Coordinates (Å) for the transition state of bowl inversion of ***t*-Bu-4** (**TS_{bowl}(*t*-Bu-4)**)

atom	x	y	z	atom	x	y	z
C	-0.522132000	1.070151000	0.000029000	C	1.553791000	3.979814000	0.000019000
C	-1.773270000	0.588193000	0.000019000	C	3.586265000	1.424971000	0.000011000
N	-1.687225000	-0.753714000	0.000023000	C	4.347367000	0.238120000	0.000007000
C	-0.404760000	-1.096086000	0.000032000	C	3.720667000	-1.024973000	0.000015000
N	0.313533000	0.017901000	0.000038000	C	5.889486000	0.282061000	-0.000013000
C	-0.161684000	2.382808000	0.000020000	C	6.421151000	-0.433048000	-1.262719000
C	-1.273887000	3.286208000	0.000011000	C	6.421184000	-0.433041000	1.262683000
C	-2.697672000	2.738684000	0.000004000	C	6.440444000	1.717827000	-0.000025000
C	-2.918865000	1.322908000	0.000003000	H	-6.090045000	-1.570530000	-0.000050000
C	0.086841000	-2.362657000	0.000022000	H	-5.629092000	-3.955476000	-0.000054000
C	1.513329000	-2.446045000	0.000026000	H	-3.390517000	-4.899416000	-0.000024000
C	2.329531000	-1.158998000	0.000026000	H	-0.980635000	-5.552887000	0.000008000
C	1.661714000	0.093099000	0.000031000	H	3.020972000	-4.006067000	0.000032000
C	-2.735972000	-1.604961000	0.000004000	H	1.427644000	-5.832864000	0.000025000
C	-2.379694000	-2.981588000	0.000000000	H	-3.924536000	4.534196000	-0.000010000
C	-0.911773000	-3.383808000	0.000012000	H	-6.035271000	3.352145000	-0.000023000
C	-4.121264000	0.560329000	-0.000007000	H	-6.259505000	0.936071000	-0.000021000
C	-4.013181000	-0.969401000	-0.000012000	H	-1.565962000	5.441418000	0.000004000
C	2.187389000	1.411295000	0.000023000	H	0.793341000	5.976616000	0.000012000
C	1.242955000	2.620990000	0.000022000	H	2.577633000	4.332805000	0.000020000
C	-5.057914000	-1.897508000	-0.000033000	H	4.101296000	2.374078000	0.000002000
C	-4.787238000	-3.274552000	-0.000036000	H	4.339952000	-1.911816000	0.000007000
C	-3.501171000	-3.822554000	-0.000019000	H	6.060862000	0.053546000	-2.171885000
C	-0.358516000	-4.666835000	0.000014000	H	7.512774000	-0.404427000	-1.274997000
C	1.964796000	-3.768017000	0.000028000	H	6.120642000	-1.481573000	-1.301135000
C	1.036962000	-4.822664000	0.000024000	H	6.060921000	0.053558000	2.171856000
C	-3.906820000	3.451262000	-0.000006000	H	7.512808000	-0.404420000	1.274930000
C	-5.126759000	2.762546000	-0.000015000	H	6.120678000	-1.481567000	1.301112000
C	-5.262947000	1.360001000	-0.000013000	H	6.134359000	2.276664000	-0.887547000
C	-0.853854000	4.625373000	0.000011000	H	7.531028000	1.684383000	-0.000043000
C	0.513329000	4.930340000	0.000015000	H	6.134387000	2.276671000	0.887502000

Table S4.8. Cartesian Coordinates (Å) for **5**

atom	*x*	*y*	*z*	*atom*	*x*	*y*	*z*
C	0.950271000	1.003139000	0.697938000	C	-1.526849000	-0.581848000	-4.726401000
C	-0.359609000	0.956669000	1.112332000	C	-0.168752000	-0.370101000	4.497031000
N	-1.167233000	0.956035000	0.000000000	C	-1.526849000	-0.581848000	4.726401000
C	-0.359609000	0.956669000	-1.112332000	C	-2.498767000	-0.399734000	3.734786000
C	0.950271000	1.003139000	-0.697938000	C	2.785269000	-0.385812000	3.537220000
C	1.997447000	0.486478000	1.457975000	C	4.018365000	-0.580682000	2.919446000
C	1.701605000	0.121451000	2.805907000	C	4.219955000	-0.368416000	1.549798000
C	0.280599000	0.114942000	3.261093000	C	4.219955000	-0.368416000	-1.549798000
C	-0.762525000	0.443171000	2.335459000	C	4.018365000	-0.580682000	-2.919446000
C	-0.762525000	0.443171000	-2.335459000	C	2.785269000	-0.385812000	-3.537220000
C	0.280599000	0.114942000	-3.261093000	H	-4.841280000	-0.597054000	2.134836000
C	1.701605000	0.121451000	-2.805907000	H	-5.996661000	-0.882522000	0.000000000
C	1.997447000	0.486478000	-1.457975000	H	-4.841280000	-0.597054000	-2.134836000
C	-2.429645000	0.424267000	0.000000000	H	-3.521697000	-0.684412000	-3.947218000
C	-2.998888000	0.105639000	-1.263225000	H	0.536531000	-0.623665000	-5.278778000
C	-2.134453000	0.094994000	-2.484399000	H	-1.837472000	-0.960685000	-5.692840000
C	-2.134453000	0.094994000	2.484399000	H	0.536531000	-0.623665000	5.278778000
C	-2.998888000	0.105639000	1.263225000	H	-1.837472000	-0.960685000	5.692840000
C	3.194573000	0.142104000	-0.753303000	H	-3.521697000	-0.684412000	3.947218000
C	3.194573000	0.142104000	0.753303000	H	2.671076000	-0.670957000	4.575876000
C	-4.320342000	-0.350906000	1.218386000	H	4.838129000	-0.975192000	3.508190000
C	-4.970919000	-0.534482000	0.000000000	H	5.172658000	-0.648777000	1.117330000
C	-4.320342000	-0.350906000	-1.218386000	H	5.172658000	-0.648777000	-1.117330000
C	-2.498767000	-0.399734000	-3.734786000	H	2.671076000	-0.670957000	-4.575876000
C	-0.168752000	-0.370101000	-4.497031000	H	4.838129000	-0.975192000	-3.508190000

6. Dynamic Light Scattering Measurements

An aqueous solution of **4a** (4×10^{-7} M) was prepared by dissolving it in deionized water. The solution was sonicated for 0.5–1.0 hour. After sonication, dynamic light scattering (DLS) size distribution of the solution was measured immediately. Time-course study was also done as shown below.

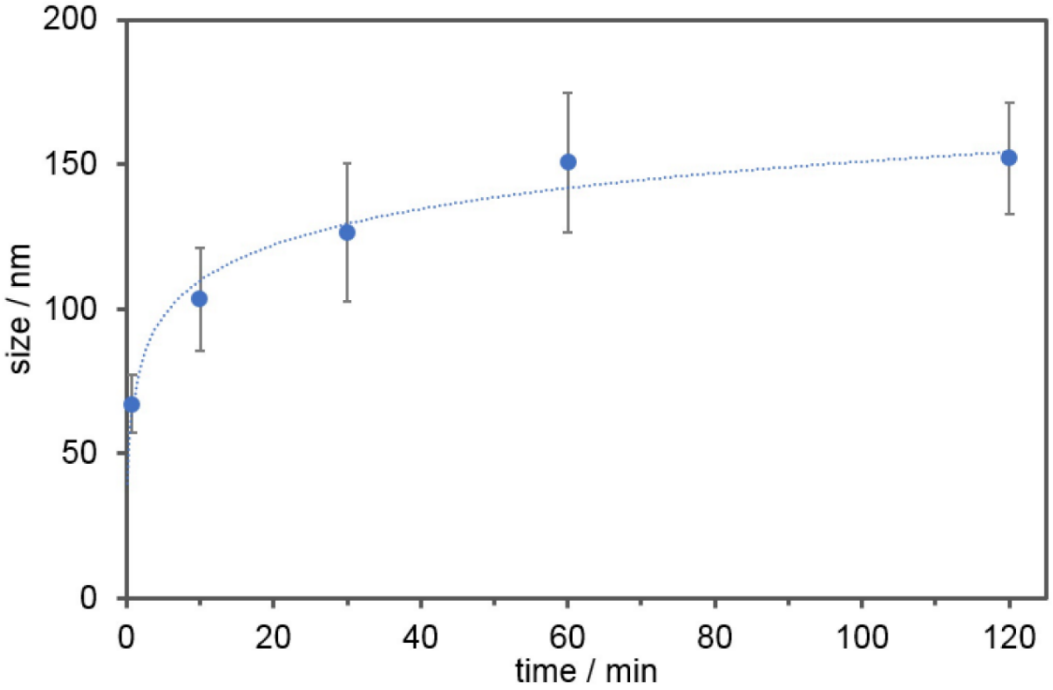

Figure S4.23. Time course study of the nanoparticle size determined DLS analysis.

Table S4.9. Time course analysis of the nanoparticle size determined DLS analysis.

Time	Size
1 min	67 ± 10 nm
10 min	103 ± 18 nm
30 min	126 ± 24 nm
60 min	150 ± 24 nm
120 min	152 ± 19 nm

7. Procedure for Determination of Lipophilicity

Lipophilicity of **4a** was measured by using a shake-flask method[63]. The octanol-water partition coefficient was measured by using UV–vis spectroscopy. Calibration curves were obtained from absorbance of standard solution (12.2–36.6 μM). Compound **4a** (36.6 μM) in octanol-saturated PBS was stirred vigorously with PBS-saturated octanol in a 1.5 mL microcentrifuge tube for 10 minutes. The solution stood for 1 minute and then was separated by centrifugation. The absorbance of **4a** in aqueous phase was measured by UV–vis spectroscopy. The absorbance at λ = 337 nm was used to calculate the partition coefficient log *P*:

$$\log P = \log [\left(\frac{A_{std}}{A_{PBS}} - 1\right)\frac{V_{PBS}}{V_O}]$$

A_{std} and A_{PBS} stand for the absorbance of standard sample (36.6 μM) and aqueous layer at λ = 337 nm, respectively. V_{PBS} and V_o stand for the volume of saturated PBS and octanol. The measurement was done for three times and the results are as follows:

Table S4.10. Results for lipophilicity measurement

octanol	abs (λ=337 nm)	log *P* (by Abs)	log *P* (average)
0	0.5946	--	--
50 μL	0.3238	1.223	1.15±0.05
75 μL	0.2913	1.143	
100 μL	0.2659	1.092	

8. Cell Viability Assay

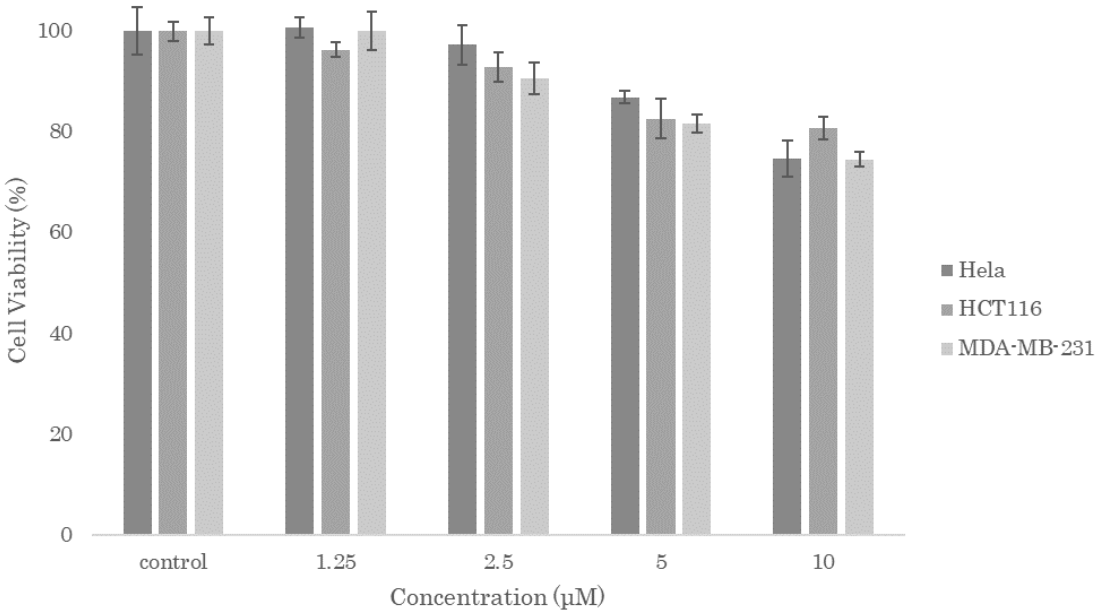

Figure S4.24. Cell toxicity effect of **4a** to HeLa, HCT 116, and MDA-MB-231 cell lines. Cells were incubated with **4a** (0–10 μM) for 24 hours. Results are mean ± SD, n = 3. Control experiments were performed in the cell culture medium only. Positive control experiments were performed in the cell culture medium contained 0.1% dimethylsulfoxide without any probes.

9. Confocal Fluorescence Imaging

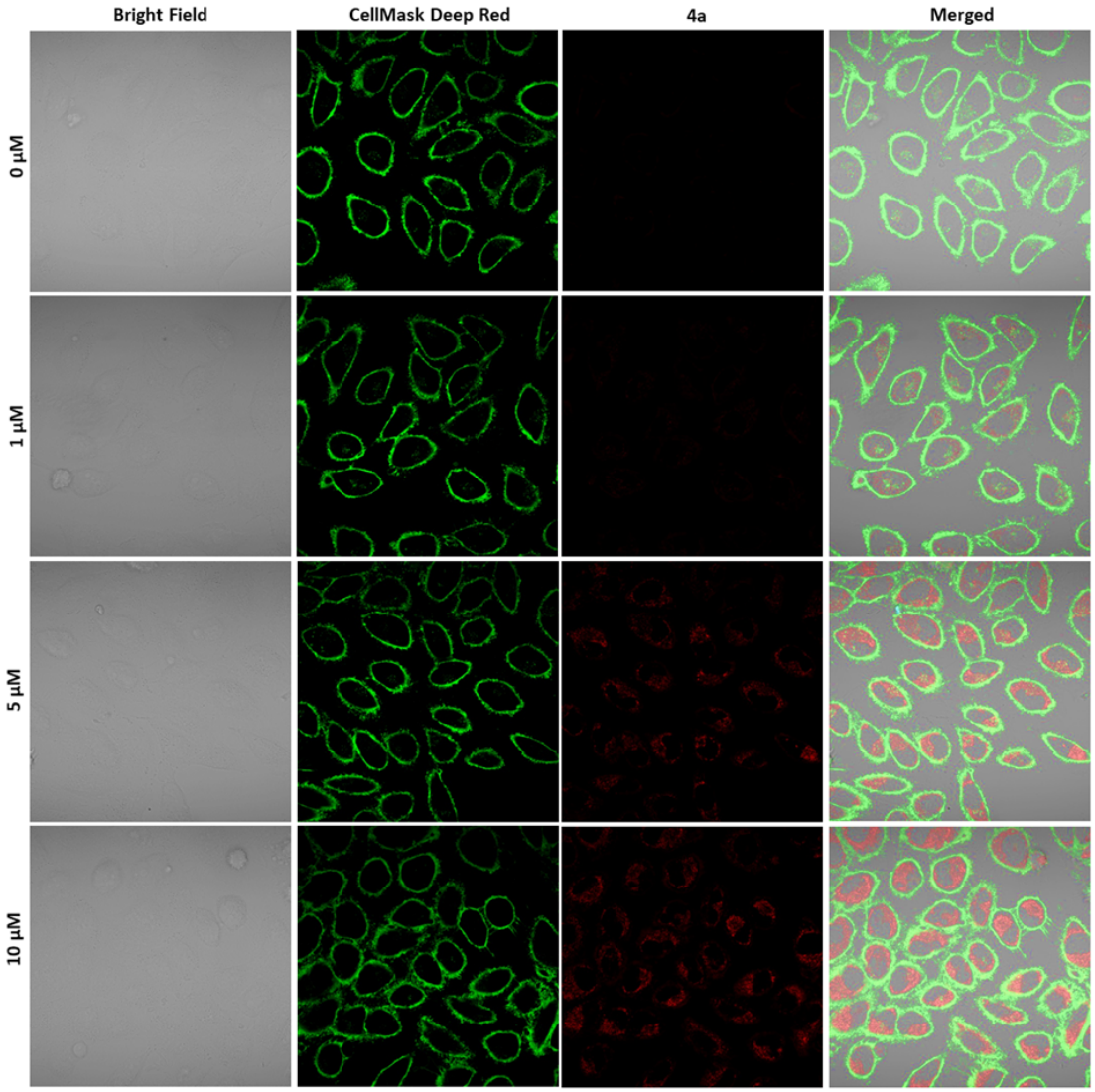

Figure S4.25. Confocal fluorescence images of HeLa cells stained with CellMask Deep Red Plasma (5 µg/ml) and **4a** (0–10 µM). Column 1: Bright field images. Column 2: CellMask Deep Red Plasma (excited with 640 nm laser) and Column 3: **4a** (excited with 488 nm laser). Column 4: Merged bright field images of CellMask Deep Red Plasma and **4a**.

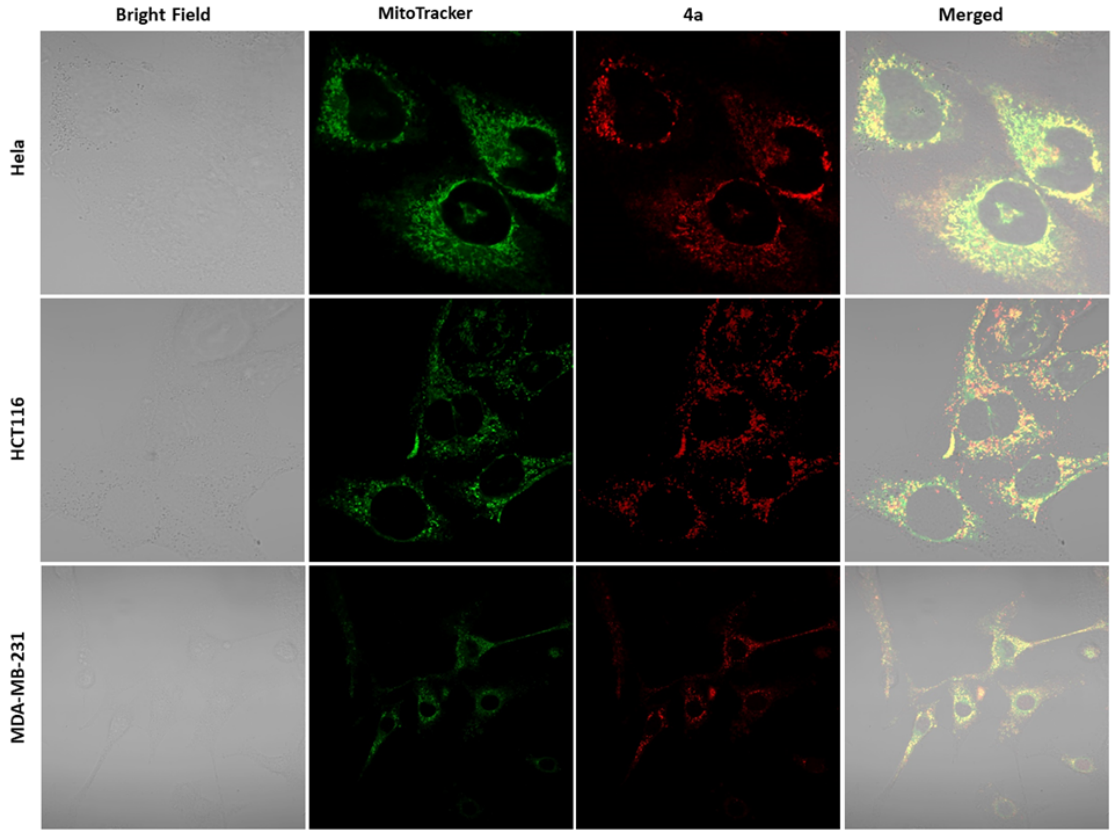

Figure S4.26. Confocal fluorescence images of HeLa cells (Row 1), HCT116 (Row 2), and MDA-MB-231 (Row 3) cell lines stained with MitoTracker (1 nM) and **4a** (5 μM). Column 1: Bright field images. Column 2: MitoTracker mitochondrial stain (excited with 561 nm laser). Column 3: **4a** (excited with 488 nm laser). Column 4: Merged images.

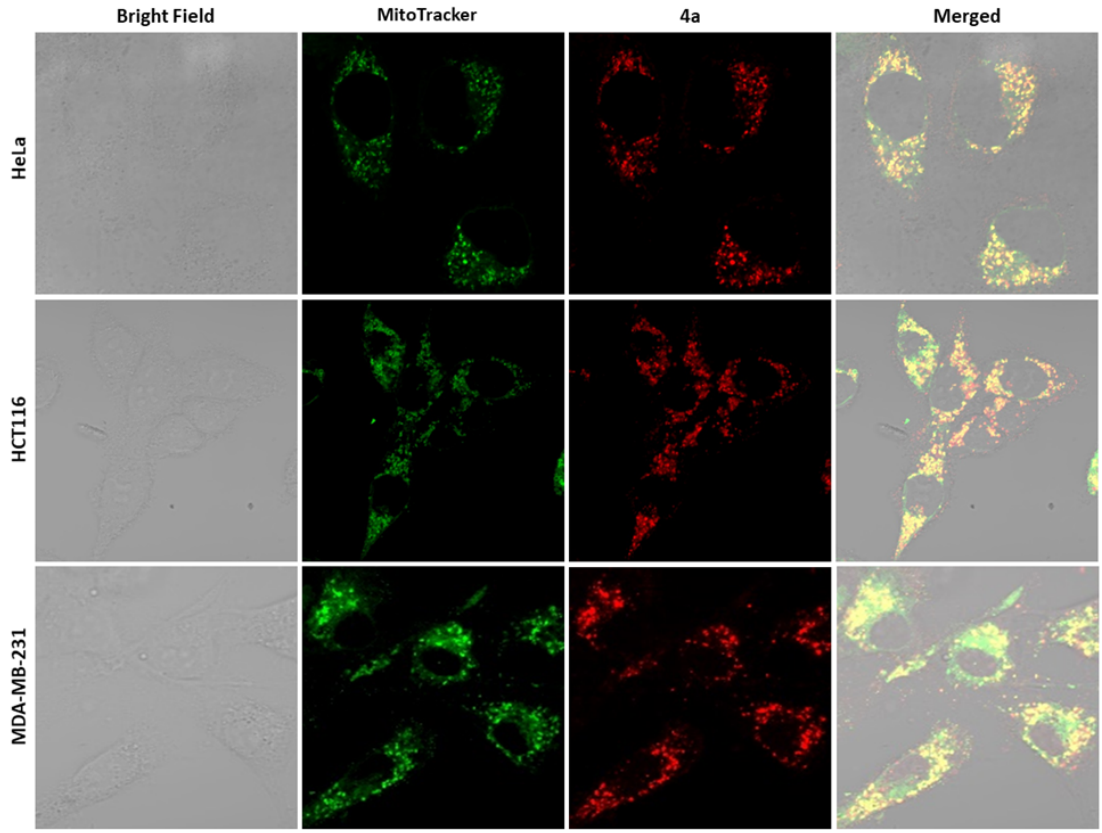

Figure S4.27. Confocal fluorescence images of HeLa cells (Row 1), HCT116 (Row 2), and MDA-MB-231 (Row 3) cell lines stained with MitoTracker (1 nM) and **4a** (10 μM). Column 1: Bright field images. Column 2: MitoTracker mitochondrial stain (excitation with 561 nm laser). Column 3: **4a** (excitation with 488 nm laser). Column 4: Merged images.

References

1. Wu, Y.-T., Siegel, J. S. *Chem. Rev*. **2006**, *106*, 4843–4867.

2. Tsefrikas, V. M., Scott, L. T. *Chem. Rev*. **2006**, *106*, 4868–4884.

3. Jiang, W., Li, Y., Wang, Z. *Chem. Soc. Rev*. **2013**, *42*, 6113–6127.

4. Narita, A., Wang, X.-Y., Feng, X., Müllen, K. *Chem. Soc. Rev*. **2015**, *44*, 6616–6643.

5. Wang, X.Y., Yao, X., Müllen, K. *Sci. China Chem*. **2019**, *62*, 1099–1144.

6. Wu, J., Pisula, W., Müllen, K. *Chem. Rev*. **2007**, *107*, 718–747.

7. Miao, Q. *Adv. Mater*. **2014**, *26*, 5541–5549.

8. Hong, G., Diao, S., Antaris, A. L., Dai, H. *Chem. Rev*. **2015**, *115*, 10816–10906.

9. Li, X. *et al*. *Biomater. Sci*. **2017**, *5*, 849–859.

10. Wu, J., Li, J., Kolb, U., Müllen, K. *Chem. Commun*. **2006**, 48–50.

11. Yin, M. et al. *J. Am. Chem. Soc*. **2009**, *131*, 14618–14619.

12. Nestoros, E., Stuparu, M. C. *Chem. Commun*. **2018**, *54*, 6503–6519.

13. Lin, H.-A. *et al*. *Angew. Chem. Int. Ed.* **2018**, *57*, 2874–2878.

14. White, B. M. *et al*. *ACS Cent. Sci.* **2018**, *4*, 1173–1178.

15. Ma, S. *et al*. *Sci. China Chem*. **2021**, *64*, 576–580.

16. Wang, Y. *et al*. *Chem. Commun*. **2021**, *57*, 5818–5821.

17. Kawasumi, K., Zhang, Q., Segawa, Y., Scott, L. T., Itami, K. *Nat. Chem.* **2013**, *5*, 739–744.

18. Ohtsuka, N. *et al*. *Chem. Commun.* **2020**, *56*, 12343–12346.

19. Márquez, I. R., Castro-Fernández, S., Millán, A., Campaña, A. G. *Chem. Commun*. **2018**, *54*, 6705–6718.

20. Saito, M., Shinokubo, H., Sakurai, H. *Mater. Chem. Front*. **2018**, *2*, 635–661.

21. Buckingham, A. D. *Discuss. Faraday Soc*. **1957**, *24*, 151–157.

22. Stępień, M., Gońka, E., Żyła, M., Sprutta, N. *Chem. Rev*. **2017**, *117*, 3479–3716.

23. Tan, Q. *et al*. *Bull. Chem. Soc. Jpn.* **2018**, *91*, 531–537.

24. Hirai, M., Tanaka, N., Sakai, M., Yamaguchi, S. *Chem. Rev*. **2019**, *119*, 8291–8331.

25. Wang, X.-Y., Yao, X., Narita, A., Müllen, K. *Acc. Chem. Res*. **2019**, *52*, 2491–2505.

26. Wang, W., Shao, X. *Org. Biomol. Chem*. **2021**, *19*, 101–122.

27. Wang, S., Li, X., Hou, X., Sun, Y., Shao, X. *Chem. Commun*. **2016**, *52*, 14486–14489.

28. Higashibayashi, S., Pandit, P., Haruki, R., Adachi, S., Kumai, R. *Angew. Chem. Int. Ed*. **2016**, *55*, 10830–10834.

29. Yokoi, H., Hiroto, S., Shinokubo, H. *J. Am. Chem. Soc.* **2018**, *140*, 4649–4655.

30. Oki, K. *et al*. *J. Am. Chem. Soc*. **2018**, *140*, 10430–10434.

31. Đorđević, L. *et al*. *Angew. Chem. Int. Ed*. **2020**, *59*, 4106–4114.

32. Babič, A. *et al*. *Adv. Funct. Mater.* **2017**, *27*, 1701839.

33. Bauer, C. *et al*. *Org. Biomol. Chem*. **2018**, *16*, 919–923.

34. Gotoh, H. *et al*. *Angew. Chem. Int. Ed*. **2021**, *60*, 12835–12840.

35. Lei, Z., Chen, B., Koo, Y.-M., MacFarlane, D. R. *Chem. Rev*. **2017**, *117*, 6633–6635 and references cited therein.

36. Vekariya, R. L. *J. Mol. Liq*. **2017**, *227*, 44–60.

37. Singh, S. K., Savoy, A. W. *J. Mol. Liq*. **2020**, *297*, 112038.

38. Herrmann, W. A., Köcher, C. *Angew. Chem. Int. Ed. Engl*. **1997**, *36*, 2162–2187.

39. de Frémont, P., Marion, N., Nolan, S. P. *Coord. Chem. Rev*. **2009**, *253*, 862–892.

40. Hopkinson, M. N., Richter, C., Schedler, M., Glorius, F. *Nature* **2014**, *510*, 485–496.

41. Gandeepan, P., Cheng, C.-H. *Chem. Asian J*. **2016**, *11*, 448–460.

42. Dutta, C., Choudhury, J. *RSC Adv*. **2018**, *8*, 27881–27891.

43. van Dijk, T. *et al*. *Angew. Chem. Int. Ed*. **2014**, *53*, 9068–9071.

44. Kawahara, K. P., Matsuoka, W., Ito, H., Itami, K. *Angew. Chem. Int. Ed*. **2020**, *59*, 6383–6388.

45. Ito, S., Tokimaru, Y., Nozaki, K. *Angew. Chem. Int. Ed*. **2015**, *54*, 7256–7260.

46. Laursen, B. W. *et al*. *J. Am. Chem. Soc*. **1998**, *120*, 12255–12263.

47. Wu, D., Pisula, W., Enkelmann, V., Feng, X., Müllen, K. *J. Am. Chem. Soc*. **2009**, *131*, 9620–9621.

48. Bando, Y. *et al*. *Chem. Eur. J*. **2016**, *22*, 7843–7850.

49. Yamada, M., Tashiro, S., Miyake, R., Shionoya, M. *Dalton Trans*. **2013**, *42*, 3300–3303.

50. Haketa, Y., Urakawa, K., Maeda, H. *Mol. Syst. Des. Eng*. **2020**, *5*, 757–771.

51. Mahadevegowda, S. H., Stuparu, M. C. *Eur. J. Org. Chem*. **2017**, 570–576.

52. Aracena, A., Rezende, M. C., Encinas, M. V., Vergara, C., Vásquez, S. O. *New J. Chem*. **2017**, *41*, 14589–14594.

53. Rösch, U., Yao, S., Wortmann, R., Würthner, F. *Angew. Chem. Int. Ed.* **2006**, *45*, 7026–7030.

54. Murphy, M. P. *Biochim. Biophys. Acta Bioenerg*. **2008**, *1777*, 1028–1031.

55. Andrés, A. *et al*. *Eur. J. Pharm. Sci*. **2015**, *76*, 181–191.

56. Wang, H. *et al*. *Front. Chem*. **2021**, *9*, 683220.

57. Tokimaru, Y., Ito, S., Nozaki, K. *Angew. Chem. Int. Ed*. **2018**, *57*, 9818–9822.

58. Zhang, Q., Cao, R., Fei, H., Zhou, M. *Dalton Trans.,* **2014***, 43,* 16872–16879.

59. Sheldrick, G. M. University of Göttingen: Göttingen, Germany, **2014**.

60. Frisch, M. J. *et al*. *Gaussian 16, Revision A.03*, Gaussian, Inc., Wallingford CT, **2016**.

61. (a) Becke, A. D. *J. Chem. Phys*. **1993**, *98*, 5648–5652. (b) Lee, C., Yang, W., Parr, R. G. *Phys. Rev. B* **1998**, *37*, 785–789.

62. (a) Hehre, W. J., Ditchfield, R., Pople, J. A. *J. Chem. Phys*. **1972**, *56*, 2257–2261. (b) Ditchfield, R., Hehre, W. J., Pople, J. A. *J. Chem. Phys.* **1971**, *54*, 724–728.

63. Andrés, A. *et al*. *Eur. J. Pharm. Sci.* **2015**, *76*, 181–191.

Chapter 5. Conclusion and Perspective

This thesis explores the synthesis and properties of mainly three polyaromatic molecules designed based on azapentabenzocorannulene. These designs are inspired by carbon-defective graphene, such as the addition of carbon or nitrogen atoms. The modifications affected the topological, optical, and electronic properties of azapentabenzocorannulene.

Chapter 2 focused on the synthesis of azahomocorannulene derivatives featuring a seven-membered (tropyl) ring. This odd-numbered ring induces the doublet ground state. The spin distribution extends from the ipso position of the seven-membered ring as the center. The molecule exhibits a planar structure due to the positive curvature stretching of azacorannulene, confirmed by X-ray crystallography. This represents a rare example of isolated tropyl radicals by X-ray crystal analysis. In addition, the crystal structure was such that each radical was relatively evenly spaced without forming a π-dimer. This may lead to further organic magnetic materials that show open-shell properties in the solid state and electrical conductivity.

Chapter 3 describes the synthesis and properties of azadihomocorannulene. The coupling reaction using the mechanoreaction makes it possible to omit conventional reaction steps in a solution system. The incorporation of two additional sp^2 carbon atoms into the azacorannulene skeleton imparts an open-shell singlet ground state. Furthermore, it is of interest to design a triradical system incorporating an additional seven-membered ring structure to investigate its influence on the spin system and topology of azacorannulene. Chapters 2 and 3 collectively demonstrate that the carbon-defective modifications, inspired by the "homo-" concept, give an open-shell nature to azacorannulene.

Chapter 4 involves incorporating a nitrogen atom into the pyrrole ring of the azacorannulene skeleton to form an imidazole structure. While the neutral species was not yet achieved, the cationic form was successfully synthesized, serving as a potential precursor to the radical form. This cationic molecule demonstrates a significantly higher affinity for water

than azacorannulene and exhibits fluorescence properties not seen in corannulene. Taking advantage of this fluorescent property, we demonstrated the possibility of using it as a fluorescent cellular probe for mitochondria. Because of its high water affinity, it has the potential for further application in biological systems.

These results show that carbon-defective modifications to polyaromatic molecules can facilitate the adoption of open-shell characteristics, which is valuable in designing organic magnetic molecules. As anticipated, modifying the azacorannulene skeleton proves to be an effective method for creating functional molecules.

The author believes incorporating carbon-defective structures into fragment molecules of carbon materials is an effective strategy for designing new functional aromatic molecules. This approach is advantageous when creating organic radical molecules as the insertion of sp^2 carbon facilitates the design of non-alternant hydrocarbons. In this study, open-shell azacorannulene derivatives were designed and tried to synthesize using carbon and nitrogen; however, inserting other heteroatoms such as boron and sulfur is also feasible. Additionally, the properties of the synthesized molecules in this thesis can be further enhanced by adding substituents. The azacorannulene framework holds significant potential for further functionalization, allowing for the design of molecules with diverse spin distribution and a wide range of applications.